Pavel Lebduška

Topografie signalizačních molekul na plazmatické membráně při aktivaci žírných buněk

Dizertační práce
z oboru molekulární a buněčné biologie

Univerzita Karlova
Přírodovědecká fakulta

Školitel: RNDr. Petr Dráber, DrSc.
Ústav molekulární genetiky Akademie věd České republiky,
Oddělení signální transdukce

Praha, červenec 2007

... lékařství pozoruje povahu churavosti a hudba
povahu nesouzvuků jen proto,
aby vytvářely jejich opak.

Plútarchos

Předmluva

Odhalování mechanizmů, jimiž buňky imunitního systému reagují na antigeny, lze zařadit mezi ty oblasti základního výzkumu, které nejen posouvají hranice obecného vědění, ale úzce se dotýkají též kvality lidského života. Z tohoto důvodu jsem si za objekt studia zvolil přenos signálu přes plazmatickou membránu žírných buněk – efektorů alergických reakcí. Výsledky práce mé a mých kolegů k tomuto tématu byly publikovány v následujících odborných článcích, které níže přikládám:

(A) Signaling assemblies formed in mast cells activated via Fcε receptor I dimers.
Ľubica Dráberová, Pavel Lebduška, Ivana Hálová, Pavel Tolar, Jitka Štokrová, Helena Tolarová, Jan Korb and Petr Dráber.
Eur. J. Immunol. 2004, 34: 2209-2219

(B) Negative regulation of mast cell signaling and function by the adaptor LAB/NTAL.
Petra Volná, Pavel Lebduška, Ľubica Dráberová, Šárka Šímová, Petr Heneberg, Michael Boubelík, Viktor Bugajev, Bernard Malissen, Bridget S. Wilson, Václav Hořejší, Marie Malissen and Petr Dráber.
J. Exp. Med. 2004, 200: 1001-1013

(C) Topography of plasma membrane microdomains and its consequences for mast cell signaling.
Petr Heneberg, Pavel Lebduška, Ľubica Dráberová, Jan Korb and Petr Dráber.
Eur. J. Immunol. 2006, 36: 2795-2806

(D) Regulation of Ca^{2+} signaling in mast cells by tyrosine-phosphorylated and unphosphorylated non-T cell activation linker, NTAL.
Ľubica Dráberová, Gouse Mohiddin Shaik, Petra Volná, Petr Heneberg, Magda Tůmová, Pavel Lebduška, Jan Korb and Petr Dráber.
Journal of Immunology, odesláno (květen 2007)

(E) Topography of signaling molecules as detected by electron microscopy on plasma membrane sheets isolated from nonadherent mast cells.
Pavel Lebduška, Jan Korb, Magda Tůmová, Petr Heneberg and Petr Dráber.
Journal of Immunological Methods, odesláno (červen 2006)

Prohlašuji, že mi tyto odborné články v minulosti nesloužily jako podklad pro získání jiného akademického titulu. Podíl mých vlastních výsledků specifikuji v průběhu následujícího textu. Vyplývá zejména z oddílů Diskuse a Závěry, kde výsledky jiných badatelů explicitně cituji.

Rád bych tímto poděkoval výše uvedeným spoluautorům předkládaných publikací, technickým pracovníkům Oddělení signální transdukce a Oddělení mikromorfologie biopolymerů na Ústavu molekulární genetiky, a v neposlední řadě svým přátelům a příbuzným, bez jejichž citové či profesní vstřícnosti by několikaletá vědecká práce byla těžší, temnější a o mnohé ochuzena.

RNDr. Pavel Lebduška
červenec 2007

***

Vypracováno na Ústavu molekulární genetiky Akademie věd České republiky v letech 2002-2007.

Obsah

Použité zkratky a upřesnění pojmů

BCR: Receptor lymfocytů B (B cell receptor)
BMMC: Žírné buňky odvozené z kostní dřeně (Bone marrow-derived mast cells)
DIG: Membrány obohacené o glykosfingolipidy a nerozpustné v Tritonu (Detergent-insoluble glycosphingolipid-enriched membranes)
DRM: Membrány rezistentní k detergentu (Detergent-resistant membranes)
FAK: Kináza fokálních adhezí (Focal adhesion kinase)
FcαR (I): Receptor imunoglobulinu A, typ I
FcγR (I, II, III): Receptor imunoglobulinu G, typ I, II, III
FcεR (I, II): Receptor imunoglobulinu E, typ I, II
FGF: Růstový faktor fibroblastů (Fibroblast growth factor)
FRET: Přenos energie fluorescenční rezonancí (Fluorescence resonance energy transfer)
GPI: Glykozylfosfatidylinozitol, glykozylfosfatidylinozitolový
GM-CSF Faktor stimulující kolonie granulocytů a makrofágů (Granulocyte-macrophage colony stimulating factor)
Ig: Imunoglobulin
IFN: Interferon
IL: Interleukin
ITAM: Imunoreceptorový tyrozinový aktivační motiv
ITIM: Imunoreceptorový tyrozinový inhibiční motiv
MAPK: Mitogenem aktivovaná proteinkináza
MAPKK: Kináza mitogenem aktivované proteinkinázy (Mitogene-activated protein kinase-kinase)
MIRR: Víceřetězcový rozpoznávací imunoreceptor (Multichain immune recognition receptor
NGF: Nervový růstový faktor (Nerve growth factor)
PI3K: Fosfatidylinozitol-3 kináza
PLC: Fosfolipáza C
RBL: Krysí bazofilní leukemie (Rat basophilic leukemia)
SCF: Faktor kmenových buněk (Stem cell factor)
T_C: Cytotoxický lymfocyt T
TCR: Receptor lymfocytů T (T cell receptor)
TGF: Transformující růstový faktor (Transforming growth factor)
T_H: Pomocný lymfocyt T
TIFF: Plovoucí frakce nerozpustná v Tritonu (Triton-insoluble floating fraction)
TLR: Receptor podobný molekule Toll (Toll-like receptor)
TNF: Faktor nekrózy nádorů (Tumor necrosis factor)
T_{Reg}: Regulační lymfocyt T

(Ostatní netradiční shluky písmen, ač původně vznikly většinou rovněž jako zkratky, používám jako vžité odborné termíny a tedy je zde neuvádím.)

Kolokalizace (vztaženo k plazmatické membráně) – míněn preferenční výskyt jednoho antigenu v oblasti výskytu antigenu druhého, nikoliv náhodný výskyt obou na tomtéž místě.

Neadherentní buňky – nepřisedající během svého růstu ke dnu kultivačních nádob určených pro tkáňové kultury.

Úvod

I) Organizace plazmatické membrány

Plazmatická membrána slouží jako víceúčelové biologické rozhraní zásadní důležitosti, které určuje a aktivně udržuje složení vnitrobuněčného prostředí a zprostředkovává dialog mezi buňkou a okolím. Tato informační funkce plazmatické membrány je již řadu let předmětem intenzivního výzkumu, který pomalu odkrývá strukturní a funkční pozadí transmembránové komunikace. Ukazuje se, že v těchto procesech nejsou možná klíčové ani tak samy proteiny, jako jejich spolupráce s lokálním lipidickým prostředím - fenomén spjatý s pojmem „lipidové rafty".

Původní představa o lipidových raftech

Když v roce 1972 Singer a Nicolson publikovali „model tekuté mozaiky" týkající se organizace plazmatické membrány, kladli důraz na laterální mobilitu jednotlivých proteinů v rámci dvojrozměrné lipidické fáze. Plazmatická membrána se jevila víceméně jako rovinný orientovaný roztok amfipatických proteinů v lipidové dvojvrstvě (*Singer a Nicolson, 1972*). Postupně se však začal prosazovat model, ve kterém lipidy plazmatické membrány na základě rozdílných vlastností svých hydrofóbních řetězců bočně segregují a spontánně tak tvoří soustavu membránových domén (*Klausner a kol., 1980; Karnovsky a kol., 1982*). Pozornost přitahovaly zejména shluky sfingolipidů s vmezeřeným cholesterolem, o nichž se předpokládalo, že tvoří jakési relativně rigidní ostrůvky, lipidové rafty, které plují jako kry v okolním fluidním prostředí plazmatické membrány tvořeném fosfolipidy s nenasycenými acylovými řetězci. Význam těchto raftů byl spatřován v transportu určitých samovolně vytříděných proteinů do konkrétní oblasti plazmatické membrány nebo příslušných organel, a byla jim též přisouzena důležitá signalizační role (*Brown a Rose, 1992; Simons a Ikonen, 1997; Simons a Toomre, 2000; Dykstra a kol., 2003*).

Podle této hypotézy působí lipidové rafty v rovině plazmatické membrány jako specifické kompartmenty sdružující zejména molekuly, které obsahují nasycené lipidické řetězce nebo řetězce s dvojnou vazbou v konfiguraci trans, tedy například palmitylované proteiny a extracelulární proteiny zakotvené pomocí glykozylfosfatidylinozitolu (GPI), uplatňují se však též interakce aminokyselin proteinového řetězce s lipidickými složkami raftů (**Obr. 1**). Imunoreceptory skupiny MIRR („víceřetězcové rozpoznávací imunoreceptory"), jako TCR lymfocytů T, BCR lymfocytů B nebo FcεRI žírných buněk, s lipidovými rafty v klidovém stavu téměř neasociují, ale agregace těchto proteinů, která iniciuje přenos signálu přes plazmatickou membránu a následné signalizační kaskády, způsobuje současně

stabilizaci jejich kontaktu s raftovými kompartmenty. Podle tohoto modelu se v lipidových raftech nacházejí aktivátory a substráty signalozomů imunoreceptorů skupiny MIRR (kinázy rodiny Src, palmitylované transmembránové adaptorové proteiny), zatímco negativní regulátory jsou vyloučeny.[*] Raft může být též funkčním pojítkem mezi extracelulárními receptory zakotvenými přes GPI a signalizačními molekulami asociovanými s intracelulárním listem plazmatické membrány (*Langlet a kol., 2000; Dykstra a kol., 2003; Hořejší a kol., 1999*).

Na počátku konceptu lipidových raftů stály studie prováděné na umělých membránách, které prověřily základní teze hypotézy o segregaci molekul v rámci planární orientované lipidické směsi (*Klausner a kol., 1980; Sankaram a Thompson, 1990a; Sankaram a Thompson, 1990b; Sankaram a Thompson, 1991; Sankaram a kol., 1992; McIntosh a kol., 1992; Dietrich a kol., 2001*). Výsledky z těchto modelových systémů ale nelze přímo aplikovat na popis chování skutečné plazmatické membrány, tedy soustavy proteinů a lipidů o mnohem větší komplexitě, kde rovněž podstatnou roli mohou hrát například interakce s podmembránovým cytoskeletem.

Široce používaným metodickým přístupem studia lipidových raftů se stala izolace tak zvaných DRM – membránové frakce vykazující zvýšenou rezistenci k působení neiontových detergentů (*Brown a Rose, 1992*). Kolem pojmu DRM („membrány rezistentní k detergentu“) vznikly terminologické zmatky, které ostatně provází celou hypotézu lipidových raftů. V obecném významu DRM představují membránový izolát vzniklý částečnou lýzou buňky neiontovým detergentem, a je proto zapotřebí specifikovat podmínky (druh detergentu, jeho koncentraci, teplotu), za kterých byl preparát získán. Často však bývá tento termín omezován na membránové izoláty připravené pomocí Tritonu X-100 při 4°C, pak bývají označovány též TIFF („plovoucí frakce nerozpustná v Tritonu“). DRM nelze zaměňovat s lipidovými rafty, neboť jsou produktem izolace, zatímco rafty předpokládáme jako reálné struktury plazmatické membrány. Přesto se tak často dělo a termíny DIG („membrány nerozpustné v detergentu a obohacené o glykosfingolipidy“) nebo GEM („membrány obohacené o glykosfingolipidy“) bývaly rovněž ztotožňovány jak s lipidovými rafty, tak s DRM. Východiskem z terminologické krize je pojímat lipidové rafty jako membránové domény bohaté na cholesterol a sfingolipidy a izolovatelné v podobě DRM (*Langlet a kol., 2000; London a Brown, 2000; Brown a London, 2000*).

Extrakce frakcí plazmatické membrány pomocí detergentu je bezesporu užitečným přístupem, který poskytuje informace o rozdílné tendenci příslušných membránových proteinů asociovat s určitým lipidickým prostředím, a získané

[*] Situace je však mnohem složitější. Například tyrozinová fosfatáza CD45, důležitý pozitivní regulátor signalizace přes MIRR, se raftů spíše straní, což koreluje se sníženou aktivitou jejích substrátů – kináz rodiny Src, které rafty preferují. Za jistých okolností je CD45 kinázám rodiny Src i negativním regulátorem. Podstatná je optimální míra kontaktu těchto tyrozinkináz s CD45 a ostatními komponentami signální kaskády v dynamickém vyváženém procesu. (*Rodgers a Rose, 1996; Montixi a kol., 1998; Penninger a kol., 2001; Zhang a kol., 2005*).

výsledky plně zapadají do konceptu lipidových raftů, nepředstavují však samy o sobě dostatečný důkaz jejich reálné existence, neboť aplikace detergentu je výrazným zásahem do biofyzikálních vlastností plazmatické membrány (*Mayor a Maxfield, 1995; Heerklotz, 2002*). Pomocí metody FRET („přenos energie fluorescenční rezonancí“) se nicméně podařilo prokázat i v plazmatické membráně živých buněk tvorbu proteinových agregátů, které závisely na přítomnosti cholesterolu a na GPI kotvě, nikoliv na samotném bílkovinném řetězci. Průměr těchto domén byl méně než 70 nm (*Varma a Mayor, 1998*). Podobné závěry vyplynuly z experimentu s kovalentním spojováním těsně asociovaných proteinů zakotvených přes GPI (*Friedrichson a Kurzchalia, 1998*). Také charakteristiky lokální difůze membránových proteinů potvrdily, že přítomnost cholesterolu vede k tvorbě relativně stabilních domén o průměru přibližně 13-40 nm, v nichž jsou obsaženy předpokládané raftové proteiny, zatímco ostatní proteiny difundují v méně viskózním prostředí (*Pralle a kol., 2000*). Ukotvení pomocí modulů myristyl-palmityl nebo palmityl-palmityl vede k agregaci v závislosti na cholesterolu, ale prenylované proteiny agregují za tvorby domén odlišných a na cholesterolu nezávislých (*Zacharias a kol., 2002*).

Pomocí fluorescenčních derivátů lipidů s nasycenými nebo nenasycenými řetězci bylo možné sledovat rozložení rigidnějších ostrůvků i fluidních oblastí plazmatické membrány jak v detailu, tak v rámci celé buňky. Organizované lipidické oblasti nedifundovaly volně, ale určitým směrem, a jejich příležitostný vznik nebo zánik se odehrával na konkrétních místech, pravděpodobně ve vztahu k vazbě cytoskeletu. Větší zastoupení těchto domén vykazovaly oblasti adheze, mezibuněčných kontaktů a panožek (*Schütz a kol., 2000; Gaus a kol., 2003*).

Zdá se, že existence lipidických heterogenit raftového typu není omezena jen na živočišné buňky, ale že analogický strukturně-funkční mechanismus využívají i rostliny a houby, byť s drobnými odlišnostmi spjatými s rozdíly v lipidickým složení a v poměru sterolů a sfingolipidů k membránovým proteinům (*Xu a kol., 2001; Bagnat a Simons, 2002; Martin a kol., 2005; Bhat a Panstruga, 2005; Opekarová a kol., 2005*).

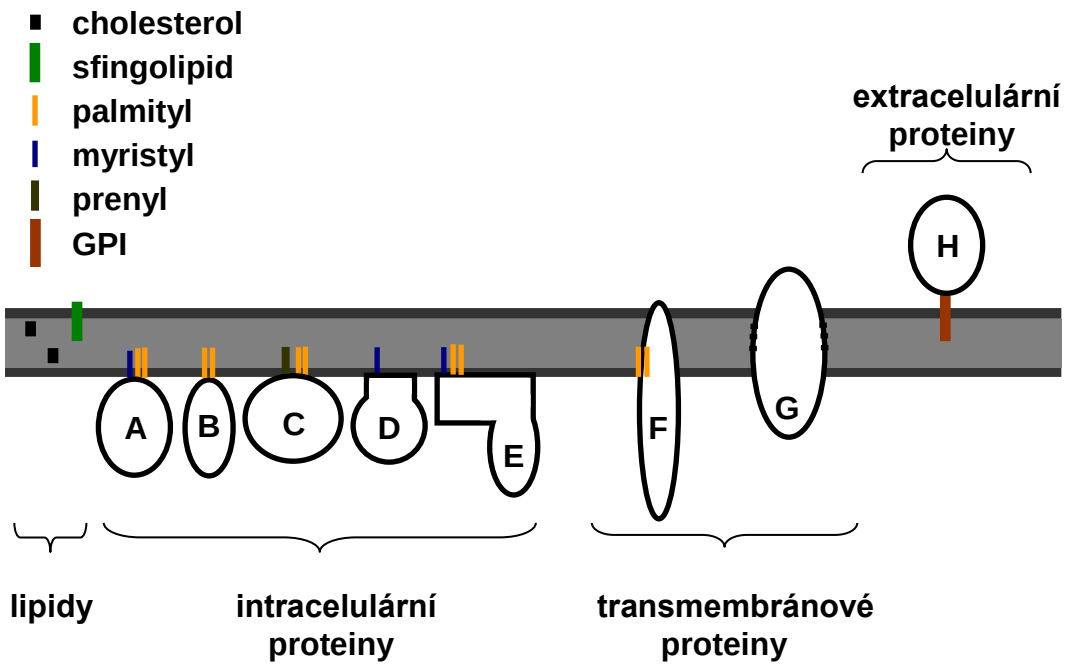

Obr. 1: Některé z tak zvaných „markerů lipidových raftů“ a jejich zakotvení v plazmatické membráně.
A) Lyn, Fyn, Lck, podjednotka α G proteinu, raftlin. **B)** GAP-43/B-50. **C)** H-ras, N-ras. **D)** NAP-22. **E)** Kaveolin, flotilin (reggie). Počet palmitylů a myristylů je u této skupiny variabilní. **F)** LAT, NTAL (LAB, LAT2), PAG (Cbp), LIME.
G) MAL/VIP17, BENE, plazmolipin, hemaglutinin, prominin. Pro tuto skupinu jsou podstatné specifické interakce mezi transmembránovou doménou a molekulami tvořícími rafty. V případě hemaglutininu navíc trojí palmitylace (nevyznačeno).
H) CD14, CD16, CD48, CD55, CD59, Thy-1 (CD90). Povaha GPI jednotek se může lišit.
(*Cinek a Hořejší, 1992; Resh, 1994; Pérez a kol., 1997; Scheiffele a kol., 1997; Arni a kol., 1998; Frank a kol., 1998; Corbeil a kol., 2001; Dunphy a kol., 2001; Epand a kol., 2001; Chatterjee a Mayor, 2001; Dykstra a kol., 2003; Saeki a kol., 2003; Pike, 2004; Pizzo a Viola, 2004; Navarro a kol., 2004; Roy a kol., 2005; Langhorst a kol., 2005*)

Nové pojetí lipidových raftů

Navzdory tomu, že se podařilo i v plazmatické membráně živých buněk dokázat existenci domén o vlastnostech připisovaných lipidovým raftům (viz výše), vyskytly se též obdobně průkazné studie, které jejich významnější zastoupení v klidové membráně (bez vyvolané agregace) zpochybňují nebo dokládají jejich překvapivě malé rozměry (*Kenworthy a Edidin, 1998; Kenworthy a kol., 2000; Vrljic a kol., 2002; Glebov a Nichols, 2004; Kenworthy a kol., 2004; Sharma a kol., 2004*). Postupně se začal formovat model, který byl současně alternativou i prohloubením původní hypotézy lipidových raftů. Předpokládá existenci kondenzovaných komplexů cholesterolu a sfingolipidů, které se stávají základními stavebními kameny raftů, a přisuzuje proteinům podstatnou roli při organizaci lipidických struktur.

I když byl koncept kondenzovaných komplexů založen na pozorování chování směsí cholesterolu a sfingolipidů v umělých membránách, stal se dobrým východiskem k vysvětlení struktury a dynamiky organizovaných domén plazmatické membrány (*Radhakrishnan a McConnell, 1999; Radhakrishnan a kol., 2000; Anderson a McConnell, 2001; Anderson a McConnell, 2002; Anderson a Jacobson, 2002*). Kondenzované lipidické komplexy mohou být v plazmatické membráně přítomny jako individuální entity obsahující pouhých 15-30 molekul, které jsou však schopny za určitých podmínek snadno vytvořit separovanou fázi. Lipidové rafty tak mohou vznikat nahloučením příslušných membránových proteinů komunikujících s okolní membránou prostřednictvím lipidického pláště tvořeného kondenzovanými komplexy. Opláštění raftových proteinů v klidovém stavu však samo o sobě pravděpodobně podléhá dynamickému procesu asociace a disociace (*Anderson a Jacobson, 2002*).

Působení extracelulárního vazebného elementu (protilátky, ligandu) na raftotvorné molekuly vyvolává vznik stabilizovaných domén vyčleněných z okolní fluidní fáze. Tyto domény mohou sdružovat též intracelulární komponenty asociované díky preferenci stejného lipidického prostředí a vázat se na cytoskelet (*Hammond a kol., 2005; Mayor a kol., 1994; Thomas a kol., 1994; Harder a kol., 1998; Suzuki a Sheetz, 2001*). Zatímco rafty klidové membrány představují zřejmě drobné a nestabilní struktury, které vznikají a zanikají v řádu nanosekund, vazba stabilizátoru pravděpodobně způsobí redukci tepelného pohybu, čímž umožní asociaci dalších molekul. Tyto sekundární raftové struktury se od primárních nestabilních raftů zásadně liší komplexitou (jak vyšší počet molekul, tak i jejich druhů), dobou trvání (v řádu minut) i velikostí (desítky nanometrů nebo i více) a zpravidla plní specifické signalizační funkce (*Subczynski a Kusumi, 2003; Kusumi a kol., 2004; Kusumi a kol., 2005*) (**Obr. 2**). V širším slova smyslu lze za podskupinu stabilizovaných raftů považovat i kaveoly nebo flotilinové domény, jejichž strukturu zpevňují agregáty speciálních membránových proteinů (*Navarro a kol., 2004; Langhorst a kol., 2005; Bauer a Pelkmans, 2006*).

Podle modelu heterogenity raftů vyvolané indukovaným přizpůsobením („The induced-fit model of raft heterogeneity“) vede rozdílná tendence raftových proteinů interagovat s raftovými lipidy k plastickému zformování takové membránové domény, jejíž struktura a obsah vychází z optimálního uspořádání souboru jednotlivých konstituentů. Agregací více proto-raftů tak může vzniknout raft o rozdílných vlastnostech, než měly jeho prekurzory, například vyloučením některých molekul a zahrnutím jiných, což ve svém důsledku může vést k dalším přestavbám dané domény (*Pike, 2004*). Tento teoretický koncept přináší možnou odpověď na otázku, proč například rozdílné proteiny zakotvené přes GPI mohou formovat rozdílné raftové útvary (*Madore a kol., 1999; Wang a kol., 2002*) – i malá odlišnost v kotvícím modulu nebo ve sterickém působení proteinových jednotek by mohla k tomu být dostatečným impulzem.

Ukazuje se, že pro specifickou lokalizaci GPI proteinů v rámci plazmatické membrány je podstatná také jejich glykozylace (*Pang a kol., 2004; Ermini a kol., 2005*). Přináší to další rozměr do možných mechanismů regulace lipidových raftů, jako doplnění ke vlivům modifikací lipidické kotvy (reverzibilní palmitylace, odštěpení proteinu od GPI), lipidického složení (modulace podílu cholesterolu a ostatních lipidů v plazmatické membráně), spektra membránových proteinů (rozdílná exprese) a vnějších vlivů (mezibuněčné kontakty, vazba volných ligandů). Stabilita těchto domén také může záviset na kovalentních i nekovalentních proteinových interakcích, ke kterým dojde již v Golgiho aparátu (*Paladino a kol., 2004*). V některých případech může podstatnou roli při asociaci proteinu s raftovými lipidy či jinými doménami plazmatické membrány hrát i spolupůsobení regulovatelných lipidických modifikací a alosterických efektů v rámci proteinové jednotky (*Hancock, 2003; Rotblat a kol., 2004; Roy a kol., 2005*).

Postupně je tedy odkrýván komplexní organizační a signalizační systém plazmatické membrány, v němž značnou (ale nikoliv jedinou) roli hrají dynamické domény proteinů a lipidů označované ze setrvačnosti jako lipidové rafty. Protože ale je vzájemné působení proteinů a lipidů v procesu formování raftů oboustranné a vzájemně podmiňující, je v současné době pojem „lipidové rafty“ stále více nahrazován výrazem „membránové rafty,“ který bychom však neměli zaměňovat s obecnějším termínem „membránové mikrodomény.“ V roce 2006 byla na sympoziu ve Steamboat Springs přijata pracovní definice membránových raftů: „*Membránové rafty jsou malé (10-200 nm), heterogenní, vysoce dynamické domény. Jsou obohacené*[*] *o steroly a sfingolipidy a kompartmentalizují buněčné procesy. Malé rafty někdy mohou být stabilizovány do rozsáhlejších platforem pomocí interakcí proteinů s proteiny i s lipidy.*“ (*Pike, 2006*). Jedná se však pouze o pokus překlenout terminologické rozpory. Příroda nezná hranice mezi uměle zavedenými kategoriemi a fenomén dynamických heterogenit plazmatické membrány nebyl dosud zcela vysvětlen, proto se lze nadít ještě dalších zvratů v jeho pojetí.

[*] Vhodnější termín by byl *bohaté.*

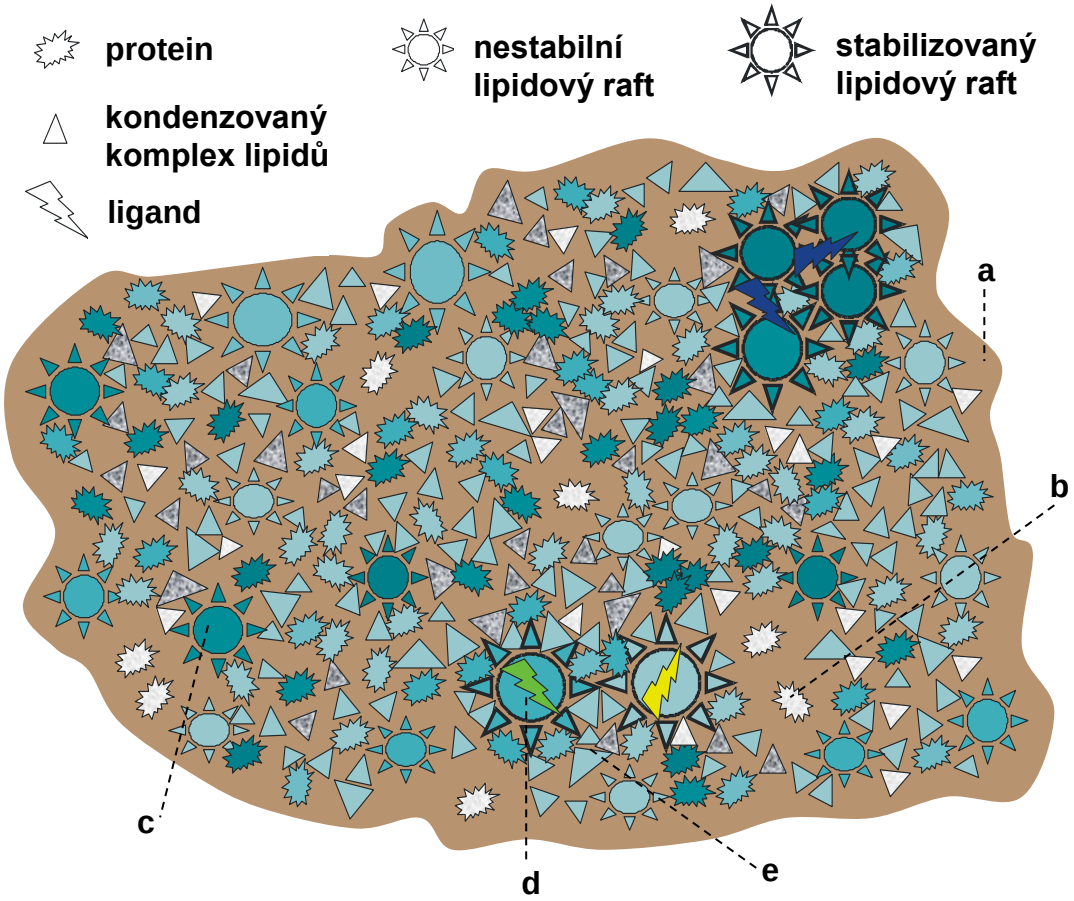

Obr. 2: Schematický pohled na rovinu plazmatické membrány podle reformovaného modelu lipidových raftů.
Ve fluidní fázi membránových lipidů **(a)** se nacházejí proteiny, které toto prostředí preferují **(b)**, avšak také takové, které se z něj v dynamickém procesu vydělují pomocí interakcí s kondenzovanými komplexy lipidů za tvorby přechodných nestabilních lipidových raftů **(c)**. Účinkem ligandu dochází ke stabilizaci lipidového raftu **(d)**, na jehož periferii vzniká přechodná zóna nestabilně asociovaných proteinů a lipidů **(e)**.
(*Anderson a Jacobson, 2002; Subczynski a Kusumi, 2003*)

II) Žírné buňky jako model přenosu signálu přes plazmatickou membránu

Žírné buňky (mastocyty) patří mezi modelové buněčné typy, na nichž jsou zkoumány mechanismy přenosu signálu přes plazmatickou membránu savčích buněk. Tato obliba odráží jak jejich roli v patologii atopických alergií, které se stávají vážným celospolečenským problémem, tak možnost sledovat dobře pozorovatelné reakce na definovaný vnější podnět, a to v horizontu sekund, minut i hodin.

Role žírných buněk v organizmu

Žírné buňky vznikají postupnou diferenciací krvetvorných kmenových buněk, jako nezralé prekurzory putují krevním řečištěm a svůj vývoj dokončují v cílových tkáních pod vlivem specifického prostředí. Tento proces není dosud uspokojivě objasněn, stejně jako vztah žírných buněk k bazofilním granulocytům, které často bývají označovány za jejich cirkulující obdobu. V myší slezině se podařilo identifikovat buněčný typ myeloidního původu, z něhož bylo možné vypěstovat jak mastocyty, tak bazofilní granulocyty a u člověka byl prokázán společný specifický prekurzor mastocytů a monocytů, nicméně stále není vyloučeno, že se žírné buňky vyvíjejí také z multipotentních progenitorů mimo myeloidní linii (*Arinobu a kol., 2005; Kirshenbaum a kol., 1999; Chen a kol., 2005; Sonoda a kol., 1983*). Pokusy *in vitro* ukázaly, že proliferace a diferenciace žírných buněk závisí na spolupůsobení cytokinů SCF, IL-3 (a někdy též IL-4) za podpory IL-9 a IL-10, zatímco GM-CSF a IFN-γ diferenciaci mastocytů inhibují a TGF-β působí proti jejich proliferaci. Také další cytokiny (TNF-α, IL-6, NGF aj.) se mohou podílet na tvorbě podmínek, které směřují k vývoji rozdílných typů žírných buněk. SCF není pro žírné buňky jen růstovým a diferenciačním faktorem, ale též jedním z chemoatraktantů a stimulátorem jejich aktivního zakotvení ve tkáních (*Metcalfe a kol., 1997; Okayama a Kawakami, 2006*).

Zdá se, že rozdíly v lokálním prostředí na jednotlivých místech organismu vedou ke vzniku mnoha specializovaných populací žírných buněk lišících se ve své morfologii i funkci. Při nejhrubším dělení bývají ale obvykle rozlišovány jen dva základní typy mastocytů – pojivové a slizniční – popsané u hlodavců, ale mající své analogie i v lidském organismu. Pojivové mastocyty z myší peritoneální dutiny dosahují velikosti 10-20 μm a jejich vývoj přímo nezávisí na lymfocytech T. Oproti tomu myší slizniční mastocyty z tenkého střeva dosahují velikosti pouze 5-10 μm, na lymfocytech T jsou závislé a od pojivových se odlišují též obsahem sekrečních granulí (jiný typ chymázy a proteoglykanů, o řád méně histaminu, zato přítomen leukotrien C_4). Lidská obdoba pojivových mastocytů (tzv. typ tryptázový-chymázový sekretující více rozdílných neutrálních peptidáz) se vyskytuje především v kůži, zatímco obdoba myších slizličních mastocytů (tzv. typ tryptázový) obývá

zejména tkáň plicních alveolů a tenkého střeva (*Metcalfe a kol., 1997*). Sama peritoneální dutina u člověka ale za normálních okolností žírné buňky neobsahuje. Prostorová a funkční organizace mastocytárního systému hlodavců a lidí je rozdílná a poznatky získané pomocí jednoho modelu nelze proto automaticky aplikovat na druhý. Myší žírné buňky se například v mnoha ohledech víc než lidským mastocytům blíží lidským bazofilům (*Bischoff, 2007; Falcone a kol., 2006*).

Nejznámější rolí žírných buněk je obrana tělních povrchů proti bakteriím a mnohobuněčným parazitům (**Obr. 3**). Vazba antigenu (alergenu) na specifické molekuly imunoglobulinu E asociované s membránovým receptorem FcεRI vede k vylití obsahu cytoplazmatických váčků do extracelulárního prostředí (k degranulaci). Uvolněné proteázy přímo či nepřímo poškozují povrch parazita a rozkládají komponenty mezibuněčné hmoty, zvyšují permeabilitu cév, stimulují produkci slizu a ovlivňují aktivitu některých cytokinů, hormonů a nervových působků; ve spolupráci s heparinem mají vliv na srážení krve. Žírné buňky mohou také stimulovat buněčnou adhezi, pozitivně působit na eozinofily i na proliferaci epitelových buněk a fibroblastů. Sekretovaný histamin způsobuje lokální stahy hladké svaloviny dýchacího a trávicího traktu (čímž přispívá k vypuzení nežádoucího cizorodého organismu) a ovlivňuje průsvit cév; peptidy kathelicidinového typu mají antimikrobiální účinky. Stimulované žírné buňky vzápětí pomocí arachidonových metabolitů a spektra cytokinů vytváří prostředí alergického zánětu. Díky receptorům TLR mastocyty reagují na patogeny i bez závislosti na mechanismech adaptivní imunity. Lze je označit za předsunuté hlídky, které v sobě spojují bezprostřední aktivní obranu ohrožené tkáně s organizováním následné komplexní ochrany. S touto rolí souvisí i udržování integrity tělních povrchů podporou hojení ran a angiogeneze (*Metcalfe a kol., 1997; Marshal, 2004*).

Žírné buňky jsou důležitými modulátory imunitních reakcí. Sekrecí cytokinů IL-3, IL-4, IL-5, IL-9, IL-13, IL-15 a IL-16 podporují lymfocyty T_H2 a B, tedy tvorbu protilátek, rovněž však mohou produkcí IFN-γ, IL-12 a IL-18 působit pozitivně na lymfocyty T_H1 a tím na zánětlivou imunitní odpověď. Vedle zánětlivých mediátorů (TNF-α, IL-1β) uvolňují protizánětlivé (IL-10, TGF- β), pomocí chemoatraktantů rovněž lákají jak lymfocyty T_H1 (IL-8), tak T_H2 (CCL5). Konkrétní průběh reakce zjevně závisí na okolnostech jejího vzniku a na předchozím specifickém vývoji dané populace mastocytů. Žírné buňky též mohou sloužit jako buňky prezentující antigen a současně k této funkci pomáhají dendritickým buňkám. Do místa alergického zánětu podle potřeby lákají neutrofily a eozinofily, umožňují jejich prostup cévní stěnou a prodlužují jejich životaschopnost, účastní se též boje proti virům spoluprácí s lymfocyty T_C. Tvoří významný regulační průsečík adaptivní a vrozené imunity (*Marshall, 2004; Frossi a kol., 2004; Galli a kol., 2005a; Galli a kol., 2005b*).

Poněkud kontroverzní je vztah žírných buněk k rakovinnému bujení. Myši se sníženým množstvím mastocytů vykazují rychlejší růst implantovaných nádorů a rovněž tak přítomnost mastocytů v lidském prsním nádoru je spojena s dobrou

prognózou. Zdá se však, že například v případě melanomů (člověk, pes), venerických nádorů (pes) nebo karcinomu žaludku (člověk) žírné buňky spíše škodí díky své podpoře angiogeneze novotvaru, je však předčasné vynášet definitivní soud. Množství výsledků týkajících se žírných buněk a rakoviny je značné, ale jejich interpretace obtížná, neboť často naráží na nejasnosti v experimentálním kontextu studia nádorů (*Burtin a kol., 1985; Rajput a kol., 2007; Toth-Jakatics a kol., 2000; Mukaratirwa a kol., 2006a; Mukaratirwa a kol., 2006b; Kondo a kol., 2006; Őzdemir, 2006*).

Ukazuje se, že se mastocyty také účastní dialogu mezi imunitním a nervovým systémem. Periferní nervová vlákna uvolňují mediátory, které místně působí na celou řadu kožních buněk (žírné buňky, dendritické buňky, keratinocyty, buňky cévní výstelky aj.) a jsou jimi též zpětně ovlivňována. Žírné buňky na periferní neurony působí nejen pomocí svých neuropeptidů, ale například též sekrecí TNF posilují lokální inervaci pokožky i škáry a svými proteázami modulují účinky neuronálních mediátorů na průběh zánětu. Podobnou regulační funkci na oblasti průniku vlivů místního a nervového stresu plní také ve sliznicích gastrointestinálního a dýchacího traktu. Podařilo se též prokázat přímý vliv mastocytů na centrální nervový systém. Patří mezi nemnoho druhů krvinek, které pronikají hematoencefalickou bariérou i u zdravých jedinců a osídlují mozek. Svou degranulací mohou způsobit aktivaci hormonální dráhy hypothalamus-hypofýza-nadledvinky, pravděpodobně jako součást obrany těla při expozici alergenu. Současně představují mechanismus dočasné přestavby konkrétních oblastí mozku v odpověď na humorální podněty, například během období páření, a to jak u savců, tak u ptáků. Žírné buňky v tomto procesu slouží jako místně specifický indukovatelný zdroj neuromodulátorů, jejichž spektrum závisí na daném živočišném druhu. V neposlední řadě mastocyty ovlivňují funkce cévního systému mozku (*Scholzen a kol., 1998; Luger, 2002; Kakurai a kol., 2006; Van Nassauw a kol., 2007; Dimitriadou a kol., 1994; Mawdsley a Rampton, 2005; Edvinsson a kol., 1977; Silver a kol., 1996; Matsumoto a kol., 2001; Kovacs a Larson, 2006*).

Vzhledem k mnohostrannému zapojení žírných buněk do regulačních mechanismů tělesné imunity je pochopitelné, že neoptimální nastavení tohoto systému může mít dalekosáhlé následky na zdravotní stav jedince, například vyústit ve vážné případy alergické přecitlivělosti a astmatu. I když lze vysledovat vliv genetických faktorů na dispozice k alergickým onemocněním, zdá se, že mnohem zásadnější je vklad nevhodného životního prostředí. Přechod od vesnického způsobu života k městskému přesvědčivě koreluje s nárůstem alergií v geneticky shodné populaci. Ve hře je zřejmě souhra absence expozice přirozeným antigenům vnějšího prostředí v dětství s vystavením působení znečištění (zplodiny nedokonalého spalování, prachové částice vázající rizikové alergeny) a stresu. Přitom se zdá, že samotné znečištění životního prostředí ve městech má na vznik alergické přecitlivělosti menší vliv než vysoká životní úroveň zkoumaných osob. Statisticky významným rizikovým faktorem pro dítě je také například rozvod rodičů, kupodivu

narozdíl od úmrtí v rodině. Alergie jsou také podporovány estrogeny ze znečištěného životního prostředí (*Bateman a Jithoo, 2007; Martinez, 2007; Sozanska a kol., 2007; van Ree a Yazdanbakhsh, 2007; Semic-Jusufagic a kol., 2006; Bockelbrink a kol., 2006; Narita a kol., 2007*).

Anafylaktický šok způsobený náhlou systemickou degranulací mastocytů a bazofilních granulocytů v odpověď na alergeny některých hmyzích a hadích jedů býval přičítán patologickému působení těchto buněk, neboť se jedná o stav mnohdy akutně ohrožující život. Na myším modelu se však podařilo prokázat protektivní roli takto masivně sekretovaných proteáz vůči vlastním účinkům toxinů. Ve svém důsledku tak anafylaktický šok ohrožoval myši méně než sám jed, mohlo by se tedy jednat o specifický obranný mechanismus (*Metz a kol., 2006*). Tato zajímavá hypotéza však zatím nebyla potvrzena na lidském modelu.

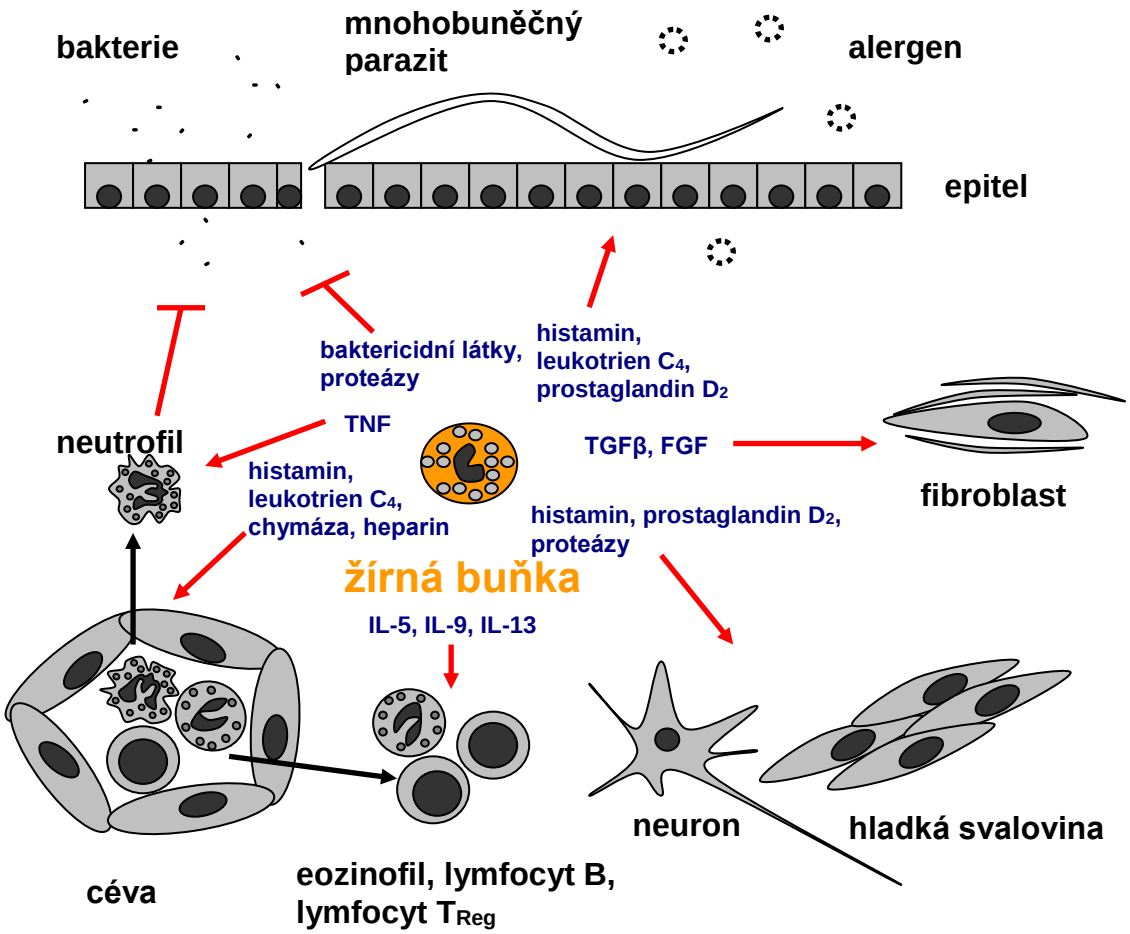

<u>Obr. 3</u>: Interakce žírných buněk při obraně tělních povrchů.
Sekrece baktericidních látek a proteáz, stimulace epitelu, podpora hojení ran, podpora peristaltiky, bronchokonstrikce, vytváření bolestivých podnětů, zvýšení prostupnosti cév a ovlivnění srážlivosti krve, chemotaxe a aktivace bílých krvinek. (Podrobně: *Bischoff, 2007*)

Signalizační kaskády žírných buněk

Dráha receptoru KIT a reakce na cytokiny

KIT je příkladem transmembránového receptoru s tyrozinkinázovou aktivitou v oblasti cytoplazmatické domény. Vyzba cytokinu SCF („faktor kmenových buněk“) z extracelulárního prostředí vede k dimerizaci a vzájemné mnohočetné fosforylaci receptorů KIT. Na fosforylovaná místa mohou nasedat adaptorové proteiny Shc a Grb2, fosfolipáza Cγ, nebo fosfolipidová kináza PI3K. Shc a Grb2 iniciují kaskádu proteinů RAS, RAF a mitogenem aktivovaných kináz, což, společně s působením kinázy PI3K, vede k transkripci genů řídících buněčný růst, diferenciaci, chemotaxi a produkci cytokinů, k čemuž přispívá i aktivace kináz rodiny JAK, které fosforylují proteiny STAT. Tyto proteiny po fosforylaci dimerizují a translokují do jádra, kde působí jako transkripční faktory. Stimulovaný receptor KIT také prostřednictvím tyrozinkináz rodiny Src (zvláště Fyn) řídí reorganizaci cytoskeletu. Signalizace přes receptor KIT má zásadní význam pro růst, vývoj a zrání žírných buněk, současně ale též posiluje jejich efektorové funkce podporou kaskády závislé na imunoglobulinu E (IgE)
(**Obr. 4**) (*Tsai a kol., 1991; O´Farrell a kol., 1996; Gilfillan a Tkaczyk, 2006; Samayawardhena a kol., 2007*).

Receptory interleukinů IL-3 a IL-5 jsou tvořeny heterodimerem specifické vazebné podjednotky α a společné podjednotky β, která po stimulaci receptoru asociuje s tyrozinkinázami rodin Src a JAK a je jimi fosforylována, čímž poskytne vazebná místa pro komponenty následné signalizace, které se rovněž účastní proteiny STAT a probíhá obdobným způsobem, jako v případě receptoru KIT. Podobné mechanismy buňka využívá též pro ostatní cytokiny, s rozdíly v podjednotkové skladbě receptorů, typu následných signalizačních molekul (zejména kináz rodiny JAK a proteinů STAT) i ve výsledném účinku (*Velazquez a kol., 2000; Suzuki a kol., 2000; Ding a kol., 2003; Gilfillan a Tkaczyk, 2006*).

Aktivace zprostředkovaná IgE

Vysokoafinitní receptor imunoglobulinu E, FcεRI, se skládá ze čtyř transmembránových podjednotek. Zatímco podjednotka α je orientována extracelulárním směrem a váže konstantní konce molekul IgE, podjednotka β a dimer podjednotek γ ve svých intracelulárních doménách obsahují fosforylovatelná vazebná místa ITAM („imunoreceptorové tyrozinové aktivační motivy“). Narozdíl od receptoru KIT nemá FcεRI vlastní tyrozinkinázovou aktivitu a je odkázán na asociaci kináz rodiny Src, zejména Lyn a Fyn. Vazebnou specifitu vůči antigenům propůjčuje receptoru teprve IgE, které svým způsobem slouží jako pátá podjednotka receptoru. Navázání tohoto imunoglobulinu na FcεRI však není jen pasivním senzitizačním krokem, ale současně stimulem, který vyvolává sekreci některých cytokinů, zvýšenou životaschopnost buňky a její adhezi k extracelulární matrix, někdy též vede k degranulaci. Mechanismus účinku IgE není dosud uspokojivě

objasněn, ale zdá se, že pro zabránění klasické aktivaci je důležitá role inozitolové fosfatázy SHIP (*Kinet, 1999; Kalesnikoff a kol., 2001; Lam a kol., 2003; Kitaura a kol., 2003; Kawakami a kol., 2005*).

Agregace FcεRI pomocí interakce vázaného IgE a antigenu vede k fosforylaci motivů ITAM v podjednotkách β a γ tyrozinkinázami rodiny Src (Lyn, Fyn). Zřejmě se jedná o spolupůsobení kináz přisedlých k částěčně fosforylovanému receptoru a těch, které s FcεRI asociovaly mechanismem stabilizace lipidových raftů. Fosforylovaná podjednotka β, na kterou se váží kinázy Lyn a Fyn, slouží jako důležitý amplifikátor signálu, ale má též modulační funkci, neboť Lyn při nadměrné stimulaci receptoru působí i jako negativní regulátor. V současné době se ukazuje také význam kinázy Hck a spolupůsobení různých členů rodiny Src v procesu aktivace žírných buněk (*Xiao a kol., 2005; Hong a kol., 2007*). Pro optimální signalizaci je rovněž podstatná souhra tyrozinových kináz s fosfatázami, a tyto děje jsou ovlivňovány reaktivními sloučeninami kyslíku, které se uvolňují v průběhu mnoha imunitních reakcí (*Heneberg a Dráber, 2002; Heneberg a Dráber, 2005*). Fosforylované podjednotky γ receptoru FcεRI mají zásadní důležitost pro další přenos informace. Nasedá na ně cytoplazmatická tyrozinkináza Syk, která vzápětí fosforyluje transmembránové adaptorové proteiny LAT a NTAL nebo cytoplazmatický adaptor SLP76, čímž z nich vytvoří ohniska následných signalizačních kaskád, zahrnujících například aktivaci fosfolipáz Cγ, fosfolipidové kinázy PI3K, proteinkináz C a A, kaskády proteinu Ras a mitogenem aktivovaných kináz aj. (Podrobně: *Gilfillan a Tkaczyk, 2006; Kraft a Kinet, 2007; Simeoni a kol., 2005*). Výsledkem je degranulace, přestavba cytoskeletu, produkce arachidonových metabolitů a transkripce genů (například pro syntézu cytokinů). Jedná se o antigenně-adaptivní odnož mastocytárních efektorových mechanismů.

Aktivace zprostředkovaná Thy-1 a jinými proteiny s GPI kotvou

Glykoprotein Thy-1 (CD90), zakotvený do plazmatické membrány pomocí GPI, představuje důležitý prvek regulace fyzických interakcí rozličných buněčných typů. Jeho přirozeným ligandem (a současně receptorem) jsou některé integriny, ale umělá agregace Thy-1 pomocí specifické protilátky vyvolává u žírných buněk děje podobné aktivaci prostřednictvím FcεRI. Dochází k mobilizaci vápenatých iontů, sekreci mediátorů i k fosforylaci celé řady proteinů, byť s nižší intenzitou než v případě stimulace FcεRI. Zřejmě se jedná o proces, ve kterém zásadní roli hraje stabilizace lipidových raftů sdružujících tyrozinkinázy rodiny Src a palmitylované transmembránové adaptorové proteiny (*Rege a Hagood, 2006; Dráberová a Dráber, 1993; Surviladze a kol., 2001*). Podobný efekt má na žírné buňky též agregace jiného proteinu zakotveného přes GPI, Tec-21. Ukazuje se, že dimerizace některých GPI proteinů (Thy-1, Tec-21, CD48) vede k neapoptotické expozici fosfatidylserinu na buněčném povrchu, zatímco u jiných (karcinoembryonální antigen) tomu tak není. Tyto experimenty jsou ale zatím v počátcích a fyziologická relevance aktivace mastocytů prostřednictvím GPI není dosud objasněna. Přinejmenším v některých

případech se může jednat o důležitý mechanismus, neboť například CD48 je jedním z receptorů, pomocí nichž žírné buňky reagují na kontakt bakterií (*Hálová a kol., 2002; Smrž a kol., 2007; Muñoz a kol., 2003*).

Adhezivní receptory

Exprese specifických sad adhezivních molekul má zásadní důležitost pro uchycení žírných buněk v cílových tkáních v závislosti na procesu diferenciace a maturace. Tyto molekuly rovněž obecně slouží jako receptory, které mastocytům poskytují kostimulační signály pro aktivaci. Jejich expozice na buněčném povrchu je regulována spektrem cytokinů, a dochází k ní též v odpověď na stimulaci kaskád vedoucích k aktivaci efektorových funkcí žírných buněk. Některé adhezivní molekuly se uplatňují při vazbě extracelulární matrix (VLA-4 = integrin $\alpha_4\beta_1$, VLA-5 = integrin $\alpha_5\beta_1$, vitronektinový receptor = integrin $\alpha_v\beta_3$, v kůži též VLA-3 = integrin $\alpha_3\beta_1$), jiné v mezibuněčných kontaktech (ICAM-1, ICAM-2, leukosialin, LFA-1, LFA-3, u nezralých žírných buněk integrin $\alpha_4\beta_7$). Mezi adhezivní molekuly patří i výše uvedený glykoprotein Thy-1 kontaktující integriny, nebo KIT, který může vázat membránovou formu cytokinu SCF. Ukotvení žírné buňky pomocí adhezivních receptorů vyústí v reorganizaci cytoskeletu, fosforylaci některých signalizačních molekul, redistribuci cytoplazmatických sekretorických váčků a přípravu k degranulaci. Těchto dějů se účastní paxilin a kináza fokálních adhezí FAK (*Hamawy a kol., 1994; Smith a Weis, 1996; Okayama, 2000*).

Jiné receptory žírných buněk

Pro roli žírných buněk v neadaptivní imunitě jsou velice důležité receptory rodiny TLR („Toll-like receptors“), které reagují na mikrobiální a virové komponenty, jako jsou lipopeptidy (rozpoznávané TLR1), peptidoglykan (TLR2, TLR6), dvouřetězcová RNA (TLR3), lipopolysacharidy a F-protein respiratorního syncitiálního viru (TLR4). Heterodimerizace receptorů TLR1 a TLR6 s TLR2 poskytuje buňce rozšíření reakčních možností. V lidských mastocytech byl popsán také TLR7, který rozpoznává jednořetězcovou virovou RNA, a TLR9, odpovídající na bakteriální DNA. Agregace receptorů TLR ligandem je spojena s procesem stabilizace lipidových raftů. Cytokinové prostředí může změnit expresi jednotlivých receptorů TLR a naopak stimulace TLR vyvolává sekreci specifických cytokinů, které směřují k obraně těla vůči mikroorganismům nebo virům, nejedná se však o degranulaci. Podobnou reakci vyvolá kontakt patogena obaleného složkami komplementové kaskády (C3b, C4b) s příslušnými receptory komplementu nebo agregace molekul IgG vázaných na receptory Fcγ, v těchto případech však dochází též k degranulaci a uvolnění proteáz a histaminu (*Marshal, 2004; Dolganiuc a kol., 2006*).

Neurotransmitery, chemokiny a chemotaktické fragmenty komplementu žírná buňka rozpoznává pomocí receptorů z rodiny heterotrimerických G-proteinů. Stejný systém využívá i na detekci adenozinu a sfingozin 1-fosfátu. Vazba ligandu vede

k disociaci podjednotky G_{α} od receptorového komplegu $G_{\beta\gamma}$. Tato podjednotka poté prostřednictvím fosfolipázy Cβ stimuluje kaskády vedoucí k sekreci některých cytokinů a podporující (nebo též vyvolávající) degranulaci. Exprese chemokinových receptorů se mění v závislosti na stupni maturace mastocytu a naopak jejich ligandy vývoj žírných buněk ovlivňují (*Forsythe a Befus, 2003; Marshal, 2004; Gilfillan a Tkaczyk, 2006*).

Žírné buňky (na rozdíl od bazofilů) exprimují nejen výše uvedený vysokoafinitní (FcεRI), ale také homotrimerický nízkoafinitní receptor pro IgE (FcεRII, CD23), jehož role je však u nich dosud nejasná. Studie na jiných buněčných typech naznačují, že by se mohl účastnit například prezentace antigenu, není to ale zatím víc než jen domněnka (*MacGlashan a kol., 1999; Montagnac a kol., 2005; Getahun a kol., 2005*). Mastocyty také mohou vázat IgG, a to pomocí různých receptorů Fcγ, jejichž zastoupení závisí na buněčném typu a daném organismu. Nízkoafinitní receptory FcγRIIIA, FcγRIIA, FcγRIIB a FcγRIIC pro účinnou vazbu potřebují agregaci ligandu, exprese vysokoafinitního receptoru FcγRI je v lidských žírných buňkách indukovatelná, v myších popsán nebyl. Některé z receptorů Fcγ (FcγRIIA, FcγRIIC, FcγRI, FcγRIII) díky aktivačním motivům ITAM, přítomným v cytoplazmatických doménách svých podjednotek, signalizaci stimulují podobným způsobem, jako FcεRI, oproti tomu FcγRIIB díky inhibičním motivům ITIM váže inozitolovou fosfatázu SHIP a signalizaci tlumí. Tato supresivní funkce FcγRIIB ale závisí na spolupráci aktivačních receptorů (*Malbec a Daëron, 2007; Bruhns a kol., 2005*). Receptor imunoglobulinu A, FcαRI, může žírné buňce poskytnout tlumivé signály, i když obsahuje aktivační motiv ITAM. Zřejmě se tak děje vazbou fosfatázy SHP1. U řady inhibičních receptorů (PIRB, MAFA, LIR1, MAIR1, LMIR1 aj.) mechanismus účinku nebo fyziologická role dosud vyjasněny nejsou (*Kraft a Kinet, 2007*).

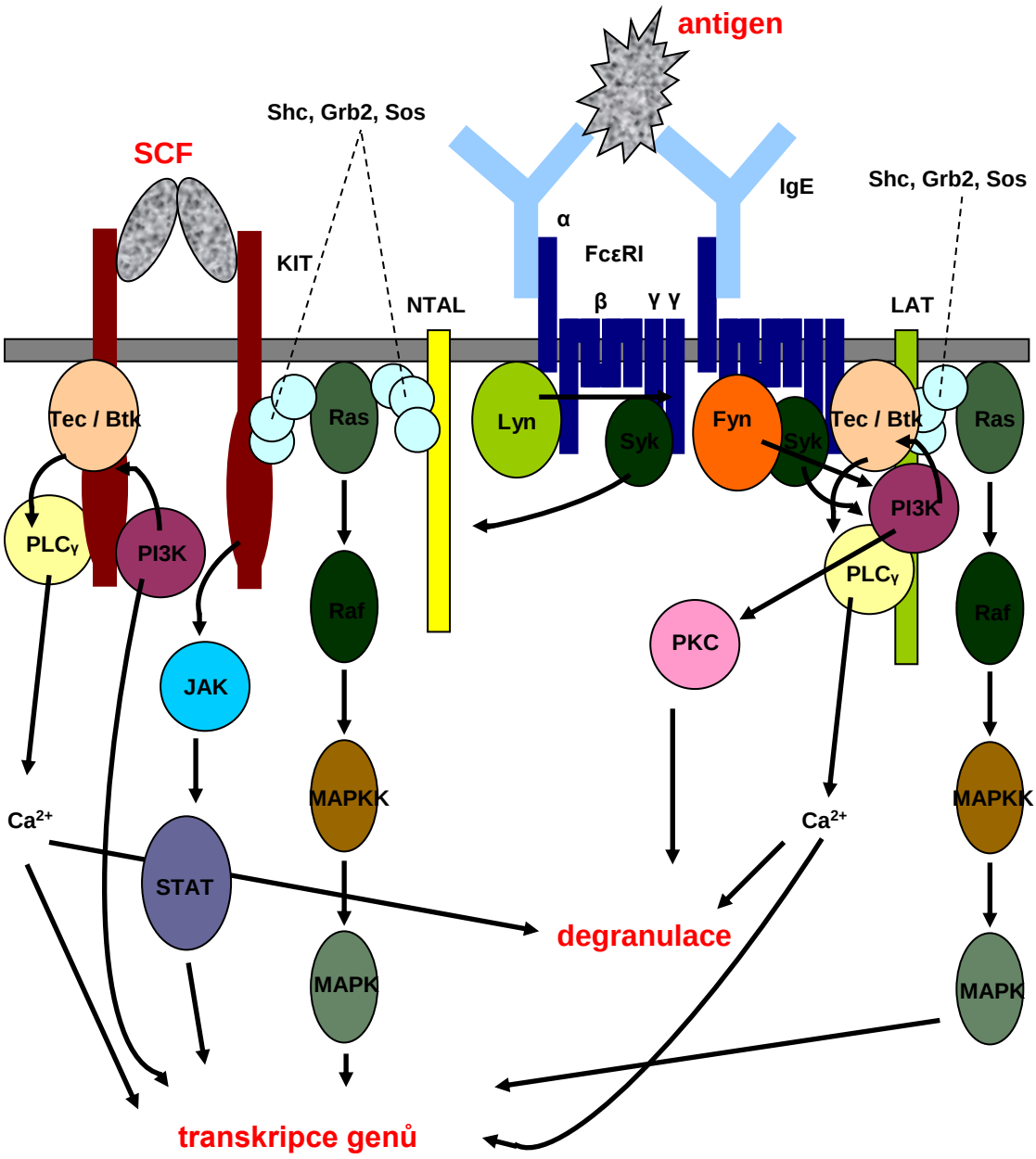

<u>Obr. 4:</u> Zjednodušený model souhry aktivace žírných buněk drahami receptorů KIT a FcεRI.

Fosforylace agregovaných receptorů FcεRI (tyrozinkinázou Lyn nebo Fyn) a KIT (autofosforylace) vede k vytvoření signalizačních ohnisek iniciujících specifickou transkripci genů. Na rozdíl od kaskády receptoru FcεRI, kaskáda vedoucí od KIT neposkytuje dobré podmínky pro degranulaci, avšak podporuje ji.
(*Gilfillan a Tkaczyk, 2006; Kraft a Kinet, 2007*)

Cíle

Záměrem této práce bylo ***přispět k upřesnění představy o funkční organizaci plazmatické membrány leukocytů s užitím topografických přístupů na modelu žírných buněk***, což současně znamenalo obohacení znalostí o samotných žírných buňkách a prohloubení metodického aparátu. Soustředil jsem se na řešení těchto dílčích otázek:

- ***Jak izolovat listy plazmatické membrány z neadherentních žírných buněk BMMC?***

Zavedenou metodu izolace (a značení) membránových listů z adherentních buněk (*Sanan a Anderson, 1991*) lze dobře aplikovat na leukemickou linii žírných buněk RBL, ale ne na netransformované neadherentní žírné buňky BMMC. Vzhledem k tomu, že topografie signalizačních molekul na membránových listech netransformovaných mastocytů nebyla známa, bylo vhodné vyvinout metodu izolace těchto listů z neadherentních buněk.
(Řešeno v článku E.)

- ***Jaká je povaha signalizačních ohnisek agregovaného receptoru FcεRI?***

Na buňkách RBL byl popsán model signalizace žírných buněk zahrnující tvorbu rozsáhlých (přibližně 200 nm) domén receptoru FcεRI (*Wilson a kol., 2002*). Otázkou však zůstávalo, zda je tvorba těchto domén jednou z podmínek dostatečné aktivace žírných buněk, nebo spíše jevem druhotným. Odpověď mohla přinést analýza buněk aktivovaných dimerizací FcεRI, nebo jiného typu mastocytů.
(Řešeno v článcích A, E.)

- ***Jak je na plazmatické membráně distribuován adaptorový protein NTAL a jaký je jeho topografický vztah k adaptoru LAT, receptoru FcεRI a glykoproteinu Thy-1?***

Analýza vzájemné topografie adaptorových proteinů LAT a NTAL, které patří spolu s Thy-1 mezi typické markery lipidových raftů, a porovnání jejich lokalizace vůči agregovanému FcεRI a Thy-1, mohla mnohé vypovídat nejen o přenosu signálu mezi receptory žírných buněk a adaptorovými proteiny, ale i o povaze systému lipidových raftů v plazmatické membráně.
(Řešeno v článcích B, C, E.)

- ***Nevede změna exprese proteinu NTAL k tvorbě atypických struktur v plazmatické membráně?***

Výsledky spoluautorů ukázaly, že NTAL působí jako negativní regulátor aktivace žírných buněk. Bylo tedy vhodné vědět, zda se nadměrná nebo snížená exprese

tohoto proteinu neprojeví v plazmatické membráně netypickou lokalizací signalizačních molekul.
(Řešeno v článku D.)

- ***Jaká je povaha domén glykoproteinu Thy-1?***

Rozličná data naznačovala značnou nezávislost markerů lipidových raftů v plazmatické membráně a hovořila proti představě těchto domén jako spontánních koagregátů více druhů signalizačních molekul. Vzájemná lokalizace dvou strukturně vysoce podobných izoforem proteinu Thy-1 (Thy-1.1 a Thy-1.2) mohla naznačit, jakým způsobem jsou v plazmatické membráně organizovány domény Thy-1.
(Řešeno v článku C.)

Metody

Stěžejním přístupem k dosažení vytyčených cílů se stala analýza topografie signalizačních molekul na izolovaných listech plazmatické membrány pomocí transmisní elektronové mikroskopie. Tomu předcházely předběžné experimenty (nepublikováno) zahrnující purifikaci protilátek, ověření jejich specifity a reaktivity v závislosti na použitém fixativu a první přiblížení topografickým změnám na plazmatické membráně při aktivaci žírných buněk za rozlišení fluorescenční mikroskopie. Na tomto místě uvádím jen stručný přehled těch přístupů, které jsem používal sám. Pro detailní informace o jednotlivých technikách odkazuji čtenáře na metodické oddíly přiložených článků.

- Kultivace žírných buněk
  (Kultivována krysí leukemická linie RBL-2H3 a žírné buňky BMMC odvozené z kostní dřeně.)

- Měření úrovně degranulace žírných buněk
  (Detekce sekretované β-glukuronidázy.)

- Purifikace protilátek; příprava buněčných lyzátů; immunoblotting; fluorescenční mikroskopie
  (Králičí polyklonální protilátka anti-NTAL izolována imunoafinitně na rekombinantním proteinu NTAL.)

- Příprava a značení izolovaných listů plazmatické membrány; elektronová mikroskopie; digitalizace dat; statistické vyhodnocení
  (Souřadnice imunoznaček převedeny do digitální formy pomocí programu Ellipse [ViDiTo; Košice, SR] a statisticky zpracovány programem GOLD nebo algoritmy skupiny Bridget Wilson z University of New Mexico s využitím systému MATLAB [MathWorks; Natick, USA].)

Výsledky

Shrnuty v následujících článcích:

(A) Signaling assemblies formed in mast cells activated via Fcε receptor I dimers.
Eur. J. Immunol. 2004, 34: 2209-2219.

(B) Negative regulation of mast cell signaling and function by the adaptor LAB/NTAL.
J. Exp. Med., 2004, 200: 1001-1013.

(C) Topography of plasma membrane microdomains and its consequences for mast cell signaling.
Eur. J. Immunol, 2006, 36: 2795-2806.

(D) Regulation of Ca^{2+} signaling in mast cells by tyrosine-phosphorylated and unphosphorylated non-T cell activation linker, NTAL.
Journal of Immunology, odesláno (květen 2007).

(E) Topography of signaling molecules as detected by electron microscopy on plasma membrane sheets isolated from nonadherent mast cells.
Journal of Immunological Methods, odesláno (červen 2007).

Tyto práce cituji pod názvem „článek A, B, C, D, E“. Pokud nebude uvedeno jinak, týkají se výsledky zmiňované v oddílech Diskuse a Závěry autora dizertace.

(A)

Signaling assemblies formed in mast cells activated via Fcε receptor I dimers.

*Eur. J. Immunol. 2004, 34: 2209-2219***.**

Signaling assemblies formed in mast cells activated via Fcε receptor I dimers

Lubica Dráberová, Pavel Lebduška, Ivana Hálová, Pavel Tolar, Jitka Štokrová, Helena Tolarová, Jan Korb and Petr Dráber

Department of Signal Transduction, Institute of Molecular Genetics, Academy of Sciences of the Czech Republic, Prague, Czech Republic

Although aggregation of the Fcε receptor I (FcεRI) is necessary for Ag-mediated mast cell triggering, the relationship between the extent of the FcεRI aggregation and subsequent biochemical and topographical events is incompletely understood. In this study, we analyzed the activation events induced by FcεRI dimers, elicited by binding of anti-FcεRI mAb to rat basophilic leukemia cells. We found that, in contrast to extensively aggregated FcεRI, receptor dimers (1) induced a less extensive association of FcεRI with detergent-resistant membranes, (2) delayed the tyrosine phosphorylation and membrane recruitment of several signaling molecules, (3) triggered a slower but more sustained increase in concentration of free cytoplasmic calcium, (4) induced degranulation which was not inhibited at higher concentrations of the cross-linking mAb, and (5) failed to produce clusters of FcεRI, Syk kinase and Grb2 adapter in osmiophilic membranes, as detected by immunogold electron microscopy on membrane sheets. Despite striking differences in the topography of FcεRI dimers and multimers, biochemical differences were less pronounced. The combined data suggest that FcεRI-activated mast cells propagate signals from small signaling domains formed around dimerized/oligomerized FcεRI; formation of large FcεRI aggregates in osmiophilic membranes seems to promote both strong receptor triggering and rapid termination of the signaling responses.

Received	10/12/03
Revised	26/4/04
Accepted	13/5/04

Key words: Mast cell / IgE receptor / Protein kinase / Receptor topography

1 Introduction

The aggregation of Fcε receptor I (FcεRI) on mast cells and basophils by multivalent Ag initiates a signaling cascade that results in degranulation. The first recognized biochemical event of the cytoplasmic signal transduction cascade is tyrosine phosphorylation of FcεRI β and γ subunits by Lyn kinase. Phosphorylation of the FcεRI γ subunits allows the protein tyrosine kinase Syk to associate with the receptor via its two Src homology (SH)2 domains. This recruitment and consequent activation of Syk leads to further downstream signaling, including tyrosine phosphorylation of LAT, Gab2 and Grb2 adapters. These proteins contribute to the formation of multicomponent signaling complexes on the plasma membrane containing phospholipase C (PLC)γ, phosphatidyinositol 3-kinase (PI3K), phosphatase SHP-2, and others (reviewed in [1, 2]).

We have previously found that Lyn in rat basophilic leukemia (RBL) cells is associated with detergent-resistant membranes (DRM) containing also the glycosylphosphatidylinositol-anchored proteins Thy-1 and TEC-21 [3, 4]. Further analysis indicated that FcεRI was only weakly associated with DRM in resting cells and that this association increased upon FcεRI aggregation [5]. Confocal microscopy with green fluorescence-labeled cytoplasmic probes proved that aggregated FcεRI colocalized with Lyn and Syk [6, 7]. Although the presence of an SH2 domain was not important for localization of Lyn in DRM, only SH2-containing Lyn constructs colocalized with aggregated FcεRI, pointing to an important role of SH2-mediated interactions in this process [6]. Surprisingly, EM showed that Lyn and Syk in activated cells appeared in topographically distinct membrane microdomains. In resting cells, FcεRI was distributed to dispersed small aggregates that often were loosely colocal-

[DOI 10.1002/eji.200322663]

Abbreviations: **$[Ca^{2+}]_i$:** Concentration of free cytoplasmic Ca^{2+} **DRM:** Detergent-resistant membranes **F-actin:** Filamentous actin **FcεRI:** Fcε receptor I **HRP:** Horseradish peroxidase **MBCD:** Methyl-β-cyclodextrin **PCF:** Pair correlation function **PCCF:** Pair cross-correlation function **PLC:** Phospholipase C **PI3K:** Phosphatidyinositol 3-kinase **PIP3:** Phosphatidylinositol 3,4,5-trisphosphate **RBL:** Rat basophilic leukemia **SH:** Src homology

ized with small Lyn aggregates. After aggregation, FcεRI redistributed to membrane microdomains that stained more intensely with osmium than the bulk membrane. Because these osmiophilic membranes accumulated several other signaling molecules, including Syk, PLCγ2, PI3K, Gab2 and Grb2, Wilson et al. suggested that they represent the primary signaling domains that function as sites of signaling from cross-linked FcεRI to downstream responses [2, 8]. This hypothesis was supported by data indicating that FcεRI dimers that did not localize in osmiophilic patches were capable of inducing tyrosine phosphorylation of FcεRI subunits, but not Syk activation and other more distant signaling events [9]. Interestingly, full activation response could be restored after induced aggregation of the FcεRI dimers. This process correlated with the redistribution of FcεRI aggregates into osmiophilic regions of the plasma membrane.

Although FcεRI aggregation is necessary for FcεRI-mediated mast cell triggering [10, 11], the relationship between the extent of aggregation and subsequent biochemical and topographical events is incompletely understood. In this study, we analyzed the early activation events in RBL cells triggered by FcεRI dimers formed after binding of anti-FcεRI mAb and compared them with those induced by FcεRI multimers produced by aggregation of FcεRI-IgE complexes by means of multivalent Ag or anti-IgE Ab.

2 Results

2.1 Differences in degranulation, calcium response and DRM recruitment between cells activated via FcεRI dimers and multimers

Using divalent anti-FcεRI mAb, it has been shown that the minimal unit capable of inducing FcεRI-coupled responses was the FcεRI dimer [11]. As these mAb reportedly failed to induce any detectable FcεRI aggregation [12], we first tested their capability to induce the association of FcεRI with DRM and correlated these changes with degranulation and calcium responses. We used two mAb, clones 5.14 and H10, which differ in their efficacy for cell activation (Fig. 1A, B). Both mAb induced degranulation at a relatively low concentration (0.02 μg/ml), which reached a maximum using 1 μg/ml and remained high at up to 10 μg/ml (not shown). At low concentrations, the H10 mAb was more potent than the 5.14 mAb. Both mAb also induced a dose-dependent increase in concentration of free cytoplasmic Ca^{2+} ($[Ca^{2+}]_i$), and again clone H10 was superior to clone 5.14 (Fig. 1C, D).

To test how the extent of aggregation of FcεRI correlates with association of the receptors with DRM, cells were exposed to ^{125}I-labeled 5.14 or H10 mAb for 5 min and solubilized in ice-cold 0.06% Triton X-100; this solubilization procedure preserves the association of aggregated FcεRI with DRM [5, 6]. In control cells exposed to ^{125}I-IgE instead of anti-FcεRI Ab, most of the ^{125}I-IgE-FcεRI complexes (94±8%; mean ± SD, n=4) were found in the high-density fractions of the sucrose gradient (fractions 11–22), and only a small portion (5.8±2.2%) was found in the low-density fractions (fractions 1–10; Fig. 1E, F). When the receptors were dimerized with anti-FcεRI Ab, a significant portion moved into the low-density fractions. Interestingly, association of FcεRI dimers with these fractions was induced by relatively low mAb concentrations and exhibited a broad density profile on the sucrose gradient. Two peaks were observed at 0.05 μg/ml, one in fractions 4 and 5 and the other one in fraction 9. A 20-fold increase in mAb concentration slightly enhanced recruitment of dimerized FcεRI into DRM, and the peak in fraction 9 became dominant. Only a small portion of dimerized receptors was found in the high-density fractions (fractions 23–25).

For comparison, we also examined the properties of cells with extensively aggregated FcεRI after exposure of FcεRI-IgE complexes to anti-IgE Ab or Ag. Data presented in Fig. 2A indicate that the secretion of β-glucuronidase increases with rising concentration of anti-IgE Ab up to a maximum observed at 1 μg/ml. At 5 and 10 μg/ml anti-IgE Ab, the secretory response was inhibited by ~20% and ~45%, respectively, compared to the maximum. In contrast, the calcium response reached its top increase in cells activated with the highest concentration of anti-IgE Ab tested (10 μg/ml). The rapid increase in $[Ca^{2+}]_i$ was followed by its fast decline. Lower concentrations of anti-IgE Ab led to a slower onset, but also a longer-lasting Ca^{2+} response (Fig. 2B). Sucrose density gradient profiles are shown in Fig. 2C. When ^{125}I-IgE-FcεRI complexes were aggregated with 0.1 μg/ml anti-IgE Ab, 17.3±1.8% (n=3) of total FcεRI was associated with DRM. A further increase in anti-IgE Ab concentration resulted in more FcεRI being associated with DRM (30.1±2.8% at 1 μg/ml, 58.4±1.5% at 5 μg/ml and 63.8±2.2% at 10 μg/ml). Extensive aggregation of FcεRI-IgE complexes induced their higher recruitment not only into DRM, but also into the high-density fractions (fractions 23–25). Such high-density complexes were also observed in cells solubilized with 0.5% Triton X-100, *i.e.* after treatment that prevented the association of aggregated FcεRI with DRM (not shown), suggesting that they represent complexes of FcεRI with the cytoskeleton [5, 10]. Pretreatment of the IgE-sensitized cells for 40 min with 10 mM methyl-β-cyclodextrin (MBCD) before adding anti-IgE Ab or anti-FcεRI mAb

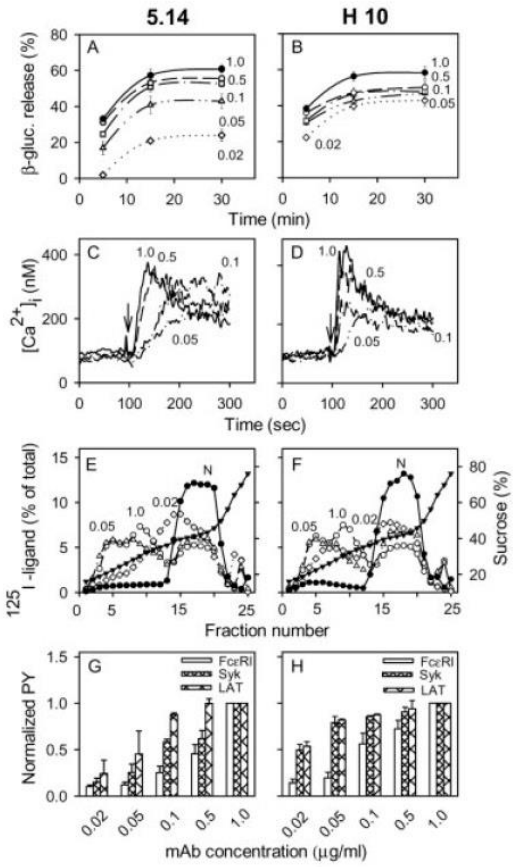

◀ *Fig. 1.* Early activation events induced by anti-FcεRI mAb, 5.14 or H10. (A, B) Secretory response. RBL cells were activated with varying concentrations (0.02–1.0 μg/ml) of mAb, and β-glucuronidase released into the supernatant was determined after various time intervals. Means ± SD of three independent experiments performed in duplicates or triplicates are shown. (C, D) Calcium response. Cells were labeled with FURA-2/AM, transferred into a cuvette kept at 37°C in a luminescence spectrometer and activated by adding mAb at rising concentrations (arrow). $[Ca^{2+}]_i$ was determined as described in Sect. 4. A typical experiment from three performed is shown. (E, F) Recruitment of FcεRI dimers into DRM. Cells were stimulated with ^{125}I-labeled 5.14 or H10 mAb at concentrations of 0.02 μg/ml (empty diamonds), 0.05 μg/ml (empty triangles) or 1.0 μg/ml (empty circles). Cells exposed to ^{125}I-IgE (N, filled circles) served as negative control. After 5 min at 37°C, cells were lysed in ice-cold lysis buffer containing 0.06% Triton X-100. Total cell lysates were loaded into the 40% sucrose fraction of a sucrose step gradient and fractionated by ultracentrifugation. Points show the percentage of total dpm in individual fractions (left axis). Sucrose concentrations in individual fractions are also indicated (filled triangles; right axis). One typical experiment from three to four performed is shown. (G, H) Tyrosine phosphorylation of FcεRI, Syk and LAT. Cells were stimulated with various concentrations of mAb and after 5 min lysed in the appropriate lysis buffer (see Sect. 4). FcεRI, Syk or LAT were immunoprecipitated and analyzed by immunoblotting with PY-20-HRP conjugates and protein-specific Ab, followed by densitometry. Densitometry data were normalized for each component analyzed by dividing the absorbance at a given mAb concentration by the absorbance of the sample showing the maximum in the given experiment; the amount of individual proteins immunoprecipitated was also taken into account. Means ± SD of three to four experiments are shown.

resulted, in accordance with previous results [13], in complete inhibition of the induced association of aggregated FcεRI with DRM (not shown). These data suggest that the formation of complexes of aggregated FcεRI with DRM is dependent on cholesterol.

2.2 Tyrosine phosphorylation of FcεRI, Syk and LAT

In further experiments, we examined whether there are any biochemical differences between cells activated via dimerized or extensively aggregated FcεRI. Data presented in Fig. 1G and H indicate that the two anti-FcεRI mAb induced a concentration-dependent increase in phosphorylation of the FcεRI β and γ subunits, Syk, and LAT; at low mAb concentrations, the H10 mAb was again superior. In cells stimulated with anti-IgE Ab at supraoptimal doses (5 and 10 μg/ml), phosphorylation of Syk, LAT and the FcεRI subunits was higher than in cells stimulated with doses optimal for degranulation (1 μg/ml; Fig. 2D).

2.3 Formation of signaling assemblies

In previous publications, we described a simple method for estimation of the formation of signaling assemblies in the course of FcεRI-mediated activation [14, 15]. This method is based on permeabilization of cells with the cholesterol-sequestering reagent saponin, followed by removal of free cytoplasmic components by washing, complete solubilization of membrane components including DRM by means of Triton X-100, and isolation of selected signaling molecules by immunoprecipitation. Using this method, which accentuates changes in subcellular localization of signaling molecules, we first examined in more detail the reported changes in Gab2

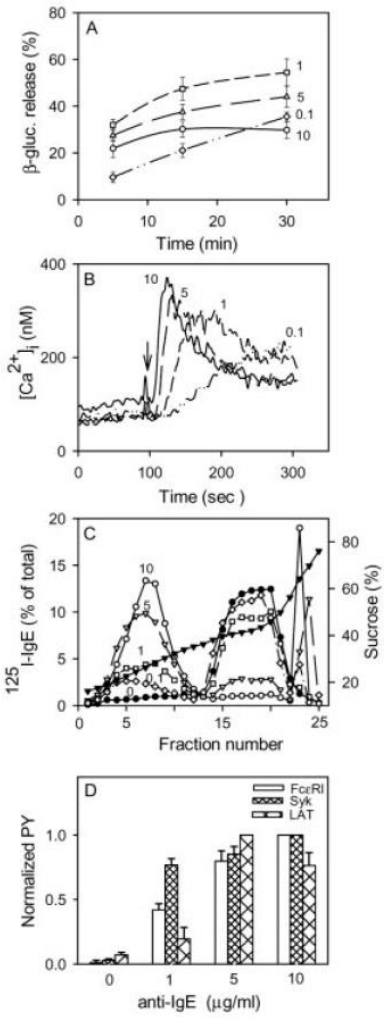

◀ *Fig. 2.* Early activation events induced in IgE-sensitized cells by anti-IgE. (A) Secretory response. Cells were sensitized with IgE (1 μg/ml), activated by exposure to anti-IgE Ab at concentrations of 0.1, 1, 5, or 10 μg/ml, and β-glucuronidase amounts were determined (for details see Fig. 1). (B) Calcium response. Cells were sensitized with IgE, loaded with FURA-2/AM, activated by adding anti-IgE Ab at various concentrations (arrow), and $[Ca^{2+}]_i$ was determined. (C) Recruitment of aggregated FcεRI in DRM. Cells were incubated for 30 min at 37°C with ^{125}I-labeled IgE (1 μg/ml). Unbound IgE was washed out and the cells were exposed to anti-IgE Ab at concentrations of 0.1 μg/ml (empty diamonds), 1 μg/ml (empty squares), 5 μg/ml (empty triangles) or 10 μg/ml (empty circles) or medium alone (filled circles). After 5 min at 37°C, the cells were lysed and analyzed by sucrose density gradient centrifugation. (D) Tyrosine phosphorylation of FcεRI, Syk and LAT. IgE-sensitized cells were stimulated with various concentrations of anti-IgE Ab, then lysed and analyzed for tyrosine phosphorylation as described in Fig. 1G and H.

adapter distribution, which in FcεRI-activated cells translocated from the cytosol to the plasma membrane [16]. Immunoblotting analyses showed a rapid association of Gab2 with macromolecular complexes in 5.14 mAb-activated cells (Fig. 3). Compared to cells activated with anti-IgE Ab, this association was lower at 0.5 min (1.6-fold versus 6.4-fold increase), but analogous at later time points. Gab2 immunoprecipitates comprised numerous tyrosine-phosphorylated proteins, as detected by immunoblotting with PY-20 mAb. At the earliest time point (0.5 min), more tyrosine-phosphorylated proteins were observed in anti-IgE Ab-activated cells than in 5.14 mAb-triggered cells. However, this situation was reversed later (2 and 5 min). One of the proteins in Gab2 precipitates was the SHP-2 phosphatase, and its amount in 5.14-activated cells was again lower only shortly after activation (0.5 min).

These studies were extended to another adapter protein, Grb2, which binds via its SH2 and SH3 domains to numerous signaling molecules including LAT adapter and PI3K [17] and undergoes significant changes in topography after FcεRI triggering [2]. Immunoblotting indicated that the amount of Grb2 bound to saponin-permeabilized cellular ghosts was increased during FcεRI-mediated signaling (Fig. 4). Grb2 immunoprecipitates harbored a number of tyrosine-phosphorylated proteins, including LAT and PI3K, and in most cases, this association was more pronounced in 5.14 mAb- than in anti-IgE Ab-stimulated cells, especially after longer time intervals.

Dramatic changes in the distribution of signaling molecules induced by FcεRI dimers were reflected in functional assays assessing the activity of PI3K (Fig. 5). In the course of 5.14 mAb-induced activation, the amount of PI3K immunoprecipitated from permeabilized cells increased (2.0-fold at 5 min). The changes were accompanied by a dramatic rise in PI3K enzymatic activity (9.8-fold at 5 min). A significant increase in PI3K activity was also observed in Gab2 and Grb2 immunoprecipitates. At the earliest time point (0.5 min), the PI3K activity in PI3K and Gab2 immunocomplexes was lower in cells activated via FcεRI dimers than via multimers. However, these differences almost disappeared later, and higher PI3K activity in Gab2 immunoprecipitates was reproducibly observed in 5.14 mAb-activated cells.

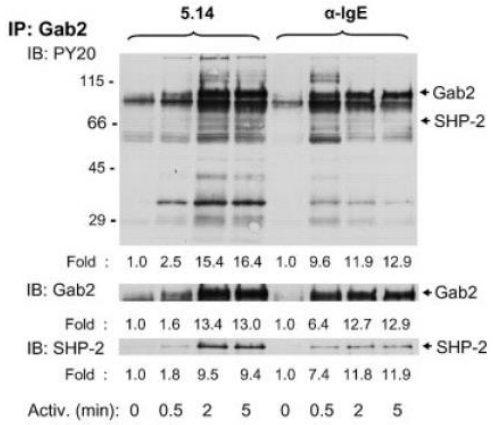

Fig. 3. Tyrosine phosphorylation and cytoplasmic localization of Gab2 and associated proteins. Cells were activated through FcεRI dimers (5.14) or multimers (α-IgE), using the Ab at 1 μg/ml concentration. At the indicated time intervals, the cells were spun down, resuspended in permeabilization buffer containing 0.1% saponin, washed, and cellular ghosts were extracted with lysis buffer containing 1% Triton X-100. Gab2 immunoprecipitates were analyzed by immunoblotting with PY-20-HRP, anti-Gab2 and anti-SHP-2 Ab. Relative amounts of Gab2 and SHP-2 and Gab2 tyrosine phosphorylation were determined by densitometry and normalized to non-activated cells. Arrows on the right and numbers on the left indicate the positions of the corresponding proteins and molecular weight standards, respectively. A typical result from four experiments performed is shown.

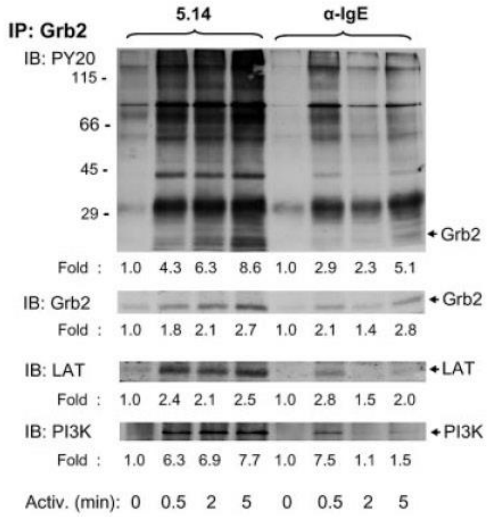

Fig. 4. Tyrosine phosphorylation and cytoplasmic localization of Grb2 and associated proteins. Cells were activated and solubilized with saponin/Triton X-100 as described in Fig. 3. Grb2 was immunoprecipitated and analyzed by immunoblotting with PY-20-HRP, anti-Grb2, anti-LAT and anti-PI3K p85 subunit Ab. Relative amounts of the proteins and Grb2 tyrosine phosphorylation were determined by densitometry of the corresponding immunoblots and normalized to non-activated cells. A typical result from three experiments performed is shown.

The increased activity of PI3K in 5.14 mAb-stimulated cells was confirmed by an analysis of phosphatidylinositol 3,4,5-trisphosphate (PIP3), an *in vivo* PI3K metabolite. Enhanced levels of PIP3 were observed after both time intervals used (2 and 5 min) and were only slightly lower in cells activated via FcεRI dimers than via multimers (Fig. 6A, B). Higher activity of PI3K was also reflected in an enhanced translocation of Akt kinase into signaling assemblies and especially in an increased Akt tyrosine phosphorylation (Fig. 6C). Interestingly, any of the two criteria showed FcεRI dimers as more potent than multimers, especially after longer time intervals.

2.4 Actin polymerization

Actin microfilaments seem to regulate the interaction between aggregated FcεRI and signal transduction molecules [18]. To quantify the levels of filamentous actin (F-actin) we measured the binding of FITC-labeled phalloidin to permeabilized cells by FCM. An exposure of RBL cells to the 5.14 mAb at a concentration of 0.1 μg/ml caused a rapid increase in the level of F-actin, which peaked at 5 min after cell triggering and then slowly declined (Fig. 7A). Higher concentration of 5.14 mAb (1 μg/ml) induced a swifter increase in the amount of F-actin, which remained enhanced at all time intervals. Extensive aggregation of FcεRI in IgE-sensitized cells achieved by adding anti-IgE Ab (1 μg/ml) induced a more rapid and extensive increase in F-actin (Fig. 7B). An increase of the anti-IgE Ab dose to 10 μg/ml caused a still quicker rise in actin polymerization peaking at 3 min, but also its rapid decline.

2.5 Electron microscopy

To throw more light on the topography of signaling molecules in cells activated through FcεRI dimers, we isolated membrane sheets from both resting and activated cells and determined the distribution of the FcεRI β subunits, Grb2 and Syk by immunogold EM. We could confirm previous data [2, 8] that FcεRI β subunits in resting cells are found homogeneously distributed as singlets and small dispersed clusters mostly containing two to five gold particles. In 5.14 mAb-activated cells, the FcεRI β subunits remained homogeneously distributed, occa-

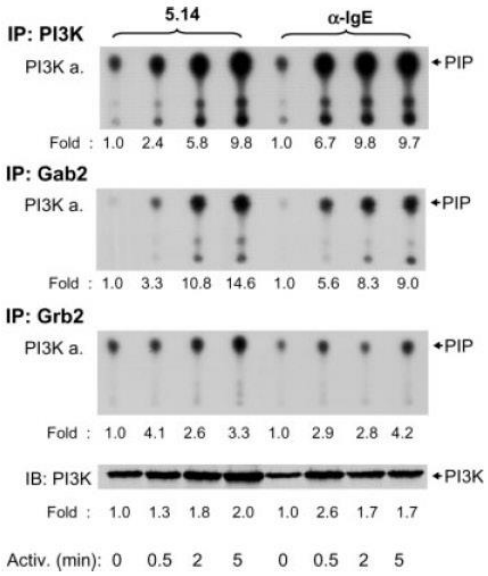

Fig. 5. PI3K enzymatic activity. Cells were activated as described in Fig. 3. PI3K, Gab2 and Grb2 were immunoprecipitated and subjected to PI3K assay. [^{32}P]Phosphatidylinositol phosphate (PIP) was quantified as described in Sect. 4 and normalized to unstimulated cells. The relative amount of PI3K in the post-nuclear supernatant was determined by immunoblotting with anti-p85 PI3K Ab and densitometry and normalized to unstimulated cells. Arrows indicate the positions of PIP and PI3K. Representative experiments from at least three performed in each group are shown.

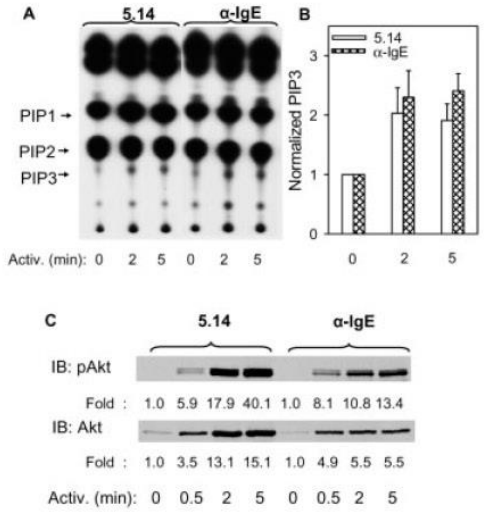

Fig. 6. PIP3 levels and properties of Akt. (A) PIP3 levels were determined in [^{32}P]orthophosphate-labeled cells before (0 min) or following stimulation with 5.14 mAb or anti-IgE Ab. The TLC separation pattern was estimated using phosphoinositide standards, phosphatidylinositol monophosphate (PIP1), phosphatidylinositol 4,5-bisphosphate (PIP2) and PIP3. A representative TLC from three performed is shown. (B) Quantitative measurements of PIP3 levels normalized to nonstimulated control cells (means ± SD, n=3). (C) Cells were activated and solubilized with saponin/Triton X-100. Post-nuclear supernatants were analyzed by immunoblotting with anti-phospho-Akt (pAkt) and anti-Akt, followed by densitometry analysis as described in Fig. 3. A typical result from two experiments is shown.

sionally associated with Syk (Fig. 8A). In contrast, Ag-mediated aggregation of FcεRI resulted in an accumulation of FcεRI β subunits in osmiophilic regions of the plasma membrane together with Syk (Fig. 8B; see also [8, 19]). A similar picture was obtained when the topography of Grb2 marked with gold particles was analyzed. Grb2 gold particles were relatively sparse on membrane sheets from untreated and IgE-sensitized cells (Fig. 9A, C), whereas in 5.14 mAb-activated cells, the amount of particles increased (see below), although they did not associate with osmiophilic regions of the plasma membrane (Fig. 9B). FcεRI multimers led to an accumulation of Grb2 in osmiophilic regions, together with FcεRI β subunits (Fig. 9D). Counting the gold particles specific for Grb2 indicated that resting cells contained 6.8±0.9 (mean ± SD, n=8) gold particles per 1 μm^2 of plasma membrane. Similar counts were obtained in IgE-sensitized cells (6.9±1.1). In cells activated for 2 min with the 5.14 mAb or a multivalent Ag, the total number of Grb2-marking particles increased to 9.9±0.2 and 14.3±3.4, respectively. Quantitative analysis of particle

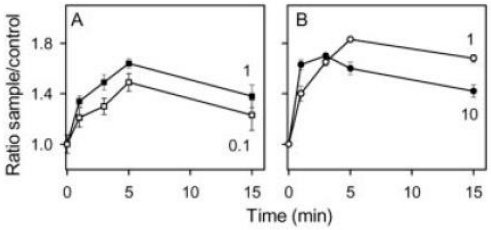

Fig. 7. FcεRI-mediated actin polymerization. FcεRI were dimerized by 5.14 mAb (0.1 or 1 μg/ml; A), or extensively aggregated by adding anti-IgE Ab (1 or 10 μg/ml) to IgE-sensitized cells (B). After various time intervals, the levels of F-actin were quantified by FCM and expressed relative to the level in non-activated cells. Means ± SD of three determinations are shown.

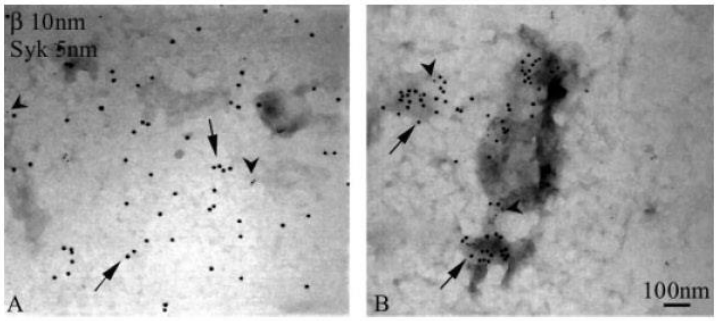

Fig. 8. Membrane topography of FcεRI **β** subunits and Syk in activated cells. Nonsensitized (A) or IgE-sensitized (B) cells were activated by exposure to 5.14 mAb (1 μg/ml) or DNP-BSA (1 μg/ml), respectively. Membrane sheets prepared from these cells were double-labeled from the inside for FcεRI **β** subunits (10-nm gold particles, arrows) and Syk (5-nm gold particles, arrowheads).

clustering, using the pair correlation function (PCF), and of colocalization of gold particles marking FcεRI **β** subunits and Grb2, using the pair cross-correlation function (PCCF), confirmed that only Ag-activated cells exhibited an enhanced formation of FcεRI clusters with increased colocalization of FcεRI and Grb2 (Fig. 10). Independent experiments confirmed that under the conditions of the EM analysis, the cells activated with 5.14 mAb or multimeric Ag released a comparable amount of β-glucuronidase (not shown). Taken together, these results demonstrate that a full secretory response is attained in cells activated through FcεRI dimers in the absence of formation of large clusters of FcεRI, Grb2 and Syk in osmiophilic membranes.

3 Discussion

The data presented here indicate that receptor dimers formed by anti-FcεRI mAb induced cell signaling events that were generally comparable to those induced by FcεRI multimers and resulting from aggregation of FcεRI-IgE complexes by anti-IgE Ab or Ag. However, certain signaling events were disparate. First, under optimal conditions, anti-FcεRI mAb induced degranulation equal to that induced by optimal doses of anti-IgE Ab or Ag. Yet, tenfold higher doses of anti-FcεRI mAb failed to inhibit the secretory response, whereas supraoptimal doses of anti-IgE Ab or Ag were inhibitory. It should be stressed that supraoptimal doses of anti-IgE Ab induced enhanced tyrosine phosphorylation of FcεRI, Syk and LAT, suggesting that early activation events were not inhibited but rather potentiated by extensively aggregated FcεRI. Second, FcεRI dimers triggered a dose-dependent increase in $[Ca^{2+}]_i$ that was slower in onset and more protracted than in cells activated via FcεRI multimers. Supraoptimal doses of anti-IgE Ab caused a faster but more transient increase in $[Ca^{2+}]_i$ than anti-IgE Ab at optimal doses; this could explain the decreased secretory responses. Third, anti-FcεRI mAb induced association of a fraction of FcεRI with DRM within a broad range of densities as determined by sucrose gradient ultracentrifugation. Interestingly, a significant portion of FcεRI remained in the detergent-soluble fractions, and only a small part was found associated with the high-density fractions containing the cytoskeleton/nuclear remnants. In contrast, FcεRI multimers showed a dose-dependent distribution to low-density fractions, and a significant amount of them (22% at 10 μg/ml anti-IgE Ab) remained associated with the high-density insoluble remnants. Fourth, FcεRI dimers usually triggered a slower but more sustained redistribution of several signaling molecules (Gab2, Grb2 and PI3K) from the cytoplasm to the newly forming signaling complexes, as evidenced by their capture in saponin-permeabilized cells. These changes were related to a slower enhancement in tyrosine phosphorylation of several substrates as well as a lower enzymatic activity of PI3K. However, at later stages of activation, tyrosine phosphorylation and/or activity of signaling molecules induced by FcεRI dimers were similar or even exceeded those elicited by FcεRI multimers. Fifth, FcεRI dimers triggered slower and less extensive actin polymerization in cells activated with optimal concentrations of cross-linking agents. Further increases in 5.14 mAb concentration had no effect on actin polymerization, whereas excessive doses of anti-IgE Ab resulted in accelerated actin polymerization, but also a faster return to baseline levels. Finally, the most remarkable difference between FcεRI dimers and multimers was in their effect on the topographical distribution of signaling molecules. Immunogold EM analysis of membrane sheets confirmed previous data [2, 8, 19]

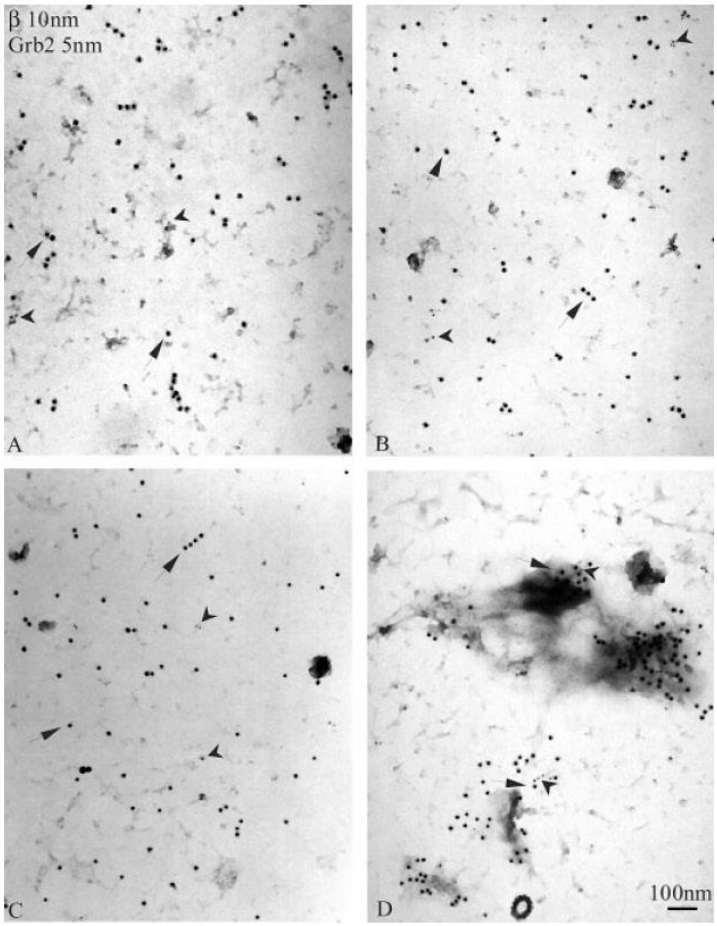

Fig. 9. Membrane topography of FcεRI β subunits and Grb2. Nonsensitized (A, B) or IgE-sensitized (C, D) cells were incubated for 2 min with no addition (A, C), 5.14 mAb (B; 1 μg/ml) or DNP-BSA (D; 1 μg/ml). Membrane sheets prepared from these cells were double-labeled from the inside for FcεRI β subunits (10-nm gold particles, arrows) and Grb2 (5-nm gold particles, arrowheads).

on the dispersed distribution of FcεRI β subunits as individual molecules, dimers or small clusters in nonactivated cells and anti-FcεRI mAb-triggered cells. Detailed analysis of gold-labeled Grb2 showed a small increase in the total number of Grb2 particles in 5.14 mAb-activated cells, but no significant colocalization of Grb2 with FcεRI β subunits in osmiophilic membranes. Similarly, there was no dramatic clustering of Syk with FcεRI β subunits in osmiophilic membranes in 5.14 mAb-activated cells. In contrast, Ag activation brought about the accumulation of FcεRI β subunits in easily detectable clusters that colocalized with Grb2 and Syk in osmiophilic membranes.

Ortega et al. reported that the H10 mAb initiated signaling through Lyn activation and FcεRI subunit phosphorylation, but caused only a modest activation of Syk and a slight increase in $[Ca^{2+}]_i$ and secretion, compared to several other FcεRI-dimerizing mAb [12]. In the present study the H10 mAb was found comparable to, or even more potent than, the 5.14 mAb with regard to its ability to induce early cell activation events. Because we used a different subclone of RBL cells and different cell culture conditions, diversities in the composition and properties of plasma membrane lipids may account for the observed discrepancies. Alternatively, an increased signaling capacity could be attributed to the presence of aggregates of mAb in the batch of H10 mAb used in this

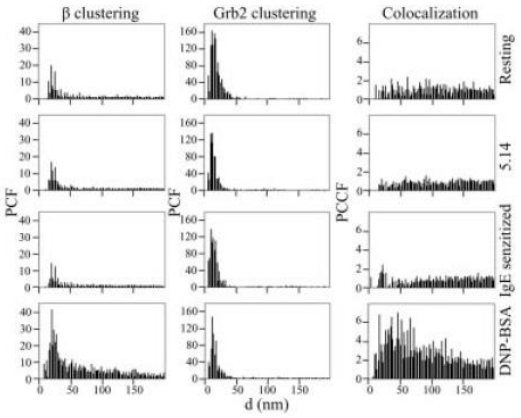

Fig. 10. Analysis of FcεRI **β** subunit and Grb2 clusters. Distribution of FcεRI **β** subunits and Grb2 on membrane sheets was determined as described in Fig. 9. PCF and PCCF values, sorted by 5-nm intervals, were determined from three independent experiments as described in Sect. 4.

study. Although the likelihood of this possibility seems to be strengthened by data showing that the aggregated H10 mAb induced activation comparable in extent to multivalent Ag [9], our own unpublished data render this explanation unlikely because the removal of aggregates by ultracentrifugation did not alter the properties of the mAb. Furthermore, confocal microscopy revealed an almost homogeneous distribution of the H10 mAb on cells incubated with the Ab for 5 min before fixation and staining (not shown). Finally, the H10 mAb-FcεRI complexes induced activation events typical for dimerizing mAb, including degranulation, calcium response and density distribution on a sucrose gradient (Fig. 1).

Previous EM studies on IgE-sensitized cells showed that addition of cross-linking agents (multivalent Ag or anti-IgE Ab) induced a striking redistribution of receptor aggregates to distinct regions of the plasma membrane that are characterized by their dark staining with osmium, adjacency of coated pits, and accumulation of several signaling proteins including Syk, PLCγ2, PI3K, Gab2 and Grb2 [2, 8]. It has been suggested that these regions are the primary sites of active signaling to downstream pathways. However, because strong FcεRI signaling is also observed in anti-FcεRI mAb-activated cells without formation of large receptor clusters associated with osmiophilic membranes, it is likely that genuine signaling domains are much smaller, formed around receptor dimers/oligomers, and that the large signaling complexes might have some other function. We favor the hypothesis that large signaling assemblies function as sites that facilitate both a rapid receptor-mediated cell triggering and an increased degradation of FcεRI complexes.

The combined data indicate that FcεRI dimers/oligomers trigger formation of signaling complexes that are small in size but possess all components necessary for signal propagation. These complexes are relatively stable and are not rapidly internalized, as suggested by the absence of an increased amount of clathrin-coated pits in the vicinity of FcεRI dimers/oligomers (see also [9]). How these small complexes are internalized remains to be solved. On the other hand, when IgE receptors are extensively aggregated, large signaling assemblies are formed that must be regulated to avert strong sustained signaling, which could lead to cell death by overstimulation. Rapid association of the signaling assemblies with osmiophilic membranes in the vicinity of clathrin-coated pits suggests that regulation of these signaling domains is mediated by receptor internalization. This is supported by previous data showing that the extent of receptor aggregation corresponded to the extent of receptor internalization [10]. Alternatively, extensively aggregated signaling complexes could attract inhibitory molecules, such as phosphatases, which could shorten the life span of the signals or down-modulate their strength.

Current models of immunoreceptor signaling envisage the formation of signaling assemblies, in which lipid and protein modifications allow the appearance of plasma membrane complexes capable of further propagating the activation signal. Initially, it was thought that these assemblies were large and involved extensive immunoreceptor clustering. For example, it has been suggested that the immunological synapse that forms between the T cell and the Ag-presenting cell facilitates T cell receptor signaling by clustering the receptor and other signaling molecules [20]. Recent studies indicated, however, that initiation of T cell receptor-mediated signaling could occur early and could largely precede the formation of the mature immunological synapse [21, 22]. Furthermore, recent *in vitro* and *in silico* experiments suggest that the immunological synapse acts as a type of adaptive controller that boosts both strong receptor triggering and increased TCR degradation [23]. Thus, both aggregated TCR and FcεRI could regulate their signal transduction pathways by similar mechanisms.

4 Materials and methods

4.1 Cells and Ab

RBL cells were maintained in culture as described [3]. The subclone RBL-2H3c80 was selected for increased secretory response. The origins of mAb specific for Syk kinase (Syk-

01/Pr), FcεRI β subunits (JRK), TNP (IgE; IGEL b4 1), phospho-tyrosine (PY-20) conjugated to horseradish peroxidase (HRP), as well as goat anti-mouse IgG conjugated to HRP, and rabbit Ab specific for Syk, LAT and IgE have been described [6]. Anti-FcεRI α subunit mAb, clones 5.14 and H10, have been described [11, 24]. Other Ab used in this study: rabbit anti-Grb2, anti-Gab2 and anti-SHP-2 (Santa Cruz Biotechnology, Santa Cruz, CA), rabbit anti-p85 subunit of PI3K (Upstate Biotechnology, Lake Placid, NY), and goat anti-mouse IgG and anti-rabbit IgG conjugated to colloidal gold particles of 10 nm and 5 nm in diameter, respectively (Amersham Pharmacia Biotech, Piscataway, NJ).

4.2 Cell activation, immunoprecipitation and immunoblotting

Cells were harvested, resuspended in culture medium at a concentration of 5×10^6 cells/ml and were sensitized or not with IgE mAb. After incubation at 37°C for 30 min in a CO_2 incubator, the cells were washed twice in BSS (20 mM HEPES pH 7.4, 135 mM NaCl, 5 mM KCl, 1.8 mM $CaCl_2$, 1 mM $MgCl_2$, 5.6 mM glucose), supplemented with 0.1% BSA, and activated at 37°C by exposure to various concentrations of anti-IgE or anti-FcεRI Ab, as specified in Sect. 2. In some experiments, cells were pretreated with MBCD as described [13]. Towards the end of the activation period, cells were briefly centrifuged and the supernatants used for determination of β-glucuronidase amounts. Cell pellets were resuspended in ice-cold lysis buffer containing 10 mM Tris-HCl pH 8.0, 50 mM NaCl, 10 mM EDTA, 1 mM Na_3VO_4, 10 mM glycerophosphate, 1 mM PMSF, aprotinin (10 μg/ml), leupeptin (10 μg/ml), and 0.2% Triton X-100. For LAT immunoprecipitation, the cells were lysed in a buffer containing 5 mM NaH_2PO_4 pH 7.2, 25 mM NaCl, 25 mM NaF, PMSF, aprotinin, leupeptin, 1% Triton X-100, 0.1% SDS, and 0.25% sodium deoxycholate. In some experiments, the cells were incubated for 5 min on ice in PBS containing 0.1% saponin, 5 mM $MgCl_2$, and 1 mM Na_3VO_4, washed in PBS and then extracted for 15 min on ice in lysis buffer supplemented with 1% Triton X-100. For immunoprecipitation, cell lysates were incubated for 2 h at 4°C with Ab, followed by 1.5 h of incubation with either UltraLink-immobilized protein A or protein G (Pierce, Rockford, IL). Immunoprecipitated proteins were resolved on 10% SDS polyacrylamide gels and analyzed by immunoblotting as described [15]. Immunoblots were quantified by Luminescent Image Analyzer LAS-3000 (Fuji Photo Film Co., Tokyo).

4.3 Electron microscopy

Cells were settled overnight on 15-mm round-glass coverslips in the presence or absence of anti-dinitrophenyl (DNP) IgE (1 μg/ml). IgE-primed cells were activated by DNP-BSA (1 μg/ml), whereas nonsensitized cells were activated by the 5.14 mAb (1 μg/ml). Plasma membrane sheets were obtained and processed as described [19]. FcεRI β subunits, Syk and Grb2 were labeled by sequential incubation with the corresponding primary Ab [JRK (3 μg/ml), anti-Syk (ascites diluted 1:500) and anti-Grb2 (8 μg/ml)], followed by gold-conjugated secondary reagents diluted 1:20 from commercial stocks. Samples were post-fixed in 2% glutaraldehyde in PBS, washed in PBS and then stained with 1% osmium in cacodylate buffer, 1% tannic acid and 1% uranyl acetate. Finally, samples were washed twice with water for 1 min, air-dried and observed with a JEOL JEM 1200EX electron microscope operating at 60 kV. Gold particle clusters and their colocalizations were analyzed using the computer program GOLD [25]. Clusters of particles of the same type were analyzed using PCF, which is a ratio of the density of gold particles at a given distance from a typical particle to the average density of these particles. To analyze the colocalization of particles, we used the PCCF, which is a ratio of the density of particles of the first type (FcεRI β subunits) at the given distance from a typical particle of the second type (Grb2) to the average density of the particles of the first type. In each of three independent experiments, we analyzed 25–30 μm^2 of plasma membranes from activated and resting cells.

4.4 Other methods

Labeling of mAb with ^{125}I by chloramine T method, sucrose density gradient ultracentrifugation and F-actin assay, as well as determination of β-glucuronidase, $[Ca^{2+}]_i$, PIP3, and PI3K activity have been described [6, 15]. ^{32}P-labeled lipids were separated by thin layer chromatography (TLC), visualized by autoradiography and quantified by Fuji Bio-Imaging Analyzer Bas 5000.

Acknowledgements: We thank H. Mrázová, R. Budovičová, J. Musilová and I. Lišková for technical assistance, Dr. I. Pecht and Z. Eshhar for anti-FcεRI mAb and Dr. B. Wilson for DNP-specific IgE. This work was supported in part by grant LN00A026 from the Ministry of Education, Youth and Sports of the Czech Republic, grants 204/03/0594, 301/03/0596, 204/00/0204 and 310/00/205 from the Grant Agency of the Czech Republic, and grants A5052005/00, A7052006/00 and A5052310 from the Grant Agency of the Academy of Sciences of the Czech Republic. The research of P. Dráber was also supported by an International Research Scholar's award from the Howard Hughes Medical Institute.

References

1 **Kinet, J. P.,** The high-affinity IgE receptor (FcεRI): from physiology to pathology. *Annu. Rev. Immunol.* 1999. **17:** 931–972.

2 **Wilson, B. S., Pfeiffer, J. R. and Oliver, J. M.,** FcεRI signaling observed from the inside of the mast cell membrane. *Mol. Immunol.* 2002. **38:** 1259–1268.

3 **Dráberová, L. and Dráber, P.,** Thy-1 glycoprotein and src-like protein-tyrosine kinase p53/p56^{lyn} are associated in large

detergent-resistant complexes in rat basophilic leukemia cells. *Proc. Natl. Acad. Sci. USA* 1993. **90:** 3611–3615.

4 **Hálová, I., Dráberová, L. and Dráber, P.,** A novel lipid raft-associated glycoprotein, TEC-21, activates rat basophilic leukemia cells independently of the type 1 Fcε receptor. *Int. Immunol.* 2002. **14:** 213–223.

5 **Field, K. A., Holowka, D. and Baird, B.,** Compartmentalized activation of the high affinity immunoglobulin E receptor within membrane domains. *J. Biol. Chem.* 1997. **272:** 4276–4280.

6 **Kovářová, M., Tolar, P., Arudchandran, R., Dráberová, L., Rivera, J. and Dráber, P.,** Structure-function analysis of Lyn kinase association with lipid rafts and initiation of early signaling events after Fcε receptor I aggregation. *Mol. Cell Biol.* 2001. **21:** 8318–8328.

7 **Stauffer, T. P. and Meyer, T.,** Compartmentalized IgE receptor-mediated signal transduction in living cells. *J. Cell Biol.* 1997. **139:** 1447–1454.

8 **Wilson, B. S., Pfeiffer, J. R., Surviladze, Z., Gaudet, E. A. and Oliver, J. M.,** High resolution mapping of mast cell membranes reveals primary and secondary domains of FcεRI and LAT. *J. Cell Biol.* 2001. **154:** 645–658.

9 **Lara, M., Ortega, E., Pecht, I., Pfeiffer, J. R., Martinez, A. M., Lee, R. J., Surviladze, Z., Wilson, B. S. and Oliver, J. M.,** Overcoming the signaling defect of Lyn-sequestering, signal-curtailing FcεRI dimers: Aggregated dimers can dissociate from Lyn and form signaling complexes with Syk. *J. Immunol.* 2001. **167:** 4329–4337.

10 **Metzger, H., Alcaraz, G., Hohman, R., Kinet, J. P., Pribluda, V. and Quarto, R.,** The receptor with high affinity for immunoglobulin E. *Annu. Rev. Immunol.* 1986. **4:** 419–470.

11 **Ortega, E., Schweitzer-Stenner, R. and Pecht, I.,** Possible orientational constraints determine secretory signals induced by aggregation of IgE receptors on mast cells. *EMBO J.* 1988. **7:** 4101–4109.

12 **Ortega, E., Lara, M., Lee, I., Santana, C., Martinez, A. M., Pfeiffer, J. R., Lee, R. J., Wilson, B. S. and Oliver, J. M.,** Lyn dissociation from phosphorylated FcεRI subunits: A new regulatory step in the FcεRI signaling cascade revealed by studies of FcεRI dimer signaling activity. *J. Immunol.* 1999. **162:** 176–185.

13 **Sheets, E. D., Holowka, D. and Baird, B.,** Critical role for cholesterol in Lyn-mediated tyrosine phosphorylation of FcεRI and their association with detergent-resistant membranes. *J. Cell Biol.* 1999. **145:** 877–887.

14 **Dráberová, L., Amoui, M. and Dráber, P.,** Thy-1-mediated activation of rat mast cells: the role of Thy-1 membrane microdomains. *Immunology* 1996. **87:** 141–148.

15 **Dráberová, L., Dudková, L., Boubelík, M., Tolarová, H., Šmíd, F. and Dráber, P.,** Exogenous administration of gangliosides inhibits FcεRI-mediated mast cell degranulation by decreasing the activity of phospholipase Cγ. *J. Immunol.* 2003. **171:** 3585–3593.

16 **Xie, Z. H., Ambudkar, I. and Siraganian, R. P.,** The adapter molecule Gab2 regulates FcεRI-mediated signal transduction in mast cells. *J. Immunol.* 2002. **168:** 4682–4691.

17 **Rivera, J.,** Molecular adapters in FcεRI signaling and the allergic response. *Curr. Opin. Immunol.* 2002. **14:** 688–693.

18 **Holowka, D., Sheets, E. D. and Baird, B.,** Interactions between FcεRI and lipid raft components are regulated by the actin cytoskeleton. *J. Cell Sci.* 2000. **113:** 1009–1019.

19 **Wilson, B. S., Pfeiffer, J. R. and Oliver, J. M.,** Observing FcεRI signaling from the inside of the mast cell membrane. *J. Cell Biol.* 2000. **149:** 1131–1142.

20 **Bromley, S. K., Burack, W. R., Johnson, K. G., Somersalo, K., Sims, T. N., Sumen, C., Davis, M. M., Shaw, A. S., Allen, P. M. and Dustin, M. L.,** The immunological synapse. *Annu. Rev. Immunol.* 2001. **19:** 375–396.

21 **Lee, K. H., Holdorf, A. D., Dustin, M. L., Chan, A. C., Allen, P. M. and Shaw, A. S.,** T cell receptor signaling precedes immunological synapse formation. *Science* 2002. **295:** 1539–1542.

22 **Freiberg, B. A., Kupfer, H., Maslanik, W., Delli, J., Kappler, J., Zaller, D. M. and Kupfer, A.,** Staging and resetting T cell activation in SMACs. *Nat. Immunol.* 2002. **3:** 911–917.

23 **Lee, K. H., Dinner, A. R., Tu, C., Campi, G., Raychaudhuri, S., Varma, R., Sims, T. N., Burack, W. R., Wu, H., Wang, J., Kanagawa, O., Markiewicz, M., Allen, P. M., Dustin, M. L., Chakraborty, A. K. and Shaw, A. S.,** The immunological synapse balances T cell receptor signaling and degradation. *Science* 2003. **302:** 1218–1222.

24 **Baniyash, M., Alkalay, I. and Eshhar, Z.,** Monoclonal antibodies specific to the α-subunit of the mast cell's FcεR block IgE binding and trigger histamine release. *J. Immunol.* 1987. **138:** 2999–3004.

25 **Philimonenko, A. A., Janáček, J. and Hozák, P.,** Statistical evaluation of colocalization patterns in immunogold labeling experiments. *J. Struct. Biol.* 2000. **132:** 201–210.

Correspondence: Lubica Dráberová, Department of Signal Transduction, Institute of Molecular Genetics, Academy of Sciences of the Czech Republic, Vídeňská 1083, CZ 142 20 Prague 4, Czech Republic
Fax: +420–241 470 339
e-mail: draberpe@biomed.cas.cz

(B)

Negative regulation of mast cell signaling and function by the adaptor LAB/NTAL.

J. Exp. Med., 2004, 200: 1001-1013.

Negative Regulation of Mast Cell Signaling and Function by the Adaptor LAB/NTAL

Petra Volná,[1] Pavel Lebduška,[1] Lubica Dráberová,[1] Šárka Šímová,[1] Petr Heneberg,[1] Michael Boubelík,[1] Viktor Bugajev,[1] Bernard Malissen,[2] Bridget S. Wilson,[3] Václav Hořejší,[1] Marie Malissen,[2] and Petr Dráber[1]

[1]*Institute of Molecular Genetics, Academy of Sciences of the Czech Republic, 142 20 Prague 4, Czech Republic*
[2]*Centre d'Immunologie de Marseille-Luminy, INSERM–CNRS–Université de la Méditerranée, 13288 Marseille Cedex 9, France*
[3]*Department of Pathology and Cancer Research, University of New Mexico Health Sciences Center, Albuquerque, NM 87131*

The Journal of Experimental Medicine

Abstract

Engagement of the Fcε receptor I (FcεRI) on mast cells and basophils initiates signaling pathways leading to degranulation. Early activation events include tyrosine phosphorylation of two transmembrane adaptor proteins, linker for activation of T cells (LAT) and non–T cell activation linker (NTAL; also called LAB; a product of *Wbscr5* gene). Previous studies showed that the secretory response was partially inhibited in bone marrow–derived mast cells (BMMCs) from LAT-deficient mice. To clarify the role of NTAL in mast cell degranulation, we compared FcεRI-mediated signaling events in BMMCs from NTAL-deficient and wild-type mice. Although NTAL is structurally similar to LAT, antigen-mediated degranulation responses were unexpectedly increased in NTAL-deficient mast cells. The earliest event affected was enhanced tyrosine phosphorylation of LAT in antigen-activated cells. This was accompanied by enhanced tyrosine phosphorylation and enzymatic activity of phospholipase C γ1 and phospholipase C γ2, resulting in elevated levels of inositol 1,4,5-trisphosphate and free intracellular Ca^{2+}. NTAL-deficient BMMCs also exhibited an enhanced activity of phosphatidylinositol 3-OH kinase and Src homology 2 domain–containing protein tyrosine phosphatase-2. Although both LAT and NTAL are considered to be localized in membrane rafts, immunogold electron microscopy on isolated membrane sheets demonstrated their independent clustering. The combined data show that NTAL is functionally and topographically different from LAT.

Key words: mast cell • signal transduction • Fcε receptor • calcium mobilization • adapter molecules

Introduction

Mast cells play a pivotal role in initiating acute inflammatory and immediate allergic reactions. The binding of multivalent antigen (Ag) to receptor-bound IgE and subsequent aggregation of the Fcε receptor I (FcεRI) provide the trigger for mast cell activation, resulting in a release of histamine, serotonin, and other preformed inflammatory mediators, as well as de novo synthesis and subsequent secretion of arachidonic acid metabolites and a variety of inflammatory cytokines. These signal transduction pathways are initiated by the engagement of protein tyrosine kinases of the Src and Syk families. Src family kinase Lyn phosphorylates immunoreceptor tyrosine-based activation motifs present on FcεRI β and γ subunits. This leads to a recruitment and subsequent activation of Syk kinase, which phosphorylates

Address correspondence to Petr Dráber, Institute of Molecular Genetics, Academy of Sciences of the Czech Republic, Vídeňská 1083, 142 20 Prague 4, Czech Republic. Phone: 420-241-062-468; Fax: 420-241-470-339; email: draberpe@biomed.cas.cz; or Marie Malissen, Centre d'Immunologie de Marseille-Luminy, INSERM–CNRS–Univ. Med., Parc Scientifique de Luminy, 13288 Marseille Cedex 9, France. Phone: 33-491269402; Fax: 33-491269430; email: malissen@ciml.univ-mrs.fr

Abbreviations used in this paper: Ag, antigen; BMMC, BM-derived mast cell; BSS, buffered saline solution; $[Ca^{2+}]_i$, concentration of free intracellular calcium; ES, embryonic stem; FcεRI, Fcε receptor I; HRP, horseradish peroxidase; IP3, inositol 1,4,5-trisphosphate; LAT, linker for activation of T cells; MAP, mitogen-activated protein; NTAL, non–T cell activation linker; PI, phosphatidylinositol; PI3K, PI 3-OH kinase; PLC, phospholipase C; PS, phosphatidylserine; SCF, stem cell factor; SH, Src homology.

 J. Exp. Med. © The Rockefeller University Press • 0022-1007/2004/10/1001/13 $8.00
Volume 200, Number 8, October 18, 2004 1001–1013
http://www.jem.org/cgi/doi/10.1084/jem.20041213

several downstream signaling molecules, including the linker for activation of T cells (LAT). Phosphorylated LAT recruits a number of signaling molecules containing Src homology (SH)2 domains, such as adaptor protein Grb2 and phospholipase C (PLC)γ1 and PLCγ2. An important intermediate is phosphatidylinositol (PI) 3-OH kinase (PI3K), which catalyzes the synthesis of PI 3,4-bisphosphate and PI 3,4,5-trisphosphate. These phospholipids contribute to recruitment to the plasma membrane of Akt and PLCγ and other molecules containing pleckstrin homology domains. PLCγ catalyzes the cleavage of the lipid substrate PI 4,5-bisphosphate into diacylglycerol, an activator of protein kinase C, and inositol 1,4,5-trisphosphate (IP3), a ligand for the IP3 receptor Ca^{2+} channel in the ER membrane that initiates a rise in cytoplasmic Ca^{2+} levels. This is followed by a more sustained influx of extracellular calcium through Ca^{2+} channels in the plasma membrane. Many of these events rely on formation of multimolecular signaling complexes that propagate the activation signal from aggregated FcεRI (1).

Recently, we have found that mast cells express a LAT-related transmembrane adaptor protein, the non–T cell activation linker (NTAL) (2). NTAL, also called LAB (3), was also found to be expressed in other cell types, such as B lymphocytes, NK cells, and monocytes but not in T lymphocytes. NTAL resembles LAT in general organization, consisting of a short extracellular domain, a single hydrophobic transmembrane domain, and a cytoplasmic tail with multiple tyrosine phosphorylation sites and two potential palmitoylation sites. The two acylation sites are likely responsible for partitioning of NTAL into detergent-resistant membrane microdomains, also called lipid rafts (4). NTAL is rapidly tyrosine phosphorylated upon engagement of FcεRI, FcγRI, or B cell receptor (2, 3). Functional similarity between LAT and NTAL was suggested by experiments in which ectopically expressed NTAL could partially restore some aspects of T cell receptor signaling in LAT-deficient cells (2). Furthermore, NTAL expressed in T cells could in part rescue the T cell development in $LAT^{-/-}$ mice (3, 5). An important functional role of NTAL in immunoreceptor signaling was suggested by experiments in which a diminution of NTAL expression by silencing RNA oligonucleotides resulted in a reduction of B cell receptor–mediated activation of mitogen-activated protein (MAP) kinase in A20 cell line (3), as well as in a reduced degranulation in FcεRI-activated human mast cells (6).

Using a genetic approach, Saitoh et al. showed that mast cell effector functions were impaired but not completely inhibited in BM-derived mast cells (BMMCs) from LAT-deficient mice (7). Accordingly, low levels of PLCγ activation and calcium response were detected in LAT-deficient BMMCs, suggesting the existence of alternative pathways. One alternative pathway independent of Lyn kinase and LAT phosphorylation but dependent on Fyn kinase and Gab2 adaptor has been described recently (8). In this study, we analyzed the signaling events in BMMCs from NTAL-deficient mice and compared them with those observed in WT mice or mice deficient in both NTAL and LAT linkers. Furthermore, we analyzed the respective topography of NTAL and LAT on membrane sheets isolated from nonactivated and activated mast cells.

Materials and Methods

Antibodies and Reagents. The following mAbs have been used: anti-Syk (9), anti-LAT (10), anti-FcεRI β subunit (JRK) (11), anti-NTAL (NAP-07) (2), TNP-specific IgE mAb (IGEL b4 1) (12), and DNP-specific IgE mAb (13). Polyclonal antibodies specific for Syk, LAT, NTAL, and IgE have been prepared by common procedures after immunizing rabbits with the corresponding proteins or their fragments (14). Polyclonal antibodies specific for PLCγ1, PLCγ2, ERK 1, phospho-ERK (specific for phosphorylated Tyr 204), Grb2, SH2-containing protein tyrosine phosphatase (SHP)-2, and horseradish peroxidase (HRP)–conjugated donkey anti–goat IgG, goat anti–mouse IgG, and goat anti–rabbit IgG were obtained from Santa Cruz Biotechnology, Inc. Rabbit anti-PI3K p85 subunit antibody (a mixture of equal amounts of antisera against the intact p85 subunit and the N-SH2 region of PI3K) was obtained from Upstate Biotechnology. Phospho-Tyr–specific mAb (PY-20) conjugated to HRP was purchased from Transduction Laboratories. Biotinylated rat anti–mouse c-kit, FITC-labeled rat anti–mouse IgE antibody, and phycoerythrin-labeled streptavidin were from BD Biosciences. Goat anti–mouse IgG and anti–rabbit IgG conjugated to colloidal gold particles of 10- and 5-nm were obtained from Amersham Biosciences. Fura-2-AM and ^{45}Ca (37 MBq; specific activity 566 MBq/mg Ca^{2+}) were purchased from Molecular Probes and MP Biomedicals, Inc., respectively. All other chemicals were obtained from Sigma-Aldrich.

Vector Construction. The targeting construct used for disruption of the *Ntal* gene is shown in Fig. 1 b. It should be noted that the official name of the gene is *Wbscr5*. The 5′ homologous sequences correspond to a gene segment encompassing nucleotide positions 79680–81447 (sequence data available from GenBank/EMBL/DDBJ under accession no. AF139987). The 3′ homologous sequences correspond to a gene segment encompassing nucleotide positions 87023–91726 (sequence data available from GenBank/EMBL/DDBJ under accession no. AF139987). In the engineered vector, the sequence containing exons 2–9 of the *Ntal* gene and coding for amino acids 1–121 of the NTAL protein was replaced by a lox P–flanked neomycin-resistance gene (neo^r). Finally, the targeting construct was abutted to a thymidine kinase expression cassette and linearized.

Isolation of Recombinant Embryonic Stem Cell Clones and Production of Mutant Mice. After electroporation of CK35 129/CV embryonic stem (ES) cells (15) and selection in G418 and gancyclovir, colonies were screened for homologous recombination by Southern blot analysis. The 5′ single copy probe corresponded to a 400-bp EcoRI–XbaI fragment. When tested on EcoRI-digested DNA, it hybridized either to a 8-kb WT fragment or to a 2.5-kb recombinant fragment. The presence of an appropriate homologous recombination event at the 3′ side was assessed using a 1051-bp XbaI–EcoRI fragment. When tested on HindIII-digested DNA, it hybridized either to a 9.5-kb WT fragment or to a 6.7-kb recombinant fragment. A neo probe was also used to ensure that adventitious nonhomologous recombination events had not occurred in the selected clones. Among the recombinant ES cell clones, one was found capable of germline transmission. The resulting mutant mouse line was first bred to Deleter mice (16) to eliminate the lox

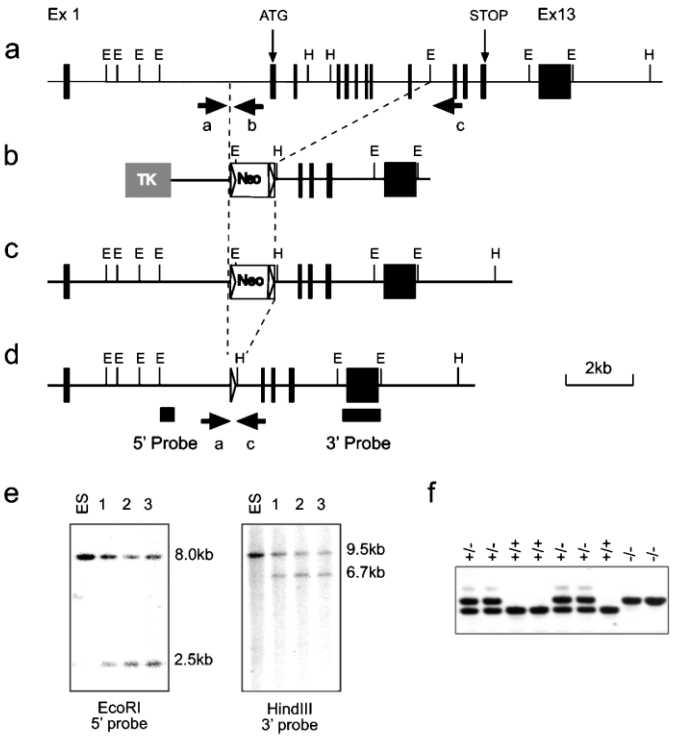

Figure 1. Generation and identification of *Ntal*-deficient mice. (a–d) Schematics of the *Ntal* knock-out strategy. (a) Partial restriction map of the WT *Ntal* gene. Exons are shown as filled boxes. The restriction sites are EcoRI (E) and Hind III (H). The exons containing the initiation (start) and the stop codon are specified. (b) Targeting vector used for the deletion of exons 2–9. Shaded or open boxes correspond to the thymidine kinase expression cassette (TK) and to the lox P–flanked neo^r cassette, respectively. Lox P sites are shown as triangles. (c) Structure of the targeted allele after homologous recombination. (d) Final structure of the targeted allele after removal of the neo^r gene via cre-mediated recombination. The 5′ and 3′ single copy probes used to verify 5′ and 3′ targeting events are indicated, and the position of the PCR primers used to genotype the resulting mice are indicated by arrows. (e) Southern blot analysis of three recombinant ES cell clones including the one that gave germline transmission (clone 1). DNA was digested as specified and hybridized with the 5′ or 3′ single copy probe. (f) PCR genotyping of *Ntal*-deficient and -proficient littermates using primers indicated in panel d.

P–flanked neomycin cassette and intercrossed to produce homozygous mutant mice. Screening of mice for the presence of the *Ntal*-null mutation was performed by PCR using the following oligonucleotides: a: 5′-CTACGGAGCTGAGTGTTCTCA-3′, b: 5′-GAACGGCTAGAACTACACAGAG-3′, c: 5′-GAGAGGAGGATAAAGTGGACCTC-3′. WT *Ntal* allele is visualized as a 383-bp fragment using the a-b pair of oligonucleotides, whereas the intended mutation is visualized as a 450-bp fragment using the a-c pair of oligonucleotides. Production of LAT$^{-/-}$ mice has been described (17). NTAL$^{-/-}$ and LAT$^{-/-}$ mice were bread to generate the NTAL$^{-/-}$/LAT$^{-/-}$ strain. All mice were maintained and used in accordance with the Institute of Molecular Genetics guidelines.

Cells. BMMCs were isolated from the femurs and tibias of the 6–10-wk-old mice. The cells were incubated for 4–8 wk in suspension cultures in freshly prepared culture media (RPMI-1640 supplemented with 20 mM Hepes, pH 7.5, 100 U/ml penicillin, 100 μg/ml streptomycin, 100 μM MEM nonessential amino acids, 1 mM sodium pyruvate, 17% FCS, 41 μM 2-ME) supplemented with IL-3 (20 ng/ml; PeproTech EC) and stem cell factor (SCF; 40 ng/ml; PeproTech EC). No discernible differences in growth properties and morphology were detected among BMMCs derived from NTAL$^{+/+}$, NTAL$^{+/-}$, NTAL$^{-/-}$, LAT$^{-/-}$, and NTAL$^{-/-}$/LAT$^{-/-}$ mice. Before activation, BMMCs were cultured for 16 h in culture medium without SCF, followed by incubation for 3–4 h in SCF- and IL-3–free medium supplemented with anti-TNP IgE (1 μg/ml). The cells were then washed in buffered saline solution (BSS) containing 20 mM Hepes, pH 7.4, 135 mM NaCl, 5 mM KCl, 1.8 mM $CaCl_2$, 5.6 mM glucose, 1 mM $MgCl_2$, and 0.1% BSA (BSS-BSA), and challenged with various concentrations of TNP-BSA.

Flow Cytometry Analyses of FcεRI and Phosphatidylserine Expression. Flow cytometry analyses of FcεRI in unfractioned freshly isolated peritoneal mast cells (c-kit positive) and BMMCs were performed as described (18) except that in the first incubation step the cells were exposed to TNP-specific IgE. To determine externalization of phosphatidylserine (PS), cells were exposed to FITC-labeled annexin V (Alexis) and then analyzed using FACSCalibur and CellQuest software (Beckton Dickinson) as described (19).

Passive Systemic Anaphylaxis and Degranulation. Mice were sensitized by i.v. tail vein injection of TNP-specific IgE (3 μg/mouse) and 24 h later challenged by i.v. tail vein injection with TNP-BSA (500 μg/mouse) or vehicle (PBS). After 1.5 min, the animals were killed, blood samples were obtained by cervical puncture, and serum was isolated. Serum histamine concentrations were determined according to the manufacturer's protocol using a histamine radioimmunoassay kit (Immunotech). Statistical significance of differences among particular groups was determined using Student's *t*-test. The degree of degranulation was determined by measuring the release of β-glucuronidase from anti-TNP IgE-sensitized and TNP-BSA–activated cells as described (20).

Immunoprecipitation and Immunoblotting. Activated and control cells were lysed in ice cold lysis buffer (50 mM Tris-HCl, pH 7.4, 150 mM NaCl, 2 mM EDTA, 10 mM β-glycerophosphate, 1 mM Na_3VO_4, 1 mM PMSF, 1 μg/ml aprotinin, 1 μg/ml leupeptin) supplemented with 1% NP-40 and 1% *n*-dodecyl β-D-maltoside (for LAT, and NTAL immunoprecipitation or for ERK immunoblotting) or 0.2% Triton X-100 (for FcεRI immunoprecipitation). In some experiments, association of the proteins under study with large macromolecular complexes was analyzed

in cells permeabilized with 0.1% saponin in PBS, thus releasing free cytoplasmic components, and the cellular ghosts were extracted for 15 min on ice in a lysis buffer supplemented with 1% Triton X-100 (21). Proteins in postnuclear supernatants were immunoprecipitated with the corresponding antibodies bound to UltraLink-immobilized protein A (Pierce Chemical Co.) and analyzed by immunoblotting as described (9). Some proteins were analyzed by direct immunoblotting of SDS-PAGE–fractionated cell lysates. Immunoblots were quantified by Luminescent Image Analyzer LAS 3000 (Fuji Photo Film Co.).

Sucrose Gradients. Cells were solubilized in lysis buffer containing 1% Brij 96 and fractionated by sucrose density gradient ultracentrifugation as described (20).

Measurements of Intracellular Ca^{2+} Concentrations and ^{45}Ca Uptake. Concentrations of free intracellular calcium $[Ca^{2+}]_i$ were determined using Fura-2-AM as a reporter. BMMCs were sensitized with anti-TNP IgE (1 μg/ml) at 37°C in culture medium supplemented with 2% FCS but devoid of SCF and IL-3. After 3–4 h, the cells were washed and resuspended at a concentration 5×10^6/ml in BSS-BSA supplemented with Fura-2-AM and probenecid at a final concentration of 1 μg/ml and 2.5 mM, respectively. After 30 min, the cells were washed in BSS-BSA supplemented with probenecid and immediately before measurement briefly centrifuged and resuspended in BSS-BSA. Calcium mobilization was determined using luminescence spectrometer LS-50B (PerkinElmer). Uptake of extracellular calcium was determined as before (22) except that the radioactivity was measured in 10 ml scintillation liquid (EcoLite; ICN Biomedicals) in QuantaSmart TM counter.

Immune Complex PI3K, PLCγ and Syk Kinase Assays, and IP3 Determination. PI3K and PLCγ activities and IP3 concentrations were determined as described previously (21). Syk kinase activity was determined by in vitro kinase assay (9).

In-gel Phosphatase Assay. SHP-2 immunoprecipitates were prepared and analyzed by in-gel phosphatase assay as described (23).

Electron Microscopy. Cells were left overnight to settle on 15-mm round-glass coverslips in the presence or absence of anti-DNP IgE (1 μg/ml). IgE-sensitized cells were activated by DNP-BSA (1 μg/ml), and membrane sheets were obtained and processed as described (24). FcεRI, NTAL, and LAT were labeled by sequential incubation with the corresponding primary antibodies followed by gold-conjugated secondary reagents diluted 1:20 from commercial stocks. Samples were postfixed in 2% glutaraldehyde in PBS, washed in PBS, and then stained with 1% OsO_4 in 0.1 M cacodylate buffer, 1% tannic acid, and 1% uranyl acetate. Samples were examined using a Hitachi 600 transmission electron microscope. Gold particles distribution was analyzed using software developed at the University of New Mexico (25). Clusters of particles of the same type were analyzed using the Hopkins and Ripley's statistics (25). In each of two independent experiments, ~30 μm^2 of plasma membranes from activated and resting cells were analyzed.

Results

Enhanced Degranulation in NTAL$^{-/-}$ Mast Cells. To explore the role of NTAL in mast cell physiology, we generated knock-out mice with a lox P sequence that replaced a central segment of the *Ntal* gene containing exons 2–9 (Fig. 1). Mice homozygous for this mutation, *Ntal*$^{-/-}$, were born at the expected Mendelian frequencies and were deprived of detectable NTAL protein (see next paragraph). First, we

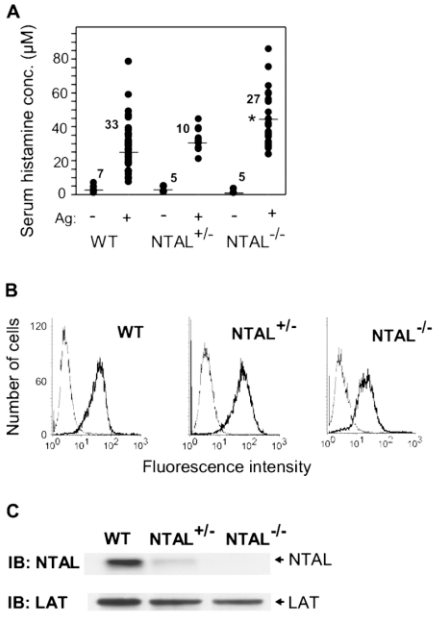

Figure 2. Enhanced passive systemic anaphylaxis in NTAL$^{-/-}$, and FcεRI and NTAL expression in BMMCs. (A) WT, NTAL$^{+/-}$, and NTAL$^{-/-}$ mice were sensitized with TNP-specific IgE, challenged with TNP-BSA (+) or with PBS alone (−), and the serum histamine levels were determined. Numbers above the mean bars indicate the numbers of mice in each group. The asterisk indicates a significant increase ($P < 0.01$) of histamine levels in NTAL$^{-/-}$ mice compared with WT mice. (B) BMMCs from WT, NTAL$^{+/-}$, and NTAL$^{-/-}$ mice were stained for surface FcεRI by sequential exposure to anti-TNP IgE (1 μg/ml, thick line) or PBS alone (thin line) followed by anti–mouse IgG–FITC conjugate. The samples were analyzed by flow cytometry. (C) NTAL expression levels in lysates from BMMCs were determined by immunoblotting (IB) using anti-NTAL mAb followed by anti–mouse IgG–HRP conjugate. As a control for protein loading the membrane was also developed with rabbit anti-LAT followed by anti–rabbit IgG–HRP conjugate.

analyzed the effect of NTAL on passive anaphylactic reaction in vivo. In controls, the basal level of serum histamine was identical in WT, NTAL$^{+/-}$, and NTAL$^{-/-}$ mice (Fig. 2 A). After challenge with Ag, the serum histamine levels were enhanced in all mice, although the levels were significantly higher in NTAL$^{-/-}$ mice. The observed increase in serum histamine was not attributable to elevated numbers of mast cells in NTAL$^{-/-}$ mice, as inferred from similar numbers of mast cells in peritoneal lavage of WT, NTAL$^{+/-}$, and NTAL$^{-/-}$ mice (2.5% ± 1.1%, mean ± SD, $n = 9$). Furthermore, peritoneal mast cells (c-kit positive) from NTAL$^{-/-}$ and WT mice did not differ in the amount of surface FcεRI as determined by flow cytometry (not depicted). These data suggested that the observed increase in serum histamine levels in NTAL$^{-/-}$ cells could reflect negative regulation of mast cell signaling by NTAL.

To investigate the underlying mechanism responsible for the enhanced degranulation response in NTAL$^{-/-}$ mice, BMMCs from WT, NTAL$^{+/-}$, or NTAL$^{-/-}$ mice were

obtained by growing BM cells for 4–8 wk in the presence of IL-3 and SCF. The cells expressed comparable amount of FcεRI (Fig. 2 B) and LAT (Fig. 2 C) and the expected amount of NTAL (Fig. 2 C). The cells were sensitized with TNP-specific IgE and activated with various doses of Ag. Data presented in Fig. 3 A indicate that FcεRI-mediated degranulation was significantly increased in NTAL$^{-/-}$ cells compared with NTAL$^{+/-}$ cells and WT cells, although the total amount of β-glucuronidase present in the cells was similar (not depicted). The most dramatic difference between WT and NTAL$^{-/-}$ cells was observed at suboptimal concentration of Ag (10 ng/ml). Under these conditions, the NTAL$^{-/-}$ cells released 40 ± 2% of the total β-glucuronidase (mean ± SD, n = 12) compared with a maximum of 22 ± 2% (n = 12) in WT cells. These data were confirmed in four independent BMMC isolates in each group. Even at optimal (100 ng/ml) and supraoptimal (500 and 1,000 ng/ml) doses of Ag, the response in NTAL$^{-/-}$ BMMCs was significantly higher. When the cells were stimulated with ionophore A23187, the differences between WT and NTAL$^{-/-}$ cells disappeared (not depicted), suggesting that NTAL affects early receptor-specific activation events which precede the calcium response.

An important feature of the degranulation process in mast cells is PS externalization (19). In nonstimulated cells, PS is found almost exclusively in the inner leaflet of the plasma membrane. FcεRI-dependent degranulation leads to an exposure of PS on the plasma membrane, detectable by binding of FITC-labeled annexin V to intact cells. Cytofluorometric analyses showed that the number of annexin V binding sites increased in WT cells with a maximum reached at 100 ng/ml (Fig. 3 C). Activated NTAL$^{-/-}$ cells exhibited higher PS externalization than activated WT cells, and again the most dramatic difference was observed at a suboptimal dose of Ag (10 ng/ml). As expected (19), no PS externalization in WT or NTAL$^{-/-}$ cells was observed in the absence of extracellular Ca^{2+} (not depicted).

Tyrosine Phosphorylation of LAT Is Enhanced in NTAL$^{-/-}$ BMMCs. Next we assessed the tyrosine phosphorylation of several proteins known to be involved in the initial stages of FcεRI signaling. When total lysates from Ag-activated cells were analyzed by immunoblotting with PY-20 mAb, the most significant difference between WT and NTAL$^{-/-}$ cells was the absence in NTAL$^{-/-}$ cells of a 30-kD phosphorylated protein corresponding in molecular weight to NTAL (Fig. 3 D). Furthermore, NTAL$^{-/-}$ cells exhibited an increased tyrosine phosphorylation of a 38-kD protein, corresponding to LAT (see end of this paragraph). If the IgE receptor was immunoprecipitated from control and Ag-activated cells, increased tyrosine phosphorylation of FcεRI β and γ subunits was observed in both WT and NTAL$^{-/-}$ cells after cell triggering, and no significant difference in the extent and/or dynamics of tyrosine phosphorylation was observed between these two groups (Fig. 4 A). Neither did the Syk kinase immunoprecipitated from the whole cell lysate exhibit any significant differences in amount, tyrosine phosphorylation, and kinase activity between WT and NTAL$^{-/-}$ cells (not depicted). However, when Syk was immunoprecipitated from cells first permeabilized with saponin in order to release free cytoplasmic components and then solubilized with Triton X-100, increased amounts of Syk and its phosphorylated form were precipitated from activated NTAL$^{-/-}$ cells relative to WT cells. This difference, which apparently reflects enhanced association of Syk with as yet unidentified plasma membrane component(s), was more pronounced at later stages (5 min) after FcεRI triggering (Fig. 4 B). The most dramatic difference observed in

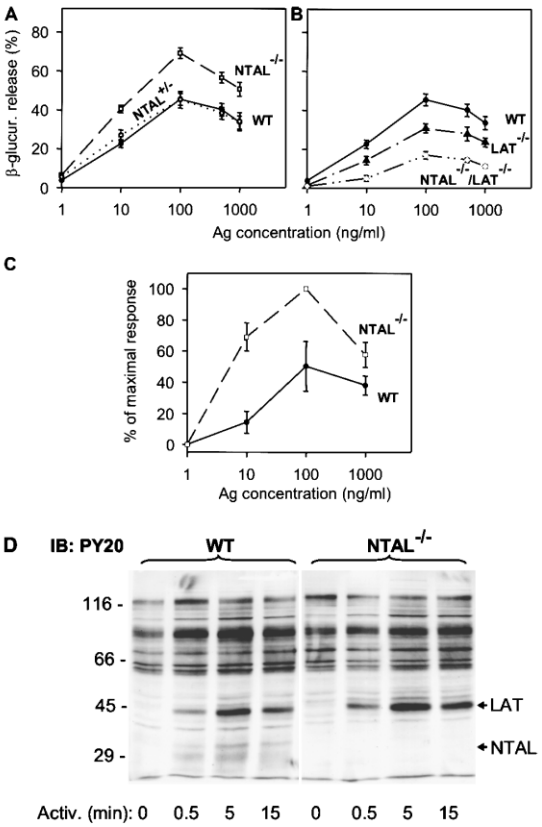

Figure 3. Enhanced degranulation, PS externalization, and tyrosine phosphorylation in NTAL$^{-/-}$ cells. BMMCs were sensitized with anti-TNP IgE (1 μg/ml) and then stimulated with Ag (TNP-BSA). (A and B) β-Glucuronidase released into supernatant from cells stimulated for 30 min with various concentrations of Ag. Data represent mean ± SD (n = 12 for WT and NTAL$^{-/-}$ cells; n = 4 for NTAL$^{+/-}$ cells; n = 6 for LAT$^{-/-}$ and NTAL$^{-/-}$/LAT$^{-/-}$ cells). (C) Externalization of PS in WT and NTAL$^{-/-}$ BMMCs stimulated for 30 min with various concentrations of Ag was determined by flow cytometry after surface staining of the cells with FITC-labeled annexin V. Data were normalized to maximal values in each assay and represent means ± SD (n = 3). (D) Cells were activated with 100 ng/ml TNP-BSA for the indicated time intervals, solubilized in 1% NP-40 and 1% n-dodecyl-β-D-maltoside, and the postnuclear supernatants were size fractionated by SDS-PAGE. The extent of tyrosine phosphorylation was determined by immunoblotting with PY-20–HRP conjugate. Positions of molecular weight standards, LAT and NTAL, are indicated on the left and right, respectively. A typical experiment from three performed is shown.

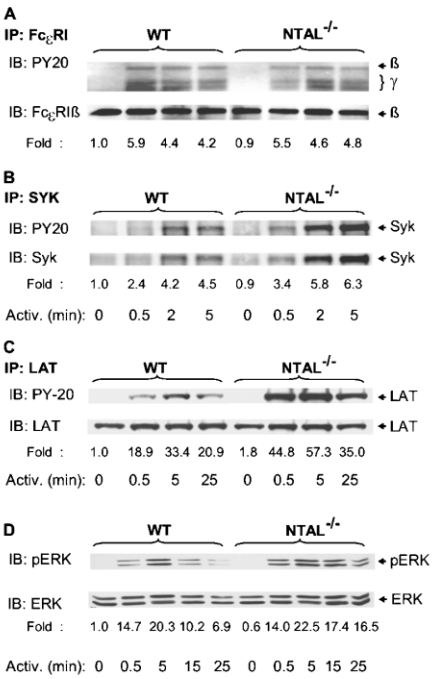

Figure 4. Tyrosine phosphorylation of FcεRI, Syk, LAT, and ERK. BMMCs from WT and NTAL$^{-/-}$ cells were sensitized with anti-TNP IgE and stimulated with TNP-BSA (100 ng/ml) for the indicated time intervals. The cells were solubilized in lysis buffer containing 0.2% Triton X-100 (A), 1% NP-40, and 1% *n*-dodecyl-β-D-maltoside (C and D) or by sequential treatment with 0.1% saponin and 1% Triton X-100 (B). FcεRI (A), Syk (B), and LAT (C) were immunoprecipitated (IP) from postnuclear supernatants with the corresponding antibodies. The immunoprecipitates were resolved by SDS-PAGE and analyzed by immunoblotting using PY-20–HRP conjugate (top). After stripping, the same membranes were reblotted with protein-specific antibodies (bottom). Phosphorylated ERK (pERK) and ERK were determined by immunoblotting in size-fractionated whole cell lysates using anti-pERK antibody, followed by stripping and immunoblotting with ERK-specific antibody (D). Fold inductions of protein tyrosine phosphorylation, normalized to nonactivated WT cells and corrected for the amount of the protein in each immunoprecipitate, are also indicated. A typical result from two to four experiments performed is presented.

NTAL$^{-/-}$ cells was an increased tyrosine phosphorylation of LAT at all time intervals analyzed (0.5–25 min; Fig. 4 C). It should be noted, however, that we were unable to coimmunoprecipitate Syk with LAT from either activated WT or NTAL$^{-/-}$ cells.

Next we examined whether NTAL is involved in FcεRI-mediated Ras–MAP kinase signaling pathway. Activation of MAP kinases was detected in total cellular lysates by immunoblotting with anti–phospho-ERK. Data in Fig. 4 D show that FcεRI-mediated tyrosine phosphorylation of the ERK was comparable in WT and NTAL$^{-/-}$ cell at early time intervals (0.5 and 5 min), but in NTAL$^{-/-}$ cells it exhibited a slower decline at later stages of activation (15 and 25 min).

NTAL Negatively Regulates the PI3K Activity. Early biochemical events in FcεRI-activated mast cells are dependent on the activity of PI3K, which functionally interacts with Gab2 and several other signaling proteins (26, 27). Therefore, we monitored the subcellular distribution and enzymatic activity of PI3K in WT and NTAL$^{-/-}$ BMMCs. PI3K was immunoprecipitated from saponin/Triton X-100–solubilized cells, and its amount was quantified by immu-

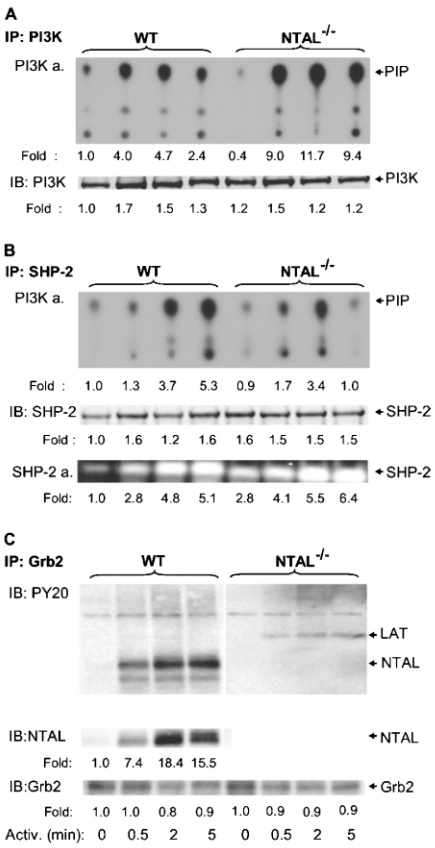

Figure 5. PI3K, SHP-2, and Grb2 immunocomplexes. BMMCs from WT and NTAL$^{-/-}$ mice were activated with TNP-BSA (100 ng/ml) for the indicated time intervals, solubilized with saponin/Triton X-100, and PI3K, SHP-2, and Grb2 immunocomplexes were isolated by immunoprecipitation with the corresponding antibodies. (A) PI3K immunoprecipitates were analyzed for (a) PI3K activity (PI3K a.) using PI as a substrate and TLC (position of [^{32}P]PI [PIP] is indicated by arrow) and (b) the amount of immunoprecipitated PI3K by immunoblotting with anti–PI3K-p85. (B) SHP-2 immunoprecipitates were analyzed for (a) SHP-2–associated PI3K activity by PI3K assay, (b) the amount of SHP-2 by immunoblotting with anti–SHP-2 antibody, and (c) SHP-2 enzymatic activity by in-gel phosphatase assay (SHP-2 a.). (C) Grb2 immunoprecipitates were analyzed by immunoblotting for the presence of tyrosine-phosphorylated proteins, NTAL and Grb2. Relative amounts of the immunoprecipitated proteins, their tyrosine phosphorylations, and/or enzymatic activities were normalized to nonactivated WT cells. Representative data from two to four experiments performed are shown.

noblotting. Enzymatic activity of PI3K in the immune complexes was determined using PI as a substrate, and the expected product [^{32}P]PI (PIP) was detected by autoradiography. Similar to a previous study performed with RBL-2H3 cells (23), we observed an activation-induced increase in recovery of PI3K from saponin-permeabilized WT BMMCs (Fig. 5 A), consistent with translocation of PI3K to the plasma membrane. The changes in the distribution of PI3K were accompanied by an enhanced PI3K enzymatic activity with peak at 2 min after FcεRI triggering. In nonactivated NTAL$^{-/-}$ cells, the enzymatic activity of PI3K was slightly lower than in WT cells. However, 0.5 min after FcεRI triggering the PI3K activity was 2.5-fold higher in NTAL$^{-/-}$ and remained higher at all time intervals analyzed.

One of the proteins interacting with PI3K is the ubiquitously expressed nonreceptor tyrosine phosphatase SHP-2 (28). Because SHP-2 regulates PI3K activity (29), we further compared the SHP-2–associated PI3K activity in WT and NTAL$^{-/-}$ cells. SHP-2 was immunoprecipitated from saponin/Triton X-100–solubilized cells, and the enzymatic activity of SHP-2–coprecipitated PI3K was determined. Data presented in Fig. 5 B show that PI3K enzymatic activity was elevated after FcεRI triggering in both WT and NTAL$^{-/-}$ cells but was more rapidly down-regulated in NTAL$^{-/-}$ cells at later time intervals (5 min). Total enzymatic activity of SHP-2 phosphatase, as detected by in-gel assay, was higher in nonactivated NTAL$^{-/-}$ than in WT cells (2.8 ± 0.3-fold increase, $n = 3$) and remained higher after FcεRI triggering at all time intervals analyzed.

NTAL Is a Major Tyrosine Phosphorylated Target of Grb2. 5 of the total 10 consensus tyrosine phosphorylation sites in NTAL, and in LAT, are of the YXN type (where X is any amino acid), and are thus potential binding sites for the SH2 domain of the cytoplasmic adaptor Grb2. Anti-NTAL immunoblotting of Grb2 immunoprecipitates showed an enhanced association of NTAL and Grb2 after FcεRI engagement in WT BMMCs (Fig. 5 C). Among the tyrosine-phosphorylated proteins in activated WT cells, NTAL was a major Grb2 target, as determined by PY-20 immunoblotting. Interestingly, more tyrosine-phosphorylated protein of 38 kD, presumably LAT, was bound to Grb2 in NTAL$^{-/-}$ cells compared with WT cells.

Enhanced PLCγ Activity and Calcium Response in NTAL$^{-/-}$ BMMCs. The observed increase in tyrosine phosphorylation of LAT implied elevated levels of PLCγ activity in NTAL$^{-/-}$ cells, and we therefore evaluated the properties of immunoisolated PLCγ. Data presented in Fig. 6 A indicate that tyrosine phosphorylation of PLCγ1 was indeed enhanced; 2 and 5 min after Ag triggering the enhancement was, respectively, 4.8- and 4-fold higher in NTAL$^{-/-}$ cells than in WT cells. Tyrosine phosphorylation of PLCγ2 isolated from NTAL$^{-/-}$ cells was also enhanced (Fig. 6 B). Next, we analyzed the PLCγ enzymatic activity. PLCγ2 was immunoprecipitated, and its enzymatic activity, resulting in the production of [^{3}H]IP3 from P[^{3}H]IP2 substrate, was determined. As shown in Fig. 6 C, PLCγ activity in FcεRI-activated cells was significantly higher in NTAL$^{-/-}$ cells than in WT cells. The enhanced PLCγ activity in NTAL$^{-/-}$ cells resulted in higher accumulation of IP3, the critical PLCγ metabolite (Fig. 6 D).

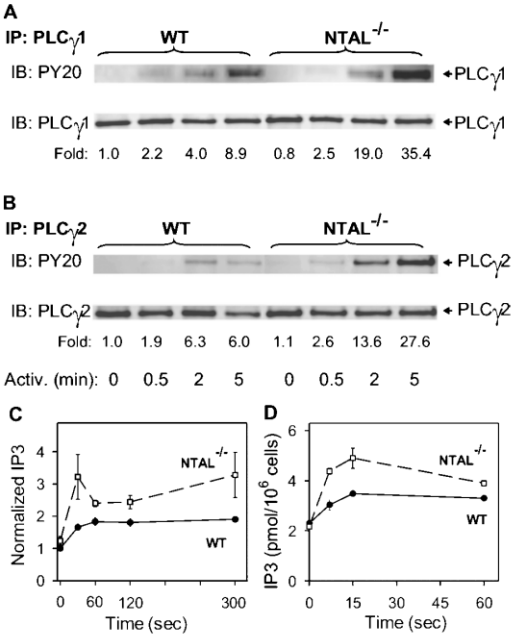

Figure 6. Tyrosine phosphorylation and enzymatic activity of PLCγ. BMMCs from WT and NTAL$^{-/-}$ mice were activated for the indicated time intervals with TNP-BSA (100 ng/ml). (A and B) The cells were solubilized with saponin/Triton X-100, and PLCγ1 (A) and PLCγ2 (B) were immunoprecipitated and analyzed by immunoblotting using phosphotyrosine-specific PY-20–HRP conjugate (top). Subsequently, after stripping the same membranes were reblotted with anti-PLCγ1 (A) and anti-PLCγ2 (B) (bottom). Representative data from two experiments performed are shown. (C) The cells were lysed in 1% Triton X-100, and enzymatic activity of the immunoprecipitated PLCγ2 was measured by immune complex PLCγ assay; the data were normalized to nonactivated WT cells. (D) IP3 levels were determined by ^{3}H-radioreceptor assay kit as described in Materials and Methods. Data in C and D represent means ± SD ($n = 3$–4).

Since an enhanced activity of PLCγ and production of IP3 are prerequisites for FcεRI-mediated calcium responses, we also estimated the $[Ca^{2+}]_i$ in WT and NTAL$^{-/-}$ cells. After an exposure of IgE-sensitized and Fura-2–loaded cells to low concentrations of Ag (5 or 10 ng/ml) in the presence of extracellular Ca^{2+}, only a small increase in $[Ca^{2+}]_i$ was observed in WT cells, whereas the response was markedly enhanced in NTAL$^{-/-}$ cells (Fig. 7, A and B). At a higher concentration of Ag (100 ng/ml), the difference between WT and NTAL$^{-/-}$ cells was less dramatic, due to enhanced calcium response in WT cells but remained significant (Fig. 7 C). An elevated calcium response was also observed in NTAL$^{-/-}$ cells activated in the absence of extracellular Ca^{2+} (Fig. 7 D).

FcεRI-mediated increase in $[Ca^{2+}]_i$ in the presence of extracellular Ca^{2+} reflects not only a transient release of in-

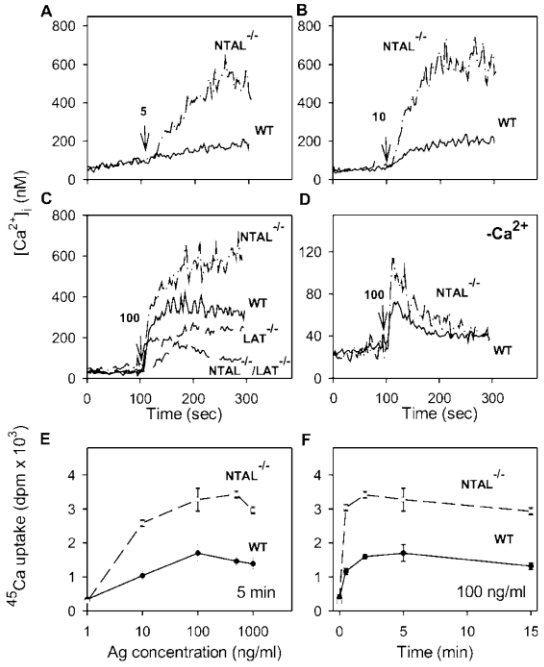

Figure 7. Ca^{2+} mobilization and extracellular ^{45}Ca uptake. (A–D) IgE-sensitized BMMCs were loaded with Fura-2-AM and stimulated with various concentrations of TNP-BSA (5 ng/ml [A], 10 ng/ml [B], or 100 ng/ml [C and D]) added at the time point indicated by arrows, in the presence (A–C) or absence (D) of 1.0 mM extracellular Ca^{2+}. The Ca^{2+} mobilization was monitored by spectrofluorometry in WT and $NTAL^{-/-}$ (A–D) and at a single concentration of TNP-BSA (100 ng/ml) also in $LAT^{-/-}$ and $NTAL^{-/-}/LAT^{-/-}$ (C) BMMCs. Representative data from at least three to five experiments are shown. (E and F) Uptake of calcium from extracellular medium was measured in IgE-sensitized WT and $NTAL^{-/-}$ cells activated in the presence of extracellular $^{45}Ca^{2+}$ (1 mM) for 5 min with various concentrations of TNP-BSA (E) or activated with 100 ng/ml of TNP-BSA for various time intervals (F). Data in E and F represent means ± SD (n = 3–6).

tracellularly stored Ca^{2+} but also a more sustained influx of Ca^{2+} from the extracellular medium through incompletely characterized store-operated channels in the plasma membrane (30). To determine whether NTAL has any effect on the influx of extracellular Ca^{2+}, we measured the uptake of ^{45}Ca from the extracellular medium. In nonactivated cells, the uptake of ^{45}Ca was low and there was no difference between WT and $NTAL^{-/-}$ cells. When the cells were exposed to increasing concentrations of TNP-BSA, the ^{45}Ca uptake rose in WT cells and even more so in $NTAL^{-/-}$ cells. The enhancement of ^{45}Ca uptake in $NTAL^{-/-}$ cells was observed at all concentrations of Ag used (up to 1 μg/ml; Fig. 7 E) and at all time intervals analyzed (up to 15 min; Fig. 7 F).

Impaired Secretory and Calcium Responses in $NTAL^{-/-}/LAT^{-/-}$ BMMCs. Although LAT and NTAL are structurally similar adaptor molecules, their absence has dramatically different consequences on FcεRI-mediated events in BMMCs. In $LAT^{-/-}$ cells, the secretory and Ca^{2+} responses are partially inhibited (7), whereas in $NTAL^{-/-}$ the same responses are potentiated (see Figs. 3–7). To determine the properties of cells defective simultaneously in both these adaptor proteins, we prepared $NTAL^{-/-}/LAT^{-/-}$ mice and examined their BMMCs. When the cells were solubilized and analyzed by immunoblotting, no proteins reactive with anti-NTAL– and anti-LAT–specific Abs were detected (not depicted). The $NTAL^{-/-}/LAT^{-/-}$ BMMCs differed from the cells expressing both adaptor proteins neither in their growth properties nor in their expression of surface FcεRI. Data presented in Fig. 3 B indicate that $NTAL^{-/-}/LAT^{-/-}$ cells exhibited lower secretory response than $LAT^{-/-}$ cells. Similarly, calcium response in $NTAL^{-/-}/LAT^{-/-}$ cells was lower than in $LAT^{-/-}$ cells (Fig. 7 C). It should be noted that although they were dramatically reduced, the secretory and calcium responses were not completely inhibited. Furthermore, there was no significant difference in degranulation and calcium responses induced by the ionophore A23187 in WT, $LAT^{-/-}$, and $NTAL^{-/-}/LAT^{-/-}$ BMMCs (not depicted), demonstrating that degranulation itself does not depend on the presence of these linker proteins.

Different Membrane Topography of NTAL and LAT in Resting and Activated Cells. Both NTAL and LAT partition into lipid rafts, as can be inferred from their detergent resistance and association with buoyant density fractions of sucrose gradient (2). However, a direct comparison of the distribution of these two adaptors in sucrose gradients has not been reported. Data presented in Fig. 8 indicate that in WT cells both LAT and NTAL are located predominantly in low density fractions of sucrose gradient (fractions 1–4). In Ag-activated cells, the amount of LAT in these fractions was decreased, and tyrosine-phosphorylated LAT was found

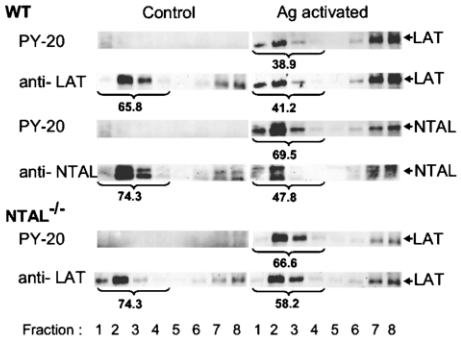

Figure 8. Distribution of NTAL and LAT in sucrose gradients. BMMCs from WT or $NTAL^{-/-}$ mice were sensitized with TNP-specific IgE and activated or not with TNP-BSA (100 ng/ml) for 5 min. The cells were solubilized in a lysis buffer containing 1% Brij 96, and the whole cell lysates were fractionated by sucrose density gradient ultracentrifugation. Individual fractions were collected and analyzed by immunoblotting for the presence of NTAL and LAT and their phosphorylated forms (PY-20). Percentage of NTAL and LAT and their phosphorylated forms in low density fractions (fraction 1–4) is indicated by numbers under fractions.

predominantly in high density fractions. Although the amount of NTAL in low density fractions also decreased in activated cells (from 74.3 to 47.8%), most of the tyrosine-phosphorylated NTAL was found in lipid rafts fractions (69.5%). Compared with WT cells, NTAL$^{-/-}$ cells exhibited higher amount of LAT in low density fractions in both nonactivated and activated cells. This difference was even more pronounced when the distribution of tyrosine-phosphorylated LAT was analyzed (38.9 versus 66.6%). These data suggested that at least a fraction of LAT and NTAL could associate with different lipid-containing structures in plasma membrane.

To throw more light on the topography of LAT and NTAL, we isolated membrane sheets from an adherent mast cell line, RBL-2H3, which also possesses the two adaptor proteins (unpublished data), and analyzed their topography by immunogold electron microscopy. In resting cells, both NTAL and LAT were found in small clusters that distributed independently of FcεRI β subunits (Fig. 9, A and C). Based on the Hopkins test, these clusters were significantly different from random patterns. After FcεRI aggregation, the FcεRI β subunits accumulated predominantly in osmiophilic regions of the plasma membrane, thus confirming previously published data (24, 31). Clusters of both NTAL and LAT were often found in the vicinity of aggregated FcεRI, without forming mixed aggregates with them (Fig. 9, B and D).

Finally, we attempted to find out whether NTAL and LAT form mixed aggregates before and/or after FcεRI aggregation. To this end, we double labeled membrane sheets for LAT and NTAL, using combinations of 5- and 10-nm gold particles (Fig. 10). The labeling with 5-nm gold particles was consistently more abundant, regardless of whether the target was LAT or NTAL. This difference reflects technical aspects of the assay, since smaller gold particles more efficiently label target molecules than large gold particles. In nonactivated cells, LAT and NTAL each formed small clusters which did not mix. The visual observations that LAT and NTAL fail to mix were confirmed using the Ripley's statistical test (not depicted). Importantly, clusters of these transmembrane adaptors can often be seen in or near osmiophilic patches of activated membranes, but again no mixing of NTAL and LAT molecules was observed. Thus, NTAL and LAT are located in distinct, nonoverlapping regions of the plasma membrane in both nonactivated and activated cells.

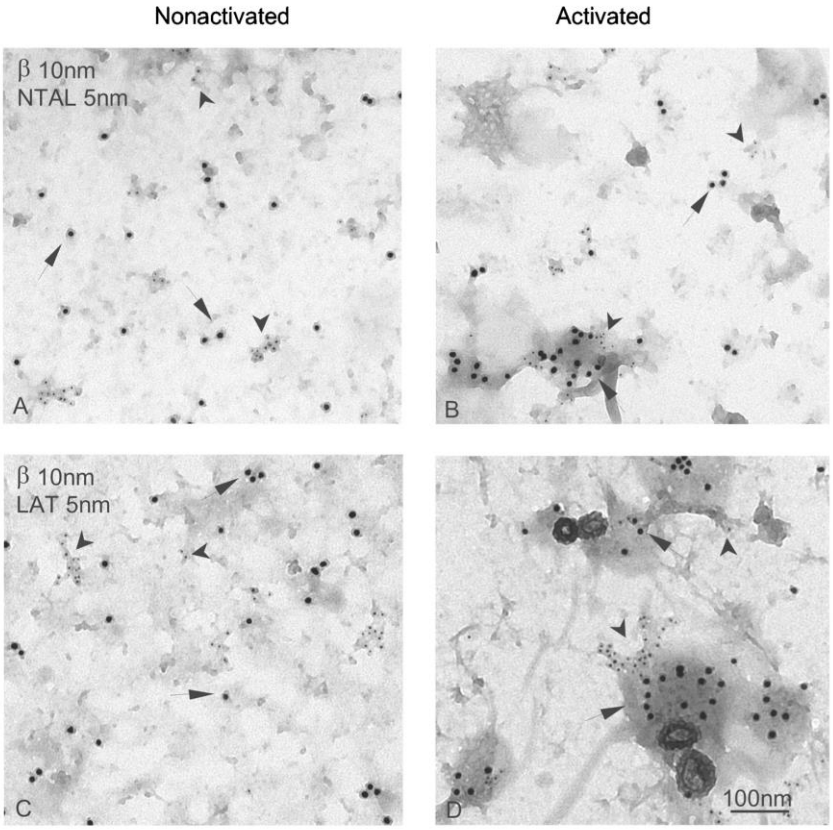

Figure 9. Membrane topography of NTAL, LAT, and FcεRI β subunit in nonactivated and Ag-activated cells. Membrane sheets were prepared from IgE-sensitized RBL-2H3 cells exposed for 2 min to PBS alone (A and C) or DNP-BSA in PBS (1 μg/ml; B and D), and double labeled from the cytoplasmic side of the plasma membrane for FcεRI β subunit (10-nm gold particles, arrows; A–D), NTAL (5-nm gold particles, arrowheads; A and B), or LAT (5-nm gold particles, arrowheads; C and D).

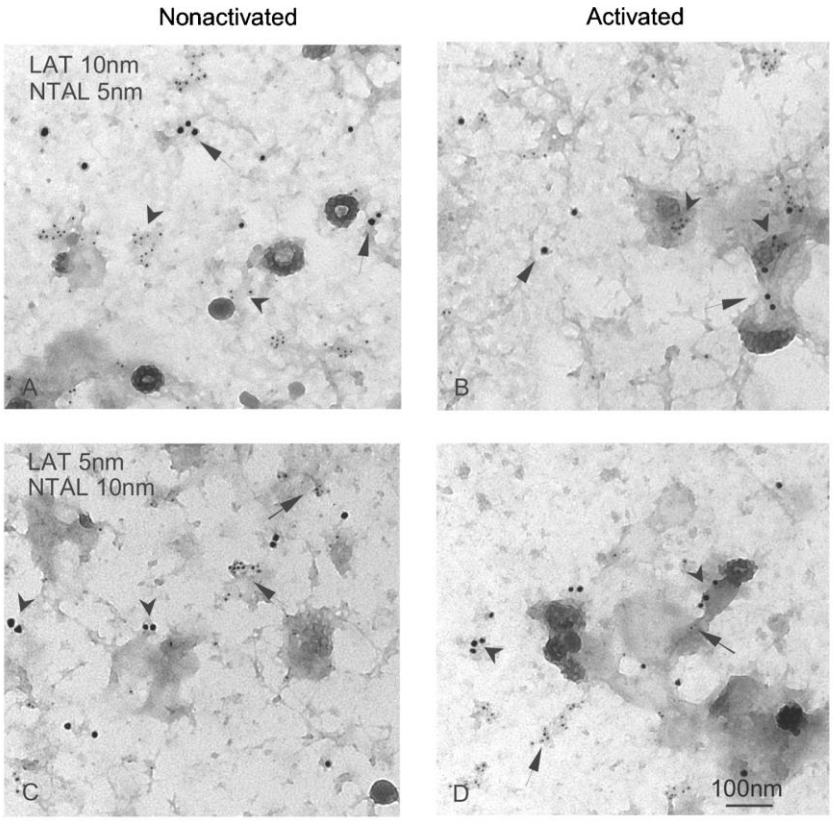

Figure 10. Different localization of NTAL and LAT clusters. Membrane sheets were prepared from nonactivated (A and C) and DNP-BSA–activated (1 μg/ml; B and D) RBL-2H3 cells and double-labeled from the inside for LAT (arrows), marked with 10-nm (A and B) or 5-nm (C and D) gold particles, and NTAL (arrowheads) marked with 5-nm (A and B) or 10-nm (C and D) gold particles.

Discussion

The structural similarity of NTAL and LAT suggested that those two proteins could have similar functions. This notion was supported by their expression pattern. Whereas NTAL is expressed in B cells, which lack LAT, the reverse is true for LAT. Studies with LAT-deficient mice revealed a complete block in T cell development (17, 32), and LAT-negative T cell lines showed a complete block in TCR signaling (33, 34). Importantly, transfection of NTAL into LAT-deficient cells or mice partially restored the defects (2, 3, 5). Mast cells express both these proteins, and LAT deficiency had no effect either on mast cell development in vivo or maturation of mast cells in vitro (7). However, BMMCs from $LAT^{-/-}$ mice exhibited defects in pathways known to be downstream of Lyn and Syk kinase activation. These included FcεRI-mediated tyrosine phosphorylation of PLCγ, production of IP3, release of Ca^{2+} from internal stores, and degranulation. Importantly, though the mast cell effector functions were impaired, they were not completely inhibited (7). These data together with enhanced tyrosine phosphorylation of NTAL in FcεRI-activated mast cells (2) and normal development of $NTAL^{-/-}$ mast cells under in vivo and in vitro conditions (this study) suggested that NTAL could be the missing adaptor protein responsible for the remaining signaling activity noted in LAT-deficient cells. However, several lines of evidence presented in this study indicate that NTAL, unlike LAT, has a negative regulatory role in FcεRI-mediated activation in mouse mast cells. First, $NTAL^{-/-}$ mice compared with WT mice exhibited an enhanced passive anaphylactic response. This systemic reaction reflects the activity of mast cells and was found reduced in $LAT^{-/-}$ cells (7). Second, BMMCs from $NTAL^{-/-}$ mice exhibited an enhanced degranulation. Third, several proteins in FcεRI-activated $NTAL^{-/-}$ cells exhibited an enhanced tyrosine phosphorylation and/or modified subcellular distribution. These proteins included Syk kinase, LAT, ERK, and PLCγ. Fourth, FcεRI-activated $NTAL^{-/-}$ cells exhibited an enhanced activity of PLCγ and PI3K, producing increased levels of IP3 and PI 3,4,5-trisphosphate, respectively. Finally, $NTAL^{-/-}$ phenotype was associated with a dramatic increase in calcium response in Ag-activated cells. This enhancement was mostly pronounced at suboptimal concentrations of the Ag and was observed even in the absence of extracellular calcium, suggesting that the enhanced release of calcium from intracellular stores contributes at least in part to this phenomenon. Thus, the conclusion based on our data seems to indicate that FcεRI-

mediated signaling events in BMMCs are negatively regulated by NTAL.

How could NTAL be involved in negative regulation of PLCγ and downstream signaling pathways? We propose that the inhibitory role of NTAL could result from its competition with LAT in lipid rafts. Furthermore, it should be noted that a major difference between LAT and NTAL is in the absence of the tyrosine residue responsible for interaction with PLCγ in the latter. In the absence of NTAL, more LAT is located in lipid rafts (Fig. 8) and is tyrosine phosphorylated (Fig. 4 C), resulting in (a) an increased recruitment of PLCγ into complexes formed around aggregated FcεRI, (b) enhanced tyrosine phosphorylation and enzymatic activities of PLCγ, (c) elevated production of IP3 and $[Ca^{2+}]_i$, and (d) more potent degranulation. Alternatively, NTAL could have a negative regulatory role in FcεRI signaling by indirect binding of phosphatases. In T cells, TCR ligation induces binding of Grb2 with SHP-2, and this interaction presumably brings the phosphatase into juxtaposition to its potential substrates (35). In stimulated mast cells, phosphorylated NTAL is a major binder of Grb2 (Fig. 5 C), and therefore, it is possible that in the absence of NTAL Grb2–phosphatase complexes are not properly targeted, and down-regulating signaling pathways are less effective. It should be mentioned that these two hypotheses are not mutually exclusive: in the absence of NTAL, more tyrosine-phosphorylated LAT in lipid rafts (Fig. 8) could better serve as a substrate for signaling molecules, and at the same time the signaling molecules could be more active due to the absence on NTAL-bound protein tyrosine phosphatases.

Our experiments with BMMCs defective in both adaptor proteins, NTAL and LAT, surprisingly reveal that NTAL, besides its negative regulatory role, may potentially also have a positive role in FcεRI signaling. Clearly, NTAL in the absence of LAT cannot play the above described inhibitory (competitive) role and it may take over, albeit with lower efficiency, some of the functions of LAT, just as it was observed in T cells (2, 3, 5). Which of these two functions would prevail could possibly depend on qualitative and/or quantitative differences in the composition of the signaling assemblies induced by FcεRI aggregation. These differences could explain why a diminution of NTAL expression by silencing RNA oligonucleotides in human mast cells resulted in an opposite phenotype (reduction of FcεRI-mediated secretory and calcium responses [6]) compared with that observed in $NTAL^{-/-}$ BMMCs (this study). In this context, it should be noted that profiles of tyrosine-phosphorylated proteins in human and mouse mast cells are very different (6). Furthermore, the influence of different tissue origins and cell culture conditions used for growth of human and mouse mast cells could also play a role.

Mast cell degranulation involves two signaling pathways proximal to FcεRI. Lyn-dependent pathway, which involves transmembrane adaptor LAT, serves as both kinetic accelerator and negative regulator of signaling, whereas Fyn-dependent pathway is essential for degranulation (8). Experiments with human mast cells suggested that NTAL could represent the transmembrane adaptor involved in the Fyn-dependent pathway (6). However, our findings that NTAL in mouse BMMCs is not essential for degranulation (Fig. 3) and that tyrosine phosphorylation of NTAL is not dependent on Fyn kinase activity but at least partially depends on Lyn kinase activity (unpublished data) suggest that NTAL is not involved in the Fyn-dependent pathway. Rather, NTAL could contribute in part to the complexity of Lyn-dependent regulatory mechanisms of mast cell signaling.

Although both NTAL and LAT are structurally similar molecules partitioning into lipid rafts in detergent-solubilized cells, a detailed analysis of their distribution on sucrose gradients indicate that they differ in physical properties, particularly in activated cells. Thus, ~60% of tyrosine-phosphorylated LAT was found in high density fractions of sucrose gradient, whereas a larger fraction (~70%) of phosphorylated NTAL was found in low density fractions (Fig. 8). These data suggest that the two molecules do not occupy the same regions of the plasma membrane. This was confirmed by electron microscopy analysis on membrane sheets. Previously, it has been shown that LAT in resting cells is found in clusters which do not mix with dispersed clusters of FcεRI β subunits (24, 31). We have confirmed these results and demonstrated that NTAL was also found in clusters that were similar in size to LAT clusters. Interestingly, NTAL clusters were topographically separated from LAT clusters. Aggregation of FcεRI induced a redistribution of the receptor into distinct areas of the plasma membrane that are characterized by their dark staining with osmium, proximity of clathrin-coated pits, and accumulation of several signaling molecules (24, 31). Although NTAL and LAT were often found in the vicinity of these aggregates, they did not form mixed aggregates.

In conclusion, our data indicate that at least in murine mast cells, NTAL mostly negatively regulates the activation through FcεRI. Therefore, it can be speculated that the absence, reduced expression, or mutations in this adaptor protein might be a contributing factor in an increased sensitivity to allergens.

We thank H. Mrázová, D. Lorenčíková, and M. Dráber for technical assistance, and Dr. J. Rivera for kindly providing the FcεRI β chain–specific antibody.

This work was supported by project LN00A026 (Center of Molecular and Cellular Immunology) from the Ministry of Education, Youth and Sports of the Czech Republic, grants 204/03/0594 and 301/03/0596 from the Grant Agency of the Czech Republic, and grant A5052310 from the Grant Agency of the Academy of Sciences of the Czech Republic. The generation of NTAL-deficient mice was supported by Institut National de la Santé et de la Recherche Médicale, Centre National de la Recherche Scientifique, and Plate-forme Rassemblement Inter Organismes. The research of P. Heneberg was supported in part by Research goal no. 002 from the 3rd Faculty of Medicine, Charles University, Prague, and the research of P. Dráber was supported by an International Research Scholar's Award from Howard Hughes Medical Institute.

The authors have no conflicting financial interests.

Submitted: 18 June 2004
Accepted: 31 August 2004

References

1. Kinet, J.P. 1999. The high-affinity IgE receptor (FcεRI): from physiology to pathology. *Annu. Rev. Immunol.* 17:931–972.
2. Brdička, T., M. Imrich, P. Angelisová, N. Brdičková, O. Horváth, J. Špička, I. Hilgert, P. Lusková, P. Dráber, P. Novák, et al. 2002. Non-T cell activation linker (NTAL): a transmembrane adaptor protein involved in immunoreceptor signaling. *J. Exp. Med.* 196:1617–1626.
3. Janssen, E., M. Zhu, W. Zhang, S. Koonpaew, and W. Zhang. 2003. LAB: a new membrane-associated adaptor molecule in B cell activation. *Nat. Immunol.* 4:117–123.
4. Harder, T., and K.R. Engelhardt. 2004. Membrane domains in lymphocytes—from lipid rafts to protein scaffolds. *Traffic.* 5:265–275.
5. Janssen, E., M. Zhu, B. Craven, and W. Zhang. 2004. Linker for activation of B cells: a functional equivalent of a mutant linker for activation of T cells deficient in phospholipase C-γ1 binding. *J. Immunol.* 172:6810–6819.
6. Tkaczyk, C., V. Horejsi, I. Shoko, P. Draber, L.E. Samelson, A.B. Satterthwaite, D.H. Nahm, D.D. Metcalfe, and A.M. Gilfillan. 2004. NTAL phosphorylation is a pivotal link between the signaling cascades leading to human mast cell degranulation following kit activation and FcεRI aggregation. *Blood.* 104:207–214.
7. Saitoh, S., R. Arudchandran, T.S. Manetz, W. Zhang, C.L. Sommers, P.E. Love, J. Rivera, and L.E. Samelson. 2000. LAT is essential for FcεRI-mediated mast cell activation. *Immunity.* 12:525–535.
8. Parravicini, V., M. Gadina, M. Kovarova, S. Odom, C. Gonzalez-Espinosa, Y. Furumoto, S. Saitoh, L.E. Samelson, J.J. O'Shea, and J. Rivera. 2002. Fyn kinase initiates complementary signals required for IgE-dependent mast cell degranulation. *Nat. Immunol.* 3:741–748.
9. Tolar, P., L. Dráberová, and P. Dráber. 1997. Protein tyrosine kinase Syk is involved in Thy-1 signaling in rat basophilic leukemia cells. *Eur. J. Immunol.* 27:3389–3397.
10. Tolar, P., M. Tumová, and P. Dráber. 2001. New monoclonal antibodies recognizing the adaptor protein LAT. *Folia Biol. (Praha).* 47:215–217.
11. Rivera, J., J.-P. Kinet, J. Kim, C. Pucillo, and H. Metzger. 1988. Studies with a monoclonal antibody to the β subunit of the receptor with high affinity for immunoglobulin E. *Mol. Immunol.* 25:647–661.
12. Rudolph, A.K., P.D. Burrows, and M.R. Wabl. 1981. Thirteen hybridomas secreting hapten-specific immunoglobulin E from mice with Ig^a or Ig^b heavy chain haplotype. *Eur. J. Immunol.* 11:527–529.
13. Liu, F.-T., J.W. Bohn, E.L. Ferry, H. Yamanoto, C.A. Molinaro, L.A. Sherman, N.R. Klinman, and D.H. Katz. 1980. Monoclonal dinitrophenyl-specific murine IgE antibody: preparation, isolation, and characterization. *J. Immunol.* 124:2728–2737.
14. Kovářová, M., P. Tolar, R. Arudchandran, L. Dráberová, J. Rivera, and P. Dráber. 2001. Structure-function analysis of Lyn kinase association with lipid rafts and initiation of early signaling events after Fcε receptor I aggregation. *Mol. Cell. Biol.* 21:8318–8328.
15. Kress, C., S. Vandormael-Pournin, P. Baldacci, M. Cohen-Tannoudji, and C. Babinet. 1998. Nonpermissiveness for mouse embryonic stem (ES) cell derivation circumvented by a single backcross to 129/Sv strain: establishment of ES cell lines bearing the Omd conditional lethal mutation. *Mamm. Genome.* 9:998–1001.
16. Schwenk, F., U. Baron, and K. Rajewsky. 1995. A cre-transgenic mouse strain for the ubiquitous deletion of loxP-flanked gene segments including deletion in germ cells. *Nudeic Acids Res.* 23:5080–5081.
17. Nunez-Cruz, S., E. Aguado, S. Richelme, B. Chetaille, A.M. Mura, M. Richelme, L. Pouyet, E. Jouvin-Marche, L. Xerri, B. Malissen, and M. Malissen. 2003. LAT regulates $\gamma\delta$ T cell homeostasis and differentiation. *Nat. Immunol.* 4:999–1008.
18. Yamaguchi, M., C.S. Lantz, H.C. Oettgen, I.M. Katona, T. Fleming, I. Miyajima, J.P. Kinet, and S.J. Galli. 1997. IgE enhances mouse mast cell FcεRI expression in vitro and in vivo: evidence for a novel amplification mechanism in IgE-dependent reactions. *J. Exp. Med.* 185:663–672.
19. Demo, S.D., E. Masuda, A.B. Rossi, B.T. Throndset, A.L. Gerard, E.H. Chan, R.J. Armstrong, B.P. Fox, J.B. Lorens, D.G. Payan, et al. 1999. Quantitative measurement of mast cell degranulation using a novel flow cytometric annexin-V binding assay. *Cytometry.* 36:340–348.
20. Surviladze, Z., L. Dráberová, M. Kovářová, M. Boubelík, and P. Dráber. 2001. Differential sensitivity to acute cholesterol lowering of activation mediated via the high-affinity IgE receptor and Thy-1 glycoprotein. *Eur. J. Immunol.* 31: 1–10.
21. Dráberová, L., L. Dudková, M. Boubelík, H. Tolarová, F. Šmíd, and P. Dráber. 2003. Exogenous administration of gangliosides inhibits FcεRI-mediated mast cell degranulation by decreasing the activity of phospholipase Cγ. *J. Immunol.* 171:3585–3593.
22. Dráberová, L. 1990. Cyclosporin A inhibits rat mast cell activation. *Eur. J. Immunol.* 20:1469–1473.
23. Tolarová, H., L. Dráberová, P. Heneberg, and P. Dráber. 2004. Involvement of filamentous actin in setting the threshold for degranulation in mast cells. *Eur. J. Immunol.* 34:1627–1636.
24. Wilson, B.S., J.R. Pfeiffer, and J.M. Oliver. 2000. Observing FcεRI signaling from the inside of the mast cell membrane. *J. Cell Biol.* 149:1131–1142.
25. Wilson, B.S., S.L. Steinberg, K. Liederman, J.R. Pfeiffer, Z. Surviladze, J. Zhang, L.E. Samelson, L.H. Yang, P.G. Kotula, and J.M. Oliver. 2004. Markers for detergent-resistant lipid rafts occupy distinct and dynamic domains in native membranes. *Mol. Biol. Cell.* 15:2580–2592.
26. Gu, H., K. Saito, L.D. Klaman, J. Shen, T. Fleming, Y. Wang, J.C. Pratt, G. Lin, B. Lim, J.-P. Kinet, and B.G. Neel. 2001. Essential role for Gab2 in the allergic response. *Nature.* 412:186–190.
27. Xie, Z.H., I. Ambudkar, and R.P. Siraganian. 2002. The adapter molecule Gab2 regulates FcεRI-mediated signal transduction in mast cells. *J. Immunol.* 168:4682–4691.
28. Wu, C.J., D.M. O'Rourke, G.S. Feng, G.R. Johnson, Q. Wang, and M.I. Greene. 2001. The tyrosine phosphatase SHP-2 is required for mediating phosphatidylinositol 3-kinase/Akt activation by growth factors. *Oncogene.* 20:6018–6025.
29. Zhang, S.Q., W.G. Tsiaras, T. Araki, G. Wen, L. Minichiello, R. Klein, and B.G. Neel. 2002. Receptor-specific regulation of phosphatidylinositol 3′-kinase activation by the protein tyrosine phosphatase Shp2. *Mol. Cell. Biol.* 22:4062–4072.
30. Putney, J.W., Jr., L.M. Broad, F.J. Braun, J.P. Lievremont, and G.S. Bird. 2001. Mechanisms of capacitative calcium entry. *J. Cell Sci.* 114:2223–2229.
31. Wilson, B.S., J.R. Pfeiffer, Z. Surviladze, E.A. Gaudet, and

J.M. Oliver. 2001. High resolution mapping of mast cell membranes reveals primary and secondary domains of FcεRI and LAT. *J. Cell Biol.* 154:645–658.
32. Zhang, W., C.L. Sommers, D.N. Burshtyn, C.C. Stebbins, J.B. DeJarnette, R.P. Trible, A. Grinberg, H.C. Tsay, H.M. Jacobs, C.M. Kessler, et al. 1999. Essential role of LAT in T cell development. *Immunity.* 10:323–332.
33. Finco, T.S., T. Kadlecek, W. Zhang, L.E. Samelson, and A. Weiss. 1998. LAT is required for TCR-mediated activation of PLCγ1 and the Ras pathway. *Immunity.* 9:617–626.
34. Zhang, W., B.J. Irvin, R.P. Trible, R.T. Abraham, and L.E. Samelson. 1999. Functional analysis of LAT in TCR-mediated signaling pathways using a LAT-deficient Jurkat cell line. *Int. Immunol.* 11:943–950.
35. Tailor, P., T. Jascur, S. Williams, M. von Willebrand, C. Couture, and T. Mustelin. 1996. Involvement of Src-homology-2-domain-containing protein-tyrosine phosphatase 2 in T cell activation. *Eur. J. Biochem.* 237:736–742.

(C)

Topography of plasma membrane microdomains and its consequences for mast cell signaling.

Eur. J. Immunol, 2006, 36: 2795-2806.

European Journal of Immunology Leukocyte signaling

Topography of plasma membrane microdomains and its consequences for mast cell signaling

Petr Heneberg[1,2], Pavel Lebduška[1], Ľubica Dráberová[1], Jan Korb[1] and Petr Dráber[1]

[1] Institute of Molecular Genetics, Academy of Sciences of the Czech Republic, Prague, Czech Republic
[2] Center for Research in Diabetes, Metabolism and Nutrition, Third Faculty of Medicine, Charles University, Prague, Czech Republic

Thy-1 (CD90) is a glycoprotein bound to the plasma membrane by a GPI anchor. Aggregation of Thy-1 in mast cells and basophils induces activation events independent of the expression of Fcε receptor I (FcεRI). Although we and others have previously suggested that plasma membrane microdomains called lipid rafts are implicated in both Thy-1 and FcεRI signaling, properties of these microdomains are still poorly understood. In this study we used rat basophilic leukemia cells and their transfectants expressing both endogenous Thy-1.1 and exogenous Thy-1.2 genes and analyzed topography of the Thy-1 isoforms and Thy-1-induced signaling events. Light microscopy showed that both Thy-1 isoforms were in the plasma membrane distributed randomly and independently. Electron microscopy on isolated membrane sheets and fluorescence resonance energy transfer analysis indicated cross-talk between Thy-1 isoforms and between Thy-1 and FcεRI. This cross-talk was dependent on actin filaments. Thy-1 aggregates colocalized with two transmembrane adaptor proteins, non-T cell activation linker (NTAL) and linker for activation of T cells (LAT), which had been shown to inhabit different membrane microdomains. Thy-1 aggregation led to tyrosine phosphorylation of these two adaptors. The combined data indicate that aggregated GPI-anchored proteins can attract different membrane proteins in different clusters and thus can trigger different signaling pathways.

Received 12/4/06
Revised 13/7/06
Accepted 22/8/06

[DOI 10.1002/eji.200636159]

Key words: Actin · Adaptor proteins · Mast cell · Thy-1 glycoprotein

Introduction

Aggregation of the Thy-1 gp (CD90) induces activation of mast cells [1, 2], which is independent of the surface expression of Fcε receptor I (FcεRI) [3]. It has been suggested that this activation is caused by an association of the GPI-anchored Thy-1 with sterol- and sphingolipid-enriched membrane microdomains called lipid rafts. Microdomains of this composition can be isolated by sucrose density gradient ultracentrifugation after solubilization of cells with Triton X-100 or other nonionic detergents [4, 5]. Biochemical studies of isolated detergent-resistant membranes (DRM) showed that they are rich not only in GPI-anchored proteins, but also in palmitoylated Src family protein tyrosine kinases [6, 7] and palmitoylated transmembrane adaptor proteins, including linker for activation of T cells (LAT) [8] and non-T cell activation linker (NTAL) [9]. Importantly, in nonactivated mast cells, the FcεRI is excluded from DRM, whereas in FcεRI-activated cells most of the receptor is associated with DRM in a cholesterol-dependent manner [10–12]. These findings

Correspondence: Dr. Petr Dráber, Department of Signal Transduction, Institute of Molecular Genetics, Academy of Sciences of the Czech Republic, Vídeňská 1083, CZ-142 20 Prague 4, Czech Republic
Fax: +420-241470339
e-mail: draberpe@biomed.cas.cz

Abbreviations: **BRA:** bivariate Ripley's analysis · **BSS:** buffered salt solution · **DRM:** detergent-resistant membranes · **F-actin:** filamentous actin · **FcεRI:** Fcε receptor I · **FRET:** fluorescence resonance energy transfer · **GαM:** goat anti-mouse · **LAT:** linker for activation of T cells · **NTAL:** non-T cell activation linker · **PM:** plasma membrane · **RαM:** rabbit anti-mouse · **RBL:** rat basophilic leukemia · **RFI:** relative fluorescence intensity · **TRITC:** tetramethylrhodamine isothiocyanate

suggested that FcεRI-mediated activation is initiated through association of the aggregated FcεRI with membrane microdomains possessing signal transduction machinery. However, solubilization of the cells with detergents could produce artifacts and misleading results [13]. Other approaches are therefore required to understand the fundamental mechanism by which clustering of membrane receptors initiates tyrosine phosphorylation of numerous substrates.

In an attempt to understand topography of plasma membrane (PM) components, EM on isolated PM sheets has been used. These studies showed that aggregated FcεRI accumulate in osmiophilic membrane regions together with several signaling molecules but with no preference for colocalization with Thy-1 or other proteins considered to be localized in lipid rafts [14, 15]. Based on these results, Wilson and co-authors suggested that the observed FcεRI aggregates could represent the true signal transduction organizing units [14]. However, we recently found that mAb-mediated FcεRI dimerization induces strong cell activation response in the absence of formation of the large signaling assemblies around FcεRI aggregates [12]. Thus, FcεRI signal transduction units could be much smaller than previously thought [14, 16], and their molecular topography and changes during the course of mast cell activation remain enigmatic.

In this study we used rat basophilic leukemia (RBL) cells and their transfectants expressing both the endogenous Thy-1.1 and transfected Thy-1.2 genes to analyze the topography of Thy-1 isoforms and some other signaling proteins. The techniques included light microscopy, fluorescence resonance energy transfer (FRET) and EM on isolated PM sheets. The role of filamentous actin (F-actin) in Thy-1-mediated signaling and in cross-talk between Thy-1, FcεRI and the adaptor proteins LAT and NTAL was also investigated.

Results

Clusters of Thy-1 isoforms move independently in the plasma membrane

We previously isolated RBL-derived cells, RBL-gT1.2/1, expressing the murine Thy-1.2 gene [2]. FACS analysis showed that all RBL-gT1.2/1 cells express FcεRI and both Thy-1.1 and Thy-1.2 (Fig. 1A). Immunoblotting examination revealed that RBL-gT1.2/1 cells express less Thy-1.1 gp than RBL cells (Fig. 1B), implying a mechanism regulating the amount of total Thy-1 produced. Using RBL-gT1.2/1 cells we analyzed topography of Thy-1.1 and Thy-1.2 by three different approaches. In the first series of experiments using immunofluorescence microscopy on cells fixed with 4% paraformaldehyde before staining, both Thy-1.1 and Thy-1.2 were found homogenously distributed over the cell surface (Fig. 1Ca–c). Aggregation of Thy-1.1 by OX7 Ab and FITC-conjugated goat anti-mouse (GαM) IgG induced formation of patches (after 10 min at 37°C, Fig. 1Cd) and caps (after 60 min at 37°C; Fig. 1Cj) of Thy-1.1, whereas Thy-1.2 remained diffusely distributed over the cell surface (Fig. 1Ce, k). Similarly, in the reverse experiment, cells with patches and caps of cross-linked Thy-1.2 (Fig. 1Ch, n) exhibited diffuse staining of Thy-1.1 (Fig. 1Cg, m). These results suggest that Thy-1.1 and Thy-1.2 gp move in the plane of the PM independently.

Next we examined topography of Thy-1 isoforms using EM on immunogold-labeled PM sheets isolated from RBL-gT1.2/1 cells. As the isolation of membrane sheets is not compatible with strong fixation, we fixed the cells with 2% paraformaldehyde, allowing effective isolation of membrane sheets but unlikely to completely inhibit the formation of small Thy-1 aggregates. Under these conditions we found that both Thy-1.1 and Thy-1.2 were localized mostly in small autonomous clusters (Fig. 2 and 3). When Thy-1.1 was aggregated with OX7 mAb and 10 nm gold-labeled GαM IgG (GαM-gold-10 nm) followed by fixation with 2% paraformaldehyde and blocking remaining free IgG-binding sites, Thy-1.2 showed significant colocalization with Thy-1.1 at distances larger than ~40 nm as detected by bivariate Ripley's analysis (BRA; Fig. 2B). Importantly, under the same experimental conditions, much stronger Thy-1.1 homoassociation was detected (Fig. 2C). Interestingly, although the size of Thy-1 clusters was smaller in prefixed cells than in cells fixed after Thy-1 labeling, the distance between individual gold labels in the clusters remained unchanged (Fig. 3A–D). Furthermore, we confirmed recent data [15] that aggregation of Thy-1 does not lead to its enhanced colocalization with FcεRI (Fig. 3E, F). These EM data support the concept that aggregated Thy-1 isoforms can move relatively independently in the plane of the PM and are localized in membrane regions with no preference for FcεRI.

Finally, we studied the topography of Thy-1 isoforms by measuring FRET efficiency. When Thy-1.1 and Thy-1.2 were labeled, respectively, with OX7-FITC and 1aG4-tetramethylrhodamine isothiocyanate (TRITC), we observed intense energy transfer leading to a decrease in relative fluorescence intensity (RFI) of 1aG4-TRITC by –26.51±0.45% (Fig. 4A). Interestingly, when both Thy-1.1-OX7-FITC and Thy-1.2–1aG4-TRITC complexes were aggregated by rabbit anti-mouse (RαM) IgG, only a small decrease of RFI (–1.06±0.47%) was observed, suggesting existence of the preformed clusters. Furthermore, when the Thy-1.2 on the cells was labeled with 1aG4-FITC and 1aG4-TRITC at a ratio 5:1, the RFI remained the same after aggregation of the Thy-1-Ab

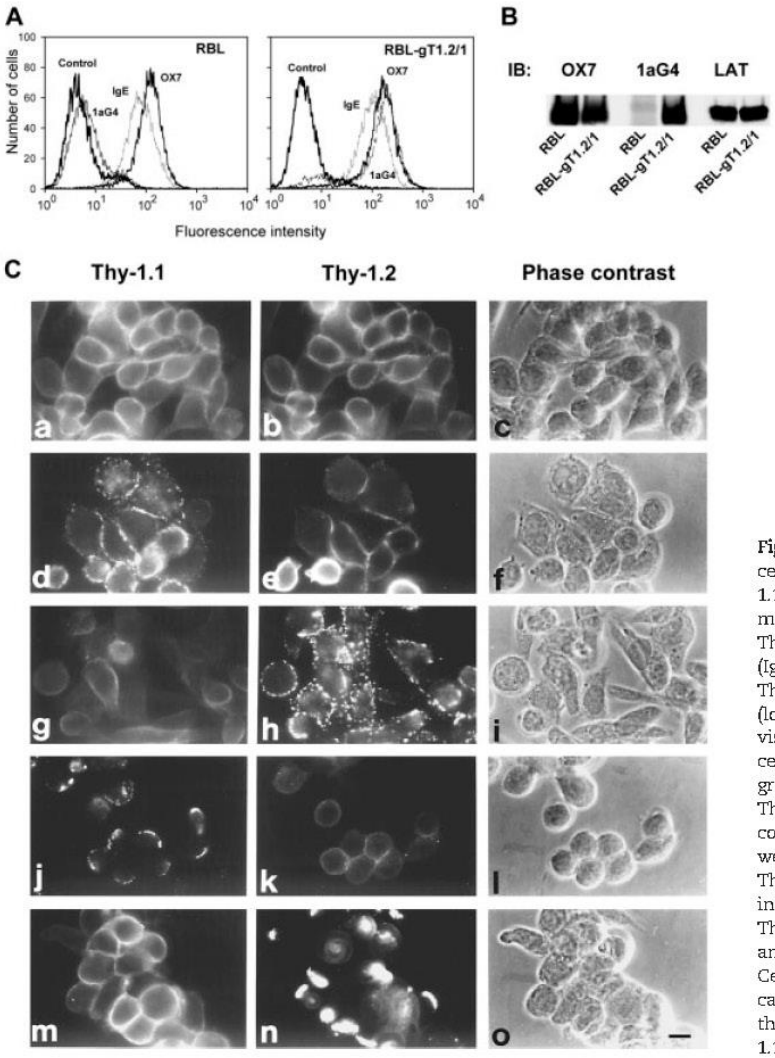

Figure 1. Properties of RBL and RBL-gT1.2/1 cells and independent movement of Thy-1.1 and Thy-1.2 as detected by light microscopy. (A) FACS analysis of surface Thy-1.1 (OX7), Thy-1.2 (1aG4) and FcεRI (IgE). (B) Immunoblotting (IB) analysis of Thy-1.1 (OX7), Thy-1.2 (1aG4) and LAT (loading control). (C) Thy-1.1 and Thy-1.2 visualized by indirect immunofluorescence on RBL-gT1.2/1 cells. The micrographs show staining for Thy-1.1 (left), Thy-1.2 (middle) and phase contrast of the corresponding fields (right). (a–c) Cells were fixed and then stained to visualize Thy-1.1 and Thy-1.2. (d–i) Cells were incubated for 10 min to induce patches of Thy-1.1 (d–f) or Thy-1.2 (g–i) and then fixed and stained for Thy-1.2 or Thy-1.1. (j–o) Cells were incubated for 60 min to induce caps of Thy-1.1 (j–l) or Thy-1.2 (m–o) and then fixed and stained for Thy-1.2 or Thy-1.1 (bar represents 10 μm).

complexes with RαM IgG (+1.57±3.05%). These data strengthen the results of EM studies indicating that the short-range distances between Thy-1 in its clusters do not dramatically change during the course of Ab-induced Thy-1 aggregation.

In the above experiments, we used whole IgG class mAb capable of dimerizing the target antigens. The observed FRET between Thy-1.1 and Thy-1.2 could thus reflect small changes in topography of the target molecules induced by their dimerization and movement into the same clusters, a situation that has been observed in another system [17]. In order to determine whether Ab-induced dimerization does indeed contribute to FRET, we labeled Thy-1.1 with either monovalent OX7(Fab)-FITC or dimerizing OX7(IgG_1)-FITC probes. Thy-1.2 was labeled with 1aG4(IgG_3)-TRITC, and FRET was analyzed by flow cytometry (Fig. 4B). At the time indicated by an arrow in Fig. 4B, Thy-1.2–1aG4-TRITC complexes were aggregated with nonlabeled isotype-specific anti-IgG_3. Monomeric Thy-1.1, labeled with OX7(Fab)-FITC, remained scattered throughout the whole cell surface after Thy-1.2 aggregation (not shown), which resulted in significantly enhanced RFI of 1aG4-TRITC (Fig. 4B, thick line), reflecting decreased FRET. However, dimeric Thy-1.1, labeled with OX7(IgG_1)-FITC, was dragged into Thy-1.2 clusters, resulting in decreased RFI values of TRITC-labeled 1aG4 (Fig. 4B, thin line). These data indicate that dimerization of Thy-1.1 results in its enhanced association with Thy-1.2 aggregates.

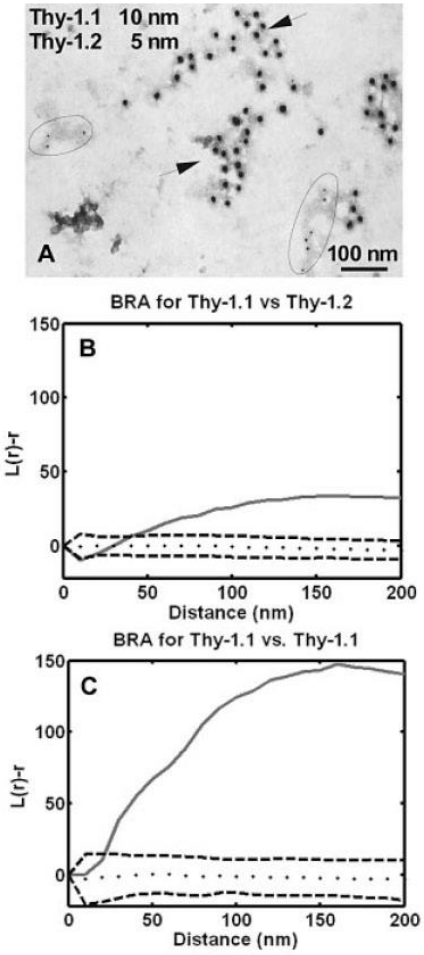

Figure 2. Topography of Thy-1.1 and Thy-1.2 as detected by EM. (A) Thy-1.1 in RBL-gT1.2/1was aggregated with OX7 mAb and GαM-gold-10 nm (arrows). The cells were fixed, free IgG binding sites were blocked with mouse IgG, and Thy-1.2 was labeled with biotinylated 1aG4 mAb followed by streptavidin-gold-5 nm (inside ellipses). (B) BRA of Thy-1.2 colocalization with aggregated Thy-1.1. (C) As a positive control, BRA is also shown for colocalization of the aggregated Thy-1.1 (labeled as above) with the remaining free Thy-1.1 in fixed cells (detected with biotinylated OX7 and streptavidin-gold-5 nm). Significant colocalization ($p<0.01$) of the proteins is shown as the position of the L-value curve (solid line) above boundaries (dashed lines) predicted for the random distribution of gold-labeled particles at a corresponding distance. Each graph represents approximately 35 μm^2 of the RBL PM from two independent experiments.

Thy-1 topography is regulated by F-actin

Distribution of PM components is regulated at least in part by submembraneous cytoskeleton [18]. In further experiments we therefore examined by means of FRET the changes in Thy-1 distribution in cells pretreated with inhibitors of actin polymerization, latrunculin B or cytochalasin D. Preincubation of RBL-gT1.2/1 cells with latrunculin for 15 min resulted in a significant increase in energy transfer between Thy-1.2–1aG4-TRITC and Thy-1.2–1aG4-FITC (Fig. 5A, column 2). These data probably reflect the formation of small Ab-Thy-1 clusters after F-actin fence removal. The homo-FRET values obtained in latrunculin-pretreated cells did not further increase by aggregation of Ab-dimerized Thy-1 with RαM IgG (Fig. 5A, column 3), suggesting that the intermolecular distances between Thy-1 remain constant even after extensive Thy-1 aggregation.

However, when Thy-1.2 was labeled with 1aG4-TRITC and Thy-1.1 with OX7-biotin-FITC, latrunculin and cytochalasin caused a decrease in the energy transfer (Fig. 5B, columns 2 and 3), which could be explained by more diffuse distribution of Thy-1.1 and Thy-1.2 dimers after F-actin fence removal. Aggregation of the Thy-1.1-OX7-biotin-FITC complexes with streptavidin caused a small but significant decrease in FRET efficiency between Thy-1.1 and Thy-1.2 (Fig. 5B, column 4). Interestingly, aggregation of Thy-1.1-OX7-biotin-FITC by streptavidin completely abolished the effect of both latrunculin and cytochalasin described above and caused, in fact, significant increase of FRET values compared to control cells (Fig. 5B, columns 5 and 6). Thus, the formation of large Thy-1.1 aggregates in cells lacking F-actin fence caused co-clustering of Thy-1.1 and Thy-1.2.

Cross-talk between Thy-1 and FcεRI

Biochemical studies with detergent-solubilized cells implied that FcεRI-mediated activation is initiated by coalescence of aggregated FcεRI with DRM [10, 12] and that F-actin is involved in this process [19, 20]. However, EM observations failed to discern any significant increase in association between Thy-1 and aggregated FcεRI [12, 15]. To elucidate these discrepancies, we further investigated the topography of Thy-1 and FcεRI by means of FRET, a method with 1–10 nm resolution. When FcεRI was dimerized by 5.14 mAb, enhanced FRET efficiency between Thy-1.1-OX7-FITC and FcεRI-IgE-TRITC complexes was observed (Fig. 6A, column 2). An even higher increase in FRET was determined after aggregation of FcεRI-IgE-TRITC complexes with multivalent antigen (TNP-BSA; Fig. 6A, column 3). These data confirm the results of biochemical studies documenting that FcεRI aggregation is indeed accompanied by movement of FcεRI aggregates into Thy-1-enriched domains [19]. As the pretreatment of cells with actin polymerization inhibitors enhanced FRET efficiency between Thy-1 and FcεRI even in control cells with nonaggregated FcεRI (Fig. 6A, columns 4 and 7), F-actin

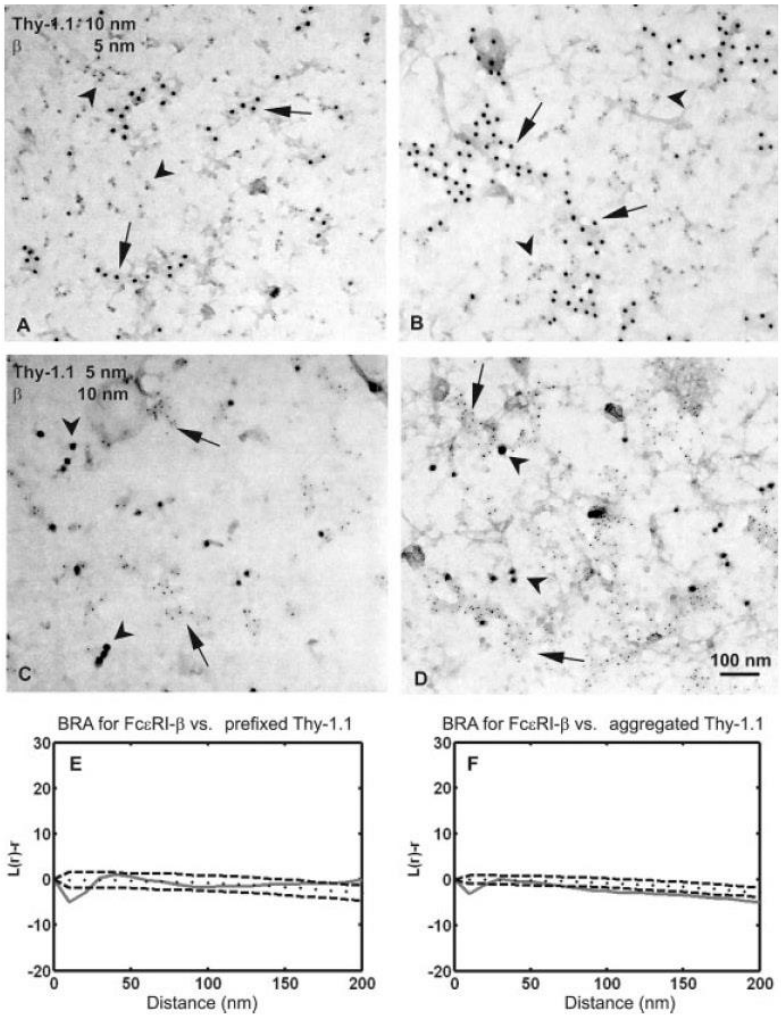

Figure 3. Topography of Thy-1.1 and FcεRI as detected by EM. RBL-2H3 cells were fixed before (A, C) or after (B, D) antibody-mediated Thy-1.1 aggregation. Thy-1.1 (arrows) was labeled on whole cells using 10 nm (A, B) or 5 nm (C, D) gold particles conjugated to OX7 mAb; FcεRI (arrowheads) was labeled on the cytoplasmic face of the PM sheets using the JRK antibody and secondary GαM-gold-5 nm (A, B) or –10 nm (C, D). BRA of colocalization of FcεRIβ subunit and nonaggregated (E) or aggregated (F) Thy-1.

could serve as a possible fence in confining FcεRI and Thy-1 in distinct membrane microdomains. Dimerization of FcεRI by 5.14 mAb in the presence of both inhibitors led to enhanced FRET between Thy-1 and FcεRI (Fig. 6A, columns 5 and 8). However, because latrunculin alone enhanced FRET efficiency by 10%, the observed difference (Fig. 6A, columns 4 and 5) was insignificant. After aggregation of FcεRI with TNP-BSA, there was even higher FRET efficiency in latrunculin-pretreated cells (Fig. 6A, columns 5 and 6, $p<0.01$), whereas in cytochalasin-pretreated cells, no further increase was observed (Fig. 6A, columns 8 and 9).

Because Thy-1 and FcεRI triggerings induce some common early activation events [21], it was important to determine whether Thy-1 aggregation has any effect on FcεRI homoassociation and whether F-actin is involved in this process. TNP-specific IgE was covalently modified either with TRITC or FITC, and the cells were labeled with both these FcεRI probes at a molar ratio 1:1. Then the cells were activated or not with dimerizing OX7 mAb or by extensive Thy-1 aggregation with Thy-1-OX7-biotin-streptavidin complexes. Data presented in Fig. 6B indicate that Thy-1 dimerization results in a small but significant enhancement of FRET, reflecting homoassociation of the FcεRI (Fig. 6B, column 2). Extensive Thy-1 aggregation had smaller effect (Fig. 6B, column 3). Pretreatment of the cells with latrunculin significantly enhanced FcεRI homo-FRET efficiency (Fig. 6B, column 4). Dimerization of Thy-1.1 and, namely, extensive Thy-1.1 aggregation in the presence of latrunculin resulted in further enhancement of IgE homoassociations (Fig. 6B, columns 5 and 6). Similar enhancement of FRET efficiencies was observed in cells pretreated with cytochalasin, except that extensive

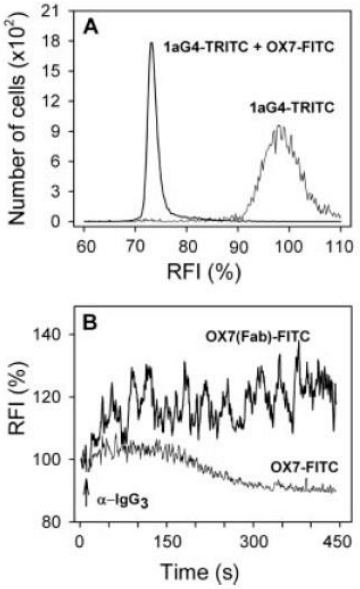

Figure 4. FRET between Thy-1.1 and Thy-1.2. (A) Representative RFI measured in RBL-gT1.2/1 cells by flow cytometry after binding of 1aG4-TRITC alone or 1aG4-TRITC and OX7-FITC. (B) Dimerization of Thy-1.1 results in its enhanced association with Thy-1.2 aggregates. Thy-1.1 was labeled either with Fab fragments of OX7-FITC or the whole OX7-FITC. Thy-1.2 was labeled with 1aG4-TRITC, and RFI were determined at various time intervals after aggregation of the Thy-1.2–1aG4-TRITC complexes with isotype-specific anti-IgG_3. Typical experiment from three performed is shown.

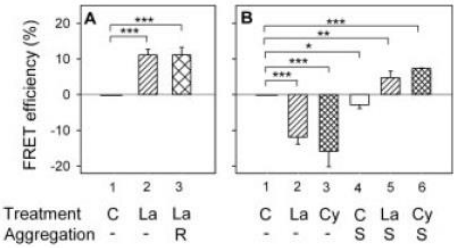

Figure 5. Different regulation of Thy-1 homo-FRET and hetero-FRET by F-actin. (A) Homo-FRET between Thy-1.2–1aG4-TRITC and Thy-1.2–1aG4-FITC. (B) Hetero-FRET between Thy-1.2–1aG4-TRITC and Thy-1.1-OX7-biotin-FITC. The cells were pretreated with latrunculin (La; 0.5 μM), cytochalasin B (Cy; 4 μM) or vehicle (C; 0.2% DMSO). In some experiments Thy-1 aggregation was induced by RαM IgG (R) or streptavidin (S). Data were normalized to vehicle-pretreated cells in column 1 (*$p<0.05$, **$p<0.01$, ***$p<0.001$).

aggregation of Thy-1 was less potent (Fig. 6B, columns 7–9). These data indicate that Thy-1 aggregation as well as actin polymerization affect the topography of FcεRI.

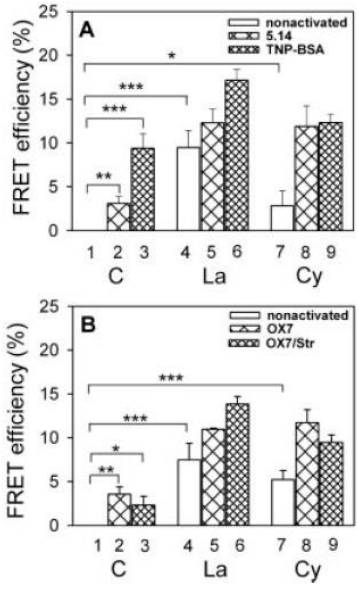

Figure 6. F-actin is involved in FRET cross-talk between Thy-1 and FcεRI. (A) FRET between Thy-1.1-OX7-FITC and FcεRI-IgE-TRITC was analyzed in RBL cells preincubated for 15 min with latrunculin (La; 0.5 μM), cytochalasin (Cy; 4 μM) or vehicle (C; 0.2% DMSO). IgE-TRITC-sensitized cells were nonactivated (1, 4, 7) or activated with 5.14 mAb (2, 5 ,8) or TNP-BSA (3, 6, 9) for 2 min, and the RFI was immediately evaluated by FACS. (B) RBL cells were either untreated or treated with latrunculin or cytochalasin and subsequently labeled with IgE-TRITC and IgE-FITC. Then the cells were either nonactivated (1, 4, 7) or activated for 5 min by Thy-1 dimerization with biotinylated OX7 (10 μg/mL; 2, 5, 8) or by extensive Thy-1 aggregation through biotinylated OX7-streptavidin complexes (3, 6, 9) (*$p<0.05$), **$p<0.01$, ***$p<0.001$).

Cross-talk between Thy-1 and the adaptor proteins LAT and NTAL

EM on PM sheets showed that LAT and NTAL are located in distinct regions of the PM [22] and that aggregated Thy-1 colocalizes with LAT [15]. To determine whether Thy-1 also colocalizes with NTAL, we used RBL cells fixed before or after Thy-1 labeling with OX7 mAb and GαM-IgG-gold-10 nm (Fig. 7 and 8). Colocalization of Thy-1 with both LAT and NTAL was occasionally observed in cells fixed before Thy-1 staining (Fig. 7A, C and 8A, C), in which NTAL and LAT are distributed in separate domains (Fig. 8E). Colocalization of both adaptors with Thy-1 was strongly enhanced after Thy-1 aggregation (Fig. 7B, D and 8B, D). Under these conditions colocalization of LAT and NTAL was observed only at distances larger than the size of LAT/NTAL clusters (Fig. 8F).

The observed colocalization of Thy-1 with NTAL and LAT could have functional consequences for initial

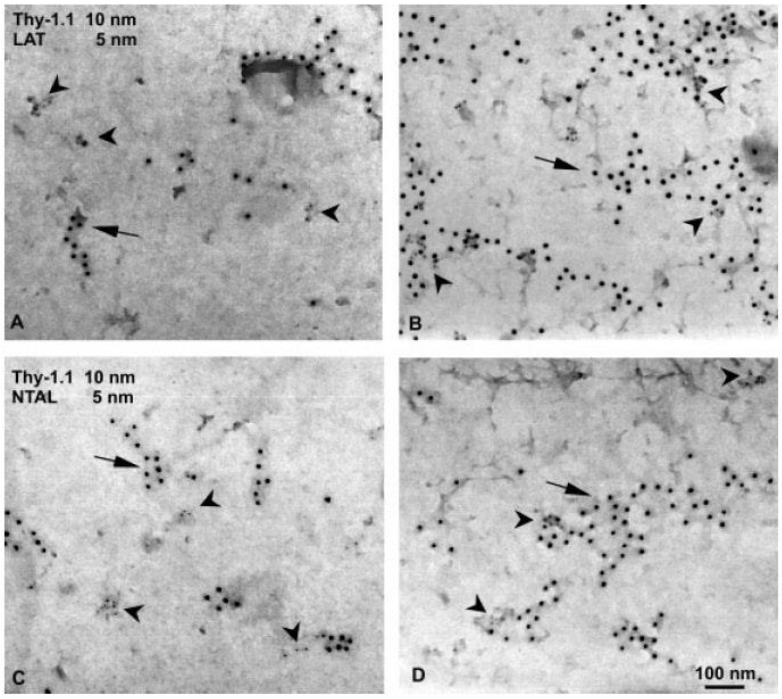

Figure 7. Colocalization of LAT and NTAL adaptors with Thy-1 clusters. Membrane topography of Thy-1.1 and adaptor proteins LAT (A, B) or NTAL (C, D) was determined in cells stained with OX7 Ab and GαM-gold-10 nm after fixation with 2% paraformaldehyde (A, C) or before fixation to induce formation of Thy-1 aggregates (B, D). Adaptors were detected with the corresponding mAb and GαM-gold-5 nm. Arrows indicate Thy-1.1; arrowheads mark LAT (A, B) or NTAL (C, D).

stages of Thy-1-induced cell activation. We therefore examined protein tyrosine phosphorylation in control and Thy-1-activated cells. The cells were lysed in 0.5% Triton X-100 and fractionated by sucrose density gradient ultracentrifugation. In nonactivated cells the major tyrosine phosphorylated protein found in DRM (fractions 1–5) is Lyn kinase, forming a typical 53/55 kDa double band (Fig. 9A, Control). Exposure of the cells to latrunculin alone resulted in weak tyrosine phosphorylation of a protein in DRM with Mr of 38 kDa, corresponding to LAT, and several other proteins in non-DRM high density fractions of the sucrose gradient (Fig. 9A, 0/La, fractions 6–9). After Thy-1-mediated activation induced by biotinylated OX7-streptavidin complexes, enhanced tyrosine phosphorylation in DRM was observed in proteins with Mr of NTAL (30 kDa) and LAT (Fig. 9A, OX7/0/Str). Aggregation of Thy-1 in the presence of latrunculin further enhanced tyrosine phosphorylation of both NTAL- and LAT-like proteins (Fig. 9A, OX7/La/Str). Further analysis showed that Syk kinase was excluded from DRM, whereas Lyn, LAT, NTAL and Thy-1 were included, as expected. Direct evidence that both NTAL and LAT are phosphorylated in Thy-1-activated cells was obtained by immunoprecipitation experiments. Thy-1 dimerization by OX7 alone induced 3.6- and 2.9-fold increases in tyrosine phosphorylation of LAT and NTAL, respectively (Fig. 9B, C). The extent of tyrosine phosphorylation was further enhanced by more extensive Thy-1 aggregation and rose even more after inhibition of actin polymerization by latrunculin. Immunoprecipitation experiments showed that latrunculin alone induced modest but reproducible dose-dependent tyrosine phosphorylation of LAT, NTAL and Syk, with peak effect at a concentration 0.5 μM (Fig. 9D).

Discussion

RBL-gT1.2/1 cells expressing both the endogenous Thy-1.1 and the transfected Thy-1.2 were used to analyze the topography of Thy-1 isoforms with three methods differing in their resolution power. Although both rat Thy-1.1 and mouse Thy-1.2 are anchored to PM through the GPI anchor and differ only in a limited number of aminoacids (82% identity), immunofluorescence microscopy showed that both isoforms are distributed in the PM randomly and are aggregated independently. These data suggest that Thy-1 domains are very small, under the resolution limit of light microscopy, and/or that forces that keep GPI-anchored molecules in the putative domains are weaker than forces leading to their antibody-mediated aggregation. Using EM on immunogold-labeled PM sheets isolated from cells fixed before labeling, we confirmed previous data [15] that Thy-1 is distributed in small clusters independently of FcεRI.

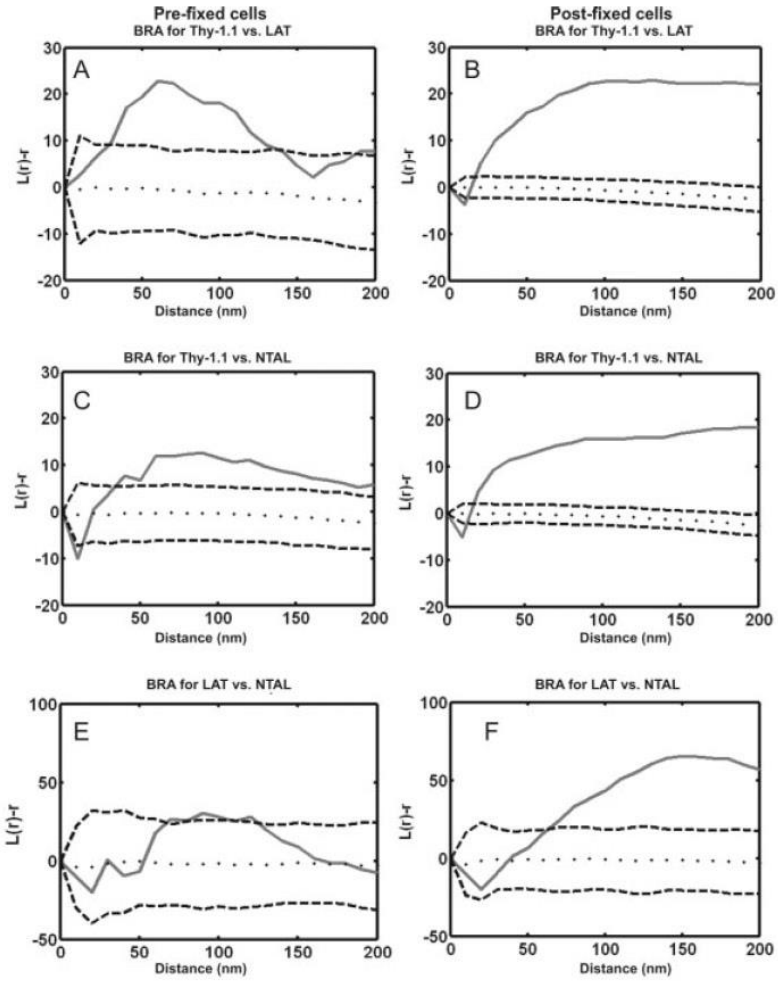

Figure 8. BRA of Thy-1.1 colocalization with LAT or NTAL in cells labeled for Thy-1 after fixation (A, C) or before fixation to induce formation of Thy-1 aggregates (B, D). BRA of LAT colocalization with NTAL in cells with nonaggregated (E) or aggregated (F) Thy-1.

However, based on these results, we cannot exclude the possibility that these clusters are induced, or that their size is enhanced, by the antibodies used for Thy-1 detection because isolation of PM sheets is incompatible with strong fixing conditions that ensure complete blocking of GPI-anchored protein movement. Antibody-induced aggregation of Thy-1 resulted in coalescence of smaller Thy-1 clusters into larger domains, as expected, yet the density of gold label in Thy-1 clusters was not enhanced; this suggests that distances between individual molecules were kept constant.

In an attempt to understand protein-protein interactions in the PM of living cells, we employed FRET-based analyses between one type of molecules (homo-FRET) or different molecules (hetero-FRET). FRET is unique in generating fluorescence signals sensitive to molecular conformations, associations and intermolecular distances in the range of 1–10 nm [23]. We found no dramatic changes in FRET efficiencies between immunolabeled Thy-1.2 and Thy-1.1 dimers after their aggregation with anti-IgG Ab. This implies that intermolecular distances do not dramatically change in the course of Thy-1 aggregation and in this sense support the results obtained by EM showing that density of gold-labeled Thy-1 in clusters is similar in cells with extensively aggregated Thy-1 (fixed after labeling) and cells fixed before Thy-1 labeling.

Previous studies suggested that segregation of lipid microdomains might be regulated by submembraneous cytoskeleton [19, 24]. Our data indicate that F-actin is involved in formation of Thy-1 clusters in PM. When polymerization of F-actin was disrupted with latrunculin, both Thy-1 isoforms distributed more randomly, as reflected in lower energy transfer between immunolabeled Thy-1.1 and Thy-1.2. These effects were almost abolished if biotinylated Thy-1.1 was crosslinked with

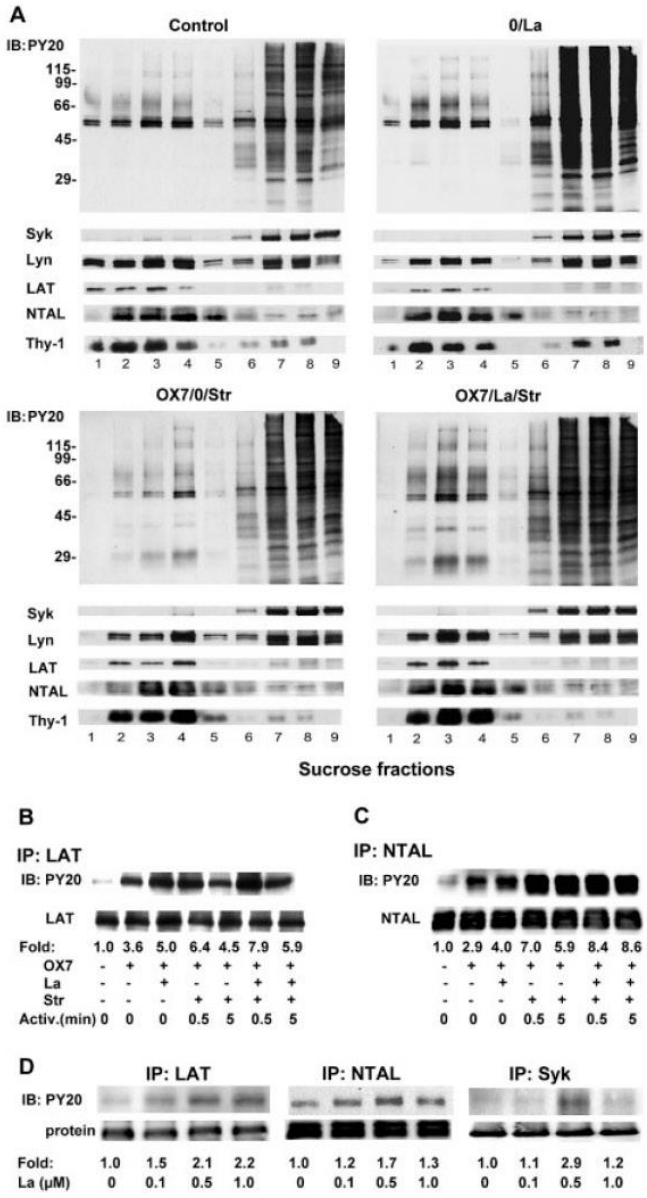

Figure 9. Tyrosine phosphorylation of NTAL and LAT in Thy-1-activated cells. (A) The cells were nonactivated (Control) or activated through Thy-1 aggregation by exposure to OX7-biotin-streptavidin (Str) complexes (OX7/0/Str). Alternatively, cells were preincubated for 15 min with latrunculin (La) and then activated in the presence of latrunculin alone (0/La) or together with OX7-biotin-streptavidin complexes (OX7/La/Str). After 5 min of incubation, the cells were solubilized, and the lysates were fractionated by sucrose density gradient ultracentrifugation. Individual fractions [1 (top) – 9 (bottom)] were collected and analyzed by immunoblotting for the presence of tyrosine phosphorylated proteins (PY-20), Syk, Lyn, LAT, NTAL and Thy-1. Numbers on the left indicate the position of Mr standards in kDa. (B–D) Extent of tyrosine phosphorylation of LAT, NTAL and Syk was determined in cells activated under different conditions as specified. The cells were solubilized and the proteins immunoprecipitated and analyzed by immunoblotting. Extent of tyrosine phosphorylation was determined by densitometry and normalized to the untreated cells and the amount of protein immunoprecipitated (Fold). A typical experiment from at least three performed in each group is shown.

streptavidin, suggesting that under these conditions cluster formation is driven by the crosslinking antibodies rather than F-actin. Thus, F-actin is crucial for the spatial distribution of Thy-1 in membrane microdomains, whereas external agents take the helm in activated cells.

Inhibition of actin polymerization leads to significant enhancement of the secretory response induced through FcεRI [25] or Thy-1 [20]. Our finding that inhibitors of actin polymerization enhance FRET efficiency between FcεRI and Thy-1.1 suggests that the decreased level of F-actin leads to loss of exclusion of the FcεRI from Thy-1 in nonactivated cells. Thus, F-actin could be the main regulator responsible for physical separation of signal transduction PM molecules. We noticed a significant difference in the effects of two inhibitors of actin polymerization, latrunculin B and cytochalasin D, which are distinct in their mode of action [26]. Latrunculin sequesters actin monomers by preventing actin polymerization and effectively disrupts both actin stress fibers and cortical actin filaments. In contrast, cytocha-

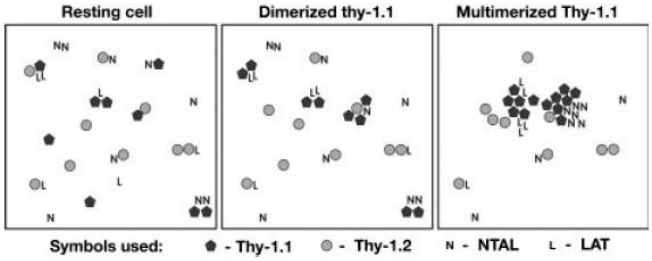

Figure 10. Schematic model of Thy-1 aggregation and interaction with transmembrane adaptors. In resting cells, both Thy-1.1 and Thy-1.2 reside scattered as single molecules or small patches of several molecules. After Thy-1.1 dimerization, Thy-1.2 remains scattered mostly independently of Thy-1.1. After Thy-1.1 multimerization, most of Thy-1.2 remains randomly scattered. However, aggregated Thy-1.1 forms large patches, recruiting transmembrane adaptors LAT and NTAL, occupying different membrane regions.

lasin binds to the barbed (growing) ends of actin filaments and prevents their elongation. Stronger inhibition of actin polymerization by latrunculin could explain why it was more potent in experiments measuring FRET efficiencies in this study.

By FACS analysis we found significantly increased FRET efficiency between Thy-1 and FcεRI after antigen-mediated FcεRI aggregation. Based on these data, we propose that at least a fraction of Thy-1 must edge towards FcεRI. However, the observed photobleaching (9.38%) after 1 min activation of the cells suggests that only a fraction of the Thy-1 was closer to aggregated FcεRI in activated cells. This finding is consistent with the results obtained by EM demonstrating that Thy-1 is not completely excluded from electron-dense patches where aggregated FcεRI accumulate [14].

Aggregated Thy-1 colocalizes with another lipid raft marker, LAT [15], which is structurally and functionally similar to NTAL. Surprisingly, LAT and NTAL are localized in different membrane microdomains in both nonactivated and activated cells [22]. Using EM we found that both LAT and NTAL colocalize with Thy-1 clusters, even though these adaptors did not form mixed clusters. Interestingly, extensive Thy-1 aggregation led to closer proximity of LAT and NTAL clusters. A schematic model of the distribution of Thy-1 isoforms, NTAL and LAT in nonactivated and Thy-1-activated cells is shown in Fig. 10. Because the two adaptors could be involved in different signaling pathways [27], our data suggest that these pathways could be affected by Thy-1 aggregation. Here we present evidence that Thy-1 aggregation induces tyrosine phosphorylation of the two adaptor proteins. Although pretreatment with latrunculin did not affect association of several signaling proteins (Lyn, LAT, NTAL and Thy-1) with DRM, it enhanced tyrosine phosphorylation of LAT, NTAL and even Syk, which is not considered to be associated with lipid rafts. It should be noted, however, that Syk could be recruited to lipid rafts through its binding to lipid raft-residing molecules such as Lyn [28] or aggregated FcεRI [10, 12]. The combined data support the notion that actin cytoskeleton is involved in setting the threshold for activation of mast cells through various pathways.

Materials and methods

Cells, antibodies and reagents

The origin and culture conditions for RBL cells (subclone 2H3) and Thy-1.2 transfectants (RBL-gT1.2/1) have been described [2]. The following mAb were used: MRC OX7 (OX7; IgG_1) recognizing Thy-1.1, F7D5 (IgM) and 1aG4 (IgG_3) directed against Thy-1.2 (their origins have been described [7]) and 5.14 (IgG_1) directed to the FcεRIα subunit [29]. The origins of IGEL b4 1 (IgE) recognizing TNP, JRK specific for the FcεRIβ subunit and antibodies against NTAL, LAT and Syk have been described [22]. GαM IgG-FITC and GαR IgM-LRSC (lissamine-rhodamine sulfonyl chloride) were obtained from Jackson Laboratories (West Grove, PA). HRP-conjugated anti-phosphotyrosine antibody PY20, RαM IgG and isotype-specific GαM IgG_3 were purchased from Sigma (St. Louis, MO). GαM-gold-10 nm and GαM-gold-5 nm were obtained from Amersham Biosciences (Uppsala, Sweden), and streptavidin-gold-5 nm was from Pelco International (Redding, CA). Fab fragments were prepared using ImmunoPure Fab Preparation Kit (Pierce, Rockford, IL). Fluorescence dyes FITC or TRITC (both from Sigma) were dissolved in DMSO at a concentration 10 mg/mL and then mixed with mAb (1:10 vol:vol). Reaction mix (1 mL containing ~2 mg antibody) was incubated for 1 h at room temperature and stopped by adding 0.1 mL 1.5 M hydroxylamine, pH 8.5. The conjugate was dialyzed against PBS and stored at –20°C. Some antibodies were biotinylated with ImmunoPure NHS-LC-biotin (Pierce) according to the manufacturer's instructions. All other reagents used were from Sigma.

Immunofluorescence microscopy

Cells were grown on coverslips to semiconfluence. The coverslips were transferred on ice, and all procedures were

performed at 0°C unless stated otherwise. For antibody dilution and cell washing, ice-cold PBS and culture medium containing 10% FCS (5:1) was used. To visualize Thy-1, the cells were incubated for 30 min with antigen-specific antibody (1:100 diluted OX7 or F7D5), washed and incubated for 30 min with the class-specific secondary reagents GαM IgG-FITC or GαM IgM-LRSC (lissamine-rhodamine sulfonyl chloride), washed and incubated at 37°C for 10 or 60 min to induce patching or capping of the target gp. Then the cells were washed in PBS, pH 7.4, fixed in 4% paraformaldehyde in PBS for 20 min at 23°C, washed sequentially with 0.1 M glycine in PBS, PBS, and culture medium containing 10% FCS and then stained for a second antigen, using the two-step procedure as described above. In some experiments, the cells were first fixed and then stained on ice with the primary antibodies (OX7 and F7D5) followed by a mixture of the class-specific secondary antibodies. After staining, the cells were fixed once more in 4% paraformaldehyde for 10 min, washed, mounted in 0.1% *p*-phenylendiamine in 50% glycerol in PBS pH 8.0 and examined with an Orthoplan (Zeiss) fluorescence microscope.

Electron microscopy

PM sheets were isolated, labeled and analyzed by EM as described [12, 15]. For labeling of both Thy-1 isoforms on the same membrane sheets, the cells were grown on coverslips and incubated for 15 min at room temperature with OX7 mAb (1 μg/mL) followed by 10 min incubation at 37°C with GαM-gold-10 nm; antibodies were diluted in buffered salt solution (BSS: 20 mM Hepes pH 7.4, 135 mM NaCl, 5 mM KCl, 1.8 mM $CaCl_2$, 5.6 mM glucose, 1 mM $MgCl_2$) supplemented with 0.1% BSA. Then the cells were fixed for 7 min in 2% paraformaldehyde in PBS at room temperature, and the remaining free IgG binding sites were blocked for 5 min in BSS-0.1% BSA with 5% normal mouse serum. Thy-1.2 gp (or Thy-1.1 gp) was detected by 15 min incubation with biotinylated 1aG4 (or OX7) in PBS-5% mouse serum. After a final 10 min incubation with streptavidin-gold-5 nm, the PM sheets were isolated and further processed.

FRET

The cells (10^6) were incubated in 1 mL BSS-0.1% BSA with fluorescently tagged antibodies at saturating concentration for 30 min in the dark. Unbound antibodies were removed by washing the cells twice in BSS-0.1% BSA, and the cells were measured immediately by FACSCalibur (Becton Dickinson) to determine FRET efficiency between FITC- and TRITC-conjugated antibodies as described [30]. Donor fluorescence of double-labeled samples was compared with that of samples where the acceptor antibody was replaced by non-labeled antibody to compensate for any competition between the donor and acceptor antibodies. FRET efficiency was calculated from the fractional decrease of the donor fluorescence in the presence of the acceptor. Forward and side angle light scattering were used to gate out debris and dead cells. Calculated values for FRET efficiency were expressed as the ratio of the number of excited donor molecules, tunneling their excitation energy to the acceptor, to the number of all excited molecules.

Cell activation, sucrose gradients and immunoblotting

RBL cells were harvested, resuspended in BSS-0.1% BSA and sensitized with biotinylated OX7 at a final concentration 10 mg/mL for 30 min at 37°C. After washing the cells were activated for 5 min at 37°C with streptavidin (10 mg/mL). In some experiments the cells were exposed for 15 min before activation to latrunculin (0.5 mM). Activated and control cells were lysed in ice-cold lysis buffer containing 0.5% Triton X-100 and fractionated by sucrose density gradient. Individual fractions from the gradient were analyzed by SDS-PAGE followed by immunoblotting as described [5]. In some experiments the cells were activated as specified in the Results, and LAT and NTAL were immunoprecipitated and analyzed as described [22].

Statistical analysis

Statistical analysis of colocalization of antigens on PM sheets was evaluated by BRA using the $L(r)$-r function as described [15]. $L(r)$-r function maps the expected value of the Ripley's K function defined similarly to the univariate function to radius r and to 0. Unless further specified, FRET data represent mean ± SD from at least three independent experiments. Statistical significance of inter-group differences was calculated by the unpaired Student's t-test.

Acknowledgements: This work was supported by project 1 M6837805001 (Center of Molecular and Cellular Immunology) from the Ministry of Education, Youth and Sports of the Czech Republic, grant IAA5052310 from the Grant Agency of the Academy of Sciences of the Czech Republic, grants S301521904 and 301/06/0361 from the Grant Agency of the Czech Republic and Institutional project AVOZ50520514. The research of P. D. and P. H. were supported by an International Research Scholar's award from the Howard Hughes Medical Institute and by Research goal MSM0021620814 from the 3rd Faculty of Medicine (Charles University, Prague), respectively.

References

1 **Dráberová, L.**, The involvement of Thy-1 antigen in the activation of rat mast cells. *Eur. J. Immunol.* 1989. **19:** 1715–1720.

2 **Dráberová, L. and Dráber, P.**, Functional expression of the endogenous Thy-1 gene and the transfected murine Thy-1.2 gene in rat basophilic leukemia cells. *Eur. J. Immunol.* 1991. **21:** 1583–1590.

3 **Dráberová, L. and Dráber, P.**, Thy-1-mediated activation of rat basophilic leukemia cells does not require co-expression of the high-affinity IgE receptor. *Eur. J. Immunol.* 1995. **25:** 2428–2432.

4 **Brown, D. A. and Rose, J. K.**, Sorting of GPI-anchored proteins to glycolipid-enriched membrane subdomains during transport to the apical cell surface. *Cell* 1992. **68:** 533–544.

5 **Surviladze, Z., Dráberová, L., Kubínová, L. and Dráber, P.**, Functional heterogeneity of Thy-1 membrane microdomains in rat basophilic leukemia cells. *Eur. J. Immunol.* 1998. **28:** 1847–1858.

6 **Štefanová, I., Hořejší, V., Ansotegui, I. J., Knapp, W. and Stockinger, H.,** GPI-anchored cell-surface molecules complexed to protein tyrosine kinases. *Science* 1991. **254:** 1016–1019.

7 **Dráberová, L. and Dráber, P.,** Thy-1 glycoprotein and src-like protein-tyrosine kinase p53/p56^{lyn} are associated in large detergent-resistant complexes in rat basophilic leukemia cells. *Proc. Natl. Acad. Sci. USA* 1993. **90:** 3611–3615.

8 **Zhang, W., Sloan-Lancaster, J., Kitchen, J., Trible, R. P. and Samelson, L. E.,** LAT: the ZAP-70 tyrosine kinase substrate that links T cell receptor to cellular activation. *Cell* 1998. **92:** 83–92.

9 **Brdička, T., Imrich, M., Angelisová, P., Brdičková, N., Horváth, O., Šička, J., Hilgert, I. *et al.*,** Non-T cell activation linker (NTAL): a transmembrane adaptor protein involved in immunoreceptor signaling. *J. Exp. Med.* 2002. **196:** 1617–1626.

10 **Field, K. A., Holowka, D. and Baird, B.,** Compartmentalized activation of the high affinity immunoglobulin E receptor within membrane domains. *J. Biol. Chem.* 1997. **272:** 4276–4280.

11 **Sheets, E. D., Holowka, D. and Baird, B.,** Critical role for cholesterol in Lyn-mediated tyrosine phosphorylation of FcεRI and their association with detergent-resistant membranes. *J. Cell Biol.* 1999. **145:** 877–887.

12 **Dráberová, L., Lebduška, P., Hálová, I., Tolar, P., Štokrová, J., Tolarová, H., Korb, J. *et al.*,** Signaling assemblies formed in mast cells activated *via* Fcε receptor I dimers. *Eur. J. Immunol.* 2004. **34:** 2209–2219.

13 **Munro, S.,** Lipid rafts: elusive or illusive? *Cell* 2003. **115:** 377–388.

14 **Wilson, B. S., Pfeiffer, J. R., Surviladze, Z., Gaudet, E. A. and Oliver, J. M.,** High resolution mapping of mast cell membranes reveals primary and secondary domains of FcεRI and LAT. *J. Cell Biol.* 2001. **154:** 645–658.

15 **Wilson, B. S., Steinberg, S. L., Liederman, K., Pfeiffer, J. R., Surviladze, Z., Zhang, J., Samelson, L. E. *et al.*,** Markers for detergent-resistant lipid rafts occupy distinct and dynamic domains in native membranes. *Mol. Biol. Cell* 2004. **15:** 2580–2592.

16 **Simons, K. and Toomre, D.,** Lipid rafts and signal transduction. *Nat. Rev. Mol. Cell Biol.* 2000. **1:** 31–39.

17 **Harder, T., Scheiffele, P., Verkade, P. and Simons, K.,** Lipid domain structure of the plasma membrane revealed by patching of membrane components. *J. Cell Biol.* 1998. **141:** 929–942.

18 **Kwik, J., Boyle, S., Fooksman, D., Margolis, L., Sheetz, M. P. and Edidin, M.,** Membrane cholesterol, lateral mobility, and the phosphatidylinositol 4,5-bisphosphate-dependent organization of cell actin. *Proc. Natl. Acad. Sci. USA* 2003. **100:** 13964–13969.

19 **Holowka, D., Sheets, E. D. and Baird, B.,** Interactions between FcεRI and lipid raft components are regulated by the actin cytoskeleton. *J. Cell Sci.* 2000. **113:** 1009–1019.

20 **Tolarová, H., Dráberová, L., Heneberg, P. and Dráber, P.,** Involvement of filamentous actin in setting the threshold for degranulation in mast cells. *Eur. J. Immunol.* 2004. **34:** 1627–1636.

21 **Dráberová, L. and Dráber, P.,** Cross-linking of Thy-1 glycoproteins or high-affinity IgE receptors induces mast cell activation *via* different mechanisms. *Immunology* 1993. **80:** 103–109.

22 **Volná, P., Lebduška, P., Dráberová, L., Šímová, Š., Heneberg, P., Boubelík, M., Bugajev, V. *et al.*,** Negative regulation of mast cell signaling and function by the adaptor LAB/NTAL. *J. Exp. Med.* 2004. **200:** 1001–1013.

23 **Jares-Erijman, E. A. and Jovin, T. M.,** FRET imaging. *Nat. Biotechnol.* 2003. **21:** 1387–1395.

24 **Harder, T. and Simons, K.,** Clusters of glycolipid and glycosylphosphatidylinositol-anchored proteins in lymphoid cells: accumulation of actin regulated by local tyrosine phosphorylation. *Eur. J. Immunol.* 1999. **29:** 556–562.

25 **Frigeri, L. and Apgar, J. R.,** The role of actin microfilaments in the down-regulation of the degranulation response in RBL-2H3 cells. *J. Immunol.* 1999. **162:** 2243–2250.

26 **Spector, I., Shochet, N. R., Blasberger, D. and Kashman, Y.,** Latrunculins–novel marine macrolides that disrupt microfilament organization and affect cell growth: I. Comparison with cytochalasin D. *Cell Motil. Cytoskeleton* 1989. **13:** 127–144.

27 **Gilfillan, A. M. and Tkaczyk, C.,** Integrated signalling pathways for mast-cell activation. *Nat. Rev. Immunol.* 2006. **6:** 218–230.

28 **Amoui, M., Dráberová, L., Tolar, P. and Dráber, P.,** Direct interaction of Syk and Lyn protein tyrosine kinases in rat basophilic leukemia cells activated *via* type I Fcε receptor. *Eur. J. Immunol.* 1997. **27:** 321–328.

29 **Baniyash, M., Alkalay, I. and Eshhar, Z.,** Monoclonal antibodies specific to the α-subunit of the mast cell's FcεR block IgE binding and trigger histamine release. *J. Immunol.* 1987. **138:** 2999–3004.

30 **Dornan, S., Sebestyen, Z., Gamble, J., Nagy, P., Bodnar, A., Alldridge, L., Doe, S. *et al.*,** Differential association of CD45 isoforms with CD4 and CD8 regulates the actions of specific pools of p56lck tyrosine kinase in T cell antigen receptor signal transduction. *J. Biol. Chem.* 2002. **277:** 1912–1918.

(D)

Regulation of Ca^{2+} signaling in mast cells by tyrosine-phosphorylated and unphosphorylated non-T cell activation linker, NTAL

Journal of Immunology, odesláno (květen 2007).

words: 10436

Regulation of Ca^{2+} signaling in mast cells by tyrosine-phosphorylated and unphosphorylated non-T cell activation linker, NTAL[1]

Lubica Dráberová,[*] Gouse Mohiddin Shaik,[*] Petra Volná,[*] Petr Heneberg,[*†] Magda Tůmová,[*] Pavel Lebduška,[*] Jan Korb,[‡] and Petr Dráber[2*]

[*]Department of Signal Transduction and [‡]Department of Micromorphology of Biopolymers, Institute of Molecular Genetics, Academy of Sciences of the Czech Republic; and [†] Center for Research in Diabetes, Metabolism and Nutrition, 3rd Medical Faculty, Charles University, Prague, Czech Republic

Running title: Multiple regulatory roles of NTAL in mast cell signaling

Keywords: Rodent, Mast Cells/Basophils, Fc Receptors, Cell Activation, Signal Transduction

[2]Address correspondence to: Dr. Petr Dráber, Department of Signal Transduction, Institute of Molecular Genetics, Academy of Sciences of the Czech Republic, Vídeňská 1083, Prague 4, CZ 142 20, Czech Republic. Phone: +420-241 062 468; Fax: +420-241 062 214; E-mail: draberpe@biomed.cas.cz.

Abstract

Engagement of the FcεRI in mast cells and basophils leads to a rapid tyrosine phosphorylation of the transmembrane adaptors LAT (linker for activation of T cells) and NTAL (non-T cell activation linker, also called LAB or LAT2). NTAL regulates activation of mast cells by a mechanism, which is incompletely understood. Here we report properties of rat basophilic leukemia cells with enhanced or reduced NTAL expression. Overexpression of NTAL led to changes in cell morphology, enhanced formation of actin filaments and inhibition of the FcεRI-induced tyrosine phosphorylation of the FcεRI subunits, Syk kinase and LAT and all downstream activation events, including calcium and secretory responses. In contrast, reduced expression of NTAL had little effect on early FcεRI-induced signaling events but inhibited calcium mobilization and secretory response. Calcium response was also repressed in Ag-activated cells defective in Grb2, a major target of phosphorylated NTAL. Unexpectedly, in cells stimulated with thapsigargin, an inhibitor of the endoplasmic reticulum Ca^{2+} ATPase, the amount of cellular NTAL directly correlated with the uptake of extracellular calcium even though no enhanced tyrosine phosphorylation of NTAL was observed. The combined data indicate that NTAL regulates FcεRI-mediated signaling at multiple steps and by different mechanisms. At early stages NTAL interferes with tyrosine phosphorylation of several substrates and formation of signaling assemblies, whereas at later stages it regulates the activity of store-operated calcium channels through a distinct mechanism independent of enhanced NTAL tyrosine phosphorylation.

Introduction

Aggregation of FcεRI in mast cells and basophils triggers numerous signaling steps, which eventually lead to degranulation and cytokine production. Early signaling events involve sequential activation of Src family protein tyrosine kinases Lyn and Fyn, and Syk/Zap family kinase Syk (1-4). The kinases phosphorylate several substrates, including β and γ subunits of the FcεRI and transmembrane adaptor protein LAT[3] (linker for activation of T cells). Phosphorylated LAT becomes a docking site for phospholipase C (PLC)γ1 and PLCγ2 and some other Src homology 2 (SH2) domain-containing signaling proteins, namely Grb2 adaptor (5, 6). Recently two groups have identified in mast cells another transmembrane adaptor protein called NTAL (non-T cell activation linker) or LAB (linker for activation of B cells) (7, 8), a product of the Williams-Beuren syndrome gene, *Wbscr5*. This protein, also expressed in B cells and NK cells but not in resting T cells, resembles LAT in possessing a short extracellular domain, a single transmembrane region, and a cytoplasmic tail with two palmitoylation cysteine residues and evolutionary conserved motifs containing tyrosine residues. Five of these motifs are of the YXN type (where X is any amino acid), and thus are potential binding sites for the SH2 domain of the cytosolic adaptor protein Grb2. However, unlike LAT, NTAL does not possess a consensus binding motif for PLCγ1 and PLCγ2 (7-9).

An important role of NTAL in immunoreceptor signaling was inferred from experiments in which diminution of NTAL expression by silencing RNA oligonucleotides resulted in reduced B cell receptor-mediated activation of MAPK in A20 cell line (8), as well as impaired degranulation in FcεRI-activated human mast cells (9). Unexpectedly, bone marrow-derived mast cells (BMMCs) isolated from NTAL-deficient mice were hyperresponsive to stimulation via the FcεRI, as evidenced by enhanced tyrosine

phosphorylation of several substrates, calcium response, degranulation and cytokine production. However, BMMCs obtained from mice lacking both LAT and NTAL had a more severe block in FcεRI-mediated signaling than BMMCs deficient in LAT alone (10, 11), suggesting that under certain circumstances NTAL may exert a positive signaling role even in BMMC.

Positive regulatory role of NTAL in immunoreceptor signaling was also observed in studies with immature chicken B-cell line, DT40 (12). In these cells, Grb2 negatively regulates the Ca^{2+} response through its binding to so far unidentified suppressor. It has been shown that SH2-mediated binding of Grb2 to tyrosine phosphorylated NTAL resulted in sequestering of the Grb2 inhibitory complex away from the cytosol, enhancing thus the calcium response. However, the role of NTAL in Ca^{2+} signaling is more complex as indicated by previous studies describing enhanced calcium responses in NTAL-deficient BMMCs (10, 11).

To enlighten the role of NTAL in FcεRI signaling we investigated by genetic and biochemical approaches the properties of rat basophilic leukemia (RBL) cells with enhanced or reduced expression of NTAL, and cells defective in Grb2 alone or in combination with NTAL. Our data indicate multiple regulatory roles of NTAL in FcεRI signaling in mast cells and document for the first time that activity of the store-operated Ca^{2+} (SOC) channels could be regulated by NTAL even in the absence of its enhanced tyrosine phosphorylation.

Materials and Methods

Antibodies, reagents, and cell cultures

The following mAbs were used: anti-Syk (13), anti-Lyn (14), anti-LAT (15), anti-FcεRI β subunit (JRK) (16), TNP-specific IgE mAb (IGEL b4 1) (17), DNP-specific IgE (18), and anti-NTAL (NAP-07; Exbio, Prague, Czech Republic). Phospho-Tyr-specific mAb (PY-20), conjugated to HRP, was purchased from Transduction Laboratories (Lexington, KY). Rabbit polyclonal Ab specific for Syk, Lyn, LAT, and NTAL, were prepared by immunization with recombinant fragments of Syk (13), Lyn (14), LAT (15) or rat NTAL (aa 30-196; GenBank accession no. Q8CGL2), respectively. Rabbit anti-IgE was prepared by immunization with whole IGEL b4 1. Polyclonal Abs specific for PLCγ1, PLCγ2, Erk1, phospho-Erk (specific for phosphorylated Tyr^{204}), Grb2, Akt1, phospho-Akt1 (specific for phosphorylated Ser^{473}) and HRP-conjugated donkey anti-goat IgG, goat anti-mouse IgG and goat anti-rabbit IgG, were obtained from Santa Cruz Biotechnology (Santa Cruz, CA). Rabbit anti-PI3K p85 subunit Ab (a mixture of equal amounts of antisera against the intact p85 subunit and the N-SH2 region of PI3K) was obtained from Upstate Biotechnology (Lake Placid, NY). Goat anti-mouse IgG and anti-rabbit IgG conjugated to colloidal gold particles of 10- or 5-nm were obtained from Amersham Pharmacia Biotech (Piscataway, NJ). Fura-2-AM and ^{45}Ca (sp. act. 566 MBq/mg Ca^{2+}) were purchased, respectively, from Molecular Probes (Eugene, OR) and MP Biomedicals (Irvine, CA). Origin of RBL cells (clone 2H3) and their culture conditions have been described (19).

Cloning of rat NTAL cDNA and its sequencing

Based on the nucleotide sequence of human *Wbscr5* (GenBank accession no. AF045555) and mouse *Wbscr5* (AF139987) we used 5' primer 5'-

AAAGAATTCGTCAGTGGTGTTGGCATCAGC-3' (EcoRI site underlined) and 3' primer 5'-AAAAAGCTTGGGCTTCCAGTCAGCACAGTC-3' (HindIII site underlined) to amplify the *NTAL* cDNA from RBL cells by RT-PCR as described (20). The PCR product was digested with EcoRI and HindIII and ligated into pGEM3Z vector (Promega, Madison, WI). The plasmid was amplified and the sequence of the insert was verified by DNA sequencing. All primers used in this study were obtained from Generi Biotech (Hradec Králové, Czech Republic).

Construction of plasmid vectors and isolation of cell lines with changes in expression of NTAL and/or Grb2

Mouse *NTAL* cDNA was obtained from V. Hořejší and cloned into EcoRI site of pcDNA3.1/Zeo vector (Invitrogen, Carlsbad, CA). The plasmid, pZeo-NTAL-1, was isolated and its sequence confirmed by sequencing. The plasmid or empty pcDNA3.1/Zeo vector (negative control) were transfected into RBL cells by electroporation (250 V and 750 μF) using Gene Pulser (Bio-Rad, Hercules, CA). Colonies resistant to zeocin (300 μg/ml) were then isolated, and clones with enhanced expression of NTAL were selected.

For production of NTAL- and Grb2-specific RNA silencing vectors, two sets of oligonucleotides, 5'-TTT GAA CTCCTA CGAGAATGTGCTCGGAAGCTTGCGAGCA CATTCTCGTAGGAGTTTTTTT-3' and 5'-CTAGAAAAAAACTCCTACGAGAATGTG CTCGCAAGCTTCCGAGCACATTCTCGTAGGAGTT-3' (for NTAL), and 5'-TTTGAA TAGATTACCACAGATCAACATAAGCTTTTGTTGATCTGTGGTAATCTATTTTTTT-3' and 5'-CTAGAAAAAAATAGATTACCACAGATCAACAAAAGCTTATGTTGATCT GTGGTAATCTATT-3' (for Grb2) were annealed and cloned into mU6pro vector as described (21). These sequences upon expression form hairpins using the loops in the middle of the sequences (underlined). The plasmids, pU6/siNTAL and pU6/siGrb2 were amplified, the sequences of the inserts were verified by DNA sequencing, and co-transfected at a ratio

10:1 with pstNeoB vector (22) into RBL cells by electroporation. In some experiments RBL cells were transfected with a mix of plasmids, pU6/siGrb2, pU6/siNTAL and pSTneoB at a ratio 5:5:1. Negative controls included empty mU6pro vector or mU6pro vector with the annealed NTAL insert as above except that 2 mismatches were introduced at positions 30 and 50 (pU6/NTAL-30/50). Clones resistant to antibiotic G418 (0.4 mg/ml) were isolated and analyzed by immunoblotting for NTAL and/or Grb2 expression.

Cell activation, immunoprecipitation, immunoblotting

Cells were harvested, resuspended in culture medium at a concentration $10x10^6$ cells/ml and sensitized with IgE (IGEL b4 1; ascites diluted 1:1000). After 30 min at 37°C the cells were washed in buffered saline solution (BSS) containing 20 mM HEPES (pH 7.4), 135 mM NaCl, 5 mM KCl, 1.8 mM $CaCl_2$, 1 mM $MgCl_2$, 5.6 mM glucose and 0.1% BSA, and challenged with Ag (TNP-BSA) for different time intervals. When the cells were activated with thapsigargin, the sensitization step was omitted. Towards the end of the activation period the cells were briefly centrifuged, and β-glucuronidase released into supernatant was determined as described (23) using 4-methylumbelliferyl β-D-glucuronide (Sigma-Aldrich, St. Louis, MO) as a substrate. The cell pellets were lysed in an ice-cold lysis buffer containing 50 mM Tris-HCl (pH 7.4), 150 mM NaCl, 2 mM EDTA, 10 mM β-glycerophosphate, 1 mM Na_3VO_4, 1 mM PMSF, 1 μg/ml aprotinin, 1 μg/ml leupeptin, and supplemented with 1% Nonidet-P40 (NP40) (for Lyn, Syk, Erk) , 0.2% Brij 96 (for FcεRI) or 1% NP40 plus 1% n-dodecyl β-D-maltoside (for NTAL and LAT). In experiments analyzing the association of proteins with large signaling assemblies, the activated or non-activated cells were resuspended in ice-cold PBS supplemented with 0.1% saponin, 5 mM $MgCl_2$ and 1 mM Na_3VO_4 (permeabilization buffer). After 5 min incubation on ice, the cells were spun down and extracted for 15 min in a lysis buffer containing 1% Triton X-100.

Postnuclear supernatants were immunoprecipitated with corresponding Abs prebound to UltraLink-immobilized protein A or G (Pierce, Rockford, IL), size-fractionated by SDS-PAGE and immunoblotted with PY-20-HRP-conjugate or with protein-specific Abs followed by an appropriate second stage HRP-conjugated anti-mouse or anti-rabbit IgG. HRP signal was detected by the ECL reagent (Amersham, Little Chalfont, GB). Tyrosine-phosphorylated Erk and Akt were determined by direct immunoblotting with phosphospecific antibodies. Immunoblots were quantified by Luminescent Image Analyzer LAS 3000 (Fuji Photo Film Co, Tokyo, Japan) and further analyzed by AIDA image analyzer software (Raytest GmbH, Straubenhardt, Germany). The amount of tyrosine phosphorylated proteins was corrected for the amount of proteins immunoprecipitated as determined by densitometry of immunoblots after stripping of the membranes, followed by development with the corresponding Abs.

Flow cytofluorometry analysis of FcεRI and F-actin

To determine the surface FcεRI, cells were exposed to 1 μg/ml anti-TNP IgE followed by FITC-conjugated anti-mouse IgG cross-reacting with mouse IgE, and probed by flow cytofluorometry using a FACSCalibur (Becton Dickinson, Mountain View, CA). The total amount of polymeric actin was measured as previously described (24, 25). Briefly, 10^6 cells in 200 μl BSS-BSA were sensitized with IgE and stimulated or not with Ag for various time intervals. The reaction was terminated by adding 300 μl of PBS containing 50 μg of lysophosphatidylcholine, 6% formaldehyde and 0.125 μg/ml FITC-phalloidin (Sigma-Aldrich). After 10 min incubation at 37°C, the cells were centrifuged and resuspended in 1 ml of PBS before flow cytofluorometry analysis. The geometric mean fluorescence intensity was determined for each sample and data points were plotted relative to the mean fluorescence intensity of nonactivated control cells.

Cytokine detection

Quantitative measurements of rat TNF-α was performed using murine TNF-α ELISA development kit (cross-reacting with rat TNF-α; PeproTech Inc. Rocky Hill, NJ) according to the manufacturer's instructions.

Lyn kinase assay

In vitro Lyn kinase assay was performed as previously described (27). Briefly, Lyn was immunoprecipitated from cells lysed by sequential treatment with 0.1% saponin and 1% Triton X-100. Saponin/Triton-extracted material was incubated with rabbit anti-Lyn Ab and the immunocomplexes were collected on protein A beads. The kinase reaction was carried out for 30 min at 37°C in kinase buffer (25 mM HEPES, pH 7.2, 3 mM $MnCl_2$, 0.1% NP-40, 100 mM Na_3VO_4, 20 mM $MgCl_2$) containing 1 μCi [γ-^{32}P] ATP (Amersham Pharmacia Biotech), 100 μM cold ATP and 0.5 μg/μl denatured enolase as exogenous substrate. The kinase reaction products were resolved by SDS-PAGE, transferred to nitrocellulose, visualized by autoradiography and quantified by Fuji Bio-Imaging Analyzer Bas 5000.

Electron microscopy

Plasma membrane sheets were prepared from nonactivated or activated cells and examined by electron microscopy as described (28) with some modifications (29).

Immune complex PI3K and PLCγ assay

PI3K and PLCγ enzymatic activity was measured as previously described (25). Briefly, FcεRI-activated or control cells ($2x10^6$) were solubilized in lysis buffer supplemented with 1% Triton-X100. PI3K in postnuclear supernatant was immunoprecipitated with anti-PI3K p85 subunit Ab and immunocomplexes were collected

on UltraLink-immobilized protein A. PI3K assay was initiated by addition of 25 µl of kinase buffer [20 mM HEPES (pH 7.4), 20 mM $MgCl_2$ and 0.25 mM EGTA] containing 10 µg of sonicated phosphatidylinositol (Sigma-Aldrich) and 37 kBq [γ-^{32}P]ATP. After 30 min at 25°C, the reaction was terminated and lipids were separated on TLC Silica gel-60 plate (Merck, Darmstadt, Germany) in a mixture of chloroform/methanol/4M ammonium hydroxide (9:7:2, v/v/v) for 1 h. ^{32}P-labeled materials were visualized by autoradiography and quantified by Fuji Bio-Imaging analyzer Bas 5000.

To determine the PLCγ enzymatic activity, postnuclear supernatants from non-activated or activated cells were immunoprecipitated with anti-PLCγ1 and immunocomplexes were collected on beads of UltraLink-immobilized protein A. The beads were washed and resuspended in 25 µl of reaction buffer followed by addition of 10 µl substrate solution [25 mM sodium phosphate, pH 6.8, 50 mM KCl, 2.5% Triton X-100, 6 µg of phosphatidylinositol 4,5-bisphosphate (PIP2)] supplemented with 1.1 kBq of P[^{3}H]IP2 (PerkinElmer Life Sciences, Boston, MA). After 30 min at 37°C, the reaction was stopped by adding 300 µl of ice-cold 0.5% BSA in PBS. The samples were centrifuged and 300 µl aliquots of the supernatant were mixed with 100 µl of ice-cold 25% (w/v) TCA. Precipitates were removed by centrifugation and supernatants were collected for quantification of released [^{3}H]inositol 1,4,5-trisphosphate (IP3) by liquid scintillation counting.

IP3 determination

The procedure used a commercially available [^{3}H]IP3 radioreceptor assay kit and followed the manufacturer's protocol (PerkinElmer Life Sciences). Briefly, IgE-sensitized cells ($6x10^6$) were stimulated or not with TNP-BSA (500 ng/ml) in 500 µl BSS-BSA. At various time intervals the reactions were terminated by adding 100 µl of ice-cold 100% TCA and the tubes were incubated on ice for 15 min. After centrifugation, supernatants were incubated for 15 min at room temperature and then mixed with a mixture of 1,1,2-trichloro-

1,2,2,-trifluoroethane-trioctylamin (3:1). The tubes were vortexed, centrifuged, and water phase was used for determination the radioactivity bound to IP3-binding protein.

Measurement of intracellular Ca^{2+} concentrations

Changes in the concentration of free intracellular Ca^{2+} $[Ca^{2+}]_i$ were determined using Fura-2/AM as a probe as previously described (23). IgE-sensitized and control cells were resuspended in BSS-BSA supplemented with 2.5 mM probenecid and 2 μM Fura-2/AM. After 40 min at 37°C, the cells were washed with BSS-BSA-probenecid and immediately before measurement briefly centrifuged and resuspended in BSS-BSA. The levels of $[Ca^{2+}]_i$ were monitored using luminescence spectrometer LS-50B (PerkinElmer, Buckinghamshire, GB) with excitation wavelengths 340 and 380 nm, and with constant emission at 510 nm. The values were calculated using ICBC Calibration PerkinElmer Fluorescence WinLab software (PerkinElmer Life Sciences).

Uptake of extracellular calcium

Calcium uptake was determined by a modified previously described procedure (30). Briefly, the cells ($2x10^6$) were resuspended in 100 μl BSS-BSA with 1 mM Ca^{2+}, mixed with 100 μl of BSS-BSA supplemented with $^{45}Ca^{2+}$ and various concentrations of thapsigargin, and incubated for 5 min at 37°C. The reaction was terminated by placing the tubes on ice followed by suspending 100 μl aliquots on the wall of the microtest tube separated by air space from the 12% BSA in PBS (300 μl) at the bottom. Cells with bound ^{45}Ca were separated from free $^{45}Ca^{2+}$ by centrifugation at 1200 x g for 15 min at 4°C through 12% BSA. The cell pellets were recovered by freezing the tubes, slicing off the tube bottom, and solubilized with 1 ml of 1% Triton X-100. The radioactivity was measured in 10 ml scintillation liquid (EcoLite ™, ICN Biomedicals, Inc) in a scintillation counter with QuantaSmart software (PerkinElmer). The efflux of calcium was determined in cells loaded

with $^{45}Ca^{2+}$ after 2 μM thapsigargin-induced $^{45}Ca^{2+}$ influx for 15 min at 37^{0}C. The cells were then washed and incubated in BSS-BSA containing 1 mM Ca^{2+} for different time intervals. The amount of cell-associated $^{45}Ca^{2+}$ was determined after removing free extracellular $^{45}Ca^{2+}$ as described above.

Results

Generation and initial characterization of mast cell lines with enhanced or reduced expression of NTAL

To prepare RNA silencing probes specific for rat NTAL, we first cloned rat NTAL (*Wbscr5*) cDNA (GenBank accession no. AY170849). As shown in Fig. 1*A*, the predicted amino acid sequence of rat NTAL (204 aa) is one amino acid longer than its mouse ortholog (GenBank accession no. NM_020044). All tyrosine motifs as well as a potential palmitoylation site (CxxC motif) are conserved in rat and mouse NTAL sequence, suggesting identical functions.

Next, we transfected RBL cells with pZeo-NTAL-1 vector containing mouse NTAL cDNA or empty pcDNA3.1/Zeo vector, and isolated stable cell lines resistant to zeocin. We also isolated RBL cells transfected with pU6/siNTAL-1, encoding rat NTAL-specific hairpin siRNA, and pstNeoB, and isolated G418-resistant stable cell lines. As controls, G418-resistant cells after transfection with pU6/NTAL-30/50 and pstNeoB were also isolated. The expression levels of NTAL in individual clones are shown in Fig. 1*B*. Compared to control RBL cells, there was an up to 7.4-fold increase in the expression of NTAL in cells after transfection with pZeo-NTAL-1, and almost no detectable endogenous NTAL in cells transfected with pU6/siNTAL-1 (>95% inhibition). Lyn (Fig. 1*B*) and several other signaling proteins (see below) were not affected by the transfection and knock-down procedure. Cells transfected with empty pcDNA3.1/Zeo, pU6/NTAL-30/50 or pstNeoB vector did not differ in NTAL expression and their secretory response from untransfected RBL cells; only control RBL cells are therefore presented in Fig. 1*B* and other figures.

After stimulation of RBL cells with Ag, NTAL was phosphorylated on tyrosine residues as detected by immunoblotting with PY-20-HRP conjugate (Fig. 1*C*; top). We

confirmed previous data (7, 8, 10-12) that phosphorylated NTAL bound the Grb2 adaptor (Fig. 1*C*; middle); the amount of bound Grb2 correlated with that of phosphorylated NTAL present.

The relationship between the amount of NTAL and FcεRI-mediated degranulation was estimated by the production of β-glucuronidase in individual cell lines at various time intervals after triggering with Ag (Fig. 1*D* and *E*). In cells expressing high levels of NTAL (3B/18, 3B/17 and 2A/4), the secretory response was reduced to ~50% of that found in control RBL cells or cells transfected with empty vector (not shown). In the cell line with lower level of exogenous NTAL expression (1A/1), the secretory response was inhibited less, indicating a correlation between the inhibitory effect and the extent of NTAL overexpression. The secretory response of 2A/4 cells was reduced at all concentrations of Ag used; two other clones with high NTAL levels (3B/18 and 3B/17) exhibited similar properties. To simplify the presentation, only data from clone 2A/4 (NTAL+) are included in Fig. 1*F* and other figures. The secretory response was also inhibited in all cell lines with decreased amount of NTAL (Fig. 1*E*) at all concentrations of Ag used; only data from clone C4 (NTAL-) are shown in Fig. 1*F* and other figures. The finding that FcεRI-mediated secretory response was inhibited in both NTAL+ and NTAL- cells was unexpected and induced further experiments.

Using IgE-sensitized cells and fluorescently labeled anti-IgE we found that all cell lines differing in NTAL expression exhibited comparable amount of FcεRI as detected by flow cytometry (Fig. 2*A*). Light microscopy of cultured NTAL+ cells (Fig. 2*B*) and other NTAL overexpressors (not shown) revealed decreased adhesion to the substrate, a more rounded morphology and less developed processes when compared to RBL cells. In contrast, NTAL- cells had fewer but more developed processes (Fig. 2*B*). The observed changes in morphology in NTAL- cells were probably related to an enhanced amount of F-

actin observed in nonactivated cells (Fig. 2*C*). After FcεRI-triggering, the amount of F-actin rose as described before (26, 31) and remained higher in NTAL- cells than RBL cells. In contrast, in NTAL+ cells activation-induced increase in F-actin was less pronounced (Fig. 2*C*).

Electron microscopy on membrane sheets isolated from nonactivated NTAL+ cells showed NTAL distributed in clusters, which resembled NTAL clusters present in RBL cells (Fig. 2*D*, a and b; 5-nm gold particles). However, the average cluster size was higher in NTAL+ cells (94.0 ± 24.8 nm; mean ± SD, n = 3) than in RBL cells (48.0 ± 8.1 nm, n = 3). As expected, the density of NTAL-bound gold particles was elevated in NTAL+ cells (68.7 ± 23.4/μm^2) compared to RBL cells (35.9 ± 13.0/μm^2). For control we also assessed the distribution of gold particles in NTAL- cells, where only background levels were found (Fig. 2*D*, c); the numbers of FcεRI β subunit were comparable in RBL, NTAL+ and NTAL- cells (Fig. 2*D*, a-c; 10-nm gold particles). In Ag-activated cells, FcεRI formed clusters within osmiophilic regions, which were often associated, but not intermixed, with NTAL clusters; the NTAL average cluster sizes and label densities were analogous to those in nonactivated cells. Ag-induced formation of FcεRI clusters in osmiophilic regions of the plasma membrane was not affected by enhanced or reduced NTAL expression (Fig. 2*D*, d-f), suggesting that the expression of NTAL does not interfere with receptor aggregation.

NTAL overexpression inhibits the FcεRI-induced tyrosine phosphorylation of FcεRI subunits, Syk and LAT

Next we assessed the tyrosine phosphorylation of several proteins known to be pivotal for initial phases of FcεRI signaling. When total cell lysates from nonactivated or Ag-activated cells were analyzed by SDS-PAGE and immunoblotting with phosphotyrosine-specific mAb, NTAL+ cells, compared to the control RBL cells, exhibited significantly

reduced tyrosine phosphorylation of several proteins (~38 kDa, ~55 kDa, ~70 kDa, ~97 kDa and ~115 kDa) and enhanced phosphorylation of some other proteins, including a protein of ~30 kDa, presumably NTAL (Fig. 3*A*). On the other hand, NTAL- cells showed a phosphorylation pattern more similar to that in control RBL cells; some proteins (e.g. ~40 kDa and 50 kDa) showed an increase, other [~30 kDa (presumably NTAL) and ~70 kDa] a decrease in phosphorylation.

To analyze individual molecules, we first immunoprecipitated FcεRI, Syk and LAT from control and Ag-activated cells and found decreased tyrosine phosphorylation of all of those proteins during activation of NTAL+ cells, compared to RBL cells (Fig. 3*B-G*). In NTAL- cells, phosphorylation of FcεRI β and γ subunit, Syk and LAT was comparable to that in RBL cells. Phosphorylation of these proteins depends on Lyn kinase activity (3); we therefore also examined the binding of Lyn to FcεRI, the first well defined intermolecular interaction step in FcεRI signaling (32), and the enzymatic activity of Lyn. Immunoprecipitation studies showed a clear activation-dependent association of Lyn with FcεRI in both control RBL and NTAL- cells (Fig. 3*B*, bottom). In contrast, no Lyn was coprecipitated with FcεRI in NTAL+ cells. To elucidate the molecular basis of this difference we assessed Lyn kinase enzymatic activity in immunocomplex kinase assay *in vitro* (Fig. 3*H*). Surprisingly, Lyn kinase autophosphorylation and phosphorylation of the Lyn substrate, enolase, was higher in NTAL+ cells than in control RBL or NTAL- cells. Thus, the observed inhibition of phosphorylation of FcεRI and several other proteins is not caused by suppressed Lyn kinase activity.

Properties of signaling assemblies depend on NTAL expression levels

To examine signaling assemblies during FcεRI-induced activation, the cells were first permeabilized with cholesterol-sequestering reagent saponin to release free cytoplasmic

components. All membrane components, including those residing in lipid rafts and otherwise insoluble in nonionic detergents, were then efficiently solubilized with Triton X-100. In our previous study, we have found that this two-step solubilization procedure allows better estimation of formation of signaling assemblies in the course of cell activation (25). Using this two-step solubilization procedure we compared the signaling assemblies formed by Grb2, which is the major adaptor protein bound to tyrosine phosphorylated NTAL (7, 8). Immunoblotting analyses of Grb2 immunoprecipitates with PY-20 mAb showed that the amount of Grb2-associated and tyrosine phosphorylated proteins increased during Ag-mediated activation (Fig. 4*A*). One of the participating tyrosine phosphorylated proteins was LAT, as determined by its molecular weight (~38 kDa) and immunoblotting with LAT-specific antibodies (Fig. 4*A*, *B* and *D*). Consistent with previous data (Fig. 3), the amount of phosphorylated LAT bound to Grb2 was reduced in NTAL+ cells and enhanced in NTAL- cells. There was only an insignificant decrease in the amount of LAT in Grb2 immunocomplexes from NTAL+ cells, compared to RBL cells (Fig. 4*D*), suggesting that reduced LAT phosphorylation did not remove all Grb2 binding sites. Another of the tyrosine phosphorylated proteins was NTAL, as determined by its molecular weight (~30 kDa) and immunoblotting with NTAL-specific antibodies (Fig. 4*A*, *C* and *E*). As expected, the amount of Grb2-associated NTAL was enhanced in NTAL+ cells and undetectable in NTAL- cells.

Recently we and others have found that Grb2 immunocomplexes from Ag-activated RBL cells possess PI3K activity (29, 33, 34). To determine whether NTAL has any effect on the formation of these complexes, we measured PI3K activity in Grb2 immunoprecipitates. Data in Fig. 4*F* indicate that in resting cells the activity of PI3K in Grb2 immunoprecipitates was higher in NTAL- cells than in RBL and NTAL+ cells. After FcεRI triggering, higher activity of PI3K in Grb2 immunocomplexes was observed at all time intervals analyzed in RBL cells and even more in NTAL- cells, whereas in NTAL+ cells only a transient increase (2.1-fold after 0.5 min) was seen. When PI3K was directly immunoprecipitated and the

immunocomplexes were tested for PI3K activity, all cell lines showed enhanced activity in response to FcεRI-mediated activation, and the dramatic differences between NTAL+ and NTAL- cells were less pronounced (Fig. 4*G*). Nevertheless, even under these conditions, PI3K activity associated with large signaling assemblies was higher in NTAL- cells than in RBL or NTAL+ cells. When NTAL was immunoprecipitated from RBL or NTAL+ cells, no PI3K activity was detected in immunoprecipitates from either nonactivated or FcεRI-activated cells (not shown). Thus, NTAL does not form complexes possessing PI3K activity, but inhibits the formation of functional PI3K-Grb2 complexes.

Enzymatic activity of PI3K results in the production of phosphatidylinositol 3,4,5-trisphosphate (PIP3). PIP3 and phosphatidylinositol 3,4-bisphosphate recruit Akt to the plasma membrane, where it is phosphorylated and activated. Phosphorylation of Akt was enhanced after FcεRI triggering in RBL cells (Fig. 5*A*). In nonactivated NTAL+ cells the amount of Akt and phospho-Akt associated with saponin-permeabilized cells was higher, but the changes faded out 2 and 5 min after FcεRI triggering. In accordance with the enhanced activity of PI3K in NTAL- cells (Fig. 4*G*), phosphorylation of Akt was also enhanced. These data support the concept that NTAL negatively regulates the formation of signaling assemblies containing PI3K and Akt.

Overexpression of NTAL inhibits MAPK pathway

The interaction of NTAL with Grb2/Sos/Shc could play a role in the regulation of cytokines production (7, 8). It has actually been reported that phosphorylation of Erk and production of several cytokines is enhanced in BMMC from NTAL$^{-/-}$ mice (10, 11). Therefore, we examined the phosphorylation of Erk and secretion of TNF-α in cells with enhanced or impaired expression of NTAL. Immunoblotting experiments showed that the amount of phosphorylated Erk in Ag-activated RBL cells was increased, reaching the peak 2

min after triggering (Fig. 5*B*). NTAL overexpression resulted in an impaired phosphorylation of Erk. In contrast, the onset of Erk phosphorylation in NTAL- cells was faster and remained higher at all time intervals tested. Inhibition of Erk phosphorylation in NTAL+ cells correlated with an inhibition of TNF-α secretion from cells activated by two different doses of Ag (Fig. 5*C*). In NTAL- cells, Ag-induced secretion of TNF-α was reduced only at lower Ag concentration (100 ng/ml), whereas no inhibition was observed at 500 ng/ml.

Expression levels of NTAL modulate activity of PLCγ

Immunoblotting analyses of PLCγ1 and PLCγ2 immunoprecipitates from saponin/Triton X-100 solubilized cells showed that the amount of tyrosine phosphorylated PLCγ1 associated with signaling assemblies decreased in both NTAL+ cells and NTAL- activated cells (Fig. 6*A*). Recruitment of PLCγ2 and degree of its phosphorylation were comparable in all cell lines (Fig. 6*B*). Enzymatic activity of PLCγ was detected by immunocomplex PLCγ assay, determining the production of [^{3}H]IP3 from P[^{3}H]IP2 substrate. In nonstimulated cells the activity of PLCγ was comparable in RBL, NTAL+ and NTAL- cells (Fig. 6*C*). After FcεRI triggering, PLCγ activity rapidly increased in all cell lines; however, in NTAL- cells, and especially in NTAL+ cells the increase was lower than in RBL cells. These findings were corroborated by direct measurements of IP3 levels (Fig. 6*D*). In nonactivated cells IP3 concentrations were similar in all cell lines under study, but in FcεRI-activated cells IP3 reached higher levels in RBL cells compared to NTAL- cells, and especially to NTAL+ cells.

Intracellular Ca^{2+} mobilization and uptake of extracellular Ca^{2+} are affected by NTAL expression level

Enhanced levels of IP3 induce a release of calcium from intracellular stores, followed by calcium influx through SOC channels in the plasma membrane (37). To determine the role of NTAL in both these steps we followed the calcium response in cells under different conditions. NTAL- cells activated with Ag in the presence of extracellular Ca^{2+}showed a lower calcium response than control cells, but identical initial kinetics. In contrast, NTAL+ cells exhibited a delay in calcium response and a slower decline to baseline levels (Fig. 7*A*). Activation of the cells by Ag in the absence of extracellular calcium resulted in ~30% inhibition of the calcium response in NTAL- cells relative to RBL cells, whereas in NTAL+ cells this response was dramatically inhibited and delayed (Fig. 7*B*). After increasing the concentration of extracellular Ca^{2+}, both RBL and NTAL- cells showed rapid increase in $[Ca^{2+}]_i$, with faster return to initial levels in NTAL- cells, whereas NTAL+ cells showed only a week response to addition of extracellular Ca^{2+} (Fig. 7*B*).

The observed dramatic decrease in calcium response in Ag-activated NTAL+ cells could be related to decreased activity of PLCγ and impaired production of IP3 (Fig. 6*C* and *D*), and/or to negative regulatory role of NTAL in Ca^{2+} mobilization at later stages. To explore the role of NTAL on Ca^{2+} mobilization independently of its effect on activity of PLCγ, cells were activated by thapsigargin, an agent that induces the release of Ca^{2+} from intracellular stores by inhibiting the endoplasmic reticulum ATPase (38). In the absence of extracellular Ca^{2+}, thapsigargin induced a small increase in $[Ca^{2+}]_i$ in all cell lines, suggesting that NTAL does not interfere with the transport of thapsigargin to its target and release of Ca^{2+} from cytoplasmic stores. Interestingly, when the extracellular Ca^{2+} level was restored, 5 independent experiments showed that the maximum $[Ca^{2+}]_i$ in NTAL+ cells was higher (750 ± 80 nM; mean ± SD) than in RBL cells (620 ± 54 nM) and NTAL- cells (580 ± 37). Furthermore, $[Ca^{2+}]_i$ reverted to baseline level more rapidly in NTAL- cells than in RBL and NTAL+ cells (Fig. 7*C*).

These data suggested that NTAL could regulate the transport of extracellular Ca^{2+} through the plasma membrane. To test this we measured the ^{45}Ca uptake in thapsigargin-stimulated cells. A direct correlation was found between the amount of NTAL expressed and calcium uptake; it was high in NTAL+ cells, medium in RBL cells and low in NTAL- cells (Fig. 7*D*). The observed correlation could imply not just an important role of NTAL in regulating Ca^{2+} uptake but also an inhibitory effect of NTAL on the release of Ca^{2+} from the cells. Next we therefore labeled the cells with $^{45}Ca^{2+}$, washed them and measured the radioactivity retained within the cells at different time intervals. Results presented in Fig. 7*E* show that all cell lines exhibited the same kinetics of $^{45}Ca^{2+}$ efflux. Together with previous findings on Ca^{2+} uptake, these data indicate that NTAL positively regulates Ca^{2+} uptake rather than Ca^{2+} efflux.

Experiments with DT40 chicken B cells suggested that phosphorylated NTAL could regulate the Ca^{2+} uptake by a mechanism involving its binding with Grb2, a negative regulator of Ca^{2+} signaling (12). We therefore attempted to find out whether or not NTAL is phosphorylated in thapsigargin-activated cells. NTAL was immunoprecipitated from nonactivated or thapsigargin-activated RBL or NTAL+ cells and its phosphorylation was assessed by immunoblotting with PY-20-HRP. Data presented in Fig. 7*F* indicate that thapsigargin had no effect on NTAL tyrosine phosphorylation in either RBL or NTAL+ cells. To determine whether Grb2 could function as a negative regulator of Ca^{2+} response in RBL cells, we transfected the cells with pU6/siGrb2 plus pSTneoB and selected G418-resistant clones, G1 and G9, with decreased amount of Grb2 (Fig. 8*A*). We also isolated RBL-derived cells with decreased amounts of both NTAL and Grb2 after transfection with pU6/siNTAL and pU6/siGrb2 and pSTneoB (Fig. 8*B*, clones NG2 and NG10). It should be noted that the amount of LAT was not affected in any transfectant (Fig. 8*A* and *B*), confirming the specificity of the knock-down procedure. Detailed analysis showed that Ag-activated RBL cells with decreased amount of Grb2 exhibited lower increase in $[Ca^{2+}]_i$ than

RBL cells transfected with empty vector (Fig. 8*C*). When the expression of both NTAL and Grb2 was reduced, an even deeper decrease in $[Ca^{2+}]_i$ was observed (Fig. 8*D*). These data indicate that Grb2 functions as a positive regulator of Ca^{2+} response in RBL cells.

Discussion

Variation of NTAL expression levels is shown to have multiple effects on FcεRI-mediated activation events in RBL cells. Permanent cell lines with low expression were isolated after transfection with U6-based expression vector producing NTAL siRNA. In contrast to previous studies in which the transfected RNA reduced the expression levels by ~70% (9), hairpin siRNA strategy lowered it by >95%. Stable cell lines with enhanced NTAL expression were obtained after transfection of mouse NTAL cDNA under cytomegalovirus promoter. We expected that NTAL overexpression would uncover additional signaling pathways undetectable in NTAL-deficient cells if they acted downstream of the early regulatory effects of NTAL.

Initial characterization revealed that cells with different expression levels of NTAL exhibited restricted secretory response after FcεRI triggering, unrelated to differences in surface expression of FcεRI and evident at all concentrations of Ag used. NTAL levels also affected morphology of the cells; NTAL+ cells being less adherent to substrate and NTAL- cells having longer processes. The observed changes in cell morphology could be related to the amount of F-actin and its formation during FcεRI signaling. Thus, NTAL- cells had more F-actin than parental RBL and NTAL+ cells, and only a weak increase in F-actin formation was induced by activation of both NTAL+ and NTAL- cells .

Previously we have examined the distribution of NTAL and LAT by electron microscopy of membrane sheets. NTAL in resting RBL cells was localized in small clusters, topographically separated from clusters of LAT and FcεRI (10), but not Thy-1 (39). When membrane sheets were isolated from NTAL overexpressors, no difference in the distribution of FcεRI and NTAL was observed except that the average cluster size and density of NTAL-bound gold particles was higher in NTAL+ than control cells. Importantly, the absence of

NTAL from the FcεRI aggregates is not confined just to control RBL cells, as reported previously (10), but applies also to NTAL+ cells (this study). Together with our finding of normal redistribution of aggregated FcεRI into osmiophilic regions in NTAL+ cells, these data suggest that the initial FcεRI aggregation step induced by multivalent Ag is not changed in NTAL overexpressors.

Immunochemical studies showed that overexpression of NTAL inhibited the tyrosine phosphorylation of FcεRI β and γ subunits, Syk and LAT in Ag-activated cells. Consequently, recruitment of PLCγ to signaling assemblies and its tyrosine phosphorylation and activation were inhibited. Reduced production of PLCγ metabolite IP3 led to a reduction in both the release of Ca^{2+} from intracellular stores and the uptake of extracellular Ca^{2+} through SOC channels. This could explain the inhibition of the secretory response in antigen-activated cells. The MAP kinase signaling pathway was also inhibited in NTAL+ cells as reflected in the impaired tyrosine phosphorylation of Erk and subsequent low secretion of TNF-α.

Decreased tyrosine phosphorylation of FcεRI subunits in NTAL+ cells suggested that the activity of Lyn kinase is inhibited. However, immunocomplex kinase assays showed Lyn kinase activity in NTAL+ cells is undiminished, implying that NTAL interferes with the accessibility of Lyn to FcεRI. This possibility is strengthened by data indicating that the amount of Lyn coprecipitated with FcεRI was higher in activated RBL cells than in NTAL+ cells. Because Lyn, like NTAL, seems to be localized in lipid rafts (7, 40), it is possible that direct or indirect interaction of Lyn with NTAL precludes the interaction between Lyn and FcεRI subunits. Although immunoprecipitation and immunocomplex kinase assays failed to show NTAL-Lyn interactions (L.D., unpublished), it is possible that procedures used to isolate NTAL immunocomplexes destroyed these interactions.

Our results indicate that the signaling assemblies formed in NTAL+ cells are different from those formed in control or NTAL- cells. Indeed, in NTAL+ cells, more NTAL and less LAT is bound to Grb2, supporting the concept of competition between NTAL and LAT for Grb2 as a substrate (10). In contrast, in Ag-activated NTAL- cells phosphorylation of FcεRI subunits, Syk and LAT was not inhibited. However, association of PLCγ with insoluble complexes, its phosphorylation and its enzymatic activity were less efficient and resulted in a partial inhibition of downstream events. The impaired function of PLCγ could reflect involvement of NTAL in the formation of signaling assemblies required for PLCγ enzymatic activity (35, 36, 41). As previously shown (10, 42, 43), Grb2 forms complexes with SHP-2 phosphatase, and these complexes could bind to NTAL to regulate early signaling events. Alternatively, if PLCγ somehow interacts with NTAL, its enzymatic activity would be inhibited in NTAL- cells even though the early FcεRI-activation events proceed normally. Although we were unable to coprecipitate PLCγ with NTAL (L.D., unpublished), it remains possible that these interaction are sensitive to the solubilization and immunoprecipitation procedures.

If IP3 signal generated by FcεRI aggregation is bypassed by thapsigargin, NTAL+ cells show a higher uptake of extracellular Ca^{2+} than control RBL cells. This suggests that NTAL could have a positive regulatory role in Ca^{2+} uptake. This is corroborated by complementary studies in which thapsigargin-activated NTAL- cells showed a lower Ca^{2+} uptake. The role of NTAL in uptake of extracellular Ca^{2+} is unclear but could be related to NTAL-dependent Ca^{2+}-regulating signal circuit recently described in DT40 B lymphocytes (12). In these cells, Grb2 plays a negative regulatory role in Ca^{2+} uptake, which appears to be eliminated upon binding to NTAL. However, several pieces of evidence indicate that in rodent mast cells NTAL plays a different role in Ca^{2+} response. First, no inhibition in $[Ca^{2+}]_i$ was observed in Ag-activated BMMC from $NTAL^{-/-}$ mice; rather, there was an enhancement

of the Ca^{2+} response (10, 11). Second, Ag-activated NTAL$^{-/-}$ BMMC showed no decrease, but rather an increase in the uptake of extracellular $^{45}Ca^{2+}$; this could be related to enhanced activity of PLCγ (10, 11). Third, there was a higher Ca^{2+} response to FcεRI triggering in NTAL- cells than in NTAL+ cells. It should be emphasized that the highest Ca^{2+} response was observed in control RBL cells, suggesting that an optimal concentration and/or topography of NTAL is required for maximum Ca^{2+} response. Different expression levels of NTAL and differences in its interaction with other signaling molecules could in part explain why, under varying conditions, NTAL has a negative (10, 11) or positive (8, 9) regulatory roles. Fourth, after activation by Ag in the absence of extracellular Ca^{2+} and restoration of Ca^{2+} level later on, there was no dramatic difference between control and NTAL- cells in initial Ca^{2+} uptake. In contrast, the response in NTAL+ was markedly inhibited. This inhibition reflected low levels of Ca^{2+} released from intracellular stores and consequently low Ca^{2+} influx through the SOC channels. Finally, $[Ca^{2+}]_i$ in cells activated with thapsigargin in the absence of extracellular Ca^{2+} was not dependent on NTAL. However, when Ca^{2+} was replenished, a significant increase in $[Ca^{2+}]_i$ occurred in the following sequence: NTAL+ > control RBL > NTAL- cells. These data suggest that NTAL could play a positive role in regulating the Ca^{2+} uptake at the level of SOC channels. Our finding of correlation between $^{45}Ca^{2+}$ uptake and the amount of NTAL in thapsigargin-activated cells supports the notion. The possibility that NTAL modulated Ca^{2+} efflux rather then its influx was excluded by experiments measuring the kinetics of calcium release from activated $^{45}Ca^{2+}$-labeled cells. Interestingly, no increase in tyrosine phosphorylation of NTAL was observed in thapsigargin-triggered cells. Thus, our data indicate that NTAL could have a novel regulatory role in Ca^{2+} uptake independent of *de novo* NTAL tyrosine phosphorylation. Possible regulatory functions of NTAL at different phases of FcεRI signaling are shown in Fig. 9. At early stages of activation (Phase I) NTAL serves as a

substrate for protein tyrosine kinases and thus interferes with phosphorylation of FcεRI and LAT by a competitive mechanism. Furthermore, phosphorylated NTAL binds Grb2 and other signaling molecules, which could modulate the activity of various enzymes, including PI3K and PLCγ. At later stages of activation (Phase II), NTAL could affect the function of SOC channels, reflecting its direct or indirect interactions with channel-forming proteins and/or their regulators such as Orai1 and/or Stim1 (44-47). This function of NTAL is not dependent on its enhanced tyrosine phosphorylation.

In summary, NTAL overexpression suppresses early FcεRI-induced activation events, but has a positive effect on the uptake of extracellular Ca^{2+} in thapsigargin-stimulated cells. Accordingly, inhibition of NTAL expression has no inhibitory effect on early signaling pathways but does suppress the late ones, including the uptake of extracellular Ca^{2+}. Expression levels of NTAL may thus regulate mast cells activation at multiple steps. In mast cells with wild-type levels of NTAL, the appropriate balance between the inhibitory and stimulatory effects of NTAL is critical for setting the thresholds for FcεRI-induced degranulation and cytokine response. This balance may be affected by numerous factors, including activity of c-kit and other receptors (48). This could explain why down-regulation of NTAL expression either inhibited (9) or enhanced (10, 11) FcεRI-induced secretory response in different mast cell types.

Acknowledgments

We thank H. Mrázová, R. Budovičová, D. Lorenčíková, M. Dráber, I. Lišková and J. Musilová for technical assistance and A. Koffer for critical reading of the manuscript.

Disclosure

The authors have no financial conflict of interest.

References

1. Eiseman, E., and J. B. Bolen. 1992. Engagement of the high-affinity IgE receptor activates *src* protein-related tyrosine kinases. *Nature* 355: 78-80.

2. Minoguchi, K., W. D. Swaim, E. H. Berenstein, and R. P. Siraganian. 1994. Src family tyrosine kinase $p53/56^{lyn}$, a serine kinase and FcεRI associate with α-galactosyl derivatives of ganglioside GD_{1b} in rat basophilic leukemia RBL-2H3 cells. *J. Biol. Chem.* 269: 5249-5254.

3. Parravicini, V., M. Gadina, M. Kovarova, S. Odom, C. Gonzalez-Espinosa, Y. Furumoto, S. Saitoh, L. E. Samelson, J. J. O'Shea, and J. Rivera. 2002. Fyn kinase initiates complementary signals required for IgE-dependent mast cell degranulation. *Nat. Immunol.* 3: 741-748.

4. Daäron, M. and R. Lesourne. 2006. Negative signaling in Fc receptor complexes. *Adv. Immunol.* 89: 39-86.

5. Zhang, W., J. Sloan-Lancaster, J. Kitchen, R. P. Trible, and L. E. Samelson. 1998. LAT: the ZAP-70 tyrosine kinase substrate that links T cell receptor to cellular activation. *Cell* 92: 83-92.

6. Saitoh, S., R. Arudchandran, T. S. Manetz, W. Zhang, C. L. Sommers, P. E. Love, J. Rivera, and L. E. Samelson. 2000. LAT is essential for FcεRI-mediated mast cell activation. *Immunity.* 12: 525-535.

7. Brdička, T., M. Imrich, P. Angelisová, N. Brdičková, O. Horváth, J. Špička, I. Hilgert, P. Lusková, P. Dráber, P. Novák, N. Engels, J. Wienands, L. Simeoni, J. Österreicher, E. Aguado, M. Malissen, B. Schraven, and V. Hořejší. 2002. Non-T cell activation linker (NTAL): a transmembrane adaptor protein involved in immunoreceptor signaling. *J. Exp. Med* 196: 1617-1626.

8. Janssen, E., M. Zhu, W. Zhang, S. Koonpaew, and W. Zhang. 2003. LAB: a new membrane-associated adaptor molecule in B cell activation. *Nat. Immunol.* 4: 117-123.

9. Tkaczyk, C., V. Horejsi, S. Iwaki, P. Draber, L. E. Samelson, A. B. Satterthwaite, D.-H. Nahm, D. D. Metcalfe, and A. M. Gilfillan. 2004. NTAL phosphorylation is a pivotal link between the signaling cascades leading to human mast cell degranulation following kit activation and FcεRI aggregation. *Blood* 104: 207-214.

10. Volná, P., P. Lebduška, L. Dráberová, Š. Šímová, P. Heneberg, M. Boubelík, V. Bugajev, B. Malissen, B. S. Wilson, V. Hořejší, M. Malissen, and P. Dráber. 2004. Negative Regulation of Mast Cell Signaling and Function by the Adaptor LAB/NTAL. *J. Exp. Med.* 200: 1001-1013.

11. Zhu, M., Y. Liu, S. Koonpaew, O. Granillo, and W. Zhang. 2004. Positive and negative regulation of FcεRI-mediated signaling by adaptor protein LAB/NTAL. *J. Exp. Med.* 200: 991-1000.

12. Stork, B., M. Engelke, J. Frey, V. Horejsi, A. Hamm-Baarke, B. Schraven, T. Kurosaki, and J. Wienands. 2004. Grb2 and the non-T cell activation linker NTAL constitute a Ca^{2+}-regulating signal circuit in B lymphocytes. *Immunity.* 21: 681-691.

13. Tolar, P., L. Dráberová, and P. Dráber. 1997. Protein tyrosine kinase Syk is involved in Thy-1 signaling in rat basophilic leukemia cells. *Eur. J. Immunol.* 27: 3389-3397.

14. Dráberová, L., M. Amoui, and P. Dráber. 1996. Thy-1-mediated activation of rat mast cells: the role of Thy-1 membrane microdomains. *Immunology* 87: 141-148.

15. Tolar, P., M. Tůmová, and P. Dráber. 2001. New monoclonal antibodies recognizing the adaptor protein LAT. *Folia Biol. (Praha)* 47: 215-217.

16. Rivera, J., J.-P. Kinet, J. Kim, C. Pucillo, and H. Metzger. 1988. Studies with a monoclonal antibody to the β subunit of the receptor with high affinity for immunoglobulin E. *Mol. Immunol.* 25: 647-661.

17. Rudolph, A. K., P. D. Burrows, and M. R. Wabl. 1981. Thirteen hybridomas secreting hapten-specific immunoglobulin E from mice with Ig^a or Ig^b heavy chain haplotype. *Eur. J. Immunol.* 11: 527-529.

18. Liu, F.-T., J. W. Bohn, E. L. Ferry, H. Yamanoto, C. A. Molinaro, L. A. Sherman, N. R. Klinman, and D. H. Katz. 1980. Monoclonal dinitrophenyl-specific murine IgE antibody: preparation, isolation, and characterization. *J. Immunol.* 124: 2728-2737.

19. Dráberová, L. and P. Dráber. 1991. Functional expression of the endogenous Thy-1 gene and the transfected murine Thy-1.2 gene in rat basophilic leukemia cells. *Eur. J. Immunol.* 21: 1583-1590.

20. Hálová, I., L. Dráberová, and P. Dráber. 2002. A novel lipid raft-associated glycoprotein, TEC-21, activates rat basophilic leukemia cells independently of the type 1 Fcε receptor. *Int. Immunol.* 14: 213-223.

21. Yu, J. Y., S. L. DeRuiter, and D. L. Turner. 2002. RNA interference by expression of short-interfering RNAs and hairpin RNAs in mammalian cells. *Proc. Natl. Acad. Sci. U S A* 99: 6047-6052.

22. Katoh, K., Y. Takahashi, S. Hayashi, and H. Kondoh. 1987. Improved mammalian vectors for high expression of G418 resistance. *Cell Struct. Funct.* 12: 575-580.

23. Surviladze, Z., L. Dráberová, M. Kovářová, M. Boubelík, and P. Dráber. 2001. Differential sensitivity to acute cholesterol lowering of activation mediated via the high-affinity IgE receptor and Thy-1 glycoprotein. *Eur. J. Immunol.* 31: 1-10.

24. Howard, T. H. and W. H. Meyer. 1984. Chemotactic peptide modulation of actin assembly and locomotion in neutrophils. *J. Cell Biol.* 98: 1265-1271.

25. Dráberová, L., L. Dudková, M. Boubelík, H. Tolarová, F. Šmíd, and P. Dráber. 2003. Exogenous administration of gangliosides inhibits FcεRI-mediated mast cell degranulation by decreasing the activity of phospholipase Cγ. *J. Immunol.* 171: 3585-3593.

26. Tolarová, H., L. Dráberová, P. Heneberg, and P. Dráber. 2004. Involvement of filamentous actin in setting the threshold for degranulation in mast cells. *Eur. J. Immunol.* 34: 1627-1636.

27. Amoui, M., P. Dráber, and L. Dráberová. 1997. Src family-selective tyrosine kinase inhibitor, PP1, inhibits both FcεRI- and Thy-1-mediated activation of rat basophilic leukemia cells. *Eur. J. Immunol.* 27: 1881-1886.

28. Wilson, B. S., J. R. Pfeiffer, and J. M. Oliver. 2000. Observing FcεRI signaling from the inside of the mast cell membrane. *J. Cell Biol.* 149: 1131-1142.

29. Dráberová, L., P. Lebduška, I. Hálová, P. Tolar, J. Štokrová, H. Tolarová, J. Korb, and P. Dráber. 2004. Signaling assemblies formed in mast cells activated via Fcε receptor I dimers. *Eur. J. Immunol.* 34: 2209-2219.

30. Dráberová, L. 1990. Cyclosporin A inhibits rat mast cell activation. *Eur. J. Immunol.* 20: 1469-1473.

31. Frigeri, L. and J. R. Apgar. 1999. The role of actin microfilaments in the down-regulation of the degranulation response in RBL-2H3 cells. *J. Immunol.* 162: 2243-2250.

32. Yamashita, T., S.-Y. Mao, and H. Metzger. 1994. Aggregation of the high-affinity IgE receptor and enhanced activity of p53/p56^{lyn} protein-tyrosine kinase. *Proc. Natl. Acad. Sci. USA* 91: 11251-11255.

33. Nishida, K., Y. Yoshida, M. Itoh, T. Fukada, T. Ohtani, T. Shirogane, T. Atsumi, M. Takahashi-Tezuka, K. Ishihara, M. Hibi, and T. Hirano. 1999. Gab-family adapter proteins act downstream of cytokine and growth factor receptors and T- and B-cell antigen receptors. *Blood* 93: 1809-1816.

34. Wilson, B. S., J. R. Pfeiffer, Z. Surviladze, E. A. Gaudet, and J. M. Oliver. 2001. High resolution mapping of mast cell membranes reveals primary and secondary domains of FcεRI and LAT. *J. Cell Biol.* 154: 645-658.

35. Gu, H., K. Saito, L. D. Klaman, J. Shen, T. Fleming, Y. Wang, J. C. Pratt, G. Lin, B. Lim, J.-P. Kinet, and B. G. Neel. 2001. Essential role for Gab2 in the allergic response. *Nature* 412: 186-190.

36. Xie, Z. H., I. Ambudkar, and R. P. Siraganian. 2002. The adapter molecule Gab2 regulates FcεRI-mediated signal transduction in mast cells. *J. Immunol.* 168: 4682-4691.

37. Putney, J. W. Jr., L. M. Broad, F.-J. Braun, J.-P. Lievremont, and G. S. J.Bird. 2001. Mechanisms of capacitative calcium entry. *J. Cell Sci.* 114: 2223-2229.

38. Thastrup, O., A. P. Dawson, O. Scharff, B. Foder, P. J. Cullen, B. K. Drobak, P. J. Bjerrum, S. B. Christensen, and M. R. Hanley. 1989. Thapsigargin, a novel molecular probe for studying intracellular calcium release and storage. *Agents Actions* 27: 17-23.

39. Heneberg, P., P. Lebduška, L. Dráberová, J. Korb, and P. Dráber. 2006. Topography of plasma membrane microdomains and its consequences for mast cell signaling. *Eur. J. Immunol.* 36: 2795-2806.

40. Dráberová, L. and P. Dráber. 1993. Thy-1 glycoprotein and src-like protein-tyrosine kinase p53/p56^{lyn} are associated in large detergent-resistant complexes in rat basophilic leukemia cells. *Proc. Natl. Acad. Sci. USA* 90: 3611-3615.

41. Zhao, C., D. H. Yu, R. Shen, and G. S. Feng. 1999. Gab2, a new pleckstrin homology domain-containing adapter protein, acts to uncouple signaling from ERK kinase to Elk-1. *J. Biol. Chem.* 274: 19649-19654.

42. Tailor, P., T. Jascur, S. Williams, M. von Willebrand, C. Couture, and T. Mustelin. 1996. Involvement of Src-homology-2-domain-containing protein-tyrosine phosphatase 2 in T cell activation. *Eur. J. Biochem.* 237: 736-742.

43. Heneberg, P. and P. Dráber. 2002. Nonreceptor protein tyrosine and lipid phosphatases in type I Fcε receptor-mediated activation of mast cells and basophils. *Int. Arch. Allergy Immunol.* 128: 253-263.

44. Liou, J., M. L. Kim, H. W. Do, J. T. Jones, J. W. Myers, J. E. Ferrell, Jr., and T. Meyer. 2005. STIM is a Ca^{2+} sensor essential for Ca^{2+}-store-depletion-triggered Ca^{2+} influx. *Curr. Biol.* 15: 1235-1241.

45. Roos, J., P. J. DiGregorio, A. V. Yeromin, K. Ohlsen, M. Lioudyno, S. Zhang, O. Safrina, J. A. Kozak, S. L. Wagner, M. D. Cahalan, G. Velicelebi, and K. A. Stauderman. 2005. STIM1, an essential and conserved component of store-operated Ca^{2+} channel function. *J. Cell Biol.* 169: 435-445.

46. Feske, S., Y. Gwack, M. Prakriya, S. Srikanth, S. H. Puppel, B. Tanasa, P. G. Hogan, R. S. Lewis, M. Daly, and A. Rao. 2006. A mutation in Orai1 causes immune deficiency by abrogating CRAC channel function. *Nature* 441: 179-185.

47. Putney, J. W. Jr. 2007. Recent breakthroughs in the molecular mechanism of capacitative calcium entry (with thoughts on how we got here). *Cell Calcium* DOI:10.1016/j.ceca.2007.01.011.

48. Gilfillan, A. M. and C. Tkaczyk. 2006. Integrated signalling pathways for mast-cell activation. *Nat. Rev. Immunol.* 6: 218-230.

Footnotes

[1]This work was supported by project 1M6837805001 (Center of Molecular and Cellular Immunology) from Ministry of Education, Youth and Sports of the Czech Republic, grants 204/03/0594, 301/03/0596 and 301/06/0361 from the Grant Agency of the Czech Republic, grants A5052310, S5052201 and 1QS500520551 from the Grant Agency of the Academy of Sciences of the Czech Republic and Institutional project AVOZ50520514. The research of P.D. and P.H. was supported, respectively, by an International Research Scholar's award from Howard Hughes Medical Institute and Research goal MSM0021620814 from the 3rd Faculty of Medicine, Charles University, Prague.

[2] Address correspondence to Dr. Petr Dráber, Department of Signal Transduction, Institute of Molecular Genetics, Academy of Sciences of the Czech Republic, Vídeňská 1083, Prague 4, CZ 142 20, Czech Republic, E-mail: draberpe@biomed.cas.cz, Tel.: 420-241 062 468; Fax: 420-241 062 214

[3] Abbreviations used in this paper: LAT, linker for activation of T cells; PLC, phospholipase C; SH2, Src homology 2; NTAL, non-T cell activation linker; BMMC, bone marrow-derived mast cell; RBL, rat basophilic leukemia; SOC, store-operated Ca^{2+}; BSS, buffered saline solution; NP40, Nonidet-P40; PIP2, phosphatidylinositol 4,5-bisphosphate; IP3, inositol 1,4,5-trisphosphate; $[Ca^{2+}]_i$, concentration of free intracellular Ca^{2+}; PIP3, phosphatidylinositol 3,4,5-trisphosphate.

Figure legends

FIGURE 1. Rat NTAL cDNA sequence and initial characterization of RBL-derived cell lines with either enhanced or reduced NTAL expression. *A*, Comparison of predicted amino acid sequence of rat NTAL (upper line) and mouse NTAL (lower line; only the different amino acids are shown). In rat NTAL, the putative transmembrane region is boxed, and potential palmitoylation sequence (CVQC) and tyrosine-containing motifs are underlined and in bold. *B*, RBL cells were transfected with vector pZeo-NTAL-1 or pU6/siNTAL-1, and stable clones with, respectively, enhanced or reduced NTAL expression were selected. Total cell lysates were analyzed by immunoblotting (IB) with anti-NTAL or anti-Lyn mAbs and amounts of the corresponding proteins were quantified by densitometry. NTAL expression was normalized to control RBL cells and to the amount of Lyn in individual samples (Fold). *C*, IgE-sensitized control RBL cells or individual transfectants with enhanced expression of NTAL were activated for 5 min by Ag (TNP-BSA, 100 ng/ml; +) or incubated with BSS-BSA alone (-). Lysates from 10^7 cells were immunoprecipitated (IP) with anti-NTAL mAb, and analyzed by immunoblotting with anti-pTyr-HRP conjugate (PY-20), anti-Grb2 and anti-NTAL antibodies. *D and E*, IgE-sensitized control RBL cells or cells with enhanced (*D*) or decreased (*E*) expression of NTAL were stimulated for the indicated time intervals (0 - 30 min) with Ag (100 ng/ml) and release of β-glucuronidase was determined in individual clones. *F*, IgE-sensitized control RBL cells, or cells with enhanced [clone 2A/4 (NTAL+)] or decreased [clone C4 cells (NTAL-)] expression of NTAL were stimulated for 30 min with different concentrations of Ag and release of β-glucuronidase was determined. Data in *D-F* represent the average of 3-4 separate experiments, and are expressed as the mean ± SD.

FIGURE 2. Expression of FcεRI, cell morphology, actin polymerization and topography of NTAL on plasma membrane sheets. *A*, The cells were stained for surface FcεRI by sequential exposure to TNP-specific IgE (thick line, 1 μg/ml) or PBS alone (negative control; thin line) followed by anti-mouse IgE-FITC conjugate. The samples were analyzed by flow cytometry. *B*, Phase contrast images of cells cultured for 48 h under standard conditions. Bar, 10 μm. *C*, Actin polymerization in nonactivated or Ag-activated cells. The cells were sensitized with TNP-specific IgE (1 μg/ml) and then activated by Ag (TNP-BSA; 100 ng/ml) for the indicated time intervals. The amount of F-actin was determined by flow cytometry. Means ± SD were calculated from 3 independent experiments. *D*, Membrane sheets were prepared from resting cells (a-c) or from Ag-activated cells (DNP-BSA, 1 μg/ml, 2 min; d-f), and double-labeled from the cytoplasmic side of the plasma membrane for FcεRI β subunit (10-nm gold particles, arrows) and NTAL (5-nm gold particles, arrowheads). Bar, 100 nm.

FIGURE 3. Overexpression of NTAL inhibits tyrosine phosphorylation of FcεRI, Syk and LAT but enhances enzymatic activity of Lyn kinase. IgE-sensitized cells were stimulated with Ag (TNP-BSA, 500 ng/ml) for the indicated time intervals. *A*, Cells were lysed in 1% NP40-containing lysis buffer and total cell lysates were analyzed for protein tyrosine phosphorylation by immunoblotting with PY-20-HRP conjugate. Numbers on the right indicate positions of molecular weight standards (in kDa). *B-D*, Cells were solubilized and the target proteins were immunoprecipitated with the corresponding antibodies and analyzed by immunoblotting with PY-20-HRP conjugate. After stripping the membranes were reblotted with protein-specific antibodies as indicated. *E-G*, Densitometry analysis of phosphotyrosine immunoblots (as in *B-D*) normalized to the amount of the proteins

immunoprecipitated and to their phosphorylation in nonactivated RBL cells. *H*, Lyn was immunoprecipitated and its enzymatic activity was determined by *in vitro* kinase assay using ^{32}P-γATP and enolase as a substrate. The kinase reaction products were quantified by autoradiography and after stripping off the membranes the amount of Lyn was determined by immunoblotting. Kinase activity of Lyn, as determined by autoradiography of ^{32}P-labeled Lyn and enolase, normalized to the parameters in nonactivated RBL cells and corrected for the amount of Lyn in each immunoprecipitate is also indicated. Means ± SD in *E-H* were calculated from 3 experiments.

FIGURE 4. Changes in Grb2 signaling assemblies. Cells were activated as in Fig. 3, solubilized with saponin/Triton X-100 procedure and Grb2 immunocomplexes were isolated by precipitation with anti-Grb2 Ab. *A*, Grb2 immunocomplexes were analyzed by immunoblotting for the presence of total tyrosine-phosphorylated proteins (PY-20), LAT, NTAL and Grb2. *B-E*, Densitometry analysis of tyrosine phosphorylated (PY) LAT (*B*) and NTAL (*C*), and total amount of LAT (*D*) and NTAL (*E*) in Grb2 immunocomplexes. Means ± SD in *B-E* were calculated from 3-4 experiments. *F*, PI3K activity associated with Grb2 immunocomplexes was estimated using ^{32}P-γATP and phosphatidylinositol as a substrate in PI3K assay (PI3K a.). Positions of [^{32}P]PI (PIP) and start (S) are indicated by arrows. *G*, PI3K immunoprecipitates were analyzed in parallel for PI3K enzymatic activity by PI3K assay and for the amount of immunoprecipitated PI3K by immunoblotting with anti-p85 subunit of PI3K. Enzymatic activity of PI3K normalized to its levels in nonactivated RBL cells and corrected for the amount of PI3K-p85 subunit precipitated is also indicated. Representative data from 3 experiments performed are shown.

FIGURE 5. Changes in tyrosine phosphorylation of Akt and Erk, and TNF-α production. *A* and *B*, Cells were activated as in Fig. 3 and then solubilized with saponin/Triton X-100 procedure (*A*) or 1% Triton X-100 (*B*). Total cell lysates were analyzed by immunoblotting with anti-phospho-Akt (*A*) or anti-phospho-Erk (*B*) antibodies, followed by stripping and immunoblotting with protein-specific antibodies. Relative amounts of proteins were normalized to nonactivated RBL cells. A typical result from 3 experiments is shown. (*C*) IgE-sensitized cells were activated with different concentrations of Ag for 3 h and the amount of TNF-α released into supernatant was determined by ELISA. Data represent means ± SD from 3 experiments performed in triplicates.

FIGURE 6. Changes in the properties of PLCγ1 and PLCγ2. *A* and *B*, Cells were activated as in Fig. 3, solubilized with saponin/Triton X-100 procedure, and PLCγ1 (*A*) and PLCγ2 (*B*) were immunoprecipitated and analyzed by immunoblotting with PY-20-HRP conjugate. After stripping the same membrane was reblotted with protein-specific antibodies. Relative amounts of proteins were normalized to nonactivated cells. Data from representative experiments from at least 3 performed are shown. *C*, Cells were lysed in 1% Triton X-100, and enzymatic activity of the immunoprecipitated PLCγ1 was measured by immune complex PLCγ assay. *D*, Cellular IP3 levels were determined by ^{3}H-radioreceptor assay kit. Data in *C and D* represent means ± SD from 3-4 experiments.

FIGURE 7. Intracellular Ca^{2+} mobilization, extracellular ^{45}Ca uptake and calcium release from the cells. *A-C*, Calcium responses in Fura-2 loaded RBL, NTAL+ and NTAL- cells. *A*, The cells were sensitized with IgE and stimulated in the presence of 1 mM extracellular calcium with TNP-BSA (500 ng/ml; arrow, Ag). Calcium levels were determined by spectrophotometry. *B*, Cells were stimulated with Ag in the absence of extracellular calcium

(arrow, Ag) and 1mM Ca^{2+} was added after Ca^{2+} calcium levels returned to original values (arrow, Ca^{2+}). *C*, Cells were exposed to thapsigargin (1μM; arrow, Th) in the absence of extracellular calcium and 1mM Ca^{2+} was added later on (arrow, Ca^{2+}). *D*, The cells were activated with various concentrations of thapsigargin in the presence of extracellular $^{45}Ca^{2+}$ (1 mM). After 5 min cells were centrifuged through 12% BSA in BSS and cell-bound radioactivity was determined. *E*, The cells were loaded with $^{45}Ca^{2+}$ during 15-min activation with thapsigargin, unbound $^{45}Ca^{2+}$ was washed out and calcium efflux was determined at different time intervals. *F*, The cells were activated with thapsigargin (2 μM) for different time intervals and solubilized in lysis buffer containing 1% NP40 plus 1% n-dodecyl β-D-maltoside. NTAL was immunoprecipitated from postnuclear supernatant and analyzed by immunoblotting with PY-20-HRP conjugate. After stripping, the membrane was reblotted with NTAL-specific Ab. Data in *A-C* and *F* are representative experiments from, respectively, 3 and 2 performed. Data in *D* and *E* represent means ± SD from 4 experiments performed in duplicates or triplicates.

FIGURE 8. Positive regulatory role of Grb2 in Ag-induced Ca^{2+} signaling. *A, B*, Immunoblotting analysis of Grb2- or Grb2/NTAL-deficient cells. RBL cells transfected with empty vector (RBL-C), pU6/siGrb2 vector (clones G1 and G9) or both pU6/siNTAL-1 and pU6/siGrb2 (clones NG2 and NG10) were lysed and postnuclear supernatants were analyzed by immunoblotting for the presence of Grb2, LAT and NTAL. Relative amounts of Grb2 and NTAL were normalized to the amount of LAT in each sample. *C* and *D*, Calcium response in Fura-2-loaded control and transfected cells. The cells were sensitized with IgE and stimulated in the presence of 1 mM extracellular Ca^{2+} with TNP-BSA (500 ng/ml, arrow, Ag). Calcium levels were determined by spectrophotometry. Data are representative of at least 2 experiments performed.

FIGURE 9. A model of NTAL function in FcεRI-mediated Ca^{2+} signaling. At early stages after FcεRI aggregation (Phase I), NTAL is rapidly tyrosine phosphorylated, competing with phosphorylation of FcεRI and LAT. Phosphorylated NTAL binds Grb2 complexes and interferes with the activity of PI3K and several other signaling molecules. NTAL affects activity of PLCγ and in this way the generation of IP3 followed by release of Ca^{2+} from internal stores. At later stages of activation (Phase II), extracellular Ca^{2+} flows into the cytoplasm through SOC channels. Activity of these channels could be modulated by direct or indirect interaction of NTAL with SOC channel proteins and/or regulators of their activity. However, this effect is independent of enhanced NTAL tyrosine phosphorylation.

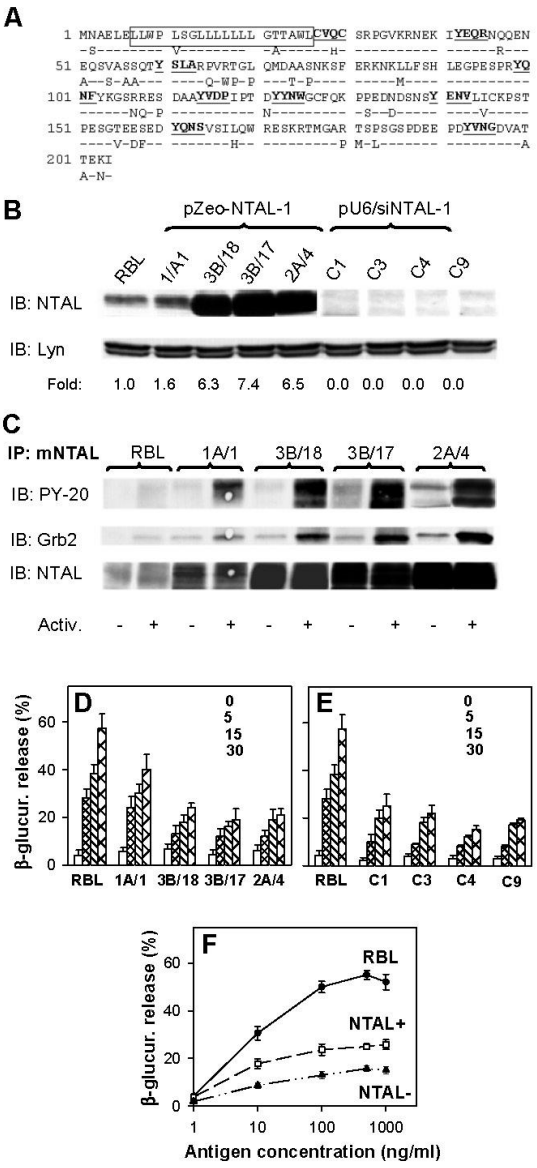

FIGURE 1

Dráberová et al.

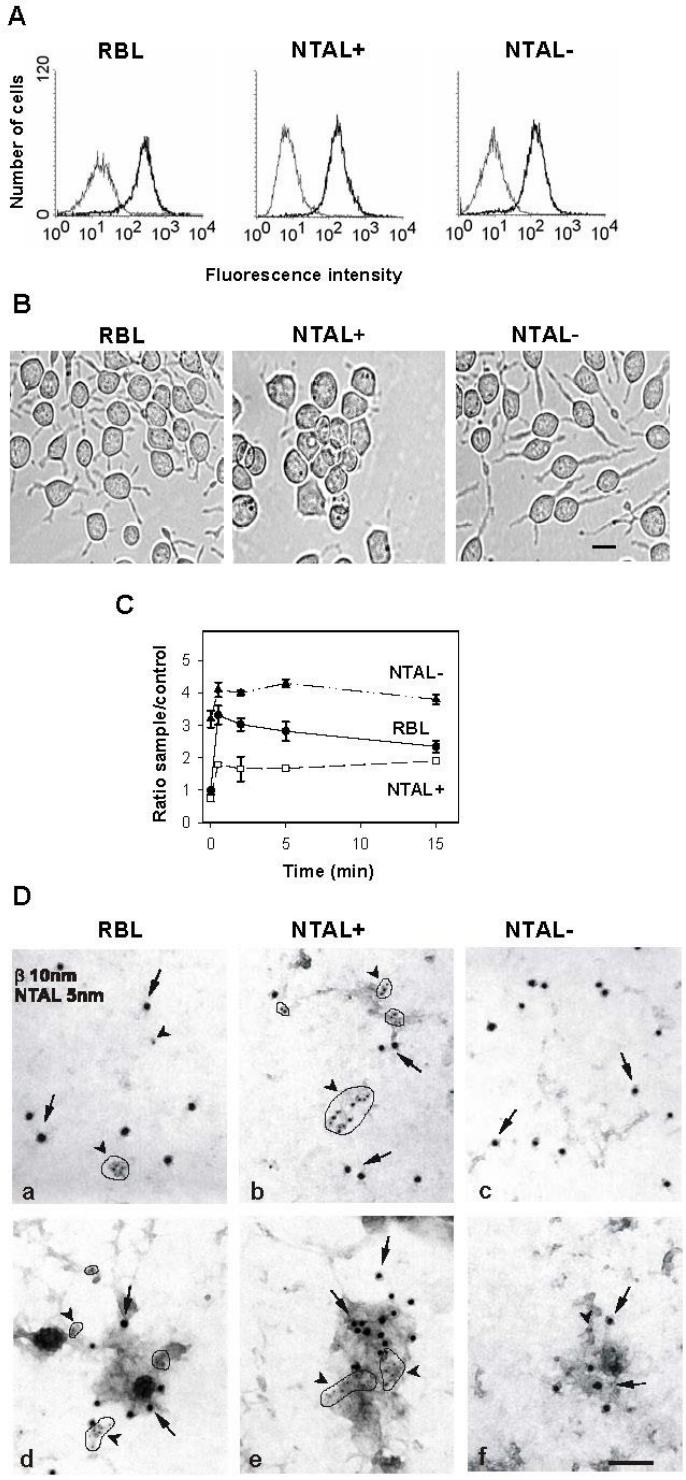

FIGURE 2

Dráberová et al.

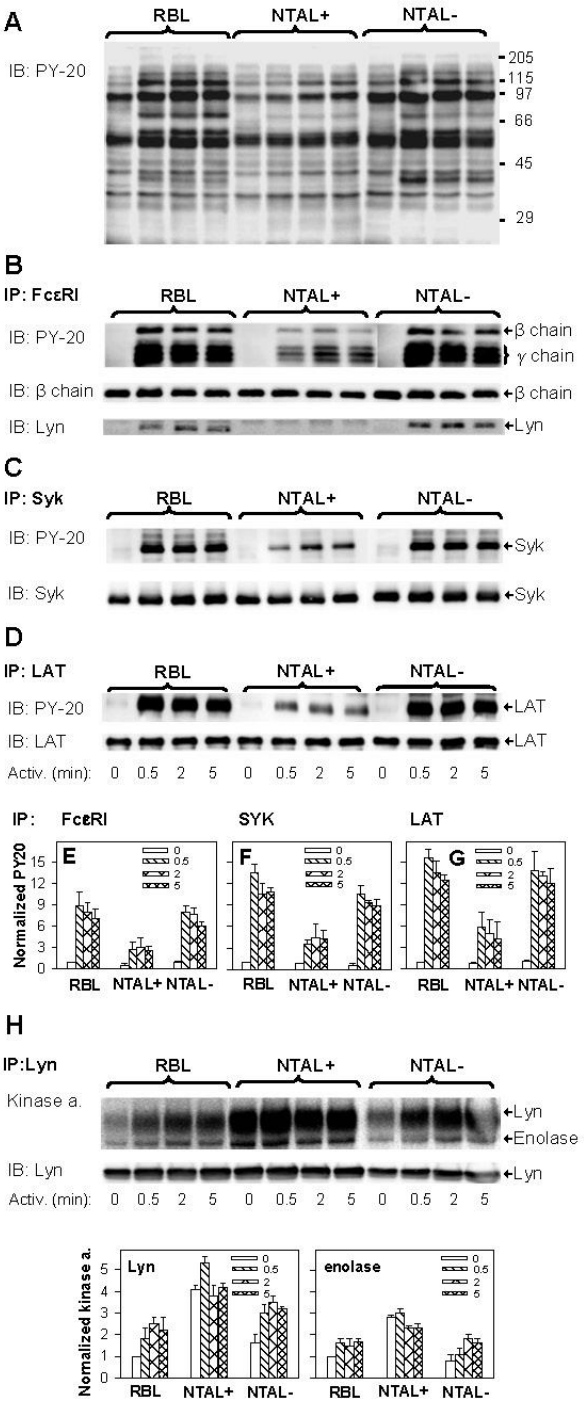

FIGURE 3

Dráberová et al.

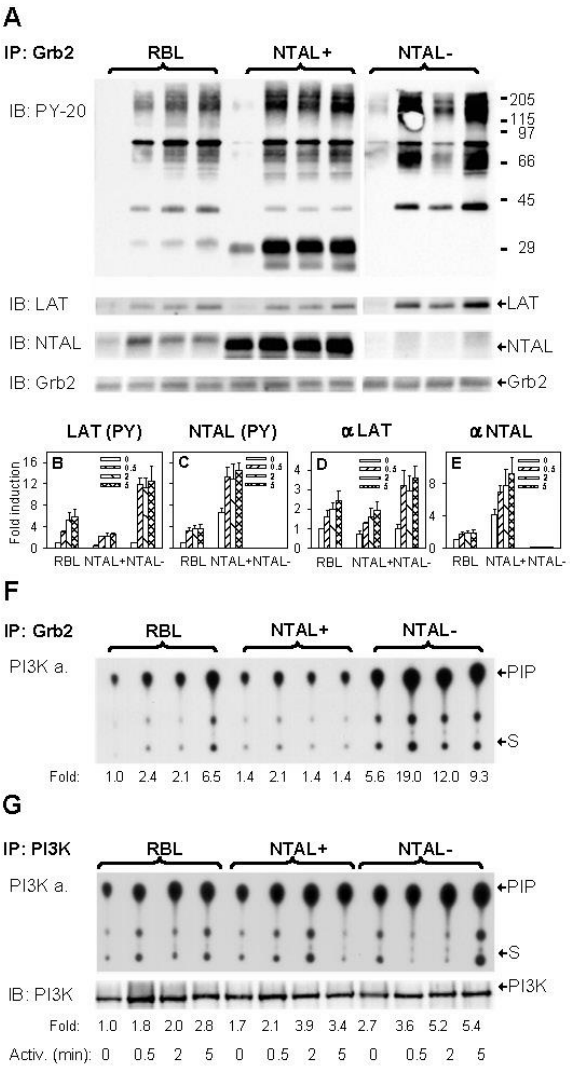

FIGURE 4

Dráberová et al.

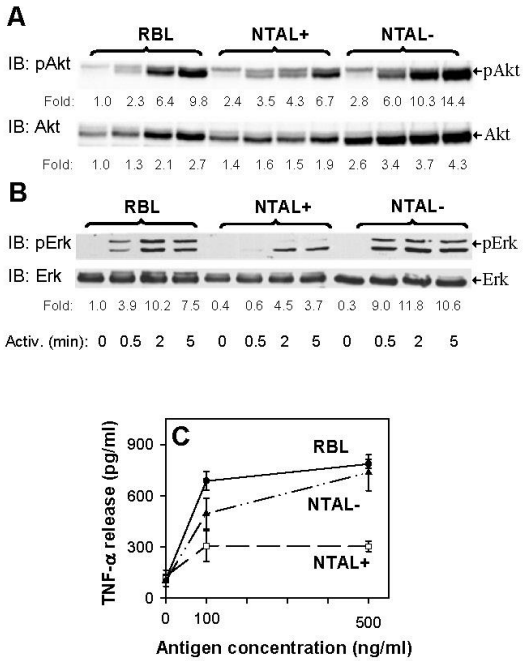

FIGURE 5 *Dráberová et al.*

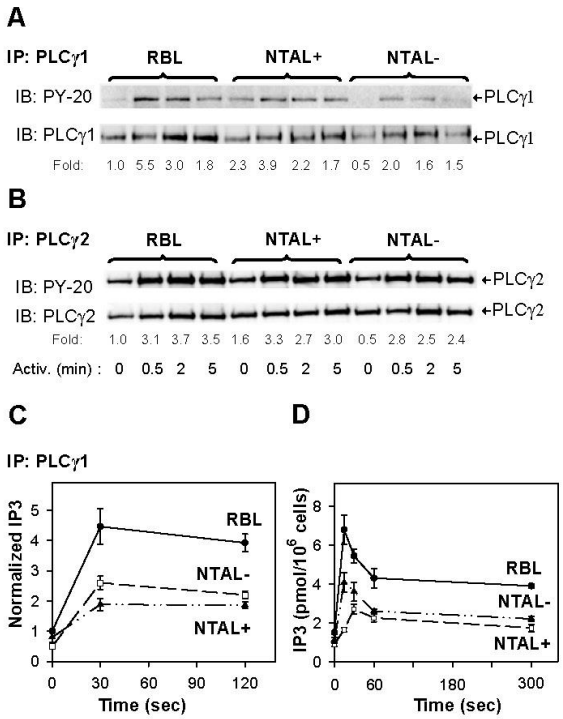

FIGURE 6

Dráberová et al.

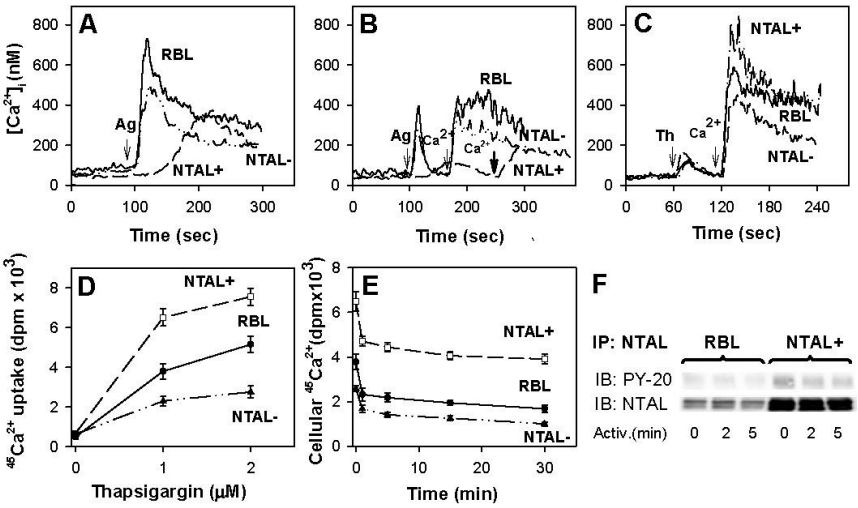

FIGURE 7

Dráberová et al.

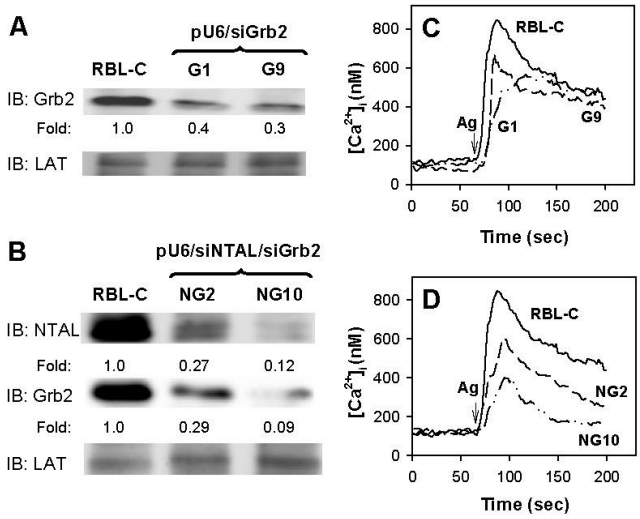

FIGURE 8

Dráberová et al.

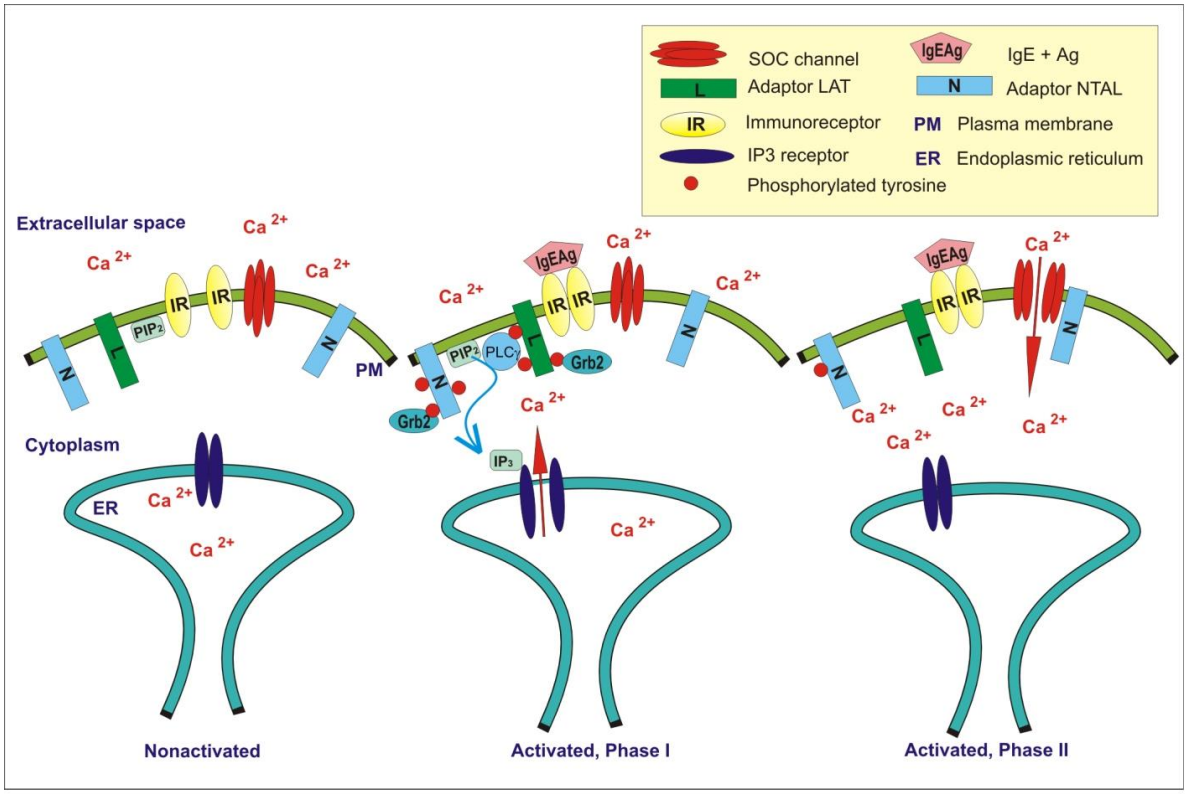

Figure 9 *Dráberová et al.*

(E)

Topography of signaling molecules as detected by electron microscopy on plasma membrane sheets isolated from nonadherent mast cells.

Journal of Immunological Methods, odesláno (červen 2007).

Topography of signaling molecules as detected by electron microscopy on plasma membrane sheets isolated from nonadherent mast cells

Pavel Lebduška, Jan Korb, Magda Tůmová, Petr Heneberg and Petr Dráber*

Department of Signal Transduction, Institute of Molecular Genetics, Academy of Sciences of the Czech Republic, v.v.i., Videňská 1083, 142 20 Prague 4, Czech Republic

Abbreviations: BMMC, bone marrow-derived mast cells; BSA, bovine serum albumin; BSS, buffered salt solution; DNP, dinitrophenyl; EM, electron microscopy; FcεRI, Fcε receptor I; FCS, fetal calf serum; FITC, fluorescein isothiocyanate; GPI, glycosylphosphatidylinositol; HEPES, N-(2-hydroxyethyl)piperazine-N'-(2-ethanesulfonic acid); IgE, immunoglobulin E; IL-3, interleukin 3; LAT, linker for activation of T cells; NC, nitrocellulose; NTAL, non-T cell activation linker; PBS, phosphate buffered saline; PCCF, pair cross-correlation function; PCF, pair correlation function; PLC, phospholipase C; PLL, poly-L-lysine; PM, plasma membrane; RBL, rat basophilic leukemia; SCF, stem cell factor

* Corresponding author: Dr. Petr Dráber, Department of Signal Transduction, Institute of Molecular Genetics, Academy of Sciences of the Czech Republic, v.v.i., Vídeňská 1083, 142 20 Prague 4, Czech Republic

Tel.: +420 241062468; fax: +420 241062214.

E-mail address: draberpe@biomed.cas.cz.

Abstract

Immunolabeling of isolated plasma membrane (PM) sheets combined with the high-resolution electron microscopy is a powerful technique for understanding the topography of PM-bound signaling molecules. However, this technique has been mostly confined to analysis of membrane sheets from adherent cells. Here we present a rapid, simple and versatile method for isolation of PM sheets from nonadherent cells, and show its use for examination of the topography of Fcε receptor I (FcεRI) and transmembrane adaptors LAT (linker for activation of T cells) and NTAL (non-T cell activation linker) in mouse bone marrow-derived mast cells (BMMC). The data were compared with those obtained with widely used but tumor-derived rat basophilic leukemia (RBL) cells. In nonactivated cells, FcεRI was distributed either individually or in small clusters of comparable size in both cell types. In multivalent antigen-activated BMMC as well as RBL cells, FcεRI was internalized to similar extent, but, strikingly, internalization in BMMC was not preceded by formation of large (~200 nm) aggregates of FcεRI, which had been previously described in activated RBL cells. On the other hand, downstream adaptor proteins LAT and NTAL were localized in independent domains in both BMMC and RBL cells before as well as after FcεRI triggering. The combined data demonstrate unexpected properties of FcεRI signaling assemblies in BMMC and emphasise the importance of studies of PM sheets isolated from nontumor cells.

Key words: **Plasma membrane · Electron microscopy · Immunolabeling · Leukocytes . Mast cells**

1. Introduction

Plasma membrane (PM) is an important cellular organelle accommodating numerous proteins involved in various functions. Although it is known that immunoreceptors and other signaling molecules interact within the PM, their topographical changes in the course of cell activation are still poorly understood. Various methods, such as fluorescence energy transfer, immunofluorescence microscopy and electron microscopy (EM) have been used to locate PM-associated molecules (Lagerholm et al., 2005). Regarding resolution, EM represents a bridge between fluorescence resonance energy transfer, working at distances under 10 nm, and fluorescence microscopy with a hundred nm-scale resolution. Transmission EM on ultrathin sections allows visualizing the PM components in the context of the whole cell. To provide a horizontal view, examination of PM sheets is the method of choice.

PM sheets from cells growing on glass coverslips have been isolated by attaching dorsal side of the cells to poly-L-lysine (PLL)-coated film on EM grids, followed by separation of PM sheets connected to the EM grid from the rest of the cell. Components in the extracellular and intracellular leaflets of the PM can be labeled before or after membrane sheets isolation, respectively. As the cells must be attached to glass coverslip prior to isolation of the PM sheets, the studies were confined mainly to adherent cells as fibroblasts, cultured neurons, Chinese hamster ovary cells, rat basophilic leukemia (RBL) cells and baby hamster kidney cells (Sanan and Anderson, 1991; Wilson et al., 2000; Wyse et al., 2003; Choy et al., 2006). Nonadherent leukocytes have been either excluded from such studies or they had to be attached to a substrate by PLL or streptavidin in procedures taking about 45-60 min (Schade and Levine, 2002; Lillemeier et al., 2006), which itself could induce cell activation.

Mast cells, the effectors of allergic reactions, have been extensively used for studies of activation events induced by aggregation of the Fcε receptor I (FcεRI) (Metcalfe et al., 1997; Gilfillan and Tkaczyk, 2006). Although FcεRI and numerous other signaling molecules involved in antigen-mediated mast cell activation have been identified, sequenced and characterized, their topography in the PM at nm-scale resolution remained almost unknown until experiments performed by Bridget Wilson's group on PM sheets isolated from adherent RBL cells (Wilson et al., 2000; Lara et al., 2001; Wilson et al., 2002; Wilson et al., 2004). These authors proposed a model of primary and secondary signaling domains formed in PM after FcεRI triggering. The primary domains consist of FcεRI patches with diameter of ~200 nm, rich in Syk kinase, phospholipase C (PLC)γ2, cytoplasmic adaptors Grb2, Gab2 and other signaling proteins. Interestingly, Lyn kinase, which phosphorylates FcεRI, was excluded from these domains. The primary signaling domains were proposed to pass the signal onto the secondary signaling domains represented by aggregates of the transmembrane adaptor LAT (linker for activation of T cells) and containing PLCγ1.

EM studies on PM sheets from RBL cells also contributed to understanding the topography of molecules thought to be localized predominantly in cholesterol- and sphingolipid-rich microdomains called lipid rafts or membrane rafts (Simons and Toomre, 2000; Pike, 2006). Some molecules considered to be associated with lipid rafts, such as glycosylphosphatidylinositol (GPI)-anchored glycoprotein Thy-1 and glycosphingolipid GM1, turned out to be localized independently in PM (Wilson et al., 2004). On the other hand, Thy-1 showed clear colocalization with palmitoylated adaptor proteins LAT and NTAL (non-T cell activation linker) (Wilson et al., 2004; Heneberg et al., 2006), even though these adaptors were found in different nonoverlapping patches in both resting and activated RBL cells (Volná et al., 2004;

Heneberg et al., 2006). RBL cells are, however, of tumor origin, and it is therefore possible that the topography of signaling molecules in these cells differs from that found in normal mast cells.

In this study we describe a new rapid, simple and versatile technique for isolation of PM sheets from nonadherent cells, and show its use for determination of topography of selected plasma membrane signaling molecules in murine bone marrow-derived mast cells (BMMC). Although these cells are more useful for analysis of signaling processes, compared to widely used tumor-derived RBL cells, BMMC had been excluded from such studies because of their growth in suspension. Direct comparison of topography of several signaling molecules in BMMC and RBL cells revealed a substantial difference in formation of FcεRI signaling spots, whereas the downstream signaling domains possessing adaptor proteins LAT and NTAL showed analogous distribution in both cell types.

2. Material and methods

2.1. Antibodies and reagents

The following mouse monoclonal antibodies were used: anti-FcεRI-β subunit (JRK, Rivera et al., 1988), anti-NTAL (Brdička et al., 2002), anti-LAT (Exbio; Czech Republic) and dinitrophenyl (DNP)-specific immunoglobulin E (IgE) (Liu et al., 1980). Rabbit polyclonal antibodies included anti-LAT (Upstate Biotechnology; NY, USA), anti-NTAL, and anti-IgE (Volná et al., 2004). DNP-BSA (bovine serum albumin) was purchased from Molecular Probes (OR, USA), goat anti-mouse and anti-rabbit secondary antibodies conjugated to 5 nm or 10 nm gold particles (diluted 1:25 for intracellular and 1:5 for extracellular labeling) were from Amersham Biosciences

(Sweden), fluorescein isothiocyanate (FITC)-conjugated donkey anti-mouse Ig was from Jackson ImmunoResearch Laboratories (PA, USA). Nickel EM grids (300 MESH), OsO_4 and pioloform were obtained from Christine Gröpl Elektronemikroskopie (Austria), and stem cell factor (SCF) and interleukin 3 (IL-3) were from PeproTech EC Ltd (UK). Poly-L-lysine (MW 300 000), fibronectin and other chemicals were purchased from Sigma (MO, USA).

2.2. Cells

RBL-2H3 cells were cultured as described (Dráberová et al., 1991). 16-18 hours before experiment, the cells were transferred into fresh complete medium containing DNP-specific IgE (1 µg/ml) and allowed to settle on an ultraclean glass coverslip (the coverslips had been thoroughly washed in a detergent, deionized water, kept overnight in concentrated HCl, thoroughly washed in deionized water and finally with ethanol, and kept in ethanol until use).

BMMC were isolated from mouse femurs and tibias and cultivated in Iscove's medium containing 10% fetal calf serum (FCS), SCF (40 ng/ml) and IL-3 (20 ng/ml). 16-18 hours before the experiment the cells were transferred into Iscove's medium without SCF, but with FCS, IL-3 and DNP-specific IgE (1µg/ml), and incubated either in suspension, or on glass coverslips covered with fibronectin [50 µg/ml in phosphate buffered saline (PBS) for 1 h at 37°C, followed by washing with PBS].

Mouse T cells were isolated from peripheral blood as described (Smrž et al., 2007).

2.3. Isolation and staining of PM sheets

2.3.1. Preparation of EM grids. On the day of the experiment, EM grids covered with pioloform and coated with carbon were glow-discharged for 45-60 s by 300 V, then incubated with 1 mg/ml PLL in H_2O for 30 min, washed once for 5 s in H_2O and dried. Immediately before the PM sheet isolation, a round nitrocellulose membrane filter (Millipore; pores, 0.45 μm) was placed onto a drop of HEPES [N-(2-hydroxyethyl)piperazine-N'-(2-ethanesulfonic acid)] buffer (25 mM HEPES, pH 7.0, 25 mM KCl, 2.5 mM magnesium acetate) on ice-cold glass support. The filter had to be fully wetted, but no liquid should appear on its upper side. Two EM grids were placed with the PLL-side up onto the filter (Fig. 1A, B).

2.3.2. *Cells.* RBL cells cultured as adherent on glass coverslips, or BMMC bound to glass coverslips covered with fibronectin (as described above), were washed with PBS and, when indicated, activated by DNP-BSA in buffered salt solution (BSS; 20 mM HEPES pH 7.4, 5 mM KCl, 135 mM NaCl, 1.8 mM $CaCl_2 \cdot 2H_2O$, 1mM $MgCl_2$, 5.6 mM glucose) at 37°C. In some experiments the cells were fixed for 7 min by 2% paraformaldehyde in PBS at room temperature, washed and incubated for 10-15 min with antibodies in PBS supplemented with 0.1% BSA (washing with PBS). Cells cultured in suspension were washed twice with BSS supplemented with 0.1% BSA and transferred to BSS without BSA. A 100 μl aliquot of the suspension (~10^6 cells/ml) was applied onto ultraclean glass coverslip (15 mm in diameter) for 1 min and, when indicated, processed for activation (by DNP-BSA in BSS, 37°C) and/or extracellular labeling (as described above). Alternatively, the cells were activated in suspension.

2.3.3. *Isolation of PM sheets:* Coverslips with adherent RBL cells or fibronectin-bound BMMC (Fig. 1A, left) as well as with glass-bound BMMC (Fig. 1A,

right) were rinsed twice in PBS and once in ice-cold HEPES buffer and, using a rubber stopper, pressed face-down to EM grids by a firm finger pressure for 10 seconds (Fig. 1C); a drop of ice-cold HEPES buffer was applied to the edge of the coverslip to maintain moisture in the following step. The coverslip was quickly side-lifted, exposing the cells to shearing forces (Fig. 1D), and the grids with attached PM sheets were immediately placed face-down onto ice-cold HEPES buffer (Fig. 1E). After 5-10 s the grids were transferred onto ice-cold 2% paraformaldehyde in HEPES buffer for 10 min. The grids were then floated on PBS for 5-30 min. Alternatively, if PM sheets were isolated from cells in suspension, 10 µl aliquots of cells suspended in BSS buffer (without BSA) were loaded onto each EM grid, then covered with an ultraclean glass coverslip (Fig. 1B), pressed and processed as described above (Fig. 1C-E).

2.3.4. Intracellular leaflet labeling and contrasting the specimen. The labeling of intracellular leaflet was performed by 30 min incubation on drops of PBS supplemented with 0.1% BSA and antibodies, followed by three 5 min washes with PBS. Samples were post-fixed with 2% glutaraldehyde in PBS for 10 min and then washed with PBS for 10 min. The specimens were further stained for 10 min with 1% OsO_4 in cacodylate buffer, washed thrice for 5 min in H_2O, incubated for 10 min with 1% aqueous tannic acid, washed thrice for 5 min in H_2O, and finally stained for 10 min with 1% aqueous uranyl acetate. After 1 min wash in H_2O, the samples were air-dried and examined by electron microscope (JEOL JEM 1200EX operating at 60kV).

2.4. Confocal microscopy and flow cytometry analysis

IgE-primed BMMC and RBL cells were fixed by 4% paraformaldehyde in PBS at various stages of their activation. Subsequently, they were washed with PBS and

immunolabeled with FITC-conjugated anti-mouse Ig. Samples were analyzed using confocal microscope Leica TCS SP with 100x oil objective or FACSCalibur™ (Becton Dickinson).

2.5. Statistics

The GOLD computer programme was used for statistical evaluation of clustering and colocalization of immunogold markers. It maps the distribution of gold particles by pair correlation function (PCF; analysis of clustering) or pair cross-correlation function (PCCF; analysis of colocalization). PCF is a ratio of the density of gold particles at a given distance from a typical particle to the average density of these particles. PCCF is a ratio of the density of particles of the first type at a given distance from a typical particle of the second type to the average density of the particles of the first type (Philimonenko et al., 2000). Data shown are means ± SD unless stated otherwise.

3. Results

3.1. New procedures for isolation of PM sheets from nonadherent cells

In pilot experiments we found that leukocytes, such as BMMC or T cells, which do not adhere to glass surface in media or buffers supplemented with serum, bound rapidly to ultraclean glass surfaces in protein-free buffer, and that this property could be used for isolation of PM sheets. The binding of cells to ultraclean glass surface occurs rapidly (within ~1 min) at room temperature and it is not dependent on actin cytoskeleton, as PM sheets were isolated with comparable efficiency from cells

pretreated with an inhibitor of actin polymerization latrunculin B (20 μM, 90 min, 37°C) as from latrunculin B-nontreated cells. Importantly, attachment of BMMC to ultraclean glass did not cause spontaneous degranulation of the cells (not shown). To elaborate this procedure for isolation of PM sheets (Fig. 1A, right) we compared it with two other methods that we developed for isolation of membrane sheets from BMMC. The first (Fig. 1A, left) makes use of the finding that BMMC at certain conditions adhere to fibronectin, a component of mast cell environment (Lam et al., 2003), thus providing relatively physiological conditions for cell adhesion. The second (Fig. 1B) is based on pressing the cells suspended in protein-free buffer to PLL-coated EM grids by ultraclean glass coverslip, thus reducing the length of attachment as much as possible. Further steps were identical in all isolation procedures used, and consisted in pressing the sandwich formed by the glass coverslip, cells and EM grid (Fig. 1C), followed by side-lifting the glass coverslip (Fig. 1D) and washing the membrane sheets attached to EM grids by floating on ice-cold HEPES buffer (Fig. 1E).

PM sheets isolated from BMMC after their binding to fibronectin (Fig. 2A), ultraclean glass (Fig. 2B) or pressing directly to PLL-covered EM grids (Fig. 2C) showed comparable distribution of the FcεRI-β subunit as detected by EM after intracellular leaflet double-step immunolabeling. Furthermore, no difference in the amount of the receptor or in the PM structure was noticed. When PM sheets were isolated 2 min after exposure to antigen (DNP-BSA), a comparable decrease in the amount of FcεRI-β subunit in PM was observed by all the three procedures (Fig. 2D). Therefore, we further used only the method based on cell adsorption to ultraclean glass.

As the density of FcεRI-β subunits on PM sheets was approximately twice higher on RBL cells (prepared by the technique of Sanan and Anderson, 1991) than on BMMC (Fig. 2E), we checked whether this difference is attributable to spreading of

RBL cells on glass surface, and thus possibly exposing the FcεRI on dorsal membrane. PM sheets isolated from RBL cells in suspension by the same procedure as from BMMC (1 min adhesion to ultraclean glass coverslips, without spreading) showed an amount of detectable FcεRI-β (24.91 ± 2.97 particles/ μm^2, n=3, 60 μm^2) comparable to that detected on PM sheets of glass-grown RBL cells (23.96 ± 2.66 particles/ μm^2, n=3, 60 μm^2).

3.2. Topography of FcεRI in the course of IgE-dependent BMMC activation

Aggregation of FcεRI by IgE and multivalent antigen leads to FcεRI internalization by a dynamin-dependent mechanism in RBL cells (Fattakhova et al., 2006). We found that both RBL cells and BMMC show analogous decrease in detectable FcεRI on PM sheets when stimulated by DNP-BSA at concentrations optimal for degranulation (1 μg/ml for RBL; 0.1 μg/ml for BMMC). No obvious difference was observed in the amount of detectable FcεRI on BMMC stimulated by either 1 or 0.1 μg/ml DNP-BSA (Fig. 2E).

It has been reported that activation of RBL cells by multivalent antigen leads to formation of FcεRI patches with several hundreds of nm in size (Wilson et al., 2000). To find out whether similar patches are also formed in BMMC, we analyzed the topography of FcεRI in resting and activated cells. To detect both FcεRI-α and FcεRI-β subunits on the same PM sheets, the IgE bound to FcεRI-α was detected by double-step immunolabeling from extracellular side, PM sheets were isolated, and FcεRI-β was labeled from the intracellular side. As expected, in resting cells both immunogold markers colocalized in the PM and were distributed in small clusters (Fig. 3A, C). Surprisingly, in antigen (DNP-BSA)-activated BMMC, no dramatic changes in FcεRI topography were observed and no large patches of FcεRI in osmiophilic regions were

formed. In fact, the number of FcεRI clusters in activated BMMC was lower than in resting cells; this was probably caused by internalization of aggregated FcεRI. The clusters that remained on PM after BMMC activation were slightly smaller than the ones before activation (Fig. 3A-D). As expected, analogous treatment of RBL cells led to formation of large (~200 nm) FcεRI aggregates (Fig. 3E-H). FcεRI clusters were of comparable size on resting BMMC and RBL cells, but they were more numerous in RBL cells, thus the difference in FcεRI content of BMMC and RBL cell PM reflects difference in number of FcεRI domains, but not in FcεRI content of the individual domains.

Further experiments showed that no large FcεRI patches were formed at any time interval after BMMC triggering, neither with low (0.1 μg/ml; Fig. 4A) nor high (1 μg/ml; Fig. 4B) concentration of antigen. When RBL cells were analyzed under comparable conditions, formation of large FcεRI aggregates was clearly observed 2 min after triggering (Fig. 4C). Thus, although FcεRI aggregates in BMMC are internalized to the same extent as in RBL cells (Fig. 2E), large patches of aggregated FcεRI are observed only in RBL cells.

For an independent view on formation of FcεRI aggregates and their internalization we also checked the topography and amount of FcεRI by confocal microscopy and flow cytometry. IgE-primed BMMC and RBL cells were fixed in resting state or after their activation with DNP-BSA, and surface IgE was labeled with FITC-conjugated goat anti-mouse Ig. Confocal microscopy confirmed that resting BMMC and RBL cells both showed a similar distribution of FcεRI (Fig. 5A, D). Antigen-mediated activation of BMMC resulted in only slightly different pattern of surface FcεRI distribution, reflecting rather a loss of some fraction of the receptor from cell surface than its aggregation (Fig. 5A-C). Conversely, activation of RBL cells led to

a more pronounced speckled pattern of surface FcεRI (Fig. 5D-F). These results support the data obtained by EM that BMMC and RBL cells differ in the size of FcεRI patches formed after FcεRI triggering. It should be noted, however, that patches of FITC-marked FcεRI detected by confocal microscopy do not directly correspond to aggregates of immunogold-labeled FcεRI observed by EM, which are much smaller and below the detection limit of light microscopy.

Quantitative changes in the total amount of PM FcεRI in the course of activation were detected by flow cytometry. Data in Fig. 5G show that both BMMC and RBL cells internalized FcεRI during DNP-mediated stimulation rapidly (approximately 40% internalized within 2 min) and to a comparable extent, and that there was no significant difference between BMMC activated by 0.1 and 1 μg/ml DNP-BSA. These results are in agreement with data obtained by EM on PM sheets.

In all previous experiments cells were activated at 37°C. It has been shown that decreasing temperature to 4°C delays all signaling events including internalization, and preserves the formation of larger signaling assemblies (Holowka et al., 2000). Next, we therefore assessed the formation of FcεRI patches in cells activated at 4°C (Fig. 6A, B). Under these conditions, enhanced FcεRI clustering in a time-dependent was found in both RBL cells and BMMC.

3.3. Independent distribution of LAT and NTAL in BMMC

We have reported previously that the transmembrane adaptor proteins LAT and NTAL are localized in independent regions of the PM sheets isolated from resting RBL cells as well as after activation via FcεRI or Thy-1 (Volná et al., 2004; Heneberg et al., 2006). This was unexpected finding because LAT and NTAL exhibit structural similarities, including submembrane localization of their palmitoylation sites and

association with detergent-resistant membranes. To exclude the possibility that the observed independent distribution of the adaptors is connected with tumor origin of RBL cells or their adhesive properties, we analyzed topography of LAT and NTAL in PM sheets isolated from BMMC. In initial control experiments LAT (Fig. 7A, D) or NTAL (Fig. 7B, E) were labeled with two different antibodies directed against the same target antigen. This resulted, as anticipated, in colocalization of the immunogold markers on PM in both BMMC and RBL cells, and was reflected in enhanced values of pair cross-correlation function (PCCF; Fig. 8A, B, black squares and black diamonds). This is an important control excluding the possibility that localization of various proteins in different domains is caused by seggregating activity of the antibodies. In contrast, when LAT and NTAL were labeled on the same membrane, both proteins were accumulated in separate domains not only in RBL cells but also in BMMC (Fig.7C, F). Analysis of colocalization confirmed the topographical independence of LAT and NTAL in the PM sheets isolated from resting or activated BMMC (Fig. 8A) and RBL cells (Fig. 8B). These data prove that LAT and NTAL are clustered in different domains in normal mast cells.

4. Discussion

Examination of isolated PM sheets by high-resolution EM is an established and powerful method for topographical analyses of various PM molecules. Originally, this method was developed for studies of cells growing as adherent to glass surface in the presence of culture media (Sanan and Anderson, 1991); such cells are, however, rare among nontransformed leukocytes. Later, the method was modified to allow isolation

of PM sheets from nonadherent T cells (Schade and Levine, 2002; Lillemeier et al., 2006). The cells were attached to glass surface by interaction with immobilized immuno-ligands or by binding to PLL at 37°C or 4°C. Alternatively, biotinylated T cells were bound to glass coverslips covered with streptavidin. In these methods, the immobilization step itself was lengthy (45 – 60 min). Here we report a new procedure for isolation of PM sheet from nonadherent leukocytes that is based on nonspecific adhesion of cells to ultraclean glass in protein-free buffer. Compared to previously described methods of membrane sheets isolation from nonadherent cells, this new one has several advantages. First, it is very rapid, requiring only ~1 min for settling the cells to ultraclean glass coverslips. This reduces the risk of artificial rearrangement of PM components during interaction of the cell with substrate. Second, it is independent of binding of the cells to PLL, which has per se been reported to cause mast cell activation (Benyon et al., 1987). It should be noted that mere binding of BMMC to ultraclean glass did not cause their degranulation. Third, it does not require preincubation of the cells at low temperature, which causes changes in organization of the PM (Magee et al., 2005). The only step required to be done at 4°C before paraformaldehyde fixation takes no more than several seconds and is almost identical with the one of the well-established procedure of plasma membrane sheets isolation from adherent cells (Sanan and Anderson, 1991; Wilson et al., 2000). Fourth, the method can be performed in the presence of actin polymerization inhibitors such as latrunculin B, because it does not require active cytoskeleton-driven adsorption. This will facilitate future studies on the role of cytoskeletal components in topography of various PM molecules.

In control experiments we analyzed PM sheets prepared from BMMC bound to fibronectin-coated surfaces, which is a process dependent on cell sensitisation. Alternatively, PM sheets were isolated from suspended cells pressed directly on PLL-

covered EM grids. As the topography of FcεRI and quality of the isolated PM sheets did not differ among these two controls and the cells adsorbed to ultraclean glass, we were using in subsequent studies the technique based on adsorption to glass. It is fast, can be universally used, and enables high effectivity even of extracellular leaflet labeling.

Changes in topography of PM signaling molecules in the course of FcεRI-mediated activation have previously been examined by the high-resolution EM almost exclusively in RBL cells (Wilson et al., 2000; Lara et al., 2001; Wilson et al., 2002; Wilson et al., 2004; Dráberová et al., 2004; Heneberg et al., 2006). Based on their findings Wilson and co-authors proposed the existence of primary signaling domains, possessing aggregated FcεRI in ~200 nm patches, and secondary signaling domains, enriched with the transmembrane adaptor protein LAT (Wilson et al., 2002). Here we present for the first time the topography of FcεRI and downstream adaptors in PM sheets isolated from BMMC. In resting BMMC the FcεRI was distributed in small clusters of comparable size to those observed on RBL cells, but the clusters were less numerous than on RBL cells. The overall amount of FcεRI-β subunit per μm^2 was reduced almost to a half in BMMC compared to RBL cell. The possibility that the enhanced amount of FcεRI-β in RBL cell is caused by transfer of the receptor from the ventral to the dorsal side during adhesive growth of the cells was excluded by experiments in which the membrane sheets from RBL cells were isolated in the same way as from BMMC and the difference was still retained.

Unexpectedly, activation of IgE-sensitized BMMC with DNP-BSA at concentrations which are either optimal (0.1 μg/ml) or supraoptimal (1 μg/ml) for degranulation did not lead to formation of large FcεRI signaling domains. This treatment caused, however, a decrease in the amount of detectable FcεRI-β on the

cytoplasmic side of the membrane sheets isolated from both BMMC and RBL cells. The observed decrease was probably caused by receptor internalization as shown using flow cytometry, which demonstrated an activation-dependent loss of cell surface FcεRI. The combined data indicate that activation of BMMC by multivalent antigen-IgE complexes leads to a rapid FcεRI internalization from multiple small patches of FcεRI aggregates. Thus, formation of large receptor aggregates, comparable in size to those formed in RBL cells activated under similar conditions, are not required for initiation of BMMC signaling events. The observed difference in size of the antigen-induced FcεRI patches between the both mast cell types is likely to reflect different local dynamics, favorizing formation of more numerous but smaller signaling domains in BMMC compared to RBL cells. When FcεRI triggering occured at 4°C, the differences between the two cell types disappeared. These data, together with our previous results that RBL cells can be activated by monoclonal antibody-mediated dimerization of the FcεRI without formation of detectable receptor clusters (Dráberová et al., 2004), suggest that primary signaling domains are much smaller than previously thought; their size in BMMC is comparable to that of FcεRI clusters observed in the PM isolated from resting cells. This calls for reconsidering the view of initiation of mast cell signaling, thereby stressing subtle and dynamic processes, as well as importance of further studies on other mast cell types.

FcεRI-mediated activation leads to rapid phosphorylation of the transmembrane adaptor proteins LAT and NTAL that serve as scaffolds for downstream signaling. Both adaptors are very similar in structure, including two acylation sites which are likely to cause enhanced resistance to solubilization in nonionic detergents. Our previous EM studies on isolated PM sheets revealed that LAT and NTAL were localized in nonoverlapping separate domains from both nonactivated and FcεRI-activated RBL

cells. When the GPI-anchored protein Thy-1 (whose aggregation causes mast cell degranulation) had been labeled in fixed state or aggregated by monoclonal antibody, both adaptors colocalized with the clustered Thy-1, but again, no mixed adaptor clusters were formed (Volná et al., 2004; Heneberg et al., 2006). Experiments with BMMC from knock-out mice revealed that LAT and NTAL had different functions (Volná et al., 2004; Zhu et al., 2004). Because the topography of these adaptors in BMMC has not yet been studied, we made use of the above described method of PM sheets isolation to address this issue. To exclude the objection that separation of both adaptors may be induced secondarily by antibodies used for detection, each of the adaptor protein was labeled with different (rabbit and mouse) antibodies together. This resulted in strong colocalization of both markers, indicating that the antibodies are not by themselves responsible for separation of the proteins. However, when the same antibodies were used for simultaneous detection of LAT and NTAL, they clearly showed different domains of both adaptors not only in RBL cells, but also in BMMC. Thus, sequestration of LAT and NTAL does not seem to be an artifact observed only in immortalized RBL cell line, or reflecting experimental procedures.

Why should these two structurally similar proteins form separate domains in PM? Perhaps, differences in aminoacid sequence of their transmembrane domains could cause association with different lipids within the membrane rafts. Alternatively, cytoplasmic domains may interact with different proteins leading to formation of variant signalosomes. The latter possibility is supported by findings that in T cells LAT associates with CD2 coreceptor and tyrosine kinase Lck in discrete PM regions, which depend on protein-protein interactions mediated through LAT phosphorylation sites but not on interactions with lipid rafts (Douglass and Vale, 2005). As the repertoir of LAT and NTAL cytoplasmic docking sites is not identical (Brdička et al., 2002), the specific

protein-protein network might result in separation of both adaptors. However, the finding that NTAL and LAT are sequestered into discrete domains even before cell triggering and therefore in the absence of their tyrosine phosphorylation, suggests that other mechanisms are also involved.

Although restricted to fixed specimen, high-resolution EM combined with immunogold labeling is a powerful technique that has brought about important findings on PM organization (Wilson et al., 2002; Prior et al., 2003; Wilson et al., 2004; Heneberg et al., 2006; Lillemeier et al., 2006). Extension of the method to rapid and simple isolation of PM sheets from nonadherent cells will contribute to its wider use and thus to better understanding of signaling events in various immune system cells which are mostly nonadherent.

Acknowledgements: We thank D. Lorenčíková, H. Mrázová, I. Lišková and J. Musilová for technical assistance. This work was supported by project 1M0506 (Center of Molecular and Cellular Immunology) from Ministry of Education, Youth and Sports of the Czech Republic, grants 204/05/H023 and 301/06/0361 from the Grant Agency of the Czech Republic, and Institutional project AVOZ50520514. Research of Petr Heneberg was supported in part by grant MSM0021620814 from the 3rd Faculty of Medicine, Charles University, Prague.

References

Benyon, R.C., Lowman, M.A., and Church, M.K., 1987. Human skin mast cells: their dispersion, purification, and secretory characterization. J. Immunol. 138, 861-867.

Brdička, T., Imrich, M., Angelisová, P., Brdičková, N., Horváth, O., Špička, J., Hilgert, I., Lusková, P., Dráber, P., Novák, P., Engels, N., Wienands, J., Simeoni, L., Ősterreicher, J., Aguado, E., Malissen, M., Schraven, B., and Hořejší, V., 2002. Non-T cell activation linker (NTAL): a transmembrane adaptor protein involved in immunoreceptor signaling. J. Exp. Med. 196, 1617-1626.

Choy, M.S., Bay, B.H., Cheng, H.C., and Cheung, N.S., 2006. PTEN is recruited to specific microdomains of the plasma membrane during lactacystin-induced neuronal apoptosis. Neurosci. Lett. 405, 120-125.

Douglass, A.D. and Vale, R.D., 2005. Single-molecule microscopy reveals plasma membrane microdomains created by protein-protein networks that exclude or trap signaling molecules in T cells. Cell 121, 937-950.

Dráberová, L. and Dráber, P., 1991. Functional expression of the endogenous Thy-1 gene and the transfected murine Thy-1.2 gene in rat basophilic leukemia cells. Eur. J. Immunol. 21, 1583-1590.

Dráberová, L., Lebduška, P., Hálová, I., Tolar, P., Štokrová, J., Tolarová, H., Korb, J., and Dráber, P., 2004. Signaling assemblies formed in mast cells activated via Fcε receptor I dimers. Eur. J. Immunol. 34, 2209-2219.

Fattakhova, G., Masilamani, M., Borrego, F., Gilfillan, A.M., Metcalfe, D.D., and Coligan, J.E., 2006. The high-affinity immunoglobulin-E receptor (FcεRI) is endocytosed by an AP-2/clathrin-independent, dynamin-dependent mechanism. Traffic 7, 673-685.

Gilfillan, A.M. and Tkaczyk, C., 2006. Integrated signalling pathways for mast-cell activation. Nat. Rev. Immunol. 6, 218-230.

Heneberg, P., Lebduška, P., Dráberová, L., Korb, J., and Dráber, P., 2006. Topography of plasma membrane microdomains and its consequences for mast cell signaling. Eur. J. Immunol. 36, 2795-2806.

Holowka, D., Sheets, E.D., and Baird, B., 2000. Interactions between FcεRI and lipid raft components are regulated by the actin cytoskeleton. J. Cell Sci. 113, 1009-1019.

Lagerholm, B.C., Weinreb, G.E., Jacobson, K., and Thompson, N.L., 2005. Detecting microdomains in intact cell membranes. Annu. Rev. Phys. Chem. 56, 309-336.

Lam, V., Kalesnikoff, J., Lee, C.W., Hernandez-Hansen, V., Wilson, B.S., Oliver, J.M., and Krystal, G., 2003. IgE alone stimulates mast cell adhesion to fibronectin via

pathways similar to those used by IgE + antigen but distinct from those used by Steel factor. Blood 102, 1405-1413.

Lara, M., Ortega, E., Pecht, I., Pfeiffer, J.R., Martinez, A.M., Lee, R.J., Surviladze, Z., Wilson, B.S., and Oliver, J.M., 2001. Overcoming the signaling defect of Lyn-sequestering, signal-curtailing FcεRI dimers: Aggregated dimers can dissociate from Lyn and form signaling complexes with Syk. J. Immunol. 167, 4329-4337.

Lillemeier, B.F., Pfeiffer, J.R., Surviladze, Z., Wilson, B.S., and Davis, M.M., 2006. Plasma membrane-associated proteins are clustered into islands attached to the cytoskeleton. Proc. Natl. Acad. Sci. USA 103, 18992-18997.

Liu, F.-T., Bohn, J.W., Ferry, E.L., Yamamoto, H., Molinaro, C.A., Sherman, L.A., Klinman, N.R., and Katz, D.H., 1980. Monoclonal dinitrophenyl-specific murine IgE antibody: preparation, isolation, and characterization. J. Immunol. 124, 2728-2737.

Magee, A.I., Adler, J., and Parmryd, I., 2005. Cold-induced coalescence of T-cell plasma membrane microdomains activates signalling pathways. J. Cell Sci. 118, 3141-3151.

Metcalfe, D.D., Baram, D., and Mekori, Y.A., 1997. Mast cells. Physiol. Rev. 77, 1033-1079.

Philimonenko, A.A., Janáček, J., and Hozák, P., 2000. Statistical evaluation of colocalization patterns in immunogold labeling experiments. J. Struct. Biol. 132, 201-210.

Pike, L.J., 2006. Rafts defined: a report on the Keystone Symposium on Lipid Rafts and Cell Function. J. Lipid Res. 47, 1597-1598.

Prior, I.A., Muncke, C., Parton, R.G., and Hancock, J.F., 2003. Direct visualization of Ras proteins in spatially distinct cell surface microdomains. J. Cell Biol. 160, 165-170.

Rivera, J., Kinet, J.-P., Kim, J., Pucillo, C., and Metzger, H., 1988. Studies with a monoclonal antibody to the beta subunit of the receptor with high affinity for immunoglobulin E. Mol. Immunol. 25, 647-661.

Sanan, D.A. and Anderson, R.G., 1991. Simultaneous visualization of LDL receptor distribution and clathrin lattices on membranes torn from the upper surface of cultured cells. J. Histochem. Cytochem. 39, 1017-1024.

Schade, A.E. and Levine, A.D., 2002. Lipid raft heterogeneity in human peripheral blood T lymphoblasts: a mechanism for regulating the initiation of TCR signal transduction. J. Immunol. 168, 2233-2239.

Simons, K. and Toomre, D., 2000. Lipid rafts and signal transduction. Nat. Rev. Mol. Cell Biol. 1, 31-39.

Smrž, D., Dráberová, L., and Dráber, P., 2007. Non-apoptotic phosphatidylserine externalization induced by engagement of glycosylphosphatidylinositol-anchored proteins. J. Biol. Chem. 282, 10487-10497.

Volná, P., Lebduška, P., Dráberová, L., Šímová, S., Heneberg, P., Boubelík, M., Bugajev, V., Malissen, B., Wilson, B.S., Hořejší, V., Malissen, M., and Dráber, P., 2004. Negative regulation of mast cell signaling and function by the adaptor LAB/NTAL. J. Exp. Med. 200, 1001-1013.

Wilson, B.S., Pfeiffer, J.R., and Oliver, J.M., 2000. Observing FcεRI signaling from the inside of the mast cell membrane. J. Cell Biol. 149, 1131-1142.

Wilson, B.S., Pfeiffer, J.R., and Oliver, J.M., 2002. FcεRI signaling observed from the inside of the mast cell membrane. Mol. Immunol. 38, 1259-1268.

Wilson, B.S., Steinberg, S.L., Liederman, K., Pfeiffer, J.R., Surviladze, Z., Zhang, J., Samelson, L.E., Yang, L.H., Kotula, P.G., and Oliver, J.M., 2004. Markers for detergent-resistant lipid rafts occupy distinct and dynamic domains in native membranes. Mol. Biol. Cell 15, 2580-2592.

Wyse, B.D., Prior, I.A., Qian, H., Morrow, I.C., Nixon, S., Muncke, C., Kurzchalia, T.V., Thomas, W.G., Parton, R.G., and Hancock, J.F., 2003. Caveolin interacts

with the angiotensin II type 1 receptor during exocytic transport but not at the plasma membrane. J. Biol. Chem. 278, 23738-23746.

Zhu, M., Liu, Y., Koonpaew, S., Granillo, O., and Zhang, W., 2004. Positive and negative regulation of FcεRI-mediated signaling by adaptor protein LAB/NTAL. J. Exp. Med. 200, 991-1000

Figure legends

Figure 1. Schematic drawing of procedures used to isolate PM sheets. (A) Glass coverslip with cells growing as adherent or attached via fibronectin (left) or ultraclean glass coverslip with cells adsorbed in protein-free buffer (right) was placed face-down onto PLL-coated EM grids laid on nitrocellulose (NC) filter wetted with HEPES buffer and kept on ice-cold basis. (B) Alternatively, cells in suspension were dropped onto individual EM grids and covered with an ultraclean glass coverslip. (C) A sandwich formed by glass coverslip, cells and EM grid was pressed by an ice-cold rubber stopper. (D) The coverslip was quickly side-lifted, leaving the dorsal PM sheets bound to EM grid. (E) The EM grid with attached PM sheets was immediately transferred face-down onto ice-cold HEPES buffer surface for several seconds and further processed (fixation, immunolabeling and contrasting steps). Schematic transversal view at high magnification of PM sheets isolation procedures is shown at the bottom of C-E.

Figure 2. Properties of PM sheets isolated by various procedures. (A-C) Examples of PM sheets isolated from resting BMMC by adhesion to fibronectin (A), adsorption to ultraclean glass coverslips (B), or direct pressing in suspension to EM grids (C). FcεRI-

β subunit was labeled on cytoplasmic side with JRK monoclonal antibody followed by goat anti-mouse IgG-10 nm gold conjugate. (D) Density of 10 nm gold immuno-labeled FcεRI-β on plasma membrane sheets isolated from resting or activated (2 min, 37°C, 0.1 μg/ml DNP-BSA) BMMC by adhesion to fibronectin (f), adsorption to ultraclean glass coverslips (g), or pressing in suspension to EM grids (s). (E) Density of 10 nm gold immuno-labeled FcεRI-β on PM sheets isolated from adherent RBL cells or ultraclean glass-adsorbed BMMC in the course of their activation with DNP-BSA at 37°C. Means and SD from 3 independent experiments are shown; each experiment covers approximately 30 μm^2 of the PM.

Figure 3. Different topography of FcεRI in activated BMMC and RBL cells. (A, B) Topography of intracellularly labeled FcεRI-β subunit (10 nm gold particles) and FcεRI-α subunit-associated extracellular IgE (5 nm gold particles, indicated by arrows) in PM sheets isolated from resting (A) or activated (B; 2 min; 37°C; 0.1 μg/ml DNP-BSA) BMMC. (C, D) Clustering of IgE (triangles) and FcεRI-β (squares) in resting (C) and activated (D) BMMC. Clustering is indicated at respective distance from a typical particle, when the pair correlation function (PCF) exceeds 1. Ideal random distribution of gold markers (PCF = 1) is pointed out by a solid line. The distance at which the peak of PCF value falls to 1 indicates size of the immunolabeled aggregates of respective membrane antigen (the real aggregates are, however, smaller, as the size of antibody sandwiches must be taken into consideration). The hight of the peak indirectly reflects density of these aggregates in PM (the higher number of distinct aggregates within certain area, the lower PCF peak) but it also reflects saturation of labeling within the aggregates (5 nm immunogold label provides more intense signal than 10 nm immunogold label). Each graph represents data from two independent experiments

covering approximately 60 μm^2. (E, F) As a control, topography of FcεRI-β subunit and FcεRI-α subunit-associated extracellular IgE in resting (E) and activated (F) RBL cells is shown. (G, H) Clustering of IgE (triangles) and FcεRI-β (squares) in resting (G) and activated (H) RBL cells was calculated as above.

Figure 4. Clustering of 10 nm-immunogold-labeled FcεRI-β in the course of BMMC and RBL cell activation. BMMC were stimulated with 0.1 μg/ml (A) or 1 μg/ml (B), RBL cells with 1 μg/ml (C) DNP-BSA at 37°C. Clustering is plotted as described in Fig. 3. Each graph represents data from two independent experiments covering approximately 60 μm^2.

Figure 5. Changes in topography and expression of FcεRI in the course of BMMC and RBL cell activation as detected by confocal microscopy and flow cytometry. (A-F) Distribution of IgE on the PM of BMMC (A-C) and RBL cells (D-F) in resting cells (A, D) or cells activated by DNP-BSA for 2 min (B, E) or 5 min (C, F). IgE was detected by FITC-conjugated donkey anti-mouse Ig on fixed cells. (G) Relative concentration of surface FcεRI on BMMC and RBL cells in the course of their activation by DNP-BSA as detected by flow cytometry. IgE was labeled by FITC-conjugated donkey anti-mouse Ig on fixed resting or activated cells. Means ± SD from 3 independent experiments are shown.

Figure 6. Enhanced FcεRI clustering in BMMC stimulated at low temperature. IgE-sensitized BMMC (A) or RBL cells (B) were incubated for 10 min on ice and FcεRI was then triggered for 2 or 5 min with DNP-BSA on ice. PM sheets were isolated and

FcεRI-β was labeled with JRK monoclonal antibody followed by goat anti-mouse IgG-10 nm gold conjugate. Clustering is plotted as described at Fig. 3. Each graph represents data from two independent experiments covering approximately 60 μm^2.

Figure 7. Topography of LAT and NTAL on the PM sheets from resting cells. PM sheets were isolated from BMMC (A-C) or RBL cells (D-F). LAT (A, D) or NTAL (B, E) were labeled by two different antibodies or they were labeled together on the same membrane (C, F). Clusters of 5 nm gold are circled.

Figure 8. Quantitative analysis of topographical relationship between LAT and NTAL. Distribution of gold particles on PM sheets isolated from BMMC (A) or RBL cells (B) was mapped by pair cross-correlation function (PCCF). Colocalization is indicated at respective distance from a typical particle when the PCCF exceeds 1. Ideal independent distribution of both gold markers (PCCF = 1) is pointed out by a solid line. The maximal width of the peak above value 1 reflects distance at which both antigens are selectively closer to each other than it would be in the case of random distribution. The hight of the peak corresponds to tendency of both antigens to colocalize and it is reduced when overall label density is higher. The black squares and black diamonds show LAT or NTAL simultaneously labeled with rabbit and mouse antibodies against the same adaptor (positive controls). Other markers show PCCF for LAT and NTAL labeled together on resting or DNP-BSA-activated cell as indicated. Each graph represents data from two independent experiments covering approximately 60 μm^2.

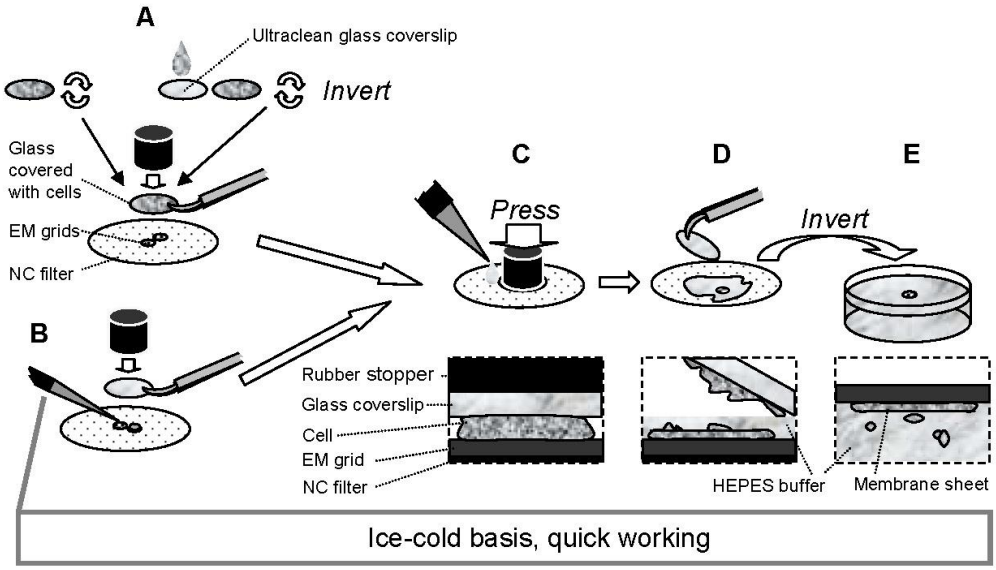

Figure 1.

Lebduška et al.

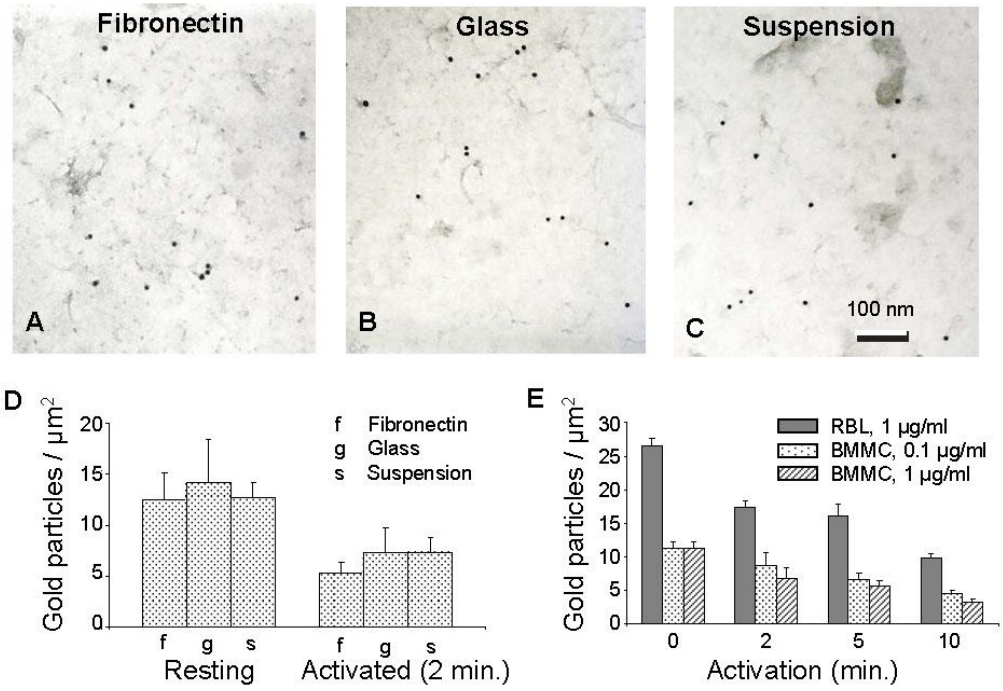

Figure 2.

Lebduška et al.

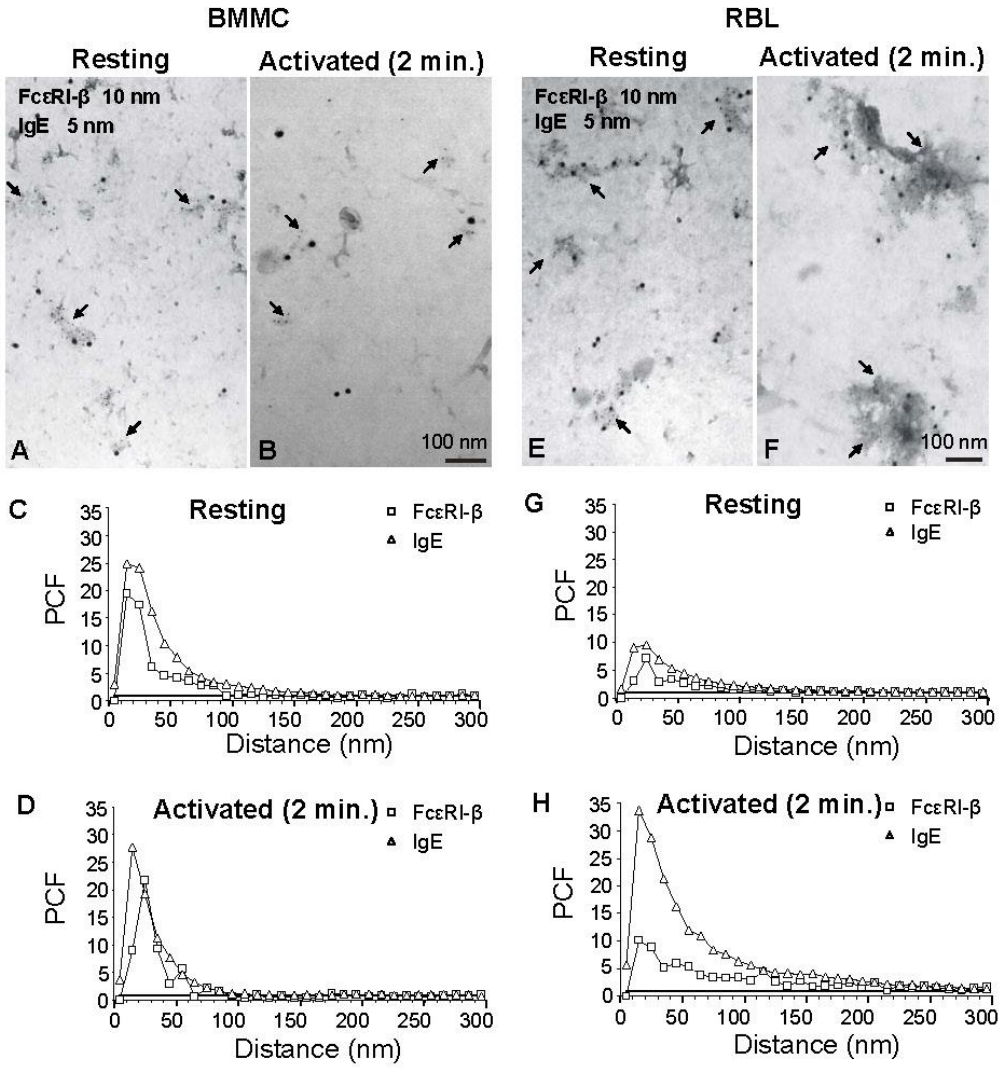

Figure 3.

Lebduška et al.

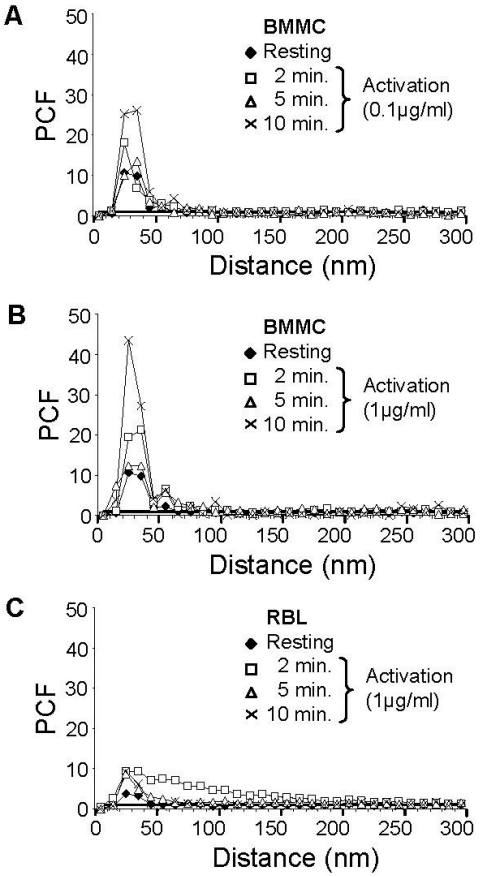

Figure 4.

Lebduška et al.

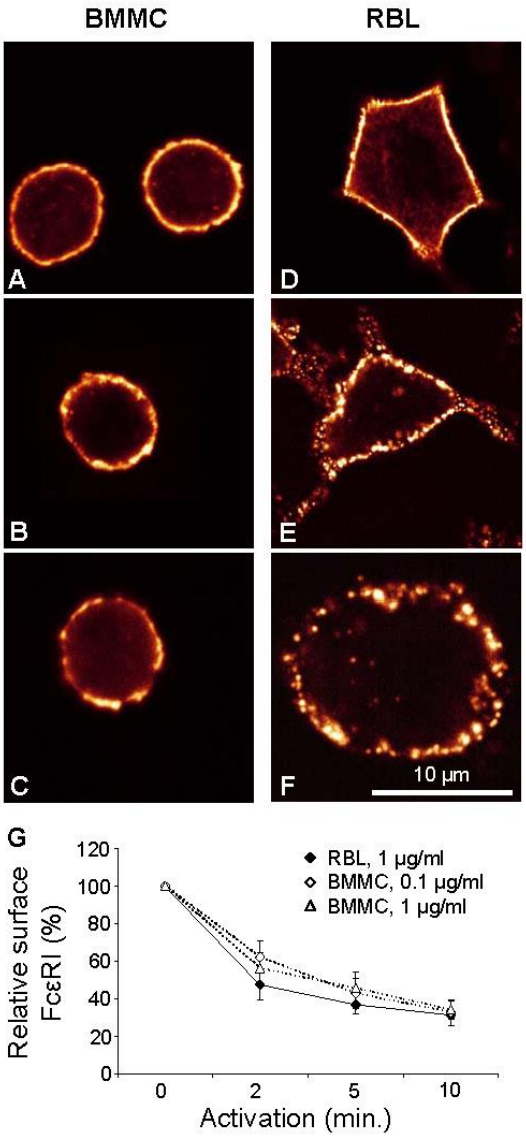

Figure 5.

Lebduška et al.

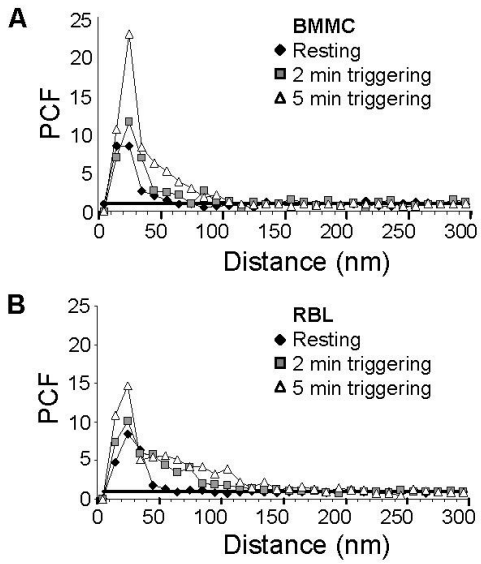

Figure 6.

Lebduška et al.

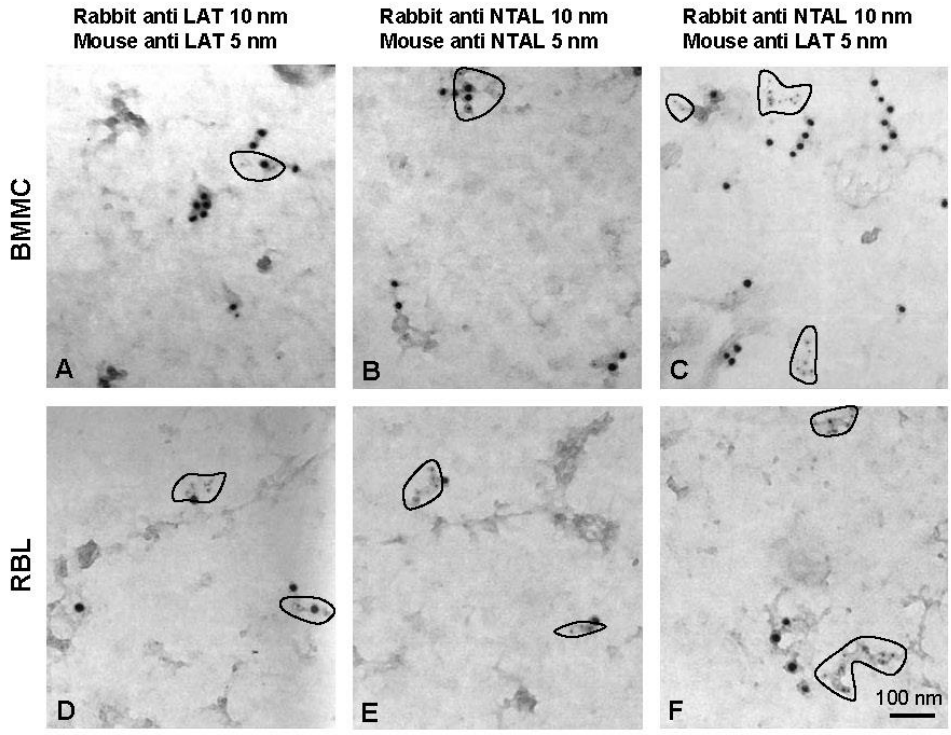

Figure 7.

Lebduška et al.

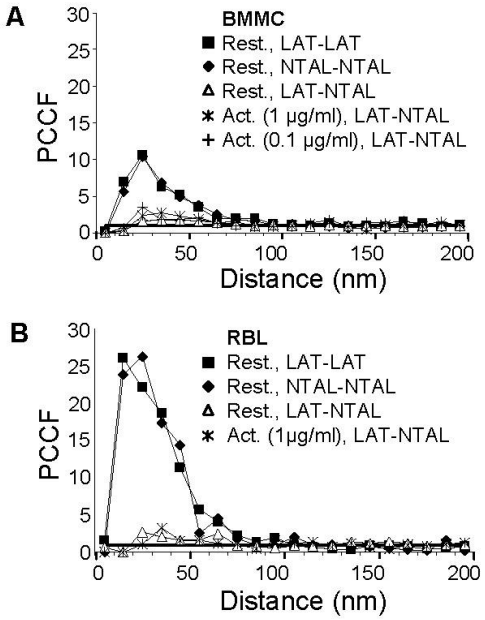

Figure 8.

Lebduška et al.

Diskuse

Na počátku té aktivace žírných buněk, která je závislá na IgE a vede ke spuštění efektorových mechanizmů alergických reakcí, stojí agregace receptoru FcεRI. Biochemickými přístupy (částečnou lýzou neiontovým detergentem a imunoprecipitací) je možné analyzovat řadu molekul, které se v tomto procesu účastní přenosu signálu přes plazmatickou membránu, a fluorescenční mikroskopie nebo skenovací elektronová mikroskopie poskytují data umožňující rámcovou představu o organizaci ohnisek těchto signalizačních kaskád, jak dokládá řada prací (*Field a kol., 1995; Kihara a Siraganian, 1994; Saitoh a kol., 2000; Holowka a kol., 2000; Barker a kol., 1998; Stump a kol., 1988*). Detailní pohled na rovinu plazmatické membrány žírných buněk však přinesla až aplikace metody izolace membránových listů zkoumatelných pomocí transmisní elektronové mikroskopie (*Wilson a kol., 2000*). Získané výsledky vypovídaly o tom, že aplikace antigenu vede u žírných buněk linie RBL k vytvoření poměrně rozsáhlých primárních signalizačních domén (o průměru až několik set nm), na jejichž periferii se nacházejí sekundární signalizační domény, které informaci přebírají a předávají dál. Primární domény mimo jiné zahrnují agregáty receptoru FcεRI, asociovanou cytoplazmatickou kinázu Syk, adaptory Grb2 a Gab2, komponenty klathrinového endocytického aparátu nebo fosfolipázu Cγ2. Jejich tvorbu provází disociace tyrozinkinázy Lyn od receptorového komplexu. Sekundární signalizační domény tvoří agregáty transmembránového adaptorového proteinu LAT a obsahují například fosfolipázu Cγ1. Fosfolipidová kináza PI3K se vyskytuje v obou typech domén (*Wilson a kol., 2000; Wilson a kol., 2002*).

Použil jsem metodu izolace a imunospecifického značení membránových listů k tomu, abych porovnal signalizační ohniska vzniklá po dimerizaci receptoru FcεRI se strukturami tvořenými po multimerizaci FcεRI zprostředkované antigenem. Jak bylo možno očekávat, aplikace antigenu vedla ke vzniku rozsáhlých (obvykle přibližně 200 nm) agregátů receptoru, kolokalizujících s tyrozinkinázou Syk a adaptorem Grb2, tedy struktur odpovídajících dříve popsaným primárním signalizačním doménám. Dimerizace receptoru monoklonální protilátkou 5.14 se oproti tomu na dané detekční úrovni na topografii signalizačních molekul nijak neprojevila – jejich distribuce odpovídala situaci na neaktivovaných buňkách. Nebyla pozorována kolokalizace FcεRI a Grb2, avšak koncentrace Grb2 na plazmatické membráně signifikantně vzrostla, byť méně, než v případě aktivace antigenem (*článek A*). Také asociace receptoru s komponentami lipidových raftů po jeho dimerizaci vzrostla, podobně jako fosforylace signalizačních proteinů, mobilizace vápenatých iontů a sekrece obsahu cytoplazmatických váčků. Tyto procesy sice opět byly méně výrazné než v případě multimerizace receptoru, přesto však řádově srovnatelné (*článek A, spoluautoři*). Nepoměr mezi topografickými změnami membránových molekul a výslednými aktivačními účinky byl zřejmý a

stavěl rozsáhlé receptorové agregáty do pozice struktur postradatelných pro vlastní efektorové funkce žírných buněk a odrážejících snad spíše proces útlumu a odklízení signalizačních komponent jako odpověď na multimerizaci receptoru FcεRI. Bylo to v souladu se skutečností, že nadměrná koncentrace antigenu při aktivaci žírných buněk RBL koreluje se snížením intenzity degranulace a vede k tvorbě rozsáhlých domén FcεRI v závislosti na aktinovém cytoskeletu (*Seagrave a kol., 1991*). Zdá se, že roli zpětnovazebného regulátoru reagujícího na přílišné nahloučení a stimulaci receptoru FcεRI by mohla hrát fosfolipidová fosfatáza SHIP (*Gimborn a kol., 2005*) a ubiquitinová ligáza Cbl, která byla vizualizována jako součást rozsáhlých primárních signalizačních domén FcεRI (*Gustin a kol., 2006; Wilson a kol., 2002*).

Otázkou zůstávalo, zda k formování takto výrazných aktivačně-inhibičních domén dochází na žírných buňkách při multimerizaci receptoru FcεRI obecně, nebo zda se jedná o jev specifický pro nádorovou linii RBL. Tato linie sice díky svému adherentnímu růstu poskytuje dobré podmínky pro izolaci membránových listů, ale jako modelový představitel žírných buněk je značně diskutabilní. Problém relevance výsledků topografických analýz na plazmatické membráně buněk RBL vyžadoval zahrnout do studií přirozenější reprezentanty žírných buněk – primární izoláty nebo krátkodobé kultiváty. Aplikaci klasické metody preparace membránových listů (*Sanan a Anderson, 1991*) však v případě těchto buněk bránila jejich neadherentnost, proto bylo zapotřebí metodu zdokonalit.

Na základě empirických poznatků z dětských let o schopnosti vazby živočišných buněk na skleněné povrchy jsem se rozhodl blíže zkoumat možnosti užití čistého skla při izolaci membránových listů z žírných buněk BMMC, kultivovaných z kostní dřeně. Zjistil jsem, že za určitých podmínek (vhodným způsobem vyčištěná a skladovaná sklíčka, buňky v pufru o nulovém nebo nízkém obsahu proteinů) také neadherentní leukocyty přilnou ke skleněnému povrchu tak efektivně, že je možné z nich snadno získat membránové listy a provádět topografické studie takového rozsahu, jako v případě studií využívajících klasickou metodu Sanana a Andesona (*Sanan a Anderson, 1991*) založenou na adhezivním růstu buněk. Tím bylo možné vyhnout se potenciálně riskantním imobilizačním krokům (jako je dlouhodobá inkubace s polylyzinem, dlouhodobá expozice nízkým teplotám) zavedeným jinými autory pro izolaci membránových listů z neadherentních lymfocytů T (*Schade a Levine, 2002; Lillemeier a kol., 2006*). Adsorpce buněk BMMC na sklo měla řadu výhod. Byla rychlá (1 min.), jednoduchá, nezpůsobovala arteficielní degranulaci, nevyžadovala chlazení buněk ani funkčnost aktinového cytoskeletu. Abych prověřil vlastnosti takto izolovaných membrán, zavedl jsem jiné dva postupy přípravy membránových listů z neadherentních buněk, které však sloužily jen jako kontrola, neboť byly méně praktické než metoda založená na adsorpci ke sklu. První přístup spočíval ve vazbě žírných buněk na komponenty extracelulární matrix, ke které docházelo po senzitizaci buněk pomocí IgE (založeno na poznatku *Lam a kol., 2003*), tedy využíval specifického mechanismu, druhý přístup redukoval adsorpční krok na minimum, neboť spočíval

v pouhém přitlačení suspendovaných buněk na mikroskopickou síťku. Jelikož jsem mezi membránovými listy připravenými výše uvedenými způsoby neshledal žádné rozdíly v morfologii membrán ani v topografických změnách receptoru FcεRI v průběhu buněčné aktivace, využil jsem metodu založenou na adsorpci ke sklu k rutinnímu zkoumání topografie signalizačních molekul žírných buněk BMMC (*článek E*).

Zjistil jsem, že denzita receptoru FcεRI na plazmatické membráně buněk BMMC je vůči buňkám RBL přibližně poloviční (*článek E*). To by mohlo vysvětlovat skutečnost, že optimální degranulace buněk BMMC je způsobována nižší koncentrací antigenu než v případě buněk RBL (*článek B, spoluautoři; článek A, spoluautoři*). Proto jsem k aktivaci buněk BMMC používal jak koncentraci optimální pro buňky BMMC, tak tu optimální pro RBL, aby srovnání topografických změn receptoru FcεRI na obou buněčných typech mělo vyšší vypovídací hodnotu. Obě koncentrace kupodivu způsobily u buněk BMMC srovnatelnou internalizaci receptoru, která odpovídala internalizaci na buňkách RBL. O to překvapivější bylo zjištění, že multimerizace receptoru FcεRI na buňkách BMMC, na rozdíl od linie RBL, nevyvolává tvorbu jeho rozsáhlých nahloučenin. Na neaktivovaných buňkách obou buněčných typů bylo možné FcεRI detekovat jako klastry o srovnatelné velikosti, které však v případě buněk RBL internalizovaly za přechodné tvorby výrazných agregátů, zatímco domény FcεRI na BMMC endocytovaly bez viditelného nárůstu velikosti. Celková míra internalizace byla u obou typů srovnatelná, ale lokální dynamika se zásadně lišila, neboť buňky BMMC preferovaly více drobných ohnisek, zatímco buňky RBL ohniska větší, ale menšího počtu (*článek E*). Ukázalo se tedy, že vžitá představa o primárních signalizačních doménách žírných buněk jako rozsáhlých agregátech receptoru FcεRI, založená na leukemické linii RBL (*Wilson a kol., 2001; Wilson a kol., 2002*), nepředstavuje obecný jev a možná nemusí odpovídat fyziologické realitě. Primární signalizační ohniska buněk BMMC jsou mnohem menší a doménám FcεRI na buňkách RBL se podobají až v případě, že multimerizace receptoru proběhne za stavu podchlazení (4°C) (*článek E*).

Sekundární signalizační domény žírných buněk byly popsány jako agregáty transmembránového adaptoru LAT, poskytující strukturní a funkční základ pro přenos signálu do nitra buňky (*Wilson a kol., 2001; Wilson a kol., 2002*). Velice podobným adaptorovým proteinem žírných buněk se ukázal být NTAL (*Brdička a kol., 2002*), jehož topografie na úrovni elektronové mikroskopie byla dosud neznámá. Analyzoval jsem membránové listy buněk RBL a prokázal, že NTAL je na plazmatické membráně distribuován v klastrech o stejné morfologii jako vykazují domény proteinu LAT a (rovněž podobně jako LAT) je možno jej nalézt při okrajích rozsáhlých agregátů receptoru FcεRI. Jak na neaktivovaných, tak na aktivovaných buňkách však proteiny LAT a NTAL tvořily separátní nepřekrývající se domény (*článek B*). To bylo poněkud překvapivé zjištění, neboť se jednalo o strukturně velice podobné palmitylované proteiny patřící mezi tak zvané markery lipidových

raftů a dalo se předpokládat, že budou sdílet společné lipidické prostředí. Ve stejném roce ale byla publikována studie dokumentující značnou topologickou nezávislost některých markerů lipidových raftů v plazmatické membráně buněk RBL (*Wilson a kol., 2004*) a pohled na lipidové rafty se začal měnit.

Rozhodl jsem se prověřit, zda separace adaptorů LAT a NTAL není specifická pro linii RBL a současně zda nemůže být důsledkem vazby detekčních protilátek. Ukázalo se, že oba adaptory tvoří nepřekrývající se domény i v buňkách BMMC a že tento jev není artefaktem procedury značení antigenů (*článek E*). Pokud tedy palmitylace propůjčuje molekulám LAT a NTAL tendenci kontaktovat společné organizované lipidické prostředí, musí existovat mechanismus, který tento účinek převáží a jejich agregáty separuje. Zdá se, že nejpravděpodobnějším vysvětlením by mohly být meziproteinové interakce v rámci signalozomů formovaných v oblasti cytoplazmatických domén těchto adaptorů, neboť soubor a rozmístění vazebných míst na molekulách LAT a NTAL se liší (*Brdička a kol., 2002*) a důležitost meziproteinových interakcí při tvorbě funkčních domén fosforylovaného proteinu LAT byla doložena v lymfocytech T (*Schade a Levine, 2002*). Tvorba a stabilizace agregátů membránových proteinů také do značné míry závisí na vazbě cytoskeletu a morfologie příslušné domény je výsledkem spolupůsobení vazeb mezi proteiny samými a mezi proteiny a lipidy (*Lillemeier a kol., 2006*).

V žírných buňkách NTAL zřejmě slouží jako negativní regulátor signalizace receptoru FcεRI, avšak je též schopen částečně nahradit pozitivní roli adaptoru LAT (*Zhu a kol., 2004; článek B, spoluautoři*). Nadměrná exprese proteinu NTAL má též, kromě útlumu aktivace, vliv na morfologii žírných buněk zasažením do procesu polymerizace aktinu (*článek D, spoluautoři*). Proto bylo teoreticky možné, že se inhibiční účinky nadměrného množství molekul NTAL projeví již v okamžiku tvorby agregátů receptoru FcεRI. Zjistil jsem však, že topografie receptoru FcεRI v průběhu aktivace žírných buněk linie RBL exprimujících obvyklé, zvýšené nebo snížené množství molekul NTAL se neliší, stejně jako vzájemná lokalizace agregátů NTAL a FcεRI. NTAL také nevytvářel za stavu nadměrné exprese žádné neobvyklé struktury, kromě toho, že jeho domény byly rozměrnější (*článek D*). Inhibiční účinek adaptoru NTAL na signalizaci žírných buněk tedy zřejmě nespočívá v ovlivnění tvorby signalizačních ohnisek FcεRI.

Navzdory výsledkům popisujícím topologickou nezávislost některých markerů lipidových raftů, pro přítomnost lipidických agregátů v plazmatické membráně svědčí skutečnost, že LAT, který postrádá extracelulární doménu, kolokalizuje s proteinem Thy-1 zakotveným do membrány extracelulárně přes GPI (*Wilson a kol., 2004*). Zajímalo mě, jestli se tolik podobný protein NTAL bude vůči Thy-1 chovat také tak, nebo zda, v souladu se svou separací od domén proteinu LAT, s Thy-1 asociovat nebude. Ukázalo se, že domény Thy-1 kolokalizují jak se shluky proteinu LAT, tak NTAL, a to zejména za podmínek extenzivní agregace Thy-1, ale ani v tomto případě oba adaptory netvořily společné ostrůvky, pouze se vyskytovaly v těsnější blízkosti než by odpovídalo náhodné distribuci (*článek C*). Protože oba

adaptorové proteiny jsou po agregaci Thy-1 fosforylovány (*článek C, spoluautoři*), domény Thy-1 vystupují jako platformy, které stimulují a sdružují nezávislé agregáty dvou funkčně příbuzných, ale do značné míry antagonistických signalizačních molekul, což by mohl být jeden ze způsobů modulace signálu pomocí lipidových raftů.

Slibným nástrojem pro analýzu struktury domén Thy-1 se stala transfekovaná linie buněk RBL, která kromě vlastní izoformy Thy-1.1 stabilně exprimovala vnesenou izoformu Thy-1.2, přičemž obě varianty tohoto glykoproteinu bylo možno odlišit a agregovat specifickými monoklonálními protilátkami. Shodný modul zakotvení do plazmatické membrány a 82% sekvenční identita těchto izoform by podle očekávání mohly způsobit jejich rovnocenné promíchání ve společných doménách, ale fluorescenční mikroskopie naznačovala jejich nezávislý pohyb (*článek C, spoluautoři*). Otázkou tedy zůstávala vzájemná topografie obou izoforem při rozlišení poskytovaném elektronovou mikroskopií, a bylo vhodné zkoumat též míru soudržnosti molekul Thy-1.1 navzájem a soudržnosti s Thy-1.2. Na membránových listech molekuly Thy-1.1 agregované (a značené) protilátkou silně kolokalizovaly s molekulami téže izoformy značenými až dodatečně po fixaci. Pokud ale byla stejným způsobem po fixaci označena izoforma Thy-1.2, agregáty Thy-1.1 s ní kolokalizovaly jen slabě, domény obou proteinů se pak nacházely sice často v těsné blízkosti, ale zachovávaly si značnou strukturní nezávislost (*článek C*). Zdá se tedy, že navzdory totožné membránové kotvě a vysoké sekvenční shodě, rozdílné izoformy Thy-1 vytvářejí v plazmatické membráně rozdílné domény, které mezi sebou vykazují jistou slabou soudržnost, ale jinak vystupují poměrně nezávisle. Jak již bylo zmíněno, na tvorbě proteinových agregátů, které jsou přítomné i v plazmatické membráně neaktivovaných buněk, se zřejmě podílí aktinový cytoskelet (*Lillemeier a kol., 2006*). Na úrovni vzdáleností několika nanometrů vede dimerizace jedné z izoforem Thy-1 ke zvýšené asociaci s agregáty druhé izoformy a aktinový cytoskelet jejich těsnější kontakt podporuje. Současně však tento cytoskelet hraje též roli separátoru, bránícího přílišnému nahloučení molekul Thy-1 stejné izoformy (*článek C, spoluautoři*).

Lipidické interakce tedy zřejmě hrají důležitou roli při tvorbě základních stabilizovaných jednotek membránových raftů (po dimerizaci), ale organizace těchto jednotek do struktur vyššího řádu je netriviálním způsobem ovlivňována spoluprácí s aktinovým cytoskeletem. Tato dizertace dokumentuje, že rozdílné raftové molekuly, byť často sekvenčně velice podobné, tíhnou k tvorbě rozdílných membránových domén. Výjimkou je silná asociace intracelulárně orientovaných transmembránových palmitylovaných proteinů LAT a NTAL s agregáty extracelulárního proteinu Thy-1. Jedním z mechanismů, které by raftové proteiny do samostatných domén mohly oddělovat, pravděpodobně bude účinek specifických vzájemných interakcí proteinových řetězců, v některých případech ale lze uvažovat například i o roli rozdílné glykozylace. Ukazuje se, že tvorba signalizačních ohnisek v plazmatické membráně je organizována systémem nejen značně komplexním, ale i vysoce

dynamickým, a že některé konkrétní projevy tohoto procesu se mohou významně lišit mezi různými modelovými zástupci daného buněčného typu. Prezentovaná metoda izolace membránových listů z neadherentních buněk by mohla výzkum v tomto oboru usnadnit. Je však třeba připomenout, že plastického obrazu o přenosu signálu přes plazmatickou membránu je možno dosáhnout jen souhrou řady rozdílných a vzájemně se doplňujících přístupů.

Závěry

Byly vytvořeny tři způsoby izolace membránových listů z neadherentních žírných buněk BMMC. Jeden z nich, založený na adsorpci leukocytů ke skleněnému povrchu, se ukázal být zvláště slibný a poskytl řadu vědeckých dat (*článek E***).**

Aktivace žírných buněk RBL dimerizací receptoru FcεRI vedla k obohacení plazmatické membrány o adaptorový protein Grb2, který však, na rozdíl od případu multimerizace receptoru, s FcεRI signifikantně nekolokalizoval a distribuce FcεRI nebyla metodou imunoznačení membránových listů odlišitelná od distribuce na neaktivovaných buňkách (*článek A***). Žírné buňky BMMC, na rozdíl od buněk RBL, netvořily po multimerizaci receptoru větší agregáty FcεRI, než buňky neaktivované. Multimerizace receptoru FcεRI vedla u buněk BMMC a RBL k jeho internalizaci o srovnatelné intenzitě i celkové dynamice, ale lokální redistribuce FcεRI se u nich zásadně lišila (***článek E***). Vžitý model rozsáhlých (přibližně 200 nm) signalizačních domén tohoto receptoru byl zpochybněn.**

Adaptorový protein NTAL byl v plazmatické membráně distribuován v klastrech obdobným způsobem jako adaptor LAT, a rovněž jejich topografické vztahy k receptoru FcεRI a glykoproteinu Thy-1 byly obdobné. Po multimerizaci FcεRI se oba adaptory u buněk RBL příležitostně nacházely na periferii agregátů tohoto receptoru, přesto však NTAL a LAT tvořily oddělené domény jak v průběhu aktivace buněk RBL, tak BMMC (*články B, E***). Oba adaptory výrazně kolokalizovaly s agregovaným glykoproteinem Thy-1, avšak i za těchto podmínek si uchovávaly charakter separátních domén (***článek C***). Tyto výsledky podporují obraz membránových raftů jako systému tvořeného souhrou proteinových a lipidických interakcí.**

Nadměrná ani snížená exprese adaptoru NTAL, který je negativním regulátorem signalizace žírných buněk, se na distribuci receptoru FcεRI v průběhu aktivace buněk RBL neprojevila. Tyto změny množství molekul NTAL v plazmatické membráně vyústily v odpovídající změny velikosti domén tohoto adaptoru, ale charakter jeho distribuce změněn nebyl (*článek D***).**

Izoformy Thy-1.1 a Thy-1.2 byly v plazmatické membráně distribuovány do značné míry nezávisle. Agregace Thy-1.1 vedla jen k slabé koagregaci Thy-1.2, oproti tomu molekuly téže izoformy vykazovaly mnohem vyšší soudržnost (*článek C***).**

English version

Pavel Lebduška

Topography of signaling molecules on the plasma membrane in the course of mast cell activation.

Dissertation thesis in molecular and cell biology

Charles University (Prague), Faculty of Sciences

Supervised by RNDr. Petr Dráber, Dr.Sc, Academy of Sciences of the Czech Republic, Institute of Molecular genetics, Department of Signal Transduction

Preface:

Revealing the mechanisms of immune cell reactions to antigens can be included among the fields of basic research that do not only extend the general knowledge, but tightly relate to the quality of human life as well. As a theme of my study, hence I have chosen the signal transduction across the plasma membrane of mast cells – the effectors of allergic reactions. The results of me and my colleagues to this topic have been published in following articles:

(A) Signaling assemblies formed in mast cells activated via Fcε receptor I dimers.
Ľubica Dráberová, Pavel Lebduška, Ivana Hálová, Pavel Tolar, Jitka Štokrová, Helena Tolarová, Jan Korb and Petr Dráber. *Eur. J. Immunol. 2004*, 34: 2209-2219

(B) Negative regulation of mast cell signaling and function by the adaptor LAB/NTAL.
Petra Volná, Pavel Lebduška, Ľubica Dráberová, Šárka Šímová, Petr Heneberg, Michael Boubelík, Viktor Bugajev, Bernard Malissen, Bridget S. Wilson, Václav Hořejší, Marie Malissen and Petr Dráber. *J. Exp. Med. 2004*, 200: 1001-1013

(C) Topography of plasma membrane microdomains and its consequences for mast cell signaling. Petr Heneberg, Pavel Lebduška, Ľubica Dráberová, Jan Korb and Petr Dráber. *Eur. J. Immunol. 2006*, 36: 2795-2806

(D) Regulation of Ca^{2+} signaling in mast cells by tyrosine-phosphorylated and unphosphorylated non-T cell activation linker, NTAL. Ľubica Dráberová, Gouse Mohiddin Shaik, Petra Volná, Petr Heneberg, Magda Tůmová, Pavel Lebduška, Jan Korb and Petr Dráber. *Journal of Immunology*, submitted (May 2007)

(E) Topography of signaling molecules as detected by electron microscopy on plasma membrane sheets isolated from nonadherent mast cells.
Pavel Lebduška, Jan Korb, Magda Tůmová, Petr Heneberg and Petr Dráber.
Journal of Immunological Methods, submitted (June 2006)

I proclaim that I have not used these articles as a background for achieving any academic degree in the past. Proportion of my own results I specify further. It arises especially from sections Discussion and Conclusions, where the results of other researchers are explicitly cited.

I would like to thank coauthors of the publications mentioned above, technicians from the Department of Signal Transduction and the Department of Micromorphology of Biopolymers at the Institute of Molecular Genetics, and, last but not least, I thank my friends and relatives, as without their emotional and professional support a several years lasting scientific work would be harder, darker and devoid of many positive features.

RNDr. Pavel Lebduška
July 2007

***

Elaborated at the Institute of Molecular Genetics, Czech Academy of Sciences in 2002-2007.

Content:

List of abbreviations and specification of terms

BCR:	B cell receptor
BMMC:	Bone marrow-derived mast cells
DIG:	Detergent-insoluble glycosphingolipid-enriched membranes
DRM:	Detergent-resistant membranes
FAK:	Focal adhesion kinase
FcαR (I):	Immunoglobulin A receptor, type I
FcγR (I, II, III):	Immunoglobulin G receptor, type I, II, III
FcεR (I, II):	Immunoglobulin E receptor, type I, II
FGF:	Fibroblast growth factor
FRET:	Fluorescence resonance energy transfer
GM-CSF:	Granulocyte-macrophage colony stimulating factor
GPI:	Glycosylphosphatidylinositol
Ig:	Immunoglobulin
IFN:	Interferon
IL:	Interleukin
ITAM:	Immune-tyrosine activation motif
ITIM:	Immune-tyrosine inhibition motif
MAPK:	Mitogene-activated protein kinase
MAPKK:	Mitogene-activated protein kinase-kinase
MIRR:	Multichain immune-recognition receptor
NGF:	Nerve growth factor
PI3K:	Phosphatidylinositol-3 kinase
PLC:	Phospholipase C
RBL:	Rat basophilic leukemia
SCF:	Stem cell factor
T_C:	Cytotoxic T cell
TCR:	T cell receptor
TGF:	Transforming growth factor
T_H:	Helper T cell
TIFF:	Triton-insoluble floating fraction
TLR:	Toll-like receptor
TNF:	Tumor necrosis factor
T_{Reg}:	Regulatory T cell

(I use the other untraditional groups of characters, though usually of abbreviation origin, as established terms, hence they are not indicated here.)

Colocalization (related to the plasma membrane) – meant as preferential location of one antigen to the area of second antigen, not as accidental location of both antigens at one place.

Nonadherent cells – growing as unattached to the bottom of tissue culture cultivation flask.

Introduction

I) Organization of the plasma membrane

Plasma membrane serves as a multipurpose biological interface of fundamental importance that determines and actively maintains the composition of intracellular milieu and mediates communication between the cell and its environment. This information function of the plasma membrane has been intensively studied for many years and the structural and functional background of transmembrane communication is being revealed gradually. It turns out that in these processes perhaps not only proteins themselves are crucial, but more likely their collaboration with local lipidic milieu – a phenomenon associated with the term of „lipid rafts".

Original hypothesis of lipid rafts

In 1972, when published their „fluid mosaic model of the structure of cell membranes", Singer and Nicolson accentuated lateral mobility of individual proteins in the field of two-dimensional lipidic phase. Plasma membrane seemed to be more or less a planar oriented solution of amphipatic proteins in lipid bilayer (*Singer and Nicolson, 1972*). Subsequently, however, a concept arose postulating that the lipids of plasma membrane laterally segregate according to different features of their hydrophobic chains and form spontaneously a system of membrane domains (*Klausner et al., 1980; Karnovsky et al., 1982*). Especially clusters of sphingolipids with intercalated cholesterol attracted the attention, being proposed as relatively rigid islets – lipid rafts – floating in surrounding fluid plasma membrane milieu composed of phospholipids with unsaturated acyl chains. The function of these rafts should consist in transport of certain autogenously sorted proteins to distinct areas of plasma membrane or to respective organelles, and they have been also attributed with important signaling role (*Brown and Rose, 1992; Simons and Ikonen, 1997; Simons and Toomre, 2000; Dykstra et al., 2003*).

According to this hypothesis lipid rafts serve as specific compartments in the field of the plasma membrane. They are supposed to conjugate especially the molecules that contain unsaturated lipid chains or the saturated chains with double bond of *trans* configuration, such as palmitoylated proteins and glycosylphosphatidylinositol (GPI)-anchored proteins, but interactions of aminoacid groups with lipidic components of the rafts are also involved (**Fig. 1**). Immunoreceptors of the MIRR family (multichain immune-recognition receptors), including TCR (T cell receptor), BCR (B cell receptor) or mast cell FcεRI (Immunoglobulin E receptor, type I) practically do not interact with lipid rafts in resting state. But aggregation of these proteins initiates signal transduction across the plasma membrane (and subsequent signaling cascades), which is accompanied with stabilization of contact of these proteins with lipid raft components. In the rough, according to this model, in lipid rafts, there are localized activators and substrates of MIRR immunoreceptor signalosomes (such as Src family kinases or palmitoylated transmembrane adaptor proteins), whereas the negative regulators are excluded.[*] The raft can also be a functional connection between extracellular GPI-anchored receptors and signaling molecules associated with the intracellular leaflet of the plasma membrane (*Langlet et al., 2000; Dykstra et al., 2003; Hořejší et al., 1999*).

[*] In fact, it is much more complicated. For example tyrosine phosphatase CD45, an important positive regulator of MIRR signaling, is rather absent from rafts, which correlates with decreased activity of its substrates – the Src family kinases that do prefer raft residency. Under certain circumstances CD45 serves also as a negative regulator of Src family kinases. The optimal dynamic and balanced contact rate of these tyrosine kinases with CD45 is substantial (*Rodgers and Rose, 1996; Montixi et al., 1998; Penninger et al., 2001; Zhang et al., 2005*).

Experiments on artificial membranes stood at the beginning of lipid raft concept. They verified the basic postulates regarding the hypothesis of segregation processes in planar oriented lipidic mixtures (*Klausner et al., 1980; Sankaram and Thompson, 1990a; Sankaram and Thompson, 1990b; Sankaram and Thompson, 1991; Sankaram et al., 1992; McIntosh et al., 1992; Dietrich et al., 2001*). The results from these model systems, however, cannot be directly applied to describe behavior of the real plasma membrane, thus of much more complex protein-lipid system, where e.g. interactions with submembrane cytoskeleton can have a substantial role.

Isolation of so called DRM (detergent-resistant membranes) – a fraction of the plasma membrane with higher resistance to nonionic detergents – has become a widely used methodical approach to study lipid rafts (*Brown and Rose, 1992*). The term DRM (as well as that of lipid rafts themselves) is connected with terminological confusions. In general, DRM represent an extract prepared by partial cell lysis using nonionic detergent, thus, it is important to specify the conditions of extraction (type of detergent, its concentration, temperature) when speaking of respective DRM. This term is often being confined to membrane fraction prepared by Triton X-100 at 4°C, than it is also called TIFF (Triton-insoluble floating fraction). DRM, a product of isolation procedure, shall not be confused with lipid rafts that are assumed as real entities within the plasma membrane. Nonetheless, it often happened, and the names DIG (detergent-insoluble glycosphingolipid-enriched membranes) or GEM (glycosphingolipid-enriched membranes) have been, unfortunately, used for DRM as well as for lipid rafts. The solution of terminological crisis may be to consider lipid rafts as cholesterol- and sphingolipid-rich membrane domains isolatable as DRM (*Langlet et al., 2000; London and Brown, 2000; Brown and London, 2000*).

Doubtless, detergent-mediated extraction of plasma membrane fractions is an helpful approach that provides information about different tendency of respective membrane proteins to associate with certain lipidic milieu. The obtained results well fit to the concept of lipid rafts, however, they are not a sufficient proof of their real existence, as application of detergent is a serious intervention into biophysical properties of the plasma membrane (*Mayor and Maxfield, 1995; Heerklotz, 2002*). Nevertheless, using FRET (fluorescence resonance energy transfer) technique, cholesterol- and GPI-anchor-dependent protein aggregates have been demonstrated even in the plasma membrane of living cells. The diameter of these domains was less than 70 nm and their formation was independent of the protein chain (*Varma and Mayor, 1998*). Similar conclusions emerged from an experiment with covalent cross-linking of closely associated GPI-anchored proteins (*Friedrichson and Kurzchalia, 1998*). Even local diffusion parameters of membrane proteins confirmed that presence of cholesterol leads to formation of relatively stable domains taking 13-40 nm in diameter. They contain the proposed lipid raft proteins, whereas the other proteins diffuse in less viscous environment (*Pralle et al., 2000*). Myristate-palmitate or palmitate-palmitate anchoring leads to cholesterol-dependent aggregation, but prenylated proteins aggregate creating different, cholesterol-independent domains (*Zacharias et al., 2002*).

Using fluorescence derivates of lipids with saturated or unsaturated chains, it has been possible to visualize distribution of relatively rigid or fluid areas of the plasma membrane both in detail and within the frame of whole cell. Organized lipid domains did not diffused freely but in certain direction, and their occasional origin or disappearance took place at particular places, probably with respect to attachment of cytoskeleton. These domains were more numerous at areas of adhesion, intercellular contacts and pseudopodia (*Schütz et al., 2000; Gaus et al., 2003*).

It seems that existence of raft-like lipidic heterogeneities is not confined to animal cells, and that analogous structurally-functional systems may be utilized by plants and fungi, however, with small differences connected with divergence of lipidic composition and of sterol-sphingolipid : membrane protein ratio (*Xu et al., 2001; Bagnat and Simons, 2002; Martin et al., 2005; Bhat and Panstruga, 2005; Opekarová et al., 2005*).

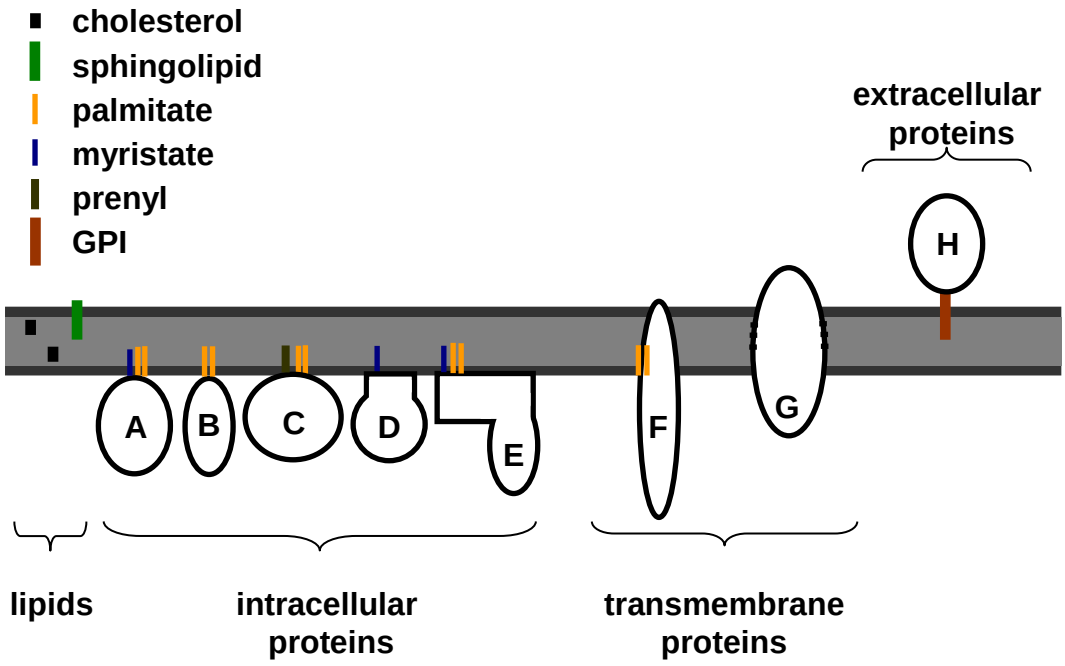

Fig. 1: Some of the so called „lipid raft markers" and their anchorage into the plasma membrane.
A) Lyn, Fyn, Lck, G protein α subunit, raftlin. **B)** GAP-43/B-50. **C)** H-ras, N-ras. **D)** NAP-22. **E)** Caveolin, flotillin (reggie). Number of palmitate and myristate units is variable within this group. **F)** LAT, NTAL (LAB, LAT2), PAG (Cbp), LIME. **G)** MAL/VIP17, BENE, plasmolipin, hemagglutinin, prominin. Specific interactions between transmembrane domain and lipid raft constituents are important for members of this group. In case of hemagglutinin, moreover, triple palmitoylation (not indicated). **H)** CD14, CD16, CD48, CD55, CD59, Thy-1 (CD90). A nature of GPI units can differ.
(*Cinek and Hořejší, 1992; Resh, 1994; Pérez et al., 1997; Scheiffele et al., 1997; Arni et al., 1998; Frank et al., 1998; Corbeil et al., 2001; Dunphy et al., 2001; Epand et al., 2001; Chatterjee and Mayor, 2001; Dykstra et al., 2003; Saeki et al., 2003; Pike, 2004; Pizzo and Viola, 2004; Navarro et al., 2004; Roy et al., 2005; Langhorst et al., 2005*)

Recent concept of lipid rafts

In spite of the fact that existence of plasma membrane domains having properties attributed to lipid rafts has been demonstrated even in living cells (see above), there appeared comparably conclusive studies that either dispute considerable presence of lipid rafts in resting membranes (without induced aggregation) or bear evidence of their surprisingly small size (*Kenworthy and Edidin, 1998; Kenworthy et al., 2000; Vrljic et al., 2002; Glebov and Nichols, 2004; Kenworthy et al., 2004; Sharma et al., 2004*). Gradually, a model arose that has been both alternative and extension of the original lipid raft hypothesis. It assumes formation of condensed complexes of cholesterol and sphingolipids as precursors of lipid rafts and attributes proteins with crutial role in lipid raft organization.

Although the concept of condensed complexes was based on behaviour of cholesterol and sphingolipids in artificial membranes, it became a good basis to explain structure and dynamics of plasma membrane organized domains (*Radhakrishnan and McConnell, 1999; Radhakrishnan et al.,*

2000; Anderson and McConnell, 2001; Anderson and McConnell, 2002; Anderson and Jacobson, 2002). Condensed complexes can exist in the plasma membrane as individual entities containing mere 15-30 molecules, but under certain conditions they can easily form a discrete phase. Lipid rafts thus can arise by aggregation of respective proteins that communicate with neighbour membrane milieu by lipidic coat composed of condensed complexes. In resting state, raft protein coating probably undergoes a dynamic process of association and dissociation (*Anderson and Jacobson, 2002*).

Effect of extracellular binding element (antibody, ligand) on raft-forming molecules leads to generation of stabilized domains sequestered from adjoining fluid phase. These domains can contain also intracellular components associated due to preference for equal lipidic milieu and can bind cytoskeleton (*Hammond et al., 2005; Mayor et al., 1994; Thomas et al., 1994; Harder et al., 1998; Suzuki and Sheetz, 2001*). Whereas the rafts of resting membrane probably are tiny and unstable structures appearing and disappearing within nanoseconds, stabilizer binding may cause reduction of thermal motion whereby enabling association of further molecules. These secondary raft structures differ substantially from the primary ones in complexity (both more molecules and their species), lasting (scale of minutes) and size (tens of nanometres or even more) and they usually perform specific signaling functions (*Subczynski and Kusumi, 2003; Kusumi et al., 2004; Kusumi et al., 2005*) (**Fig. 2**). In a broad sense, caveolae or flotillin domains, whose structure is consolidated by aggregates of specialized proteins, can be considered as subgroups of stabilized lipid rafts (*Navarro et al., 2004; Langhorst et al., 2005; Bauer and Pelkmans, 2006*).

According to the induced-fit model of raft heterogeneity, different tendency of raft proteins to interact with raft lipids leads to plastic forming of such a membrane domain whose structure and content emanates from optimal collocation of its constituents. Aggregation of proto-rafts thus can lead to formation of lipid raft that has different properties than were those of the precursors, e.g. by exclusion of some molecules and inclusion of others, which, consequently, could lead to further re-building the domain (*Pike, 2004*). This theoretical concept might resolve the question why for example different GPI-anchored proteins can form different raft structures (*Madore et al., 1999; Wang et al., 2002*) – even a small variance in anchoring module or in steric effects of the protein units may be a sufficient impulse for domain separation.

It turns out that, for specific location of GPI-proteins, also appropriate glycosylation is important (*Pang et al., 2004; Ermini et al., 2005*). It brings a further dimension to possible mechanisms of lipid raft regulation, supplementing the effect of lipid anchor modification (reversible palmitoylation, cutting a protein from GPI), changes of lipidic composition (e.g. modulation of cholesterol content) or protein spectra (different gene expression) and the effect of external stimuli (intercellular contacts, binding of soluble ligands). Stability of these domains can also depend on covalent and noncovalent interactions that occur already in Golgi apparatus (*Paladino et al., 2004*). In some cases, an interplay between controllable lipid modifications and allosteric effects within the protein unit can have a substantial role in targeting the protein to or out of lipid rafts or other plasma membrane domains (*Hancock, 2003; Rotblat et al., 2004; Roy et al., 2005*).

Step by step, thus, a complex system of plasma membrane organization and signaling is being revealed. Dynamic protein-lipid domains, traditionally denotated as lipid rafts, play a substantial (but not the only) role in this mechanism. As the interactions between proteins and lipids in the process of raft forming are mutual and bilaterally conditional, recently the term „lipid rafts“ has been more and more often replaced by „membrane rafts,“ which, however, should not be confused with a wider term „membrane microdomains.“ In 2006, at the symposium in Steamboat Springs, a working definition of membrane rafts was submitted: „*Membrane rafts are small (10-200 nm), heterogeneous, highly dynamic, sterol- and sphingolipid-enriched*[*] *domains that compartmentalize cellular processes. Small rafts can sometimes be stabilized to form larger platforms through protein-protein and protein-lipid interactions.*“ (*Pike, 2006*). It is but only an attempt to bridge terminological inconsistencies. The

[*] Better may be *rich*.

nature does not know divider lines between artificially introduced categories, and the phenomenon of dynamic heterogeneities within the plasma membrane has not been fully explained yet, so one can expect further changes of its concept.

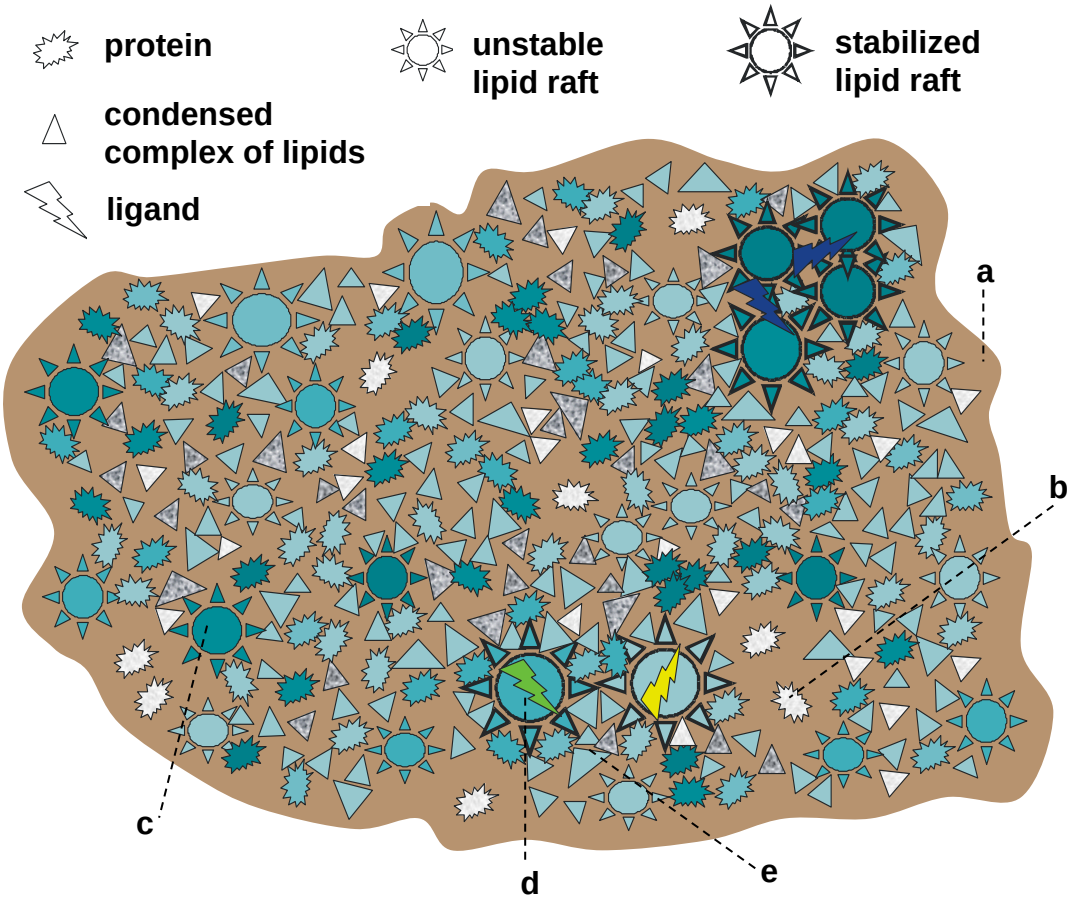

Fig. 2: Schematic view of the plasma membrane plane according to the reformed model of lipid rafts.
Within fluid phase of membrane lipids **(a)** there are localized proteins that prefer this milieu **(b)**, but also such proteins that are dynamically being detached by interactions with lipidic condensed complexes, forming unstable lipid rafts **(c)**. By effect of ligand, a lipid raft is being stabilized **(d)**, and at its periphery there arises an intermediary zone of unstably-associated proteins and lipids **(e)**. (*Anderson and Jacobson, 2002; Subczynski and Kusumi, 2003*)

II) Mast cells as a model of signal transduction across the plasma membrane

Mast cells belong to model cell types which have been extensively used for investigation of signal transduction mechanisms that occur at the plasma membrane of mammalian cells. Popularity of mast cells reflects their role in pathology of atopic allergies, that are becoming a serious all-society problem, as well as possibility to study well-observable reactions to defined external stimuli within scales of seconds, minutes and hours.

Roles of mast cells in organism

Mast cells originate by gradual differentiation of stem cells, and as immature precursors they migrate through blood system to target tissues where they complete their development affected by specific environment. This process has not been fully elucidated, as well as the relation of mast cells to basophilic granulocytes, which have often been called as their circulatory analogues. In mouse spleen, there has been identified a myeloid cell type that could generate both mast cells and basophils. Similarly, a human common specific precursor of mast cells and monocytes has been discovered, but still it cannot be excluded that mast cells evolve also from multipotent progenitors out of myeloid line (*Arinobu et al., 2005; Kirshenbaum et al., 1999; Chen et al., 2005; Sonoda et al., 1983*). *In vitro* experiments showed that mast cell proliferation and differenciation depends on interaction of cytokines SCF, IL-3 (sometimes also IL-4) supported with IL-9 and IL-10, whereas GM-CSF and IFN-γ inhibit mast cell differentiation and TGF-β acts against their proliferation. Also other cytokines (TNF-α, IL-6, NGF etc.) can participate in formation of conditions leading to development of different mast cell types. For mast cells, SCF is not only a growth and differentiation factor, but it is also one of their chemoattractants and tissue settling stimulator (*Metcalfe et al., 1997; Okayama and Kawakami, 2006*).

It seems that differences in local environments at particular places in the body lead to origination of many specialized population of mast cells, which are variant in morphology and function. Roughly divided, however, usually only two basic types are distinguished – the connective and mucosal – described in rodents but having analogies even in human organism. Connective mast cells from murine peritoneal cavity span 10-20 μm and their development is not dependent on T cells. By contrast, murine mucosal mast cells span only 5-10 μm, they are T cell dependent and from the connective ones they also differ in content of secretion granules (another types of chymase and proteoglycans; one place value less of histamine; leukotriene C_4 is present). Human analogues of connective mast cells (so called tryptase-chymase type, secreting more kinds of neutral peptidases), occur mainly in skin, whereas the analogues of murine mucosal mast cells (so called tryptase type) inhabit mostly lung alveolar tissue and small intestine (*Metcalfe et al., 1997*). Human peritoneal cavity itself, however, under normal circumstances does not contain mast cells. Spatial and functional organization of mastocytal system differs between humans and rodents, thus the results obtained using one of the models cannot be directly applied to the other one. For example, murine mast cells in many aspects resemble to human basophils rather than to human mast cells (*Bischoff, 2007; Falcone et al., 2006*).

The most widely known role of mast cells is the defence of body surfaces against bacteria and multicellular parasites (**Fig. 3**). Binding of antigen (allergen) to specific immunoglobulin E molecules associated with membrane receptor FcεRI leads to release of cytoplasmic vesicles content (to degranulation). The secreted proteases directly or indirectly damage surface of the parasite, degrade components of extracellular matrix, enhance blood vessel wall permeability, stimulate production of mucus and influence activity of some cytokines, hormones and nerve mediators; cooperating with heparin they affect blood coagulation. Mast cells also can stimulate cell adhesion, they positively act

on eosinophils and on epithelial cell and fibroblast proliferation. The secreted histamine causes local contractions of respiratory and gastrointestinal tract smooth muscles (contributing to expulsion the undesirable allochtonous organism) and affects vessel calibre; cathelicidin-type peptides have antimicrobial effects. Stimulated mast cells subsequently create allergic inflammation environment by arachidonic metabolites and spectrum of cytokines. Due to Toll-like receptors (TLR) they react to pathogens even without dependence on mechanisms of adaptive immunity. Mast cells can be termed as sentinels with functions both in proximate guarding and in organization of subsequent complex defence. These roles are connected also with maintaining body surface integrity by supporting wound healing and angiogenesis (*Metcalfe et al., 1997; Marshal, 2004*).

Mast cells are important modulators of immune reactions. Secreting cytokines IL-3, IL-4, IL-5, IL-9, IL-13, IL-15 and IL-16 they support T_H2 and B cells, thus production of antibodies, but they can also positively affect T_H1 cells, and hence the inflammatory response, by production of IFN-γ, IL-12 and IL-18. Besides pro-inflammatory mediators (TNF-α, IL-1β) they can release the anti-inflammatory ones (IL-10, TGF- β), similarly, they attract both T_H1 cells (by IL-8) and T_H2 cells (by CCL5). The particular course of immune reaction evidently depends on circumstances of its origin and on previous specific development of given mast cell population. Mast cells can serve as antigen-presenting cells and, as well, they help dendritic cells to this function. When needed, they attract neutrophils or eosinophils into the atopic inflammation place, enable their transmission through blood vessel wall and prolong their viability. They also participate anti-viral defence by cooperation with T_C cells. Mast cells represent an important regulatory intersection of adaptive and innate immunity (*Marshall, 2004; Frossi et al., 2004; Galli et al., 2005a; Galli et al., 2005b*).

Relation of mast cells to cancers is rather controversial. Mice with decreased number of mast cells show faster growth of implanted tumors, and, similarly, presence of mast cells in human breast cancer is connected with good prognosis. It seems, however, that for example in case of melanomas (man, dog), veneric carcinomas (dog) or gastric cancer (man) mast cells, instead, disserve to the organism due to their support to tumor angiogenesis, but it is preliminary to adjudigate them. Number of results regarding mast cells and cancers is quite high, but their interpretation is difficult, on account of unclarities in experimental context of cancer research (*Burtin et al., 1985; Rajput et al., 2007; Toth-Jakatics et al., 2000; Mukaratirwa et al., 2006a; Mukaratirwa et al., 2006b; Kondo et al., 2006; Őzdemir, 2006*).

It turns out that mast cells also participate in cross-talk between immune and nervous system. Peripheral neural fibres release mediators that locally influence many types of skin cells (mast cells, dendritic cells, keratinocytes, blood vessel endothelial cells etc.) and they are influenced by them in return. Mast cells affect peripheral neurons not only by neuropeptides, but they e.g. support topical inervation of epidermis and dermis by secretion of TNF and, by secreted proteases, they modulate effects of neuronal mediators on inflammation process. Similar regulatory function at intersection of local and nervous stress they perform also in gastrointestinal and respiratory tract mucosa. Direct effect of mast cells on central nervous system has also been demonstrated. They belong to the few of blood cells that penetrate across haemato-encephalic barrier even of healthy individuals and settle the brain. By degranulation they can cause activation of hypothalamus-pituitary-adrenal axis, probably as a part of defence mechanism upon allergen challenge. Likewise, they represent a system of transient remodelling of certain brain areas in response to humoral stimuli, e.g. during breeding period of mammals and birds. In this process mast cells serve as site-specific inducible source of neuromodulators whose spectra depend on respective animal species. Last but not least, mast cells influence functions of vascular system in brain (*Scholzen et al., 1998; Luger, 2002; Kakurai et al., 2006; Van Nassauw et al., 2007; Dimitriadou et al., 1994; Mawdsley and Rampton, 2005; Edvinsson et al., 1977; Silver et al., 1996; Matsumoto et al., 2001; Kovacs and Larson, 2006*).

With regard to multilateral engagement of mast cells in regulatory mechanisms of somatic immunity, it is inferrable that suboptimal adjustment of this system can have far-reaching consequences to individual health, e.g. it can result in severe forms of allergic hypersensitivity and

asthma. Although there have been revealed genetic dispositions to allergic diseases, it seems that the effect of improper environment is much more important, as conversion from rural to urban living style convincingly correlates with rising incidence of allergies in genetically equivalent population. There is probably involved absence to natural antigens of external environment during childhood, combined with exposition to pollution products of incomplete combustion, to dust particles binding hazardous allergens) and to psychical stress. Nevertheless, it seems that the polluted city environment itself has smaller effect on development of allergic hypersensitization than the high living style of the examined people has. A divorce of parents, but surprisingly not a death in family, is for a child a statistically significant risk factor of allergy development as well. The allergies are also supported by estrogens from contaminated environment (*Bateman and Jithoo, 2007; Martinez, 2007; Sozanska et al., 2007; van Ree and Yazdanbakhsh, 2007; Semic-Jusufagic et al., 2006; Bockelbrink et al., 2006; Narita et al., 2007*).

Anaphylactic shock caused by sudden systemic degranulation of mast cells and basophils in response to allergens of some snake or insect venoms has been attributed to pathological activity of these cells, because it is a life-threatening state. In mice, however, a protective role of proteases, massively secreted during this process, against the toxins themselves has been demonstrated. In consequence, the anaphylactic shock represented smaller danger to the mice than the toxin, thus, it could be a specific protective mechanism (*Metz et al., 2006*). This interesting hypothesis but has not been confirmed on human model yet.

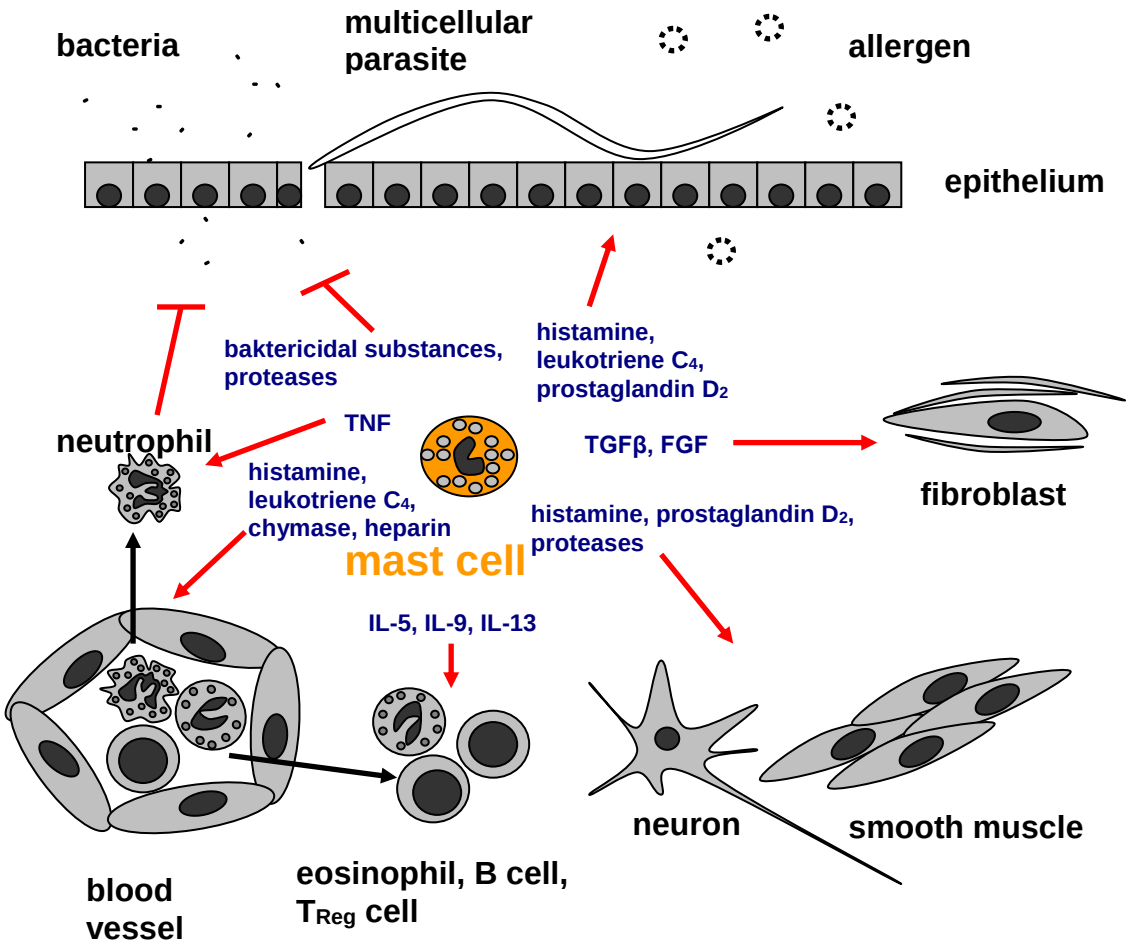

Fig. 3: Mast cell interactions in defence of cell surfaces.
Secretion of bactericidal substances and proteases, stimulation of epithelium, support of wound healing, peristalsis, bronchoconstriction, induction of pain, enhancement of vascular permeability, effects on coagulation, chemotaxis and activation of leukocytes.
(In detail: *Bischoff, 2007*)

Mast cell signaling cascades

KIT receptor pathway and reactions to cytokines

KIT is an example of transmembrane receptor with tyrosine kinase activity in cytoplasmic domain. Stem cell factor (SCF) binding at the extracellular side of the plasma membrane leads to dimerization and multiple phosphorylation of KIT receptor. The phosphorylated sites can serve as anchor for adaptor proteins Shc and Grb2, phospholipase Cγ, or phospholipid kinase PI3K. Shc and Grb2 initiate cascade of RAS, RAF and mitogen-activated kinases, which, together with action of PI3K, leads to transcription of genes governing cell growth, differenciation, chemotaxis and cytokine production, supported by activation of JAK-family kinases that phosphorylate STAT proteins. These proteins subsequently dimerize and translocate to nucleus where they act as transcription factors. By Src-family tyrosine kinases (mainly Fyn), stimulated KIT also directs cytoskeleton reorganization. Kit receptor signaling has fundamental role in mast cell growth, development and maturation, and it also strengthens their effector functions by support of immunoglobulin E (IgE)-dependent cascade (**Fig. 4**). (*Tsai et al., 1991; O´Farrell et al., 1996; Gilfillan and Tkaczyk, 2006; Samayawardhena et al., 2007*).

Receptors for IL-3 and IL-5 are composed of heterodimerized specific binding α-subunit and common β-subunit that associates, upon receptor stimulation, with Src- and JAK-family kinases and is phosphorylated by them, whereby providing binding sites for components of subsequent signaling cascades, when STAT proteins again participate, as in the case of KIT-mediated pathways. The cell uses similar mechanisms also for other cytokines sensing, with differences in subunit composition of receptors, in types of downstream signaling molecules (especially JAK kinases and STAT proteins) and in final effect (*Velazquez et al., 2000; Suzuki et al., 2000; Ding et al., 2003; Gilfillan and Tkaczyk, 2006*).

IgE-mediated activation

FcεRI, the high-affinity IgE receptor, is composed of four transmembrane subunits. Whereas the α-subunit is extracellularly oriented and binds constant termini of IgE molecules, the β-subunit and the γ-subunit dimer contain phosphorylatable ITAM (immune-tyrosine activation motives) sites in their intracellular domains. Unlike KIT receptor, FcεRI does not possess intrinsic tyrosine kinase activity and it is dependent on Src-family kinases association, mainly on Lyn and Fyn. Antigen-binding specificity is provided to the FcεRI by IgE, which, in a way, serves as fifth subunit of the receptor. IgE binding, however, is not only a passive sensitization step, but it is also a stimulus, that induces secretion of some cytokines, sustained cell viability and increased adhesiveness to extracellular matrix, sometimes it leads also to degranulation. The mechanism of IgE effect has not been satisfactorily elucidated yet, but it seems that inositol phosphatase SHIP plays an important role in prevention of the effector-way activation after IgE binding (*Kinet, 1999; Kalesnikoff et al., 2001; Lam et al., 2003; Kitaura et al., 2003; Kawakami et al., 2005*).

In response to antigen binding, aggregation of IgE-FcεRI complexes leads to phosphorylation of β- and γ-subunit ITAM sites by Src-family tyrosine kinases (Lyn, Fyn). There probably take place kinases attached to partially phosphorylated receptor and the kinases that associated with FcεRI by stabilization of lipid rafts. Phosphorylated β-subunit (binding Lyn and Fyn) serves as important signal amplifier, but it has also modulator function, as Lyn can serve as negative regulator after excessive stimulation. Recently, importance of Hck kinase and collaboration of various members of Src family kinases for mast cell activation has been revealed (*Xiao et al., 2005; Hong et al., 2007*). For optimal signaling, a teamwork of tyrosine kinases and phosphatases is also important, and this mechanism is influenced by reactive oxygen substances that are produced during many immune processes (*Heneberg and Dráber, 2002; Heneberg and Dráber, 2005*). Phosphorylated FcεRI γ-subunits are crutial for further signal transmission. They are contacted by cytoplasmic tyrosine kinase Syk, which subsequently phosphorylates transmembrane adaptor proteins LAT and NTAL or cytoplasmic

adaptor SLP76, therethrough organizing downstream signaling cascades, including e.g. activation of phospholipases Cγ, phospholipid kinase PI3K, protein kinases C and A, cascades of Ras protein and mitogen-activated kinases etc. (in detail: *Gilfillan and Tkaczyk, 2006; Kraft and Kinet, 2007; Simeoni et al., 2005*). These pathways result in degranulation, cytoskeleton remodelling, production of arachidonic metabolites and gene transcription (e.g. synthesis of cytokines). It is an antigen-adaptive branch of mast cell effector mechanisms.

Activation mediated by Thy-1 and other GPI-anchored proteins

Thy-1 glycoprotein (CD90), anchored to the plasma membrane by GPI, represents an important regulation element of physical interactions among various cell types. Its natural ligands (and receptors) are certain integrins, but artificial aggregation of Thy-1 by specific antibody invokes in mast cells processes similar to those induced upon FcεRI-dependent activation – calcium ions are mobilized, mediators secreted and many proteins are phosphorylated, though less intensively than in case of FcεRI stimulation. In these processes stabilization of lipid rafts conjugating Src-family kinases and palmitoylated transmembrane adaptor proteins probably plays crutial role (*Rege and Hagood, 2006; Dráberová and Dráber, 1993; Surviladze et al., 2001*). Also aggregation of Tec-21, another protein anchored by GPI, has similar effect on mast cells. It turns out that dimerization of some GPI-anchored proteins (Thy-1, Tec-21, CD48) leads to nonapoptotic exposure of phosphatidylserine on cell surface, whereas some other (carcinoembryonic antigen) do not cause it. These experiments, however, are still at the beginning, and physiological relevance of mast cell activation via GPI-anchored proteins has not been much elucidated yet. At least in some cases it may be an important mechanism, as e.g. CD48 belongs to the receptors that serve mast cell to sense bacteria (*Hálová et al., 2002; Smrž et al., 2007; Muñoz et al., 2003*).

Adhesive receptors

Expression of specific sets of adhesion molecules has fundamental importance for mast cell colonization of target tissues depending upon differenciation and maturation process. These molecules generally also serve as receptors that provide mast cells with costimulatory signals for activation. Their exposition on cell surface is regulated by cytokines, and occurs also in response to stimulation of cascades that lead to activation of mast cell effector mechanisms. Some adhesive molecules serve to binding extracellular matrix (VLA-4 = $\alpha_4\beta_1$ integrin, VLA-5 = $\alpha_5\beta_1$ integrin, vitronectin receptor = $\alpha_v\beta_3$ integrin, in skin also VLA-3 = $\alpha_3\beta_1$ integrin), other in intercellular contacts (ICAM-1, ICAM-2, leukosialin, LFA-1, LFA-3, in immature mast cells $\alpha_4\beta_7$ integrin). Even the Thy-1 glycoprotein mentioned above (contacting integrins) belongs among adhesive molecules, as well as KIT, which can bind membrane form of SCF cytokine. Mast cell anchoring by adhesion receptors results in cytoskeleton reorganization, phosphorylation of some signaling molecules, redistribution of cytoplasmic secretory vesicles and preparation to degranulation. In these processes, paxillin and focal adhesion kinase (FAK) participate (*Hamawy et al., 1994; Smith and Weis, 1996; Okayama, 2000*).

Some other mast cell receptors

For mast cell role in nonadaptive immunity, Toll-like receptors (TLR) are very important. They respond to microbial and viral components, such as lipopeptides (recognized by TLR1), peptidoglycan (TLR2, TLR6), doublestrand RNA (TLR3), lipopolysaccharides, and F-protein of respiratory syncytial virus (TLR4). Heterodimerization of TLR1 a TLR6 with TLR2 receptors affords to the cell perfection of reaction scope. In human mast cells also TLR7 (recognizing viral singlestrand RNA) and TLR9 (responding to bacterial DNA) have been described. Aggregation of TLR by ligand is connected with process of lipid raft stabilization. Cytokine environment can change expression of respective TLR receptors and, vice versa, TLR stimulation invokes secretion of specific cytokines that lead to body defence against microorganisms and viruses, but not by degranulation. Similar response is induced by contact of pathogen covered with compounds of complement cascade (C3b,

C4b) with respective complement receptors, or by aggregation of IgG molecules bound to Fcγ receptors. In these examples, however, also degranulation and release of proteases and histamine occurs (*Marshal, 2004; Dolganiuc et al., 2006*).

Neurotransmitters, chemokines and chemotactic fragments of complement are recognized by mast cell receptors of heterotrimeric G-protein family. Mast cell utilizes the same system for detection of adenosine and also sphingosine 1-phosphate. Ligand binding leads to dissociation of G_{α} subunit from receptor complex $G_{\beta\gamma}$. Through phospholipase Cβ, G_{α} stimulates cascades leading to secretion of certain cytokines and supporting (or promoting) degranulation. Expression of chemokine receptors depends on maturation stage and, vice versa, their ligands affect mast cell development (*Forsythe and Befus, 2003; Marshal, 2004; Gilfillan and Tkaczyk, 2006*).

Unlike basophils, mast cells express not only the above mentioned high-affinity FcεRI, but also homotrimeric low-affinity IgE receptor (FcεRII, CD23), however, its role is still unclear. Studies on other cell types suggest that it might act e.g. in antigen presentation, it is but not more than a hypothesis (*MacGlashan a kol., 1999; Montagnac a kol., 2005; Getahun a kol., 2005*). Mast cells can also bind IgG by various Fcγ receptors. Their content depends on cell type and respective organism. The low-affinity FcγRIIIA, FcγRIIA, FcγRIIB and FcγRIIC receptors need aggregated ligand for its effective binding. Expression of the high-affinity FcγRI is inducible in human mast cells and it has not been described in murine ones. Some of Fcγ receptors (FcγRIIA, FcγRIIC, FcγRI, FcγRIII) stimulate mast cell signaling similar to the FcεRI-mediated, due to activation (ITAM) motives within intracellular domains of their subunits. By contrast, FcγRIIB, due to inhibition (ITIM) motives, binds inositol phosphatase SHIP and suppresses the signaling. This inhibition function of FcγRIIB, however, depends on cooperation of activation receptors (*Malbec a Daëron, 2007; Bruhns a kol., 2005*). Immunoglobulin A receptor, FcαRI, can afford to mast cell suppressive signals, although containing activation ITAM motive, probably by binding SHP1 phosphatase. The physiological role or function mechanism of many mast cell inhibition receptors (such as PIRB, MAFA, LIR1, MAIR1, LMIR1) has not been sufficiently elucidated yet (*Kraft a Kinet, 2007*).

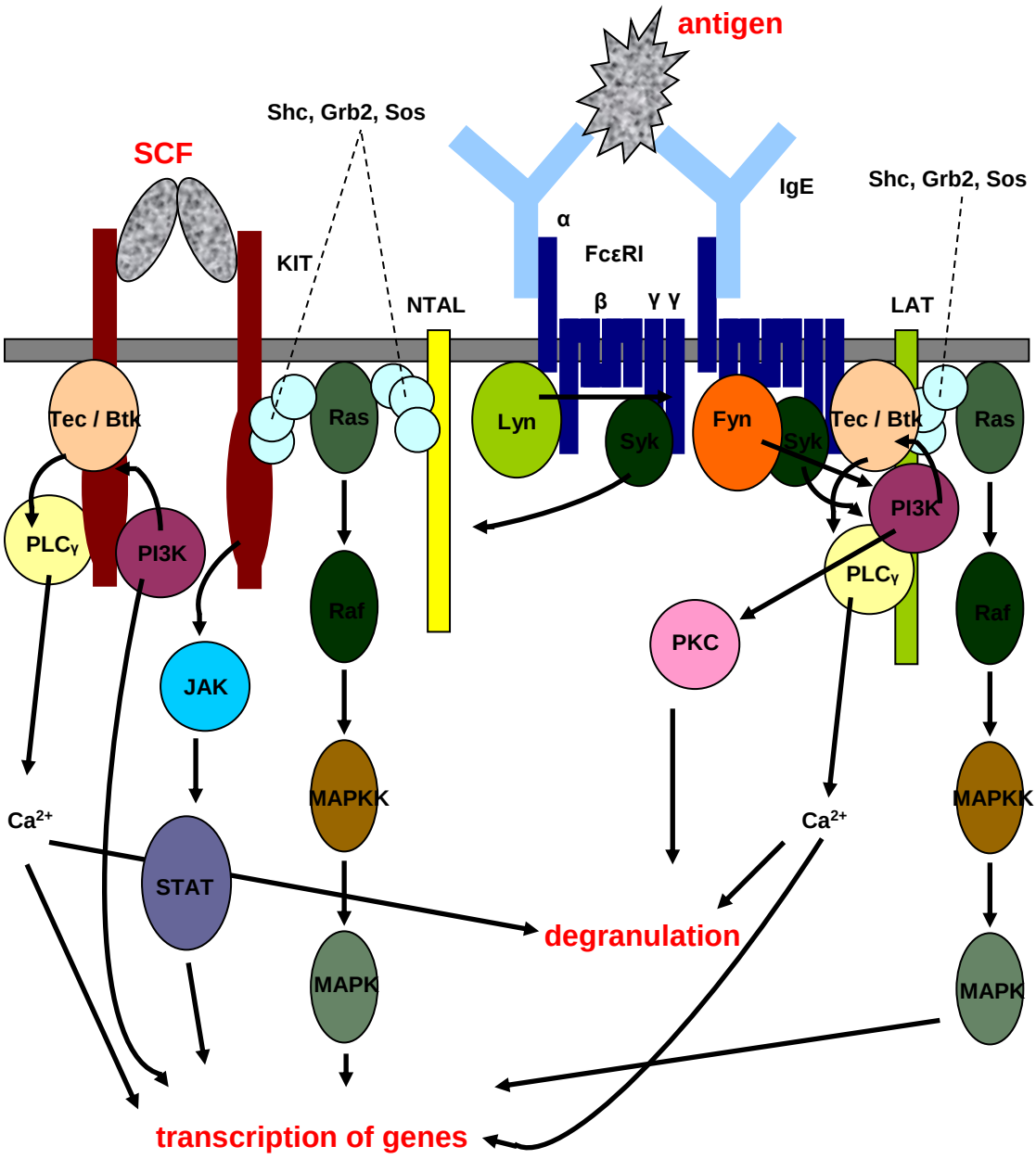

Fig. 4: Simplified model of KIT and FcεRI cooperation during mast cell activation.
Phosphorylation of aggregated FcεRI (by tyrosine kinases Lyn or Fyn) and KIT (autophosphorylation) leads to formation of signaling spots initiating specific gene transcription. Unlike FcεRI, the KIT receptor cascade itself does not provide good conditions for degranulation, but supports it.
(*Gilfillan and Tkaczyk, 2006; Kraft and Kinet, 2007*)

Aims

Aim of this thesis has been ***to contribute to elucidation of functional organization of leukocyte plasma membrane by utilizing topographical approaches on mast cell model.*** It also led to enrichment of knowledge about mast cells themselves and widening of methodical device. I have focused on these partial questions:

- ***How to isolate plasma membrane sheets from nonadherent BMMC mast cells?***

The established approach of plasma membrane sheet isolation (and labeling) from adherent cells (*Sanan and Anderson, 1991*) could be successfully applied on tumor RBL mast cell line, but not on nontransformed nonadherent BMMC mast cells. As the topography of signaling molecules on the plasma membrane sheets of nontransformed mast cells had not been known, it was advisable to develop method of plasma membrane sheet isolation from these nonadherent cells.
(Analyzed in article E.)

- ***What is the nature of signaling assemblies of aggregated FcεRI receptor?***

A model of mast cell signaling that included formation of large (approximately 200 nm) FcεRI domains has been described on RBL cells (*Wilson et al., 2002*). A question, however, remained whether assembly of these domains is one of requirements of sufficient mast cell activation, or rather an accessory feature. The answer might be achieved by examination of the cells activated by FcεRI dimerization, or of another mast cell type.
(Analyzed in articles A, E.)

- ***How is NTAL adaptor protein distributed in the plasma membrane and what is its topographic relation to LAT adaptor, FcεRI receptor and Thy-1 glycoprotein?***

Analysis of relative topography of LAT and NTAL adaptor proteins, which belong together with Thy-1 among typical lipid raft markers, and comparison of their localization regarding aggregated FcεRI and Thy-1, could reveal many things not only about signal transduction between mast cell receptors and adaptor proteins, but also about nature of lipid raft system in the plasma membrane.
(Analyzed in articles B, C, E.)

- **Does a change in NTAL expression lead to formation of atypical structures in the plasma membrane?**

Results of coauthors showed that NTAL serves as a negative regulator of mast cell activation. It was thus convenient to know whether excessive or decreased expression of this protein would reflect in atypical localization of plasma membrane signaling molecules.
(Analyzed in article D.)

- **What is the nature of Thy-1 glycoprotein domains?**

Various data suggested substantial independence of many markers of lipid rafts within the plasma membrane and evidenced against the view that considered these domains as spontaneous coaggregates of heterogeneous signaling molecules. Relative localization of two structurally very similar Thy-1 isoforms (Thy-1.1 and Thy-1.2) could indicate how are in the plasma membrane organized Thy-1 domains.
(Analyzed in article C.)

Methods

Analysis of topography of signaling molecules on isolated plasma membrane sheets, performed by electron microscopy, has become the crutial approach to achieve aims of this dissertation. However, pilot experiments (unpublished) had to be done, including purification and confirming specificity of antibodies and confirming their reactivity depending on fixation procedures, as well as first approximation to topographical changes within the plasma membrane during mast cell activation at fluorescence microscopy level. In this section, I extract brief list of the approaches that I performed myself. For details of respective techniques, reader is referred to methodic paragraphs of publications enclosed.

- Mast cell culturing
  (Cultured rat leukemic line RBL-2H3 and mast cells BMMC derived from bone marrow.)

- Measuring of mast cell degranulation extent
  (Detected secreted β-glucuronidase.)

- Purification of antibodies; preparation of cell lysates; immunoblotting; fluorescence microscopy
  (Rabbit polyclonal antibody anti-NTAL was isolated immunoaffinitly by recombinant NTAL protein.)

- Preparation and labeling of plasma membrane sheets; electron microscopy; digitalization of data; statistical evaluation
  (Coordinates of immunolabels were digitalized by programme Ellipse [ViDiTo; Košice, SR] and statistically elaborated by programme GOLD or by algorithms of Bridget Wilson's group, University of New Mexico, utilizing MATLAB system [MathWorks; Natick, USA].)

Results

Summarized in following articles:

These articles are cited throughout as „article A, B, C, D, E". The results presented in sections Discussion and Conclusions pertain to the author of this dissetation, unless stated otherwise.

Discussion

Aggregation of FcεRI receptor is the initial step of IgE-dependent mast cell signaling that leads to activation of allergic effector mechanisms. Biochemical approaches (such as partial lysis by nonionic detergents and immunoprecipitation) have been extensively used for analysis of a wide range of molecules participating in this process of signal transduction across the plasma membrane. Similarly, fluorescence microscopy or scanning electron microscopy provided data that gave basic knowledge on organization of signaling assemblies (*Field et al., 1995; Kihara and Siraganian, 1994; Saitoh et al., 2000; Holowka et al., 2000; Barker et al., 1998; Stump et al., 1988*). Detail view on the plane of mast cell plasma membrane, however, had not been performed before introduction of method of plasma membrane sheet isolation and examination under transmission electron microscope (*Wilson et al., 2000*). The obtained results documented that in RBL mast cell line, application of antigen induces formation of quite large (hundreds nm in diametre) primary signaling domains. At their periphery there are localized secondary signaling domains, which take on and transmit the signal. Primary domains are composed typically of FcεRI aggregates, associated cytoplasmic Syk tyrosine kinase, Grb2 and Gab2 adaptors, components of clathrin endocytic apparatus or phospholipase Cγ2 and their formation is accompanied by dissociation of Lyn tyrosine kinase from the receptor complex. Secondary signaling domains contain aggregates of transmembrane adaptor protein LAT or phospholipase Cγ1. PI3K phospholipid kinase can be found in both types of domains (*Wilson et al., 2000; Wilson et al., 2002*).

To analyze the topography of mast cell signaling assemblies after FcεRI dimerization and to compare them with those formed after antigen-mediated FcεRI multimerization, I performed the method of isolation and immunolabeling of plasma membrane sheets. As expected, application of antigen led to formation of large (usually approximately 200 nm) receptor aggregates that colocalized with Syk tyrosine kinase and Grb2 adaptor. These structures thus corresponded to previously reported primary domains. By contrast, at given detection level, receptor dimerization by 5.14 monoclonal antibody had no effect on topography of signaling molecules whose distribution corresponded to the situation on nonactivated cells. No colocalization of FcεRI and Grb2 was observed, but the Grb2 concentration on the plasma membrane significantly increased, though less than in case of antigen-mediated activation (*article A*). Likewise, association of the receptor with components of lipid rafts, phosphorylation of signaling proteins, mobilization of calcium ions and secretion of content of cytoplasmic granules increased after receptor dimerization. These processes were, however, again less intense than in case of receptor multimerization, but they were still generally comparable (*article A, coauthors*). There was thus obvious disproportion between topographical changes of membrane molecules and resulting activation effects. The large aggregates of FcεRI turned out to be structures dispensable for mast cell effector functions and reflecting possibly rather process of attenuation and silencing of the signaling components in response to FcεRI multimerization. It was compatible with the fact that excessive concentration of antigen correlates with decrease intensity of degranulation during mast cell activation and leads to actin cytoskeleton-dependent formation of extensive FcεRI domains (*Seagrave et al., 1991*). It seems that the role of feedback regulator responding to effusive FcεRI accumulation and stimulation could be played by phospholipid phosphatase SHIP (*Gimborn et al., 2005*) and ubiquitin ligase Cbl, which has been visualized as a component of large primary signaling domains of FcεRI (*Gustin et al., 2006; Wilson et al., 2002*).

There remained, however, an opened question whether such pronounced activation-inhibitory domains are formed during mast cell FcεRI multimerization generally, or whether it is a feature specific to RBL cell line. This tumor line provides good conditions for membrane sheet isolation due to ability of adhesive growth but it is quite disputable as a model of mast cells. Relevance of results of topographical analyses obtained by RBL cell plasma membranes should have been confirmed by examining more natural mast cell representatives, such as isolated or short-term cultivated cells. As

these cells, because of their nonadherence, could not have been processed by the classical method of membrane sheet preparation (*Sanan and Anderson, 1991*), the method had to be improved.

Based on my childhood empiric findings on affinity of animal cells to glass surfaces, I decided to examine usage of clean glass to isolate plasma membrane sheets from bone marrow-derived mast cells (BMMC). I found that under certain conditions (appropriately cleaned and stored glass coverslips, cells in buffer of no or low protein content) even nonadherent leukocytes adhered to glass surface so strongly that they could be easily processed to membrane sheet isolation. The obtained membrane sheets were usable for topographical studies of extent comparable to studies employing the classical technique by Sanan and Anderson (*Sanan and Anderson, 1991*) based on adhesive cell growth. It was thus possible to avoid the potentially risky immobilization steps (such as long-term incubation with polylysine, long-term exposition to low temperatures) introduced by other authors to isolate membrane sheets from nonadherent T cells (*Schade and Levine, 2002; Lillemeier et al., 2006*). Adsorption of BMMC to glass had several advantages. It was quick (1 min.) and simple, it did not cause artificial degranulation and did not need cooling of cells nor functional actin cytoskeleton. To check properties of plasma membranes isolated in this way, I have introduced two other approaches of membrane sheet isolation from nonadherent cells. These approaches, however, served only as controls, for they were less practical than the method based on adsorption to glass. The first approach consisted in active binding of mast cells to components of extracellular matrix in response to priming by IgE (based on finding of *Lam et al., 2003*), it thus make use of a specific mechanism; the second control technique reduced the adsorption step to minimum, for consisted in mere pressing suspended cells to electron microscopy grid. As I did not find any difference in membrane morphology nor in topographical changes of FcεRI in the course of mast cell activation between plasma membrane sheets prepared by all the three techniques, I further used only the method based on adsorption to glass for routine examination of topography of BMMC signaling molecules (*article E*).

I found that the density of FcεRI on the plasma membrane of BMMC was roughly twice lower than on RBL cell plasma membrane (*article E*), which might possibly explain the fact that optimal BMMC degranulation was caused by lower concentration of antigen than in case of RBL cells (*article B, coauthors; article A, coauthors*). To activate BMMC, hence I was using both the antigen concentration optimal for BMMC and for RBL cells, to make comparison of FcεRI topography on both cell types more predicative. Interestingly, the both concentrations induced comparable internalization of FcεRI in BMMC, corresponding to internalization in RBL cells. The finding indicating that FcεRI multimerization on BMMC did not lead to formation of large FcεRI aggregates was all the more striking. On nonactivated BMMC and RBL cells, FcεRI could be detected as clusters of comparable size, but these clusters internalized forming temporary pronounced aggregates in RBL cells, whereas in BMMC, the FcεRI domains endocytosed without observable increase in their size. The overall extent of internalization was comparable in both cell types, but the local dynamics markedly differed, as BMMC preferred higher number of small spots, whereas RBL cells preferred larger platforms but of lower number (*article E*). Thus, the established view describing mast cell primary signaling domains as large aggregates of FcεRI, based on leukemic RBL cell line (*Wilson et al., 2001; Wilson et al., 2002*), may not correspond to physiological reality and does not represent a general phenomenon. Primary signaling spots of BMMC are far smaller and they resemble the large FcεRI domains of RBL cells when the receptor is aggregated at low temperature (4°C) but not at normal conditions (*article E*).

Secondary signaling domains of mast cells were described as aggregates of transmembrane adaptor protein LAT that provides structural and functional support for signal transduction into the cell interior (*Wilson et al., 2001; Wilson et al., 2002*). NTAL turned out to be an adaptor protein very similar to LAT (*Brdička et al., 2002*), but its topography at elelectron microscopy level was unknown. I thus analysed RBL cell membrane sheets and demonstrated that in the plasma membrane, NTAL is distributed in clusters of the same morphology that is shown by LAT, and (again similarly to LAT) NTAL can be found at periphery of large FcεRI aggregates. However, LAT and NTAL were

forming nonoverlapping domains both in activated and nonactivated cells (*article B*). This was a rather surprising finding, as the both structurally similar palmitoylated proteins belonged to the so called lipid raft markers and it could be thus supposed that they would share common lipidic milieu. In the same year, however, a study has been published documenting substantial topographical independence of some lipid raft markers in RBL cell plasma membrane (*Wilson et al., 2004*) and the view of lipid rafts started to be changed.

I decided to check whether the separation of LAT and NTAL adaptors is specific to RBL cell line and whether the phenomenon could artificially result from binding of detection antibodies. It turned out that the both adaptors formed nonoverlapping domains even in BMMC and that this effect was not caused by labeling procedure (*article E*). Provided that palmitoylation is responsible for tendency of LAT and NTAL to contact common organized lipidic milieu, there must exist a mechanism that outweighs this effect and separates their aggregates. It seems that the most probable explanation could be protein-protein interactions within signalosomes formed around cytoplasmic domains of these adaptors, as the content and distribution of LAT and NTAL binding sites differs (*Brdička et al., 2002*) and importance of protein-protein interactions in the process of forming functional domains of phosphorylated LAT has been demonstrated in T cells (*Schade and Levine, 2002*). Establishment and stabilization of membrane protein aggregates, to a large extent also depends on cytoskeleton binding, and the morphology of respective domain is a result of both protein-protein and protein-lipid interactions (*Lillemeier et al., 2006*).

In mast cells, NTAL serves as a negative regulator of FcεRI signaling, but it is also able to compensate for positive role of LAT adaptor (*Zhu et al., 2004; article B, coauthors*). Excessive NTAL expression has also (besides supressing the activation) effect on mast cell morphology, which is caused by affecting actin polymerization (*article D, coauthors*). Hence, it was possible that the inhibitory effects of over-expressed NTAL could display already in the moment of FcεRI aggregate formation. However, I found that FcεRI topography in the course of RBL cell activation and localization of NTAL regarding FcεRI did not differ between cells expressing normal, higher or lower amount of NTAL. Over-expressed NTAL itself also did not form any unusual structures, except the fact that its domains were larger (*article D*). Inhibitory effect of NTAL on mast cell activation thus probably does not consist in affecting formation of FcεRI signaling assemblies.

In spite of results describing topographical independence of some lipid raft markers, presence of lipidic aggregates within the plasma membrane is supported by the fact that LAT, which lacks extracellular domain, colocalizes with Thy-1 glycoprotein, which is extracellularly anchored to the plasma membrane via GPI anchor (*Wilson et al., 2004*). I was interested whether so similar NTAL protein would have similar close topographical relationship to Thy-1 as LAT had, or whether these proteins would be separated in concordance with independent localization of LAT and NTAL. It turned out that Thy-1 domains colocalized with both LAT and NTAL clusters, especially after extensive aggregation of Thy-1, and that even under these conditions the both adaptors were not forming common islets. However, they were localized closer to each other than it would be in case of random distribution (*article C*). Because both adaptor proteins were phosphorylated upon Thy-1 aggregation (*article C, coauthors*), domains of Thy-1 seem to serve as platforms that stimulate and conjugate independent aggregates of two functionally related but to a large extent antagonistic signaling molecules, which could be one of mechanisms of lipid raft-mediated signal modulation.

As a suitable tool for analysis of Thy-1 domain structure, an RBL transfectant expressing not only endogenous Thy-1.1 but also allochtonous Thy-1.2 isoform was used. The both Thy-1 variants could be distinguished and aggregated by specific monoclonal antibodies. The same anchoring module of Thy-1.1 and Thy-1.2, as well as 82% amino acid identity of these isoforms could possibly cause their mixing in common domains. Fluorescence microscopy, however, suggested their independent movement (*article C, coauthors*). The question remained topography of both proteins at resolution of electron microscopy and also the also intensity of coherence between Thy-1.1 molecules and between Thy-1.1 and Thy-1.2 should be analyzed. On plasma membrane sheets, antibody-

induced (and labeled) Thy-1.1 aggregates strongly colocalized with molecules of the same isoform labeled additionally after fixation. Under the same conditions, labeled after fixation, however, Thy-1.2 isoform colocalized only weakly with Thy-1.1 aggregates – in this case domains of both proteins were often localized in close vicinity, but they kept considerable structural independence (*article C*). It seems thus that despite equal membrane anchor and high sequence identity, different Thy-1 isoforms form different domains in the plasma membrane. Between these domains certain weak coherence may exist, but they seem to be relatively independent. As already mentioned, formation of protein aggregates, that are present even in the plasma membrane of nonactivated cells, is apparently affected by actin cytoskeleton (*Lillemeier et al., 2006*). Within scale of several nanometres, dimerization of one of Thy-1 isoforms leads to increased association with aggregates of the other isoform, and actin cytoskeleton supports their contact. By contrast, this cytoskeleton serves as spacer preserving molecules of one isoform from excessive packing (*article C, coauthors*).

Taken together, lipidic interactions seem to play important role in establishment of basic stabilized lipid raft units (after dimerization), but organization of these elementary structures into higher-order domains is affected by cooperation with actin cytoskeleton in an ambiguous process. This dissertation documents that different raft-residing molecules, although often of very similar sequence, tend to formation of different membrane domains. An exception is strong colocalization of intracellularly oriented palmitoylated transmembrane adaptor proteins LAT and NTAL with aggregates of extracellular protein Thy-1. One of the mechanisms separating raft proteins to distinct domains probably may be effect of specific protein-protein interactions, in some cases for example also variant glycosylation might play a role. It turns out that formation of signaling spots in the plasma membrane is organized not only by considerably complex, but also highly dynamic system, and that some particular features accompanying this process can substantially differ between various model exemplars of a given cell type. The presented technique of plasma membrane sheet preparation from nonadherent cells may facilitate research in this field. It must be, however, mentioned that a plastic view of signal transduction across the plasma membrane can be achieved only by combination of various mutually complementary approaches.

Conclusions

Three techniques of isolation of plasma membrane sheets from nonadherent BMMC mast cells have been developed. One of them, based on adsorption of leukocytes to glass surface, turned out to be very promising and provided many scientific data (*article E***).**

Activation of RBL mast cells by FcεRI receptor dimerization led to increase of Grb2 adaptor content in the plasma membrane. However, by contrast to the case of receptor multimerization, this Grb2 did not significantly colocalize with FcεRI, and, by immunolabeling of membrane sheets, distribution of FcεRI was not distinguishable from the distribution on nonactivated cells (*article A***). BMMC, in contrast to RBL cells, after multimerization of FcεRI did not form larger aggregates of this receptor than nonactivated cells did. FcεRI multimerization led to its internalization of comparable intensity and overall dynamics in BMMC and RBL cells, but local redistribution of FcεRI fundamentally differed between these two cell types (***article E***). Established model of large (approximately 200 nm) signaling domains of FcεRI receptor has been challenged.**

NTAL adaptor protein has been clustered in the plasma membrane and distributed analogously to LAT adaptor, and also their topographic relations to FcεRI receptor and Thy-1 glycoprotein were analogous. In RBL cells, after FcεRI multimerization, both adaptors were occasionally localized at the periphery of FcεRI aggregates; despite it, however, LAT and NTAL were organized in distinct domains in the course of BMMC as well as RBL cell activation (*articles B, E***). Both adaptors strongly colocalized with aggregated Thy-1 glycoprotein, but even under these conditions they preserved their distribution in separate domains (***article C***). These results support the view of membrane rafts as a system constituted by interplay of lipidic and protein interactions.**

Neither excessive, nor decreased expression of NTAL adaptor, which is a negative regulator of mast cell signaling, affected FcεRI distribution in the course of RBL cell activation. These changes in amount of NTAL molecules in the plasma membrane caused corresponding changes of NTAL domain size, but the character of NTAL distribution was not changed (*article D***).**

Thy-1.1 and Thy-1.2 isoforms were localized to a great extent independently within the plasma membrane. Aggregation of Thy-1.1 lead to only weak coaggregation of Thy-1.2. By contrast, molecules of identical isoform showed much higher coherence (*article C***).**

Literatura

Anderson R. G. W., Jacobson K. (2002) A role for lipid shells in targeting proteins to caveolae, rafts, and other lipid domains. *Science 296: 1821-1825*

Anderson T. G., McConnell H. M. (2001) Condensed complexes and the calorimetry of cholesterol-phospholipid bilayers. *Biophys. J. 81: 2774-2785*

Anderson T. G., McConnell H. M. (2002) A thermodynamic model for extended complexes of cholesterol and phospholipid. *Biophys. J. 83: 2039-2052*

Arinobu Y., Iwasaki H., Gurish M. F., Mizuno S., Shigematsu H., Ozawa H., Tenen D. G., Austen K. F., Akashi K. (2005) Developmental checkpoints of the basophil/mast cell lineages in adult murine hematopoiesis. *Proc. Natl. Acad. Sci. USA 102: 18105-18110*

Arni B., Keilbaugh S. A., Ostermeyer A. G., Brown D. A. (1998) Association of GAP-43 with detergent-resistant membranes requires two palmitoylated cysteine residues. *J. Biol. Chem. 273: 28478-28485*

Bagnat M., Simons K. (2002) Lipid rafts in protein sorting and cell polarity in budding yeast Saccharomyces cerevisiae. *Biol. Chem. 383: 1475-1480*

Barker S. A., Caldwell K. K., Pfeiffer J. R., Wilson B. S. (1998) Wortmannin-sensitive phosphorylation, translocation, and activation of PLCγ1, but not PLCγ2, in antigen-stimulated RBL-2H3 mast cells. *Mol. Biol. Cell 9: 483-496*

Bateman E. D., Jithoo A. (2007) Asthma and allergy – a global perspective. *Allergy 62: 213-215*

Bauer M., Pelkmans L. (2006) A new paradigm for membrane-organizing and -shaping scaffolds. *FEBS Lett. 580: 5559-5564*

Bhat R. A., Panstruga R. (2005) Lipid rafts in plants. *Planta 223: 5-19*

Bischoff S. C. (2007) Role of mast cells in allergic and non-allergic immune responses: comparison of human and murine data. *Nat. Rev. Immunol. 7: 93-104*

Bockelbrink A., Heinrich J., Schäfer I., Zutavern A., Borte M., Herbarth O., Schaaf B., von Berg A., Schäfer T. (2006) Atopic eczema in children: another harmful sequel of divorce. *Allergy 61: 1397-1402*

Brdička T., Imrich M., Angelisová P., Brdičková N., Horváth O., Špička J., Hilgert I., Lusková P., Dráber P., Novák P., Engels N., Wienands J., Simeoni L., Österreicher J., Aguado E., Malissen M., Schraven B., Hořejší V. (2002) Non-T cell activation linker (NTAL): a transmembrane adaptor protein involved in immunoreceptor signaling. *J. Exp. Med. 196: 1617-1626*

Brown D. A., London E. (2000) Structure and function of sphingolipid- and cholesterol-rich membrane rafts. *J. Biol. Chem. 275: 17221-17224*

Brown D. A., Rose J. K. (1992) Sorting of GPI-anchored proteins to glycolipid-enriched membrane subdomains during transport to the apical cell surface. *Cell 68: 533-544*

Bruhns P., Frémont S., Daëron M. (2005) Regulation of allergy by Fc receptors. *Curr. Opin. Immunol. 17: 662-669*

Burtin C., Ponvert C., Fray A., Scheinmann P., Lespinats G., Loridon B., Canu P., Paupe J. (1985) Inverse correlation between tumor incidence and tissue histamine levels in W/WV, WV/+, and +/+ mice. *J. Natl. Cancer Inst. 74: 671-674*

Chatterjee S., Mayor S. (2001) The GPI-anchor and protein sorting. *Cell. Mol. Life Sci. 58: 1969-1987*

Chen C.-C., Grimbaldeston M. A., Tsai M., Weissman I. L., Galli S. J. (2005) Identification of mast cell progenitors in adult mice. *Proc. Natl. Acad. Sci. USA 102: 11408-11413*

Cinek T., Hořejší V. (1992) The nature of large noncovalent complexes containing glycosyl-phosphatidylinositol-anchored membrane glycoproteins and protein tyrosine kinases. *J. Immunol. 149: 2262-2270*

Corbeil D., Röper K., Fargeas C. A., Joester A., Huttner W. B. (2001) Prominin: a story of cholesterol, plasma membrane protrusions and human pathology. *Traffic 2: 82-91*

Dietrich C., Bagatolli L. A., Volovyk Z. N., Thompson N. L., Levi M., Jacobson K., Gratton E. (2001) Lipid rafts reconstituted in model membranes. *Biophys. J. 80: 1417-1428*

Dimitriadou V., Rouleau A., Dam Trung Tuong M., Newlands G. J. Miller H. R., Luffau G., Schwartz J. C., Garbarg M. (1994) Functional relationship between mast cells and C-sensitive nerve fibres evidenced by histamine H3-receptor modulation in rat lung and spleen. *Clin. Sci. (Lond.) 87: 151-163*

Ding Y., Chen D., Tarcsafalvi A., Su R., Qin L., Bromberg J. S. (2003) Supressor of cytokine signaling 1 inhibits IL-10-mediated immune responses. *J. Immunol. 170: 1383-1391*

Dolganiuc A., Bakis G., Kodys K., Mandrekar P., Szabo G. (2006) Acute ethanol treatment modulates Toll-like receptor-4 association with lipid rafts. *Alcohol Clin. Exp. Res. 30: 76-85*

Dráberová L., Dráber P. (1993) Cross-linking of Thy-1 glycoproteins or high-affinity IgE receptors induces mast cell activation via different mechanisms. *Immunology 80: 103-109*

Dunphy J. T., Greentree W. K., Linder M. E. (2001) Enrichment of G-protein palmitoyltransferase activity in low density membranes. *J. Biol. Chem. 276: 43300-43304*

Dykstra M., Cherukuri A., Sohn H. W., Tzeng S. J., Pierce S. K. (2003) Location is everything: lipid rafts and immune cell signaling. *Annu. Rev. Immunol. 21: 457-481*

Edvinsson L., Cervos-Navarro J., Larsson L. I., Owman C., Ronnberg A. L. (1977) Regional distribution of mast cells containing histamine, dopamine, or 5-hydroxytryptamine in the mammalian brain. *Neurology 27: 878-883*

Epand R. M., Maekawa S., Yip C. M., Epand R. F. (2001) Protein-induced formation of cholesterol-rich domains. *Biochemistry 40: 10514-10521*

Ermini L., Secciani F., La Sala G. B. Sabatini L., Fineschi D., Hale G., Rosati F. (2005) Different glycoforms of the human GPI-anchored antigen CD52 associate differently with lipid microdomains in leukocytes and sperm membranes. *Biochem. Biophys. Res. Com. 338: 1275-1283*

Falcone F. H., Zillikens D., Gibbs B. F. (2006) The 21st century renaissance of the basophil? Current insights into its role in allergic responses and innate immunity. *Exp. Dermatol. 15: 855-864*

Field K. A., Holowka D., Baird B. (1995) FcεRI-mediated recruitment of p53/56^{lyn} to detergent-resistant membrane domains accompanies cellular signaling. *Proc. Natl. Acad. Sci. USA 92: 9201-9205*

Forsythe P., Befus A. D. (2003) CCR3: a key to mast cell phenotypic and functional diversity? *Am. J. Respir. Cell Mol. Biol. 28: 405-409*

Frank M., van der Haar M. E., Schaeren-Wiemers N., Schwab M. E. (1998) rMAL is a glycosphingolipid-associated protein of myelin and apical membranes of epithelial cells in kidney and stomach. *J. Neurosci. 18: 4901-4913*

Friedrichson T., Kurzchalia T. V. (1998) Microdomains of GPI-anchored proteins in living cells revealed by crosslinking. *Nature 394, 802-805*

Frossi B., De Carli M., Pucillo C. (2004) The mast cell: an antenna of the microenvironment that directs the immune response. *J. Leukoc. Biol. 75: 579-585*

Galli S. J., Kalesnikoff J., Grimbaldeston M. A., Piliponsky A. M., Williams C. M. M., Tsai M. (2005a) Mast cells as a „tunable" effector and immunoregulatory cells: recent advances. *Annu. Rev. Immunol. 23: 749-786*

Galli S. J., Nakae S., Tsai M. (2005b) Mast cells in the development of adaptive immune responses. *Nat. Immunol. 6: 135-142*

Gaus K., Gratton E., Kable E. P. W., Jones A. S., Gelissen I., Kritharides L., Jessup W. (2003) Visualizing lipid structure and raft domains in living cells with two-photon microscopy. *Proc. Natl. Acad. Sci. USA 100: 15554-15559*

Getahun A., Hjelm F., Heyman B. (2005) IgE enhances antibody and T cell responses in vivo via CD23^{+} B cells. *J. Immunol. 175: 1473-1482*

Gilfillan A. M., Tkaczyk C. (2006) Integrated signalling pathways for mast-cell activation. *Nat. Rev. Immunol. 6: 218-230*

Gimborn K., Lessmann E., Kuppig S., Krystal G., Huber M. (2005) SHIP down-regulates FcεRI-induced degranulation at supraoptimal IgE or antigen levels. *J. Immunol. 174: 507-516*

Glebov O. O., Nichols B. J. (2004) Lipid raft proteins have a random distribution during localized activation of the T-cell receptor. *Nat. Cell Biol. 6: 238-243*

Gustin S. E., Thien C. B., Langdon W. Y. (2006) Cbl-b is a negative regulator of inflammatory cytokines produced by IgE-activated mast cells. J. Immunol. 177: 5980-5989

Hálová I., Dráberová L., Dráber P. (2002) A novel lipid raft-associated glycoprotein, TEC-21, activates rat basophilic leukemia cells independently of the type 1 Fcε receptor. *Int. Immunol. 14: 213-223*

Hamawy M. M., Mergenhagen S. E., Siraganian R. P. (1994) Adhesion molecules as regulators of mast-cell and basophil function. *Immunol. Today 15: 62-66*

Hammond A. T., Heberle F. A., Baumgart T. Holowka D., Baird B., Feigenson G. W. (2005) Crosslinking a lipid raft component triggers liquid ordered-liquid disordered phase separation in model plasma membranes. *Proc. Natl. Acad. Sci. USA 102: 6320-6325*

Hancock J. F. (2003) Ras proteins: different signals from different locations. *Nat. Rev. Mol. Cell Biol. 4: 373-384*

Harder T., Scheiffele P., Verkade P., Simons K. (1998) Lipid domain structure of the plasma membrane revealed by patching of membrane components. *J. Cell Biol. 141: 929-942*

Heerklotz H. (2002) Triton promotes domain formation in lipid raft mixtures. *Biophys. J. 83: 2693-2701*

Heneberg P., Dráber P. (2002) Nonreceptor protein tyrosine and lipid phosphatases in type I Fcε receptor-mediated activation of mast cells and basophils. *Int. Arch. Allergy Immunol. 128: 253-263*

Heneberg P., Dráber P. (2005) Regulation of Cys-based protein tyrosine phosphatases via reactive oxygen and nitrogen species in mast cells and basophils. *Curr. Med. Chem. 12: 1859-1871*

Holowka D., Sheets E. D., Baird B. (2000) Interactions between FcεRI and lipid raft components are regulated by the actin cytoskeleton. *J. Cell Sci. 113: 1009-1019*

Hong H., Kitaura J., Xiao W., Hořejší V., Ra C., Lowell C. A., Kawakami Y., Kawakami T. (2007) The Src family kinase Hck regulates mast cell activation by suppressing an inhibitory Src family kinase Lyn. *Blood (May 18, Epub. ahead of print)*

Hořejší V., Drbal K., Cebecauer M., Černý J., Brdička T., Angelisová P., Stockinger H. (1999) GPI-microdomains: a role in signalling via immunoreceptors. *Immunol. Today 20: 356-61*

Chatterjee S., Mayor S. (2001) The GPI-anchor and protein sorting. *Cell. Mol. Life Sci. 58: 1969-1987*

Chen C.-C., Grimbaldeston M. A., Tsai M., Weissman I. L., Galli S. J. (2005) Identification of mast cell progenitors in adult mice. *Proc. Natl. Acad. Sci. USA 102: 11408-11413*

Kakurai M., Monteforte R., Suto H., Tsai M., Nakae S., Galli SJ. (2006) Mast cell-derived tumor necrosis factor can promote nerve fiber elongation in the skin during contact hypersensitivity in mice. *Am. J. Pathol. 169:1713-1721*

Kalesnikoff J., Huber M., Lam V., Damen J. E., Zhang J., Siraganian R. P., Krystal G. (2001) Monomeric IgE stimulates signaling pathways in mast cells that lead to cytokine production and cell survival. *Immunity 14: 801-811*

Karnovsky M. J., Kleinfeld A. M., Hoover R. L., Klausner R. D. (1982) The concept of lipid domains in membranes. *J. Cell Biol. 94: 1-6*

Kawakami T., Kitaura J., Xiao W., Kawakami Y. (2005) IgE regulation of mast cell survival and function. *Novartis Found. Symp. 271: 100-107*

Kenworthy A. K., Edidin M. (1998) Distribution of a glycosylphosphatidylinositol-anchored protein at the apical surface of MDCK cells examined at a resolution of < 100 Å using imaging fluorescence resonance energy transfer. *J. Cell Biol. 142: 69-84*

Kenworthy A. K., Nichols B. J., Remmert C. L., Hendrix G. M., Kumar M., Zimmerberg J., Lippincott-Schwartz J. (2004) Dynamics of putative raft-associated proteins at the cell surface. *J. Cell Biol. 165: 735-746*

Kenworthy A. K., Petráňová N., Edidin M. (2000) High-resolution FRET microscopy of cholera toxin B-subunit and GPI-anchored proteins in cell plasma membranes. *Mol. Biol. Cell 11: 1645-1655*

Kihara H., Siraganian R. P. (1994) Src homology 2 domains of Syk and Lyn bind to tyrosine-phosphorylated subunits of the high affinity IgE receptor. *J. Biol. Chem. 269: 22427-22432*

Kinet J.-P. (1999) The high affinity IgE receptor (FcεRI): from physiology to pathology. *Annu. Rev. Immunol. 17: 931-972*

Kirshenbaum A. S., Goff J. P., Semere T., Foster B., Scott L. M., Metcalfe D. D. (1999) Demonstration that human mast cells arise from a progenitor cell population that is $CD34^+$, c-kit^+, and expresses aminopeptidase n (CD13). *Blood 94: 2333-2342*

Kitaura J., Song J., Tsai M., Asai K., Maeda-Yamamoto M., Mocsai A., Kawakami Y., Liu F.-T., Lowell C. A., Barisas B. G., Galli S. J., Kawakami T. (2003) Evidence that IgE molecules mediate a spectrum of effects on mast cell survival and activation via aggregation of the FcεRI. *Proc. Natl. Acad. Sci. USA 100: 12911-12916*

Klausner R. D., Kleinfeld A. M., Hoover R. L., Karnovsky M. J. (1980) Lipid domains in membranes. *J. Biol. Chem. 255: 1286-1295*

Kondo K., Muramatsu M., Okamoto Y., Jin D., Takai S., Tanigawa N., Miyazaki M. (2006) Expression of chymase-positive cells in gastric cancer and its correlation with the angiogenesis. *J. Surg. Oncol. 94: 260-262*

Kovacs K. J., Larson A. A. (2006) Mast cells accumulate in the anogenital region of somatosensory thalamic nuclei during estrus in female mice. *Brain Res. 1114: 85-97*

Kraft S., Kinet J.-P. (2007) New developments in FcεRI regulation, function and inhibition. *Nat. Rev. Immunol. 7: 365-378*

Kusumi A., Ike H., Nakada C., Murase K., Fujiwara T. (2005) Single-molecule tracking of membrane molecules: plasma membrane compartmentalization and dynamic assembly of raft-philic signaling molecules. *Semin. Immunol. 17: 3-21*

Kusumi A., Koyama-Honda I., Suzuki K. (2004) Molecular dynamics and interactions for creation of stimulation-induced stabilized rafts from small unstable steady-state rafts. *Traffic 5: 213-230*

Lam V., Kalesnikoff J., Lee C. W., Hernandez-Hansen V., Wilson B. S., Oliver J. M., Krystal G. (2003) IgE alone stimulates mast cell adhesion to fibronectin via pathways similar to those used by IgE + antigen but distinct from those used by Steel factor. *Blood 102: 1405-1413*

Langhorst M. F., Reuter A., Stuermer C. A. O. (2005) Scaffolding microdomains and beyond: the function of reggie/flotillin proteins. *Cell. Mol. Life Sci. 62: 2228-2240*

Langlet C., Bernard A.-M., Drevot P., He H.-T. (2000) Membrane rafts and signaling by the multichain immune recognition receptors. *Current Opin. Immunol. 12: 250-255*

Lillemeier B. F., Pfeiffer J. R., Surviladze Z., Wilson B. S., Davis M. M. (2006) Plasma membrane-associated proteins are clustered into islands attached to the cytoskeleton. *Proc. Natl. Acad. Sci. 103: 18992-18997*

London E., Brown D. A. (2000) Insolubility of lipids in Triton X-100: physical origin and relationship to sphingolipid/cholesterol membrane domains (rafts). *Biochim. Biophys. Acta 1508: 182-195*

Luger T. A. (2002) Neuromediators – a crucial component of the skin immune system. *J. Dermatol. Sci. 30: 87-93*

MacGlashan D. Jr., Lichtenstein L. M., McKenzie-White J., Chichester K., Henry A. J., Sutton B. J., Gould H. J. (1999) Upregulation of FcεRI on human basophils by IgE antibody is mediated by interaction of IgE with FcεRI. *J. Allergy Clin. Immunol. 104: 492-498*

Madore N., Smith K. L., Graham C. H., Jen A., Brady K., Hall S., Morris R. (1999) Functionally different GPI proteins are organized in different domains on the neuronal surface. *EMBO J. 18: 6917-6926*

Malbec O., Daëron M. (2007) The mast cell IgG receptors and their roles in tissue inflammation. *Immunol. Rev. 217: 206-221*

Marshall J. S. (2004) Mast-cell responses to pathogens. *Nat. Rev. Immunol. 4: 787-799*

Martin S. W., Glover B. J., Davies J. M. (2005) Lipid microdomains – plant membranes get organized. *Trends Plant. Sci. 10: 263-265*

Martinez F. D. (2007) Gene-environment interactions in asthma: with apologies to william of Ockham. *Proc. Am. Thorac. Soc. 4: 26-31*

Matsumoto I., Inoue Y., Shimada T., Aikawa T. (2001) Brain mast cells act as an immune gate to the hypothalamic-pituitary-adrenal axis in dogs. *J. Exp. Med. 194: 71-78*

Mawdsley J. E., Rampton D. S. (2006) Psychological stress in IBD: new insights into pathogenic and therapeutic implications. *Gut 54: 1481-1491*

Mayor S., Maxfield F. R. (1995) Insolubility and redistribution of GPI-anchored proteins at the cell surface after detergent treatment. *Mol. Biol. Cell 6: 929-944*

Mayor S., Rothberg K. G., Maxfield F. R. (1994) Sequestration of GPI-anchored proteins in caveolae triggered by cross-linking. *Science 264: 1948-1951*

McIntosh T. J., Simon S. A., Needham D., Huang C. H. (1992) Structure and cohesive properties of sphingomyelin/cholesterol bilayers. *Biochemistry 31: 2012-2020*

Metcalfe D. D., Baram D., Mekori Y. A. (1997) Mast cells. *Physiol. Rev. 77: 1033-1079*

Metz M., Piliponski A. M., Cheng C.-C., Lammel V., Åbrink M., Pejler G., Tsai M., Galli S. J. (2006) Mast cells can enhance resistance to snake and honeybee venoms. *Science 313: 526-530*

Montagnac G., Mollà-Herman A., Bouchet J., Yu L. C. H., Conrad D. H., Perdue M. H., Benmerah A. (2005) Intracellular trafficking of CD23: differential regulation in humans and mice by both extracellular and intracellular exons. *J. Immunol. 174: 5562-5572*

Montixi C., Langlet C., Bernard A.-M., Thimonier J., Dubois C., Wurbel M.-A., Chauvin J.-P., Pierres M., He H.-T. (1998) Engagement of T cell receptor triggers its recruitment to low-density detergent-insoluble membrane domains. *EMBO J. 17: 5334-5348*

Mukaratirwa S., Chikafa L., Dliwayo R., Moyo N. (2006a) Mast cells and angiogenesis in canine melanomas: malignancy and clinicopathological factors. *Vet. Dermatol. 17: 141-146*

Mukaratirwa S. Chiwome T., Chitanga S., Bhebhe E. (2006b) Canine transmissible venereal tumour: assessment of mast cell numbers as indicators of the growth phase. *Vet. Res. Commun. 30: 613-621*

Muñoz S., Hernández-Pando R., Abraham S. N., Enciso J. A. (2003) Mast cell activation by *Mycobacterium tuberculosis*: mediator release and role of CD48. *J. Immunol. 170: 5590-5596*

Narita S., Goldblum R. M., Watson C. S., Brooks E. G., Estes D. M., Curran E. M., Midoro-Horiuti T. (2007) Environmental estrogens induce mast cell degranulation and enhance IgE-mediated release of allergic mediators. *Environ. Health. Perspect. 115: 48-52*

Navarro A., Anand-Apte B., Parat M. O. (2004) A role for caveolae in cell migration. *FASEB J. 18: 1801-1811*

O´Farrell A.-M., Ichihara M., Mui A. L.-F., Miyajima A. (1996) Signaling pathways activated in a unique mast cell line where interleukin-3 supports survival and stem cell factor is required for a proliferative response. *Blood 87: 3655-3668*

Okayama Y. (2000) Mast cell matrix interactions. *Clin. Exp. Allergy 30: 455-457*

Okayama Y., Kawakami T. (2006) Development, migration and survival of mast cells. *Immunol. Res. 34: 97-115*

Opekarová M., Malínská K., Nováková L., Tanner W. (2005) Differential effect of phosphatidylethanolamine depletion on raft proteins. Further evidence for diversity of rafts in Saccharomyces cerevisiae. *Biochim. Biophys. Acta 1711: 87-95*

Őzdemir Ő. (2006) Mast cells and the tumor-associated neoangiogenesis. *Med. Sci. Monit. 12: RA53-56*

Paladino S., Sarnataro D., Pillich R., Tivodar S., Nitsch L., Zurzolo C. (2004) Protein oligomerization modulates raft partitioning and apicas sorting of GPI-anchored proteins. *J. Cell Biol. 167: 699-709*

Pang S., Urquhart P., Hooper N. M. (2004) N-glycans, not the GPI anchor, mediate the apical targeting of a naturally glycosylated, GPI-anchored protein in polarised epithelial cells. *J. Cell Sci. 117: 5079-5086*

Penninger J. M., Irie-Sasaki J., Sasaki T., Oliveira-dos-Santos A. J. (2001) CD45: new jobs for an old acquaintance. *Nat. Immunol. 2: 389-396*

Pérez P., Puertollano R., Alonso M. A. (1997) Structural and biochemical similarities reveal a family of proteins related to the MAL proteolipid, a

component of detergent-insoluble membrane microdomains. *Biochem. Biophys. Res. Com. 232: 618-621*

Pike L. J. (2004) Lipid rafts: heterogeneity on the high seas. *Biochem. J. 378: 281-292*

Pike L. J. (2006) Rafts defined: a report on the Keystone symposium on lipid rafts and cell function. *J. Lipid Res. 47: 1597-1598*

Pizzo P., Viola A. (2004) Lipid rafts in lymphocyte activation. *Microbes Infect. 6: 686-692*

Pralle A., Keller P., Florin E. L., Simons K., Hörber J. K. H. (2000) Sphingolipid-cholesterol rafts diffuse as small entities in the plasma membrane of mammalian cells. *J. Cell Biol. 148: 997-1007*

Radhakrishnan A., Anderson T. G., McConnell H. M. (2000) Condensed complexes, rafts, and the chemical activity of cholesterol in membranes. *Proc. Natl. Acad. Sci. USA 97: 12422-12427*

Radhakrishnan A., McConnell H. M. (1999) Condensed complexes of cholesterol and phospholipids. *Biophys. J. 77: 1507-1517*

Rajput A. B., Turbin D. A., Cheang M. C., Voduc D. K., Leung S., Gelmon K. A., Gilks C. B., Huntsman D. G. (2007) Stromal mast cells in invasive breast cancer are a marker of favourable prognosis: a study of 4,444 cases. Breast Cancer Res. Treat. (March 13, Epub. ahead of print)

Rege T. A., Hagood J. S. (2006) Thy-1 as a regulator of cell-cell and cell-matrix interactions in axon regeneration, apoptosis, adhesion, migration, cancer, and fibrosis. *FASEB J. 20: 1045-1054*

Resh M. D. (1994) Myristylation and palmitylation of Src family members: the fats of the matter. *Cell 76: 411-413*

Rodgers W., Rose J. K. (1996) Exclusion of CD45 inhibits activity of $p56^{lck}$ associated with glycolipid-enriched membrane domains. *J. Cell Biol. 135: 1515-1523*

Rotblat B., Prior I. A., Muncke C., Parton R. G., Kloog Y., Henis Y. I., Hancock J. F. (2004) Three separable domains regulate GTP-dependent association of H-ras with the plasma membrane. *Mol. Cell. Biol. 24: 6799-6810*

Roy S., Plowman S., Rotblat B., Prior I. A., Muncke C., Grainger S., Parton R. G., Henis Y. I., Kloog Y., Hancock J. F. (2005) Individual palmitoyl residues serve distinct roles in H-ras trafficking, microlocalization, and signaling. *Mol. Cell. Biol. 25: 6722-6733*

Saeki K., Miura Y., Aki D., Kurosaki T., Yoshimura A. (2003) The B cell-specific major raft protein, raftlin, is necessary for the integrity of lipid raft and BCR signal transduction. *EMBO J. 22: 3015-3026*

Saitoh S., Arudchandran R., Manetz T. S., Zhang W., Sommers C. L., Love P. E., Rivera J., Samelson L. E. (2000) LAT is essential for FcεRI-mediated mast cell activation. *Immunity 12: 525-535*

Samayawardhena L. A., Kapur R., Craig A. W. B. (2007) Involvement of Fyn kinase in Kit and integrin-mediated Rac activation, cytoskeletal reorganization, and chemotaxis of mast cells. *Blood 109: 3679-3686*

Sanan D. A., Anderson R. G. W. (1991) Simultaneous visualization of LDL receptor distribution and clathrin lattices on membranes torn from the upper surface of cultured cells. *J. Histochem. Cytochem. 39: 1017-1024*

Sankaram M. B., Thompson T. E. (1990a) Interaction of cholesterol with various glycerophospholipids and sphingomyelin. *Biochemistry 29: 10670-10675*

Sankaram M. B., Thompson T. E. (1990b) Modulation of phospholipid acyl chain order by cholesterol. A solid-state 2H nuclear magnetic resonance study. *Biochemistry 29: 10676-10684*

Sankaram M. B., Thompson T. E. (1991) Cholesterol-induced fluid-phase immiscibility in membranes. *Proc. Natl. Acad. Sci. USA 88: 8686-8690*

Sankaram M. B., Marsh D., Thompson T. E. (1992) Determination of fluid and gel domain sizes in two-component, two-phase lipid bilayers. *Biophys. J. 63: 340-349*

Schade A. E., Levine A. D. (2002) Lipid raft heterogeneity in human peripheral blood T lymphoblasts: a mechanism for regulating the initiation of TCR signal transduction. *J. Immunol. 168: 2233-2239*

Scheiffele P., Roth M. G., Simons K. (1997) Interaction of influenza virus haemagglutinin with sphingolipid-cholesterol membrane domains via its transmembrane domain. *EMBO J. 16: 5501-5508*

Scholzen T., Armstrong C. A., Bunnett N. W. Luger T. A., Olerud J. E., Ansel J. C. (1998) Neuropeptides in the skin: interactions between the neuroendocrine and the skin immune systems. *Exp. Dermatol. 7: 81-96*

Schütz G. J., Kada G., Pastushenko V. P., Schindler H. (2000) Properties of lipid microdomains in a muscle cell membrane visualized by single molecule microscopy. *EMBO J. 19: 892-901*

Seagrave J., Pfeiffer J. R., Wofsy C., Oliver J. M. (1991) Relationship of IgE receptor topography to secretion in RBL-2H3 mast cells. *J. Cell Physiol. 148: 139-151*

Semic-Jusufagic A., Simpson A., Custovic A. (2006) Environmental exposures, genetic predisposition and allergic diseases: one size never fits all. *Allergy 61: 397-399*

Sharma P., Varma R., Sarasij R. C., Ira, Gousset K., Krishnamoorthy G., Rao M., Mayor S. (2004) Nanoscale organization of multiple GPI-anchored proteins in living cell membranes. *Cell 116: 577-589*

Schade A. E., Levine A. D. (2002) Lipid raft heterogeneity in human peripheral blood T lymphoblasts: a mechanism for regulating the initiation of TCR signal transduction. *J. Immunol. 168: 2233-2239*

Scheiffele P., Roth M. G., Simons K. (1997) Interaction of influenza virus haemagglutinin with sphingolipid-cholesterol membrane domains via its transmembrane domain. *EMBO J. 16: 5501-5508*

Scholzen T., Armstrong C. A., Bunnett N. W. Luger T. A., Olerud J. E., Ansel J. C. (1998) Neuropeptides in the skin: interactions between the neuroendocrine and the skin immune systems. *Exp. Dermatol. 7: 81-96*

Schütz G. J., Kada G., Pastushenko V. P., Schindler H. (2000) Properties of lipid microdomains in a muscle cell membrane visualized by single molecule microscopy. *EMBO J. 19: 892-901*

Silver R., Silverman A. J., Vitković L., Lederhendler I. I. (1996) Mast cells in the brain: evidence and functional significance. *Trends Neurosci. 19: 25-31*

Simeoni L., Smida M., Posevitz V., Schraven B., Lindquist J. A. (2005) Right time, right place: the organization of membrane proximal signaling. *Semin. Immunol. 17: 35-49*

Simons K., Ikonen E. (1997) Functional rafts in cell membranes. *Nature 387: 569-572*

Simons K., Toomre D. (2000) Lipid rafts and signal transduction. *Nat. Rev. Mol. Cell Biol. 1: 31-39*

Singer S. J., Nicolson G. L. (1972) The fluid mosaic model of the structure of cell membranes. *Science 175: 720-731*

Smith T. J., Weis J. H. (1996) Mucosal T cells and mast cells share common adhesion receptors. *Immunol. Today 17: 60-63*

Smrž D., Dráberová L., Dráber P. (2007) Non-apoptotic phosphatidylserine externalization induced by engagement of glycosylphosphatidylinositol-anchored proteins. *J. Biol. Chem. 282: 10487-10497*

Sonoda T., Kitamura Y., Haku Y., Hara H., Mori K. J. (1983) Mast-cell precursors in various haematopoietic colonies of mice produced in vivo and in vitro. *Br. J. Haematol. 53: 611-620*

Sozanska B., MacNeill S. J., Kajderowicz-Kowalik M., Danielewicz H., Wheatley M., Newman Taylor A. J., Boznanski A., Cullinan P. (2007) Atopy and asthma in rural Poland: a paradigm for the emergence of childhood respiratory allergies in Europe. *Allergy 62: 394-400*

Stump R. F., Pfeiffer J. R., Seagrave J., Oliver J. M. (1988) Mapping gold-labeled IgE receptors on mast cells by scanning electron microscopy: receptor distributions revealed by silver enhancement, backscattered electron imaging, and digital image analysis. *J. Histochem. Cytochem. 36: 493-502*

Subczynski W. K., Kusumi A. (2003) Dynamics of raft molecules in the cell and artificial membranes: approaches by pulse EPR spin labeling and single molecule optical microscopy. *Biochim. Biophys. Acta 1610: 231-243*

Surviladze Z., Dráberová L., Kovářová M., Boubelík M., Dráber P. (2001) Differential sensitivity to acute cholesterol lowering of activation mediated via the high-affinity IgE receptor and Thy-1 glycoprotein. *Eur. J. Immunol. 31: 1-10*

Suzuki K., Nakajima H., Watanabe N., Kagami S., Suto A., Saito Y., Saito T., Iwamoto I. (2000) Role of common receptor γ chain (γ_c)- and Jak3-dependent signaling in the proliferation and survival of murine mast cells. *Blood 96: 2172-2180*

Suzuki K., Sheetz M. P. (2001) Binding of cross-linked glycosylphosphatidylinositol-anchored proteins to discrete actin-associated sites and cholesterol-dependent domains. *Biophys. J. 81: 2181-2189*

Thomas J. L., Holowka D., Baird B., Webb W. W. (1994) Large-scale co-aggregation of fluorescent lipid probes with cell surface proteins. *J. Cell Biol. 125: 795-802*

Toth-Jakatics R., Jimi S., Takebayashi S., Kawamoto N. (2000) Cutaneous malignant melanoma: correlation between neovascularization and peritumor accumulation of mast cells overexpressing vascular endothelial growth factor. *Hum. Pathol. 31: 955-960*

Tsai M., Takeishi T., Thompson H., Langley K. E., Zsebo K. M., Metcalfe D. D., Geissler E. N., Galli S. J. (1991) Induction of mast cell proliferation, maturation, and heparin synthesis by the rat c-kit ligand, stem cell factor. *Proc. Natl. Acad. Sci. USA 88: 6382-6386*

Van Nassauw L., Adriaensen D., Timmermans J. P. (2007) The bidirectional communication between neurons and mast cells within the gastrointestinal tract. *Auton. Neurosci. 133: 91-103*

van Ree R., Yazdanbakhsh M. (2007) Allergic disorders in African countries: linking immunology to accurate phenotype. *Allergy 62: 237-246*

Varma R., Mayor S. (1998) GPI-anchored proteins are organized in submikron domains at the cell surface. *Nature 394: 798-801*

Velazquez L., Gish G. D., van der Geer P., Taylor L., Shulman J., Pawson T. (2000) The Shc adaptor protein forms interdependent phosphotyrosine-mediated protein complexes in mast cells stimulated with interleukin 3. *Blood 96: 132-138*

Vrljic M., Nishimura S. Y., Brasselet S., Moerner W. E., McConnell H. M. (2002) Translational diffusion of individual class II MHC membrane proteins in cells. *Biophys. J. 83: 2681-2692*

Wang J., Gunning W., Kelley K. M. M., Ratnam M. (2002) Evidence for segregation of heterologous GPI-anchored proteins into separate lipid rafts within plasma membrane. *J. Membrane Biol. 189: 35-43*

Wilson B. S., Pfeiffer J. R., Oliver J. M. (2000) Observing FcεRI signaling from the inside of the mast cell membrane. *J. Cell Biol. 149: 1131-1142*

Wilson B. S., Pfeiffer J. R., Oliver J. M. (2002) FcεRI signaling observed from the inside of the mast cell membrane. *Mol. Immunol. 38: 1259-1268*

Wilson B. S., Pfeiffer J. R., Surviladze Z., Gaudet E. A., Oliver J. M. (2001) High resolution mapping of mast cell membranes reveals primary and secondary domains of FcεRI and LAT. *J. Cell Biol. 154: 645-658*

Wilson B. S., Steinberg S. L., Liederman K., Pfeiffer J. R., Surviladze Z., Zhang J., Samelson L. A., Yang L., Kotula P. G., Oliver J. M. (2004) Markers for detergent-resistant lipid rafts occupy distinct and dynamic domains in native membranes. *Mol. Biol. Cell 15: 2580-2592*

Xiao W., Nishimoto H., Hong H., Kitaura J., Nunomura S., Maeda-Yamamoto M., Kawakami Y., Lowell C. A., Ra C., Kawakami T. (2005) Positive and negative regulation of mast cell activation by Lyn via the FcεRI. *J. Immunol. 175: 6885-6892*

Xu X., Bittman R., Duportail G., Heissler D., Vilcheze C., London E. (2001) Effect of the structure of natural sterols and sphingolipids on the formation of ordered sphingolipid/sterol domains (rafts). *J. Biol. Chem. 276: 33540-33546*

Zacharias D. A., Violin J. D., Newton A. C., Tsien R. Y. (2002) Partitioning of lipid-modified monomeric GFPs into membrane microdomains of live cells. *Science 296: 913-916*

Zhang M., Moran M. Round J., Low T. A., Patel V. P., Tomassian T., Hernandez J. D. Miceli M. C. (2005) CD45 signals outside of lipid rafts to promote ERK activation, synaptic raft clustering, and IL-2 production. *J. Immunol. 174: 1479-1490*

Zhu M., Liu Y., Koonpaew S., Granillo O., Zhang W. (2004) Positive and negative regulation of FcεRI-mediated signaling by the adaptor protein LAB/NTAL. *J. Exp. Med. 200: 991-1000*